

THE UNIVERSITY of EDINBURGH

This thesis has been submitted in fulfilment of the requirements for a postgraduate degree (e.g. PhD, MPhil, DClinPsychol) at the University of Edinburgh. Please note the following terms and conditions of use:

This work is protected by copyright and other intellectual property rights, which are retained by the thesis author, unless otherwise stated.

A copy can be downloaded for personal non-commercial research or study, without prior permission or charge.

This thesis cannot be reproduced or quoted extensively from without first obtaining permission in writing from the author.

The content must not be changed in any way or sold commercially in any format or medium without the formal permission of the author.

When referring to this work, full bibliographic details including the author, title, awarding institution and date of the thesis must be given.



THE UNIVERSITY *of* EDINBURGH

Regulation of proteostasis during cell division

Shoukang Du

A thesis submitted for the degree of Doctor of Philosophy

The University of Edinburgh

2025

Abstract

Misfolding and aggregation of proteins not only disrupt their functions but also perturb the functions of other proteins by co-aggregation. These processes challenge protein homeostasis (proteostasis) and subsequently lead to cellular aging and neurodegenerative disorders. To maintain proteostasis, cells utilize several protein quality control (PQC) systems including the regulation of protein synthesis, folding, degradation, and the spatial sequestration of misfolded protein aggregates. How cells employ PQC systems is extensively studied, however, less is known about how cells regulate their proteostasis during division.

To investigate how PQC systems maintain proteostasis in dividing cells, firefly luciferase with two destabilizing mutations (FlucDM), a live-cell proteostasis reporter, was fused to enhanced green fluorescent protein (eGFP) and expressed in mammalian cells undergoing symmetric division. Upon heat shock, FlucDM-eGFP formed protein aggregates in mitotic cells, indicating that the FlucDM system effectively reports proteostasis during cell division. To further explore how mitotic cells regulate proteostasis, small-molecule inhibitors were utilized to disrupt key elements of the proteostasis network and live-cell imaging was used to monitor the aggregation of FlucDM-eGFP. The results demonstrated that the 26S proteasome and heat shock protein 70 (Hsp70) played critical roles in eliminating misfolded proteins during mitosis. Moreover, both the attenuation of protein translation and the induction of endoplasmic reticulum (ER) stress relieved proteostasis stress in mitotic cells. Interestingly, the inhibitor of the 26S proteasome alone induced protein aggregates in interphase cells but not in mitotic cells, suggesting that mitotic cells possess a stronger ability to relieve proteostasis stress caused by proteasome inhibition.

Unexpectedly, in various mammalian cell lines, ER-targeted FlucDM-eGFP (ER-FlucDM-eGFP) assembled into protein aggregates in the nucleus. Interestingly, these aggregates were encapsulated by the ER membrane, similar to the structural feature of the nucleoplasmic reticulum (NR). Similar protein aggregates also formed in cells overexpressing other ER-targeted proteins such as ER-targeted eGFP. However, either perturbation of ER homeostasis by small molecules or the overexpression of human

pathological misfolding-prone proteins in the ER did not induce similar aggregates. Surprisingly, ER-FlucDM-eGFP aggregates no longer formed upon the knockdown of binding immunoglobulin protein (BiP), an ER-resident member of the Hsp70 chaperone family. Furthermore, immunofluorescence staining showed that BiP colocalized with these aggregates. This suggested that despite its expected role in disaggregating misfolded protein aggregates, BiP may facilitate the aggregation of misfolding-prone proteins. Moreover, aggregates in mitotic cells exhibited faster fluorescence recovery kinetics after photobleaching than those in interphase cells.

Live-cell imaging demonstrated that these aggregates were cleared only during cell division. Proteomic analysis revealed that ER-FlucDM-eGFP overexpression upregulated multiple proteins related to the unfolded protein response (UPR) and several proteins associated with cell cycle regulation. Using small-molecule inhibitors, it was found that aggregate clearance required the inactivation of cyclin-dependent kinase 1 (Cdk1) and the activity of Aurora kinase A. Moreover, the inhibition of the Hsp70 family chaperones, especially BiP, not only abolished aggregate clearance but also altered the ER membrane structure in dividing cells, suggesting mitotic ER remodeling facilitates aggregate clearance. The following perturbations on ER remodeling by both the disassembly of microtubules and the knockdown of the ER membrane fusion protein atlastins inhibited aggregate clearance. Furthermore, overexpression of the ER luminal spacer cytoskeleton-linking membrane protein 63 (CLIMP63) facilitated the clearance of aggregates. Notably, the total protein abundance of ER-FlucDM-eGFP remained mostly unchanged before and after cell division, suggesting that aggregate clearance primarily results from ER remodeling rather than protein degradation.

In conclusion, this study reveals several novel mechanisms regulating proteostasis in mammalian dividing cells. Results from Chapter 3 and Chapter 5 indicate that misfolding-prone proteins are less likely to aggregate during cell division. Results from Chapter 4 and Chapter 5 demonstrate that interphase cells confine misfolded proteins from the ER to the nucleus and assemble them into aggregates. These aggregates are cleared during cell division, a process dependent on ER remodeling.

Keywords: Cell division; Mitosis; Proteostasis; Protein aggregates

Abstract in Chinese

蛋白质的错误折叠与聚集不仅会破坏其自身的功能，还会通过共聚集干扰其他蛋白质的正常功能，从而挑战蛋白质稳态 (proteostasis) 并导致细胞衰老和神经退行性疾病。为维持蛋白质稳态，细胞采用了多种蛋白质质量控制 (protein quality control, PQC) 系统，这些系统涵盖了蛋白质合成、折叠、降解以及对错误折叠蛋白聚集物的空间隔离。虽然细胞如何利用 PQC 系统已被广泛研究，但是分裂时期的细胞如何调控其蛋白质稳态的认识却相对较少。

为了探究 PQC 系统如何在细胞分裂过程中维持蛋白质稳态，本研究在进行对称分裂的哺乳动物细胞中表达了一种带有两个去稳定化突变的萤火虫荧光素酶 (firefly luciferase with two destabilizing mutations, FlucDM) 作为活细胞蛋白质稳态的报告工具。在热休克条件下，FlucDM-eGFP 在有丝分裂细胞中形成蛋白聚集体，表明该系统能有效反映有丝分裂期间的蛋白质稳态。为进一步探讨有丝分裂细胞调控蛋白质稳态的机制，我利用小分子抑制剂干扰蛋白质稳态网络的关键组分，并通过活细胞成像监测 FlucDM-eGFP 的聚集情况。结果表明，26S 蛋白酶体 (26S proteasome) 和 70 kDa 热休克蛋白 (heat shock protein 70, Hsp70) 在清除有丝分裂细胞中错误折叠蛋白方面发挥了关键作用。此外，降低蛋白质合成以及诱导内质网 (endoplasmic reticulum, ER) 应激均能缓解有丝分裂细胞受到的蛋白质稳态压力。有趣的是，仅使用 26S 蛋白酶体抑制剂会在间期细胞中诱导蛋白聚集，但在有丝分裂细胞中却没有这种效应，这表明有丝分裂细胞具有更强的能力去缓解因蛋白酶体抑制所引发的蛋白质稳态压力。

在多种哺乳动物细胞系中，靶向内质网的 FlucDM-eGFP (ER-FlucDM-eGFP) 出乎意料地在细胞核中组装成了蛋白质聚集体。这些聚集体被内质网膜包裹，呈现出类似核质网 (nucleoplasmic reticulum, NR) 的结构特征。当过表达其他内质网靶向蛋白比如靶向内质网的 eGFP 时，也观察到了类似的蛋白质聚集体。然而，通过小分子干扰内质网稳态或在内质网中过表达易于错误折叠的病理蛋白均未

诱导出此类聚集体。令人惊讶的是，敲低内质网中 Hsp70 家族成员免疫球蛋白结合蛋白 (binding immunoglobulin protein, BiP) 后，ER-FlucDM-eGFP 的聚集体不再形成。同时免疫荧光染色显示 BiP 与这些聚集体共定位。这表明尽管 BiP 通常被认为有助于解聚错误折叠的蛋白质，但在本研究中，它可能促进了易错误折叠的蛋白质形成聚集体。另外，相比间期细胞，有丝分裂细胞中的蛋白质聚集体在光漂白后表现出更快的荧光恢复速度。

有趣的是，活细胞成像显示这些聚集体仅在细胞分裂过程中被清除。蛋白质组学分析发现 ER-FlucDM-eGFP 的过表达上调了多种与未折叠蛋白反应 (unfolded protein response, UPR) 相关的蛋白以及一些与细胞周期调控相关的蛋白。使用小分子抑制剂的实验发现，聚集体的清除依赖于细胞周期蛋白依赖性激酶 1 (cyclin-dependent kinase 1, Cdk1) 的失活和极光激酶 A (Aurora kinase A) 的活性。此外，抑制 Hsp70 家族分子伴侣尤其是 BiP 不仅阻碍了聚集体的清除还改变了细胞分裂时的内质网结构。这表明 ER 在细胞分裂时的形态重塑可能有助于聚集体的清除。其他破坏 ER 重塑的方法比如解聚微管或者敲低 ER 膜融合蛋白 atlastins 都会抑制聚集体的清除。另外，过表达作为内质网腔间隔体 (ER luminal spacer) 的细胞骨架连接膜蛋白 63 (cytoskeleton-linking membrane protein 63, CLIMP63) 则加速清除蛋白质聚集体。值得注意的是，细胞分裂前后 ER-FlucDM-eGFP 的总蛋白量几乎没有变化，这表明蛋白质聚集体的清除主要是由于有丝分裂期间内质网的重塑导致，而非蛋白质的降解。

本研究揭示了哺乳动物细胞分裂时调控蛋白质稳态的若干新机制。第三章和第五章的研究结果表明，在细胞分裂过程中，易错误折叠的蛋白发生聚集的可能性降低。第四章和第五章的结果揭示，间期细胞会将内质网里的错误折叠蛋白限制在细胞核内，并将其组装成聚集体，而这些聚集体在细胞分裂过程中被清除。这个清除过程依赖于 ER 在细胞分裂时的重塑。

关键词：细胞分裂；有丝分裂；蛋白质稳态；蛋白质聚集体

Lay Summary

Proteins fold into three-dimensional structures and proper folding is essential for their function. Accumulation of misfolded proteins is a hallmark of several human diseases such as Alzheimer's and Parkinson's disease. In cells, protein quality control (PQC) systems ensure correct protein folding and eliminate misfolded species. In PQC, molecular chaperones assist in folding polypeptide chains into functional proteins. Misfolded proteins are either degraded or sequestered into specialized compartments, forming protein aggregates to minimize their deleterious effects on cellular health. Cell division is the process by which a single cell divides into two daughter cells. In asymmetrically dividing cells such as the budding yeast, protein aggregates are preferentially retained in the mother cell, allowing the daughter cell to start with a refreshed proteome. However, how cells undergoing division symmetrically maintain their proteome health is less explored.

To investigate this, I expressed a protein health reporter in human cells and discovered that fewer protein aggregates are assembled in dividing cells upon the inhibition of protein degradation. Furthermore, my study demonstrates that misfolded proteins expressed in the endoplasmic reticulum assemble into protein aggregates in the cell nucleus. Moreover, these aggregates are cleared during cell division. This clearance depends on structural remodeling events in dividing cells.

In brief, my study observed several novel proteostasis maintenance strategies and revealed that mammalian cells are less likely to assemble protein aggregates during cell division.

Abbreviations

°C	Centigrade
AAT	α1-antitrypsin
APC/C	Anaphase-promoting complex/cyclosome
APC/Ci	APC/C inhibitor
ATL2	Atlastin 2
ATL3	Atlastin 3
Baf	Bafilomycin A1
BiP	Binding immunoglobulin protein
Cal	Calcimycin
CANX	Calnexin
CCT	Chaperonin containing TCP1
Cdc	Cell division cycle
Cdk1	Cyclin-dependent kinase 1
CFTR	Cystic fibrosis transmembrane conductance regulator
CHO	Chinese hamster ovary
CHX	Cycloheximide
CLIMP63	Cytoskeleton-linking membrane protein 63
CMA	Chaperone-mediated autophagy
CRISPRi	Clustered regularly interspaced palindromic repeats interference
DAPI	4’,6-Diamidino-2-phenylindole
DMEM	Dulbecco’s modified eagle medium
DMSO	Dimethyl Sulfoxide
DNA	Deoxyribonucleic acid
Drp1	Dynamin-related protein 1
EF	Elongation factor
eGFP	Enhanced green fluorescent protein
eIF	Eukaryotic initiation factor
eIF2	Eukaryotic initiation factor 2
eIF2α	α subunit of eukaryotic initiation factor 2
EM	Electron microscope
ER	Endoplasmic reticulum
ERAD	ER assisted degradation
Ero1	ER sulfhydryl oxidase 1
ERSU	ER stress surveillance
FACS	Fluorescence activated cell sorting
Fluc	Firefly luciferase
FlucDM	Firefly luciferase with double mutations
FlucSM	Firefly luciferase with single mutation
FlucWT	Firefly luciferase wild-type
FRAP	Fluorescence recovery after photobleaching
FSHR	Follicle stimulating hormone receptor
GAPDH	Glyceraldehyde-3-phosphate dehydrogenase
GFP	Green fluorescent protein
HaloDM	Halo tag with double mutations
hGeminin	Human geminin
Hsc70	Heat shock cognate protein 70
Hsp	Heat shock protein
Hsp40	Heat shock protein 40
Hsp60	Heat shock protein 60
Hsp70	Heat shock protein 70
Hsp90	Heat shock protein 90
HSPA1A	Heat shock protein family A member 1A

HSPA5	Heat shock protein family A member 5
HSPA8	Heat shock protein family A member 8
HSPB8	Heat shock protein family B member 8
IF	Initiation factor
INM	Inner nuclear membrane
INQ	Intranuclear quality-control compartment
IPOD	Insoluble protein deposit
IRES	Internal ribosome entry sites
JUNQ	Juxtanuclear quality-control compartment
KD	Knockdown
L	Liter
LDS	Lithium dodecyl sulfate
M	Molar
mg	Milligram
min	Minutes
mL	Milliliter
mRNA	Messenger ribonucleic acid
MTOC	Microtubule-organizing center
NDD	Neurodegenerative diseases
NEB	Nuclear envelope breakdown
NLS	Nuclear targeting sequence
nM	Nano molar
Noco	Nocodazole
NR	Nucleoplasmic reticulum
ONM	Outer nuclear membrane
PBS	Phosphate-buffered saline
PCR	Polymerase chain reaction
PDI	Protein disulfide isomerases
Plk1	Polo-like kinase 1
PQC	Protein quality control
qRT-PCR	Quantitative real-time PCR
REEP	Receptor expression-enhancing protein
RNA	Ribonucleic acid
RO	RO-3306
RTN	Reticulon
SD	Standard deviation
sgRNA	Single guide RNA
sHsp	Small heat shock protein
SRP	Signal recognition particle
TAOK2	Thousand and one amino acid kinase 2
TBS	Tris buffered saline
TBST	Tris buffered saline with Tween-20
TCP1	Tailless complex polypeptide 1
TEM	Transmission electron microscopy
Thaps	Thapsigargin
ThT	Thioflavin T
TRiC	TCP1 ring complex
tRNA	Transfer ribonucleic acid
Tuni	Tunicamycin
UPR	Unfolded protein response
UPS	Ubiquitin-proteasome system
VER	VER-155008
µg	Microgram
µl	Microliter
µM	Micromolar

List of Figures

Figure 1.1 Elements of the proteostasis network……2

Figure 1.2 A summary of early milestones in proteostasis research……7

Figure 1.3 Compartmentalization of misfolded proteins……21

Figure 1.4 Reorganization of organelles during cell division……24

Figure 1.5 Protein aggregate inheritance during cell division……33

Figure 1.6 Diagram of oxidative protein folding in the ER……37

Figure 1.7 Diagram of the proteostasis reporter system……44

Figure 2.1 Quantifying aggregates by Trainable Weka Segmentation……62

Figure 2.2 Workflow of heat shock treatment in dividing cells……64

Figure 3.1 The Fluc proteostasis reporter in MG132-treated cell……68

Figure 3.2 Mitotic MCF10A cells expressing FlucDM-eGFP upon heat shock……69

Figure 3.3 Effects of cycloheximide on protein aggregation in mitotic cells……70

Figure 3.4 Effects of VER-155008 on protein aggregation in mitotic cells……71

Figure 3.5 MG132 induces protein aggregation in interphase cells but not in mitotic cells...72

Figure 3.6 Effects of MG132 on protein aggregation in mitotic cells upon heat shock……..73

Figure 3.7 Effects of combined MG132 and CHX treatment on protein aggregation in mitotic cells upon heat shock……74

Figure 3.8 Effects of ER stress inducers, calcimycin or thapsigargin, on protein aggregation in mitotic cells upon heat shock……75

Figure 4.1 ER-FlucDM-eGFP is largely soluble, as revealed by protein immunoblotting….84

Figure 4.2 ER-FlucDM-eGFP is less functional revealed by luciferase activity test……..85

Figure 4.3 ER-FlucDM-eGFP assembles into protein aggregates in the cell nucleus……86

Figure 4.4 ER-FlucDM aggregates in the nucleus are encapsulated by the ER membrane…87

Figure 4.5 The expression of NLS-FlucDM-eGFP in cells……89

Figure 4.6 ER-FlucDM colocalizes with anti-GFP and Thioflavin T……90

Figure 4.7 Correlation between BiP and protein aggregates……92

Figure 4.8 ER-FlucDM-eGFP assembles into protein aggregates in various cell lines……93

Figure 4.9 Various ER-targeted proteins induce protein aggregation……95

Figure 4.10 Expression of α-1 antitrypsin and CFTR mutants in cells……96

Figure 4.11 Proteostasis perturbation by small molecules does not induce ER membrane appearance in the cell nucleus……97

Figure 4.12 Fluorescence recovery after photobleaching (FRAP) of protein aggregates in the cell nucleus……..99

Figure 4.13 Differential aggregate dynamics in interphase and mitosis……100

Figure 5.1 The quantity and area of aggregates correlate with stages of cell division…..…113

Figure 5.2 Protein aggregates are cleared during cell division……114

Figure 5.3 Protein aggregates are encapsulated by the ER membrane in dividing cells…...115

Figure 5.4 Protein aggregates of ER-HaloDM-eGFP are also cleared during cell division.116

Figure 5.5 MG132 inhibits protein aggregate clearance during cell division……..…117

Figure 5.6 APC/C is not involved in aggregate clearance during cell division……119

Figure 5.7 Effects of bafilomycin A1 on protein aggregate clearance during cell division..120

Figure 5.8 Cycloheximide chase experiments of cells expressing ER-FlucDM-eGFP……122

Figure 5.9 Relative intensity of ER-FlucDM-eGFP in early versus late dividing cells……123

Figure 5.10 Volcano plot of proteomics analysis and the validation by qRT-PCR……...124

Figure 5.11 Thapsigargin inhibits protein aggregate clearance during cell division……126

Figure 5.12 Effects of tunicamycin on protein aggregate clearance during cell division….127

Figure 5.13 Inhibition of Hsp70 and BiP abolishes aggregate clearance…….129

Figure 5.14 BiP inhibition alters ER structure in dividing cells……...130

Figure 5.15 Nocodazole inhibits aggregate clearance during cell division……..131

Figure 5.16 Cdk1 inhibition in MG132-arrested cells accelerates aggregate clearance…...132

Figure 5.17 Nocodazole inhibits the acceleration of aggregate clearance induced by Cdk1 inactivation…….……133

Figure 5.18 CLIMP63 overexpression accelerates aggregate clearance……..……134

Figure 5.19 Simultaneous knockdown of atlastin 2 and 3 inhibits aggregate clearance…...135

Figure 5.20 Aurora kinase A inhibition abolishes aggregate clearance…….……...136

Figure 6.1 A summary of the working models in Chapter 4 and Chapter 5…….……..…147

List of Tables

Table 2.1: Plasmid information.....45
Table 2.2: The recipe for DNA fragments preparation 47
Table 2.3: The recipe for Gibson assembly.....47
Table 2.4: The recipe for DNA fragments annealing.....48
Table 2.5: The recipe for T4 ligation 48
Table 2.6: The recipe for colony PCR.....49
Table 2.7: The sequence of single guide RNA 52
Table 2.8: Drugs used 53
Table 2.9: Buffers used in western blot 55
Table 2.10: Antibodies used in western blot 55
Table 2.11: Primers used in quantitative real-time PCR.....58

Acknowledgments

I would like to thank my advisor, Dr. Chew Ting Gang, for giving me the opportunity to pursue a Ph.D. in his laboratory. I am also grateful for his continuous encouragement, constant support to my projects and his excellent guidance.

I thank my thesis committee members, Dr. David Hay, Dr. Matthew Brook and Dr. Mike Shipston, for their guidance and valuable suggestions.

I would like to express my sincere thanks to Dr. Edward Avezov, Dr. Mikael Björklund, and Dr. Pierre Bagnaninch for attending my viva and for providing valuable suggestions on this thesis.

I express my thanks to all present and past members of Ting Gang Lab for their help. I thank Dr. Wang Chao and Dr. Ding Jingjing for teaching me how to do experiments. I thank all graduate students in lab especially Wang Yuhan for assistance on my projects. I also thank Yang Hui and Wang Chenxin in lab. I thank all undergraduate students especially Chen Bowen, Chen Xuqi, Gao Xukai, Chu Zihan and Miao Yuyang for their help on experiments. I also thank other professors and students in my institute for helps on my projects, especially Dr. Chan Kuan Yoow, Drs. Xie Shuangshuang and Dr. Mikael Björklund for providing reagents used in my study.

I would like to thank members from Chinese Society for Cell Biology awarding me one the best posters during the annual meeting. I thank professors and students sharing me with valuable comments on my project at the meeting.

Finally, I thank my family and friends for their supports. I thank those who have shown me that there are other possibilities in life. Thank you for making me more complete, even whole.

Shoukang Du

Declaration

I declare that this thesis is my own original work with only minor contributions from others as state. This thesis has not been submitted for any other degree or professional certification. To avoid the potential risk of self-plagiarism, I declare that some of the work in Chapter 4 and Chapter 5 has been published in an *eLife* article and on bioRxiv.

Shoukang Du

Contents

Abstract ..... **I**

Abstract in Chinese ..... **III**

Lay Summary ..... **V**

Abbreviations ..... **VI**

List of Figures ..... **VIII**

List of Tables ..... **X**

Acknowledgments ..... **XI**

Declaration ..... **XII**

Chapter 1 Introduction **1**

1.1 Proteostasis network **1**

1.1.1 Overview 1

1.1.2 Protein synthesis 3

1.1.2.1 Early concepts of protein synthesis 3

1.1.2.2 Current understanding of protein synthesis within proteostasis 7

1.1.3 Protein folding and conformation maintenance 8

1.1.3.1 Early concepts of protein folding and the discovery of chaperones 8

1.1.3.2 Current insights into protein folding and conformational maintenance 12

1.1.4 Protein degradation 14

1.1.4.1 Early discoveries of lysosomes and autophagy 14

1.1.4.2 Early discovery of the ubiquitin-proteasome system (UPS) 17

1.1.4.3 Current understanding of UPS and autophagy within proteostasis 18

1.1.5 Compartmentalization of misfolded proteins 19

1.2 Proteostasis maintenance during cell division **22**

1.2.1 General introduction of cell division 22

1.2.2 Proteostasis during cell division 25

1.2.2.1 Protein synthesis in dividing cells 25

1.2.2.2 Protein folding and conformational maintenance in dividing cells 26

1.2.2.3 The ubiquitin-proteasome system (UPS) in dividing cells 28

1.2.2.4 Autophagy and lysosomes in dividing cells 29

1.2.2.5 Protein aggregates in dividing cells 30
1.3 The endoplasmic reticulum (ER) 33
1.3.1 The early discovery of the ER 33
1.3.2 Protein folding in the ER 34
1.3.3 The ER and protein misfolding in diseases 38
1.3.4 ER remodeling and cell division 41
1.4 Tools to report proteostasis in live cells **41**
1.4.1 General introduction 41
1.4.2 Firefly luciferase mutants as proteostasis reporters 42
1.5 Aims of this thesis **44**

Chapter 2 Materials and Methods **45**
2.1 Plasmids and cloning **45**
2.1.1 Plasmid list 45
2.1.2 Molecular cloning methods 47
2.1.2.1 Vector preparation 47
2.1.2.2 DNA fragments preparation before Gibson assembly 47
2.1.2.3 Gibson assembly 47
2.1.2.4 Short DNA fragments annealing 48
2.1.2.5 T4 ligation 48
2.1.2.6 Plasmid transformation 48
2.1.2.7 Colony PCR 49
2.1.2.8 DNA sequencing of cloning products 49
2.1.2.9 Plasmids extraction 49
2.2 Cell line culture and preparation **50**
2.2.1 General cell culture conditions 50
2.2.2 Chemical transfection 50
2.2.3 Lentivirus transduction 50
2.2.3.1 Lentivirus packaging 51
2.2.3.2 Transduction 51
2.2.3.3 CRISPRi knockdown 51
2.2.4 Fluorescence-activated cell sorting (FACS) 52

2.2.5 Mitotic cell preparation 52
2.2.6 Drug list....52
2.3 Biochemistry methods....53
2.3.1 Western blots (WB) 53
2.3.1.1 General WB workflow....53
2.3.1.2 Supernatant and pellet fraction preparation 54
2.3.1.3 List of reagents used in WB....54
2.3.2 Immunofluorescence staining....56
2.3.3 Luciferase activity test....57
2.3.4 Quantitative real-time PCR (qRT-PCR) 57
2.4 Microscopy imaging techniques 58
2.4.1 Transmission electron microscopy (TEM) 58
2.4.2 Live-cell staining....59
2.4.3 Spinning-disk confocal microscopy methods....59
2.4.4 Image analysis and processing 60
2.5 Heat shock treatment 63
2.6 Proteomics methods 63
2.7 Statistics....64

Chapter 3 Proteostasis Maintenance in Mammalian Cells during Mitosis 65
3.1 Introduction 65
3.2 Results....67
3.2.1 Validation of FlucDM reporter system in MCF10A cells 67
3.2.2 Aggregation of FlucDM-eGFP in dividing cells under heat shock 68
3.2.3 Inhibition of protein translation decreases protein aggregation in dividing cells upon heat shock 68
3.2.4 Hsp70 ATPase inhibition increases protein aggregation in heat-shocked mitotic cells....69
3.2.5 26S proteasome inhibition by MG132 increases protein aggregation in heat-shocked mitotic cells but only MG132 does not induce protein aggregation in mitotic cells....70
3.2.6 ER stress inducers relieve protein aggregation in heat-shocked mitotic cells73

3.3 Discussion 75
3.3.1 Summary of results in this chapter 75
3.3.2 How to further verify only MG132 does not induce visible protein aggregates in mitotic cells? 75
3.3.3 How to explain why MG132 does not induce protein aggregates in mitotic cells? 76
3.3.4 The speculation on protein aggregates in the ER during cell division 78

Chapter 4 ER-Targeted Proteins Form Aggregates in the Nucleus 79
4.1 Introduction 79
4.2 Results 82
4.2.1 ER-FlucDM-eGFP is largely soluble as revealed by western blot 82
4.2.2 ER-FlucDM-eGFP is less functional proved by luciferase activity test 83
4.2.3 ER-FlucDM-eGFP forms protein aggregates in the cell nucleus while being surrounded by ER membranes 85
4.2.4 NLS-FlucDM-eGFP alone does not induce protein aggregates 87
4.2.5 ER-FlucDM-eGFP protein aggregates are stained by Thioflavin T 88
4.2.6 BiP is involved in ER-FlucDM-eGFP aggregation 90
4.2.7 Protein aggregates induced by ER-FlucDM-eGFP in the cell nucleus are independent of cell lines 92
4.2.8 Various ER targeted proteins induce protein aggregates 93
4.2.9 Pathologically misfolded proteins expressed in the ER do not induce protein aggregates in the cell nucleus 94
4.2.10 Proteostasis perturbations by small molecules treatment do not induce protein aggregates in the cell nucleus 95
4.2.11 Differential aggregate dynamics in cells at interphase and mitosis 97
4.3 Discussion 100
4.3.1 Summary of results in this chapter 100
4.3.2 The properties of ER-FlucDM-eGFP protein aggregates 101
4.3.3 How do the aggregates assemble in the cell nucleus while being embedded in the ER membrane? 103
4.3.4 Why are ER-FlucDM-eGFP aggregates partially encapsulated by the lamin? 105

4.3.5 Potential crosstalk among misfolded proteins in the ER, the inner nuclear envelope, and the cell nucleus 106
4.3.6 Under which conditions do protein aggregates invaginate into the cell nucleus? 107

Chapter 5 Clearance of Protein Aggregates during Cell Division 109
5.1 Introduction 109
5.2 Results 111
5.2.1 The quantity and area of protein aggregates depend on the cell stages in naturally dividing cells 111
5.2.2 Live-cell imaging reveals ER-FlucDM-eGFP aggregates are cleared during cell division 112
5.2.3 ER-FlucDM-eGFP aggregates in dividing cells are surrounded by the ER membrane 114
5.2.4 ER-HaloDM-eGFP aggregates are also cleared during cell division 115
5.2.5 Proteasome inhibition undermines aggregate clearance 115
5.2.6 APC/C is not involved in aggregate clearance during cell division 117
5.2.7 Lysosome acidification inhibition hinders aggregate clearance 119
5.2.8 Total GFP levels barely change along with aggregate clearance 120
5.2.9 The expression of ER-FlucDM-eGFP induces the unfolded protein response 122
5.2.10 Effects of ER stressors on aggregate clearance 124
5.2.10.1 Thapsigargin inhibits aggregate clearance 124
5.2.10.2 Tunicamycin short treatment does not inhibit aggregate clearance while its pretreatment accelerates aggregate clearance 126
5.2.11 Inhibition of either Hsp70 or its family member BiP prevents aggregate clearance 127
5.2.12 ER structure remodeling ensures aggregate clearance 129
5.2.12.1 ER membrane structures are perturbed upon BiP inhibition in mitotic cells 129
5.2.12.2 Nocodazole, a microtubules depolymerizer, inhibits aggregate clearance 130

5.2.12.3 RO-3306, a Cdk1 inhibitor, accelerates aggregate clearance in metaphase-arrested cells 131
5.2.12.4 Nocodazole inhibits the accelerated aggregate clearance induced by Cdk1 inactivation.....132
5.2.12.5 CLIMP63 overexpression accelerates aggregate clearance.....133
5.2.12.6 Atlastin 2 and 3 knockdown inhibits aggregate clearance.....134
5.2.12.7 Aurora kinase A inhibition by MLN-8237 inhibits aggregate clearance 135
5.3 Discussion 136
5.3.1 Summary of results in this chapter 136
5.3.2 Evidence supporting degradation is incorporated into a disassembly model137
5.3.3 Evidence supporting the disassembly model is difficult to integrate into a degradation model 138
5.3.4 Why are protein aggregates cleared only during cell division? 140
5.3.5 The proposed model of aggregate clearance 141
5.3.6 Future studies to elucidate the mechanism of protein aggregate clearance during cell division 142
5.3.7 The significance and limitations of this study.....144

Chapter 6 Conclusions and General Discussion 145
6.1 Summary of this thesis.....145
6.2 Crosstalk of proteostasis across subcellular compartments 147
6.3 Aggregation and disaggregation of protein aggregates in the ER.....148
6.4 Organelle dynamics and proteostasis during cell division.....149
6.5 Leave the protein aggregates to be dealt with during cell division.....150
6.6 The inheritance and maintenance of cellular materials during division 151

Reference 153
List of the Publication.....180

Chapter 1 Introduction

1.1 Proteostasis network

1.1.1 Overview

A typical human cell expresses over 10,000 distinct protein species. The abundances of these proteins vary significantly from a few dozen copies for specific transcription factors to more than 10 million copies such as histones and tubulin per cell (Geiger et al., 2012). To maintain functionality, these proteins must remain properly folded despite constant environmental fluctuations and cellular stress. Additionally, a substantial proportion of proteins are intrinsically disordered or contain unstructured regions (Liu et al., 2020). The structural ensemble of these proteins is tightly regulated by their localization and concentration, further increasing the complexity of the cellular proteome (Hipp et al., 2019). Even proteins generally considered stable are continuously subjected to conformational challenges caused from various endogenous (internal) and exogenous (external) stressors.

Proteostasis, or protein homeostasis, encompasses the cellular regulation of protein synthesis, folding, distribution, and degradation throughout their life cycle (Hipp et al., 2019). Disruptions in proteostasis are major contributors to the onset and progression of various diseases, including type 2 diabetes, lysosomal storage disorders, cystic fibrosis and neurodegenerative diseases such as Alzheimer's and Huntington's disease (Hartl et al., 2011).

To avoid the detrimental effects of impaired proteostasis, cells evolve an intricate system known as the proteostasis network. In human cells, this network comprises approximately 2,000 proteins that play multifaceted roles in maintaining protein homeostasis through the regulation of synthesis, folding, distribution, and degradation of proteins (Jayaraj et al., 2020). It not only ensures that proteins fold into their functional states immediately after translation but it also continuously monitors their

conformations throughout lifetimes and regulates their abundance to maintain proper function (Hipp et al., 2014). Furthermore, the proteostasis network prevents protein misfolding and aggregation since the accumulation of misfolded proteins could be toxic to cells. For example, proteins with complex amino acid sequences are prone to forming intermediate structures that expose hydrophobic regions, thus increasing the risk of aggregation (Klaips et al., 2018). The proteostasis network addresses this challenge through molecular chaperones that facilitate the correct folding and stabilization of proteins. Furthermore, the proteostasis network eliminates defective or excess proteins by employing its protein degradation pathways including lysosome- and proteasome-mediated processes (Hartl et al., 2011). Moreover, the proteostasis network sequesters protein aggregates into specific subcellular compartments to mitigate their potential toxicity (Miller et al., 2015).

In brief, for a single cell, its proteostasis network can be classified into four interconnected branches: protein synthesis, protein folding and conformation maintenance, protein degradation, and the compartmentalization of damaged proteins **(Figure 1.1)** (Hipp et al., 2019).

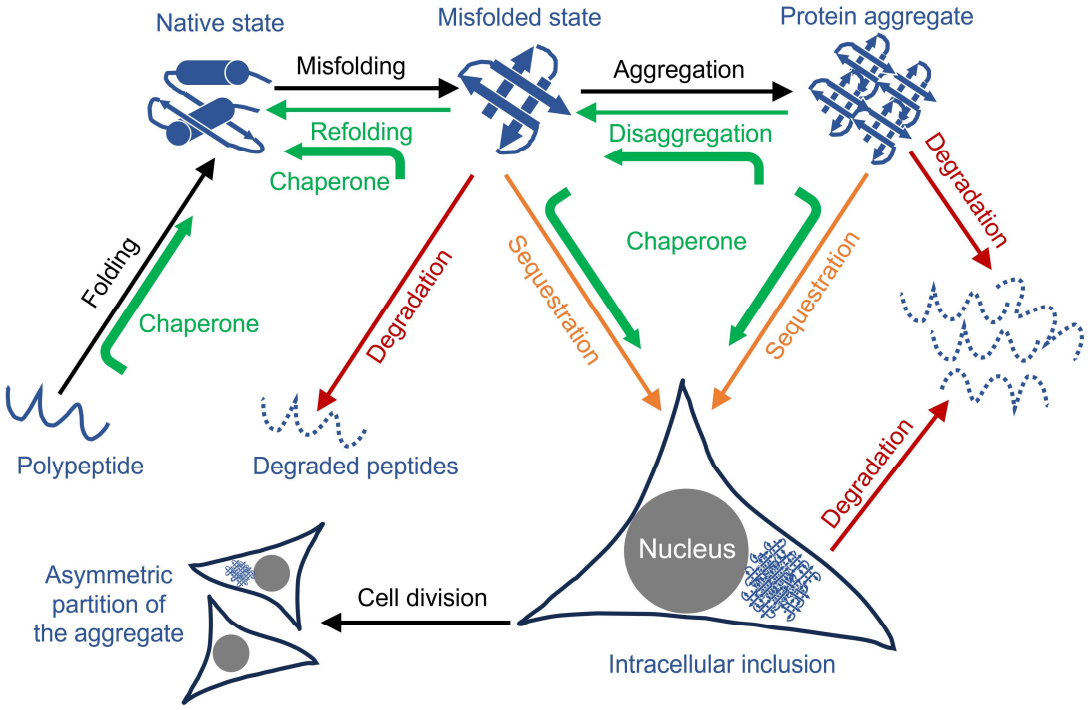


Figure 1.1: Elements of the proteostasis network. Cells employ various strategies to

eliminate misfolded proteins and their aggregates. Molecular chaperones assist in the folding of polypeptides to their native state, refold misfolded proteins, prevent aggregation, and disassemble protein aggregates. Moreover, molecular chaperones sequester protein aggregates into intracellular inclusions. During cell division, these inclusions can be partially retained in the mother cell, thereby rejuvenating the daughter cell.

1.1.2 Protein synthesis

1.1.2.1 Early concepts of protein synthesis

In the 1930s, physiological questions about protein synthesis were primarily addressed in a descriptive way by studies using tissues, tissue slices, or whole animals (Tahmasebi et al., 2019). At that time, the prevailing assumption was that bodily structural proteins remained stable and static, whereas ingested proteins were completely metabolized and their end-products excreted (Ciechanover, 2005a; Ratner, 1979). This concept was refuted by a series of studies conducted by Rudolph Schönheimer and his colleagues around 1940 (Ratner et al., 1940). They introduced the isotopic tracer method in metabolic studies and fed adult rats with ^{15}N-labelled glycine and collected their urine. They found that about 40% of the nitrogen was isotopic, suggesting that glycine is used to synthesize new proteins in these non-growing rats. Together with other studies from that era, these findings contributed to the gradual recognition that protein synthesis is a continuous process in animals.

During the 1940s, there were two significant findings and one pivotal hypothesis. Jean Brachet and Torbjörn Caspersson demonstrated that protein synthesis predominantly occurs in the cytoplasm and observed that cells synthesizing more proteins exhibit higher ribonucleic acid (RNA) concentrations (Cobb, 2015). In 1947, knowing that bacteria contained two to three times more RNA than deoxyribonucleic acid (DNA) and that the DNA content was relatively uniform among different bovine tissues, André Boivin proposed that DNA regulates the production of cytoplasmic proteins by controlling RNA synthesis (Boivin and Vendrely, 1947; Cavaillon, 2020).

Until 1950, the mechanisms of protein translation that are widely accepted today were

not known. However, the field underwent a transformative change in the 1950s, driven by newly developed techniques and foundational insights into protein synthesis. In 1951, Frederick Sanger refined the reagents used in partition chromatography and reported the first protein sequence (Sanger and Tuppy, 1951). He found that the bovine insulin B chain has a defined composition and sequence. If we extend this conclusion, any protein should possess a specific amino acid sequence, challenging the prevailing assumption that proteins were amorphous in that era.

In 1952, the synthesis of proteins was explained by two theories. The first theory emphasized the role of enzymes and postulated that a multitude of highly specific enzymes catalyzed the formation of peptide bonds between adjacent amino acids. The second theory emphasized the existence of "templates." For example, the template theory, also known as the nucleic acid template hypothesis, was first proposed in 1952 by Alexander Dounce (Dounce, 1952). This theory assumed that a specific amino acid sequence originates from a corresponding unique RNA arrangement. According to this hypothesis, RNA molecules act as templates that interact with other RNAs or amino acids to form either double-stranded RNA complexes or peptide chains. (Campbell and Work, 1953).

In 1953, Francis Crick and James Watson deciphered the structure of DNA using X-ray crystallography, describing the double-helix structure of DNA and imagining its genetic implications (Watson and Crick, 1953a) (Watson and Crick, 1953b). In the same year, Alexander Dounce refined and completed the template theory he had proposed in 1952. He overall considered observations such as the continued protein synthesis in enucleated cells and the genetic nature of DNA. Then he proposed a model consisting of a template sequence from DNA to RNA and to protein with the additional postulate that RNA synthesis could occur independently using RNA as its own template (Dounce, 1953).

In 1954, inspired by the DNA structure proposed by Watson and Crick, George Gamow,

a physicist who proposed the Big Bang theory before, discussed the possibility that DNA might act as a direct template for protein synthesis. He proposed that amino acids recognized specific “holes” in the double helix (Gamow, 1954). To be specific, every four bases of DNA formed a diamond-shaped hole for amino acids to recognize and there were 20 different combinations of holes, representing 20 different amino acids (Gamow, 1954). Although Gamow’s theory was later disproven due to the vast structural differences between DNA and amino acids, it was the first prediction about the existence of a genetic code, thereby inspiring the concept of codons. Furthermore, his theory emphasized that the sequence of amino acids in proteins solely originated from the nucleotide sequence rather than from the three-dimensional structure of DNA. In the same year, Gamow established the RNA Tie Club to decipher the mysteries of RNA structure and understand its role in protein synthesis.

In 1955, in a note from RNA Tie Club, Francis Crick postulated the existence of molecules capable of carrying specific amino acids and interacting with nucleic acid templates through corresponding enzymes. Crick’s adaptor hypothesis was formalized during a lecture in 1957 and published in 1958 with the central dogma (Crick, 1958), which emphasized that there is no way for genetic information to transport from proteins to DNA (Cobb, 2017; Crick, 1970). Also, around this time, Paul Zamecnik and his colleagues who had developed a cell-free protein synthesis system independently found there indeed existed a small fraction of soluble RNA labelled with isotopes from ^{14}C-leucine in the supernatant although high molecular weight ribosomal RNA were supposed to be centrifuged down (Zamecnik, 1969; Zamecnik et al., 1957). This amino acid-bound soluble RNA was thought to be the adaptor molecule proposed by Crick and is now known as transfer RNA (tRNA). In 1955, by electron microscopy, George Palade observed particles attached to the endoplasmic reticulum (ER) membrane (Palade, 1955). These particles were later isolated, identified as the center of protein synthesis and later termed ribosomes (Tahmasebi et al., 2019).

In summary, the 1950s marked a transformative era for understanding protein synthesis

at the molecular level **(Figure 1.2)**. Theoretical breakthroughs elucidated how DNA mediated protein synthesis by controlling the production of RNA. Concurrently, researchers recognized the existence of at least two distinct RNA species with different properties. Although their defined roles in protein synthesis were still ambiguous, it was known that one species robustly colocalized with ribonucleoprotein while another category of RNA was not upon ultracentrifugation. Instead, the latter one transiently bound to amino acids. At the time, the prevailing hypothesis posited that one gene directed the synthesis of one protein via a corresponding ribosome (Tahmasebi et al., 2019). However, this concept was challenged in the early 1960s.

In 1961, it was found that bacteria do not synthesize new ribosomes upon phage infection. Instead, RNA was actively synthesized and degraded (Brenner et al., 1961). Thus, it was speculated that protein synthesis relies on pre-existing ribosomes and unstable intermediate RNAs that act as "messengers" (Jacob and Monod, 1961). Later that year, another research group led by James Watson also provided evidence for the existence of messenger RNA (mRNA) (Gros et al., 1961). The establishment of the messenger RNA hypothesis ultimately revolutionized our understanding of protein synthesis.

During the 1960s and 1970s, key functional elements involved in protein synthesis, such as the initiation factor (IF) and the elongation factor (EF), were discovered, encouraging researchers to investigate their functions based on the foundational assumptions established in the 1950s with molecular biology and biochemical evidence (Tahmasebi et al., 2019). In the 1980s and 1990s, further insights into the molecular mechanisms regulating protein translation emerged, particularly regarding the precise phosphorylation of various eukaryotic initiation factors (eIFs) and elongation factors, and the physiological consequences of these modifications (Tahmasebi et al., 2019). For instance, in 1972, it was shown that eukaryotic initiation factor 2 (eIF2) is capable of binding and delivering the initiator tRNA to the ribosome (Chen et al., 1972). In 1977, the phosphorylation of the α subunit of eIF2 (eIF2α) was found to impair the

loading of the 40S ribosomal subunit with Met-tRNA$_f$, thereby inhibiting protein translation (Farrell et al., 1977). In 1993, eIF2α phosphorylation was demonstrated to be a response to endoplasmic reticulum (ER) stress induced by calcium ion depletion (Prostko et al., 1993). Two years later, double-stranded RNA-dependent protein kinase (PKR) was identified as a mediator of eIF2α phosphorylation during ER stress (Srivastava et al., 1995). After entering the 21st century, advanced techniques have continued to deepen our understanding of the mechanisms governing protein synthesis, providing increasingly multifaceted and quantitatively robust insights into their roles under physiological conditions.

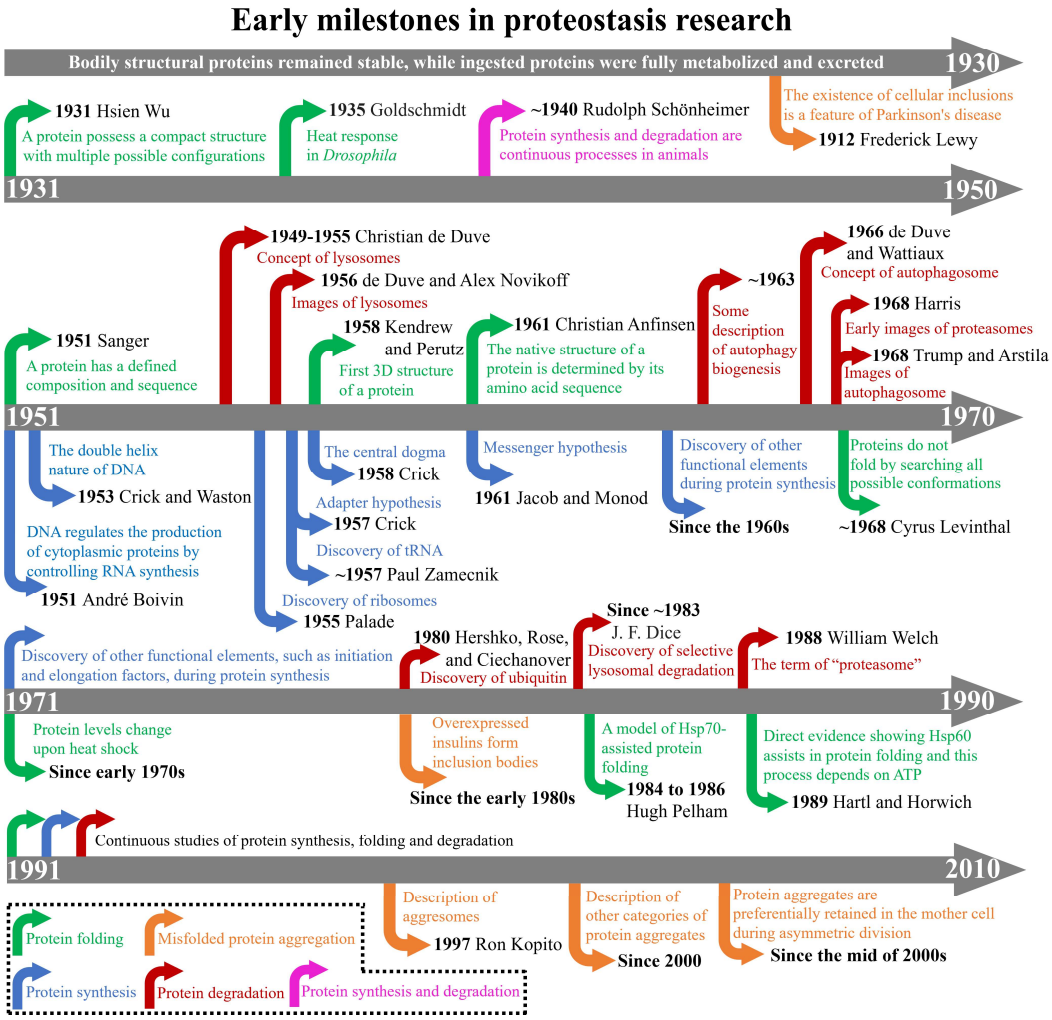


Figure 1.2: A summary of early milestones in proteostasis research. This image only contains landmarks introduced in this thesis.

1.1.2.2 Current understanding of protein synthesis within proteostasis

It is now known that the majority of cellular proteins are synthesized by cytosolic

ribosomes and their associated machinery, with each ribosome adding approximately five to six amino acids per second (Ingolia et al., 2011). This rapid pace results in over a billion protein molecules per human cell (Milo, 2013), with an average length of about 560 amino acids (Balchin et al., 2016). However, protein synthesis is intrinsically imperfect. There is a misincorporation rate of about 1 in every 1,000 to 10,000 amino acids (Zaher and Green, 2009). Consequently, roughly 15% of newly synthesized proteins contain amino acid sequence errors (Drummond and Wilke, 2009), potentially causing improper folding or decreased stability. To relieve the proteostasis stress during protein translation, cells have evolved multiple strategies such as the ribosome-associated protein quality control (PQC) pathway that clears polypeptides stalled on ribosomes (Brandman and Hegde, 2016).

In addition to spontaneous errors, cells actively regulate protein translation in response to environmental and internal signals. Under conditions of proteostasis stress such as proteasome inhibition, cells reduce protein synthesis to alleviate the burden on PQC systems (Liu et al., 2013). This reduction is mediated by controlling the phosphorylation of translation initiation and elongation factors (Spriggs et al., 2010). Furthermore, these translation factors promote the upregulation of genes encoding chaperones and proteasome subunits, further improving the cell's ability to counteract proteostasis stress (Karagöz et al., 2019). Indeed, the protein quality control strategy during translation is closely related to the function of molecular chaperones. For instance, the accumulation of misfolded proteins can overwhelm the Hsp70 chaperone system. Subsequently, newly synthesized polypeptides in ribosomes are inefficiently pulled due to insufficient Hsp70, causing early elongation pauses and subsequently shutting down translation to ameliorate proteome stress (Liu et al., 2013). Next, the discovery of chaperones and early concepts of protein folding will be introduced.

1.1.3 Protein folding and conformation maintenance

1.1.3.1 Early concepts of protein folding and the discovery of chaperones

According to a reprinted article originated from the *Chinese Journal of Physiology* in

1931 (Wu, 1995), Hsien Wu proposed that natural and soluble proteins are not composed of flexible open chains. Instead, they possess a compact structure with multiple possible configurations and these well-organized conformations become disordered upon denaturation (Wu, 1995) (Edsall, 1995). Additionally, Wu argued that a protein's biological specificity originates from a limited subset of configurations. Although his pioneering theory is influential, significant advancements in the study of protein folding and conformation were not realized until the late 1950s and early 1960s **(Figure 1.2)**.

In 1958 and 1960, benefiting from a specialized X-ray diffractometer (Thomas, 2012), John Kendrew and Max Perutz, along with their colleagues, resolved the first and second three-dimensional structures of proteins, myoglobin and haemoglobin (Kendrew et al., 1958) (Perutz et al., 1960). With other protein structures reported during this era, a question emerged: How does a protein fold into its native three-dimensional conformation? Around 1961, Christian Anfinsen discovered that urea-denatured bovine pancreatic RNase can spontaneously refold into its functional state. This led him to speculate that the native secondary and tertiary structures of a protein are determined by its amino acid sequence (Haber and Anfinsen, 1961). Anfinsen's findings suggested that protein folding might be a spontaneous process, which raises a question: How do proteins "know" their natural conformations before starting to fold?

To address this question, around 1968, Cyrus Levinthal performed a theoretical calculation showing that if a protein folded by randomly searching all possible configurations, it would take an astronomically long time (Levinthal, 1968). For example, if we assume each bond connecting two amino acids has three possible states and there is a protein containing one hundred amino acids, then this protein has approximately $3^{100} \approx 5 \times 10^{47}$ potential configurations. Even if the protein scans configurations at a rate of 10^{14} per second (about 3×10^{21} per year), it would still require roughly 10^{26} years to explore them all. This time scale far exceeds the age of the Earth, which is approximately 4.5×10^{10} years (Patterson, 1956). However, protein folding

generally occurs in a relatively short range from microseconds to hours (Guzman and Gruebele, 2014). To resolve this paradox, protein physicists and chemists proposed various models that assume the existence of folding pathways and intermediates (Dill and MacCallum, 2012).

For biologists, as another main line of studying protein folding, the heat response in *Drosophila* had already been investigated as early as the 1930s (Goldschmidt, 1935; Richter et al., 2010). In 1962, large chromosomal expansions (referred to as chromosomal puffs, an indication of localized transcriptional activation) were observed in *Drosophila* larvae upon heat shock at temperatures above 36°C and these puffs reversed when allowing the larvae to recover at 25°C (Ritossa, 1962). In 1974,it was founded that heat shock increased the expression of several proteins in various organelles and this upregulation correlated with the patterns of chromosomal puffs (Tissieres et al., 1974). By the late 1970s, similar heat shock-induced protein expression changes were reported in prokaryotes and other eukaryotes, indicating that the heat shock response is a ubiquitous pathway (Richter et al., 2010). Additionally, these upregulated proteins were identified as heat shock proteins (Hsp), although their precise biological functions remained unclear before the 1980s (Richter et al., 2010).

In the 1980s, the study on protein folding and heat shock proteins started to merge. In 1984, Hugh Pelham reported that the immunofluorescence staining pattern of Hsp70 in the cell nucleus shifted from being excluded from nucleoli to partial colocalization with nucleoli upon heat shock (Pelham, 1984). This transition reversed upon recovery at 37°C and the overexpression of Hsp70 accelerated this recovery (Pelham, 1984). A year later, William Welch and Joseph Suhan also observed that Hsp70 localizes to nucleoli in rat fibroblasts subjected to heat shock (Welch and Suhan, 1985). In the same year, Lewis and Pelham found that the release of client proteins from Hsp70 is ATP-dependent *in vitro* (Lewis and Pelham, 1985). Pelham then pioneeringly proposed a tentative model about how Hsp70 works: during heat shock, proteins expose hydrophobic regions, leading to aggregation. Hsp70 binds these exposed surfaces,

preventing aggregation, and then releases the proteins in an ATP-dependent manner, allowing them to refold (Pelham, 1986).

Functional studies on Hsp70 paved the path to several landmark works about how heat shock protein 60 (Hsp60) assists protein folding in mitochondria. In 1985 and 1986, work from the laboratories of Walter Neupert and Gottfried Schatz suggested that proteins must first unfold before being imported into mitochondria (Schleyer and Neupert, 1985) (Eilers and Schatz, 1986). In 1988, studies from the labs of Günter Blobel, Elizabeth Craig, and Randy Schekman demonstrated that Hsp70 functions as an "unfoldase" for unfolding client proteins before their translocation (Chirico et al., 1988; Deshaies et al., 1988). However, it was unknown how these unfolded proteins folded again inside mitochondria. By 1988, two homologs of Hsp60, GroEL from *E. coli* and the Rubisco subunit-binding protein from chloroplasts, were identified as mediators of protein assembly and termed "chaperonins" by John Ellis and colleagues (Hemmingsen et al., 1988). However, whether chaperonins assisted protein folding was unknown. Landmark evidence supporting the function of Hsp60 in protein folding emerged in 1989.

In 1989, Ulrich Hartl and Art Horwich identified a temperature-sensitive mutant yeast strain with normal mitochondrial import function. However, in this mutant, imported proteins in mitochondria failed to assemble into their native oligomeric state, which might originate from refolding failure (Cheng et al., 1989). Then they reported that this mutation occurred in the gene encoding Hsp60. This was the first evidence demonstrating that proteins in cells need molecular assistance to fold correctly and these folding helpers are now known as chaperones. In the same year, Hartl and Horwich also provided evidence showing that Hsp60 facilitated the folding of dihydrofolate reductase in isolated mitochondria, a process dependent on ATP binding and hydrolysis, further indicating protein folding in cells is actively regulated (Ostermann et al., 1989). Since the 1990s, research on chaperones has been largely focused on how they assist in protein folding and conformational maintenance.

1.1.3.2 Current insights into protein folding and conformational maintenance

The prevailing definition of the molecular chaperone is that the protein that interacts with, stabilizes or assists another protein in acquiring its functionally active conformation without becoming part of its final structure (Hartl, 1996). In eukaryotes, the first line of defense in protein folding begins at the ribosome, where certain chaperones operate near the polypeptide exit site. These chaperones, typically not stress-induced (Albanèse et al., 2006), include complexes such as the nascent chain-associated complex (Kirstein-Miles et al., 2013) and the ribosome-associated complex (Zhang et al., 2017). Their function is to bind newly synthesized polypeptides at hydrophobic regions, keeping them in an unfolded state to prevent aggregation or incorrect folding until enough structural elements are present to initiate proper folding. Although some small proteins are able to achieve their native structure when passing through the tunnel of ribosomes, proteins with more intricate or multidomain architectures often require further assistance from additional chaperone systems (Klaips et al., 2018).

The Hsp70 family engages partially folded or newly synthesized proteins during or after their production to address more complex folding requirements. The substrate-binding domain of Hsp70 recognizes short hydrophobic segments of client proteins, with its activity tightly regulated by ATP binding and hydrolysis in its nucleotide-binding domain (Clerico et al., 2015). The efficiency of this system is enhanced by heat shock protein 40 (Hsp40) co-chaperones, also known as J-proteins, which initially bind non-native proteins and direct them to Hsp70 (Mogk et al., 2018). These cofactors trigger ATP hydrolysis, allowing the substrate-binding domain of Hsp70 to clamp securely around the target protein. Human cells encode dozens of Hsp40 proteins, each with distinct subcellular localizations and structural features, broadening the functionality of the Hsp70 system (Kampinga and Craig, 2010). This versatility enables Hsp70 to facilitate initial folding, maintain proper protein conformation, disassemble aggregates, and mark misfolded proteins for degradation. Additionally, nucleotide exchange factors are essential for resetting Hsp70, allowing repeated cycles of binding

and release (Bracher and Verghese, 2015).

For proteins that fail to reach their correct conformation with the help of Hsp70, chaperonins provide the next level of assistance. These specialized complexes, including mitochondrial Hsp60 and TCP1 ring complex (TRiC) in the cytoplasm, encapsulate misfolded proteins inside a chamber-like structure, shielding them from aggregation and accelerating their folding (Horovitz et al., 2022). Although chaperonins assisted only about 10% of cellular proteins (Hartl et al., 2011), their substrates often include essential and abundant proteins such as tubulin and actin (Kelly et al., 2022). Loss of chaperonin function is linked to severe conditions, including neurodegenerative disorders associated with mitochondrial Hsp60 dysfunction and recently identified “TRiCopathies” caused by mutations in TRiC (Bross et al., 2012) (Kraft et al., 2024).

The heat shock protein 90 (Hsp90), another vital chaperone, takes over downstream of Hsp70 and ensures that key signaling proteins obtain and maintain their functional states. More than 400 client proteins are assisted by Hsp90 (Gu et al., 2025). Functioning as a homodimer, Hsp90 utilizes ATP-driven conformational shifts to stabilize near-native client proteins, including kinases and steroid hormone receptors, preparing them for activation (Schopf et al., 2017).

Even after achieving their initial folded state, many proteins rely on continuous monitoring by chaperones to maintain their functional structure. Proteins often operate near their stability threshold, making them vulnerable to disruptions under stress. In this scenario, the Hsp70 system and the small heat shock proteins (sHsps) are two key players in maintaining proteome integrity. sHsps function as oligomeric complexes with diverse structural forms (Reinle et al., 2022). During acute stress such as heat shock, up to 30% of cytosolic proteins are potential clients of sHsps, highlighting their crucial role in stabilizing the proteome (Mymrikov et al., 2017). However, when the chaperone network becomes overwhelmed, misfolded proteins accumulate and form

aggregates. In such cases, sHsps, acting as “holdases” (in contrast to the “foldase” role of ATP-dependent chaperones like Hsp70), directly associate with these aggregates, facilitating their resolution during the recovery phase (Carra et al., 2017). This interaction allows downstream processing, with chaperone cofactors and the combined action of Hsp70, Hsp40, and Hsp110 systems aiding in disaggregation and restoring proteostasis.

Moreover, under stress conditions, the transcription of molecular chaperones could be actively regulated by compartment-specific signaling pathways, such as the heat shock response in the cytosol (Pessa et al., 2024) and the unfolded protein response (UPR) in the endoplasmic reticulum (Hetz et al., 2020) or mitochondria (Torres et al., 2024). Once proteotoxic stress calms down and free chaperone capacity is restored, the stress response system re-equilibrates, returning to its balanced state of proteostasis.

Proteins that fail to achieve proper folding or refolding, even with chaperone assistance, are targeted for degradation to prevent potentially toxic aggregation. These terminally misfolded proteins are primarily degraded by the ubiquitin-proteasome system (UPS) or through the autophagosomal-lysosomal pathway.

1.1.4 Protein degradation

In the late 1930s to early 1940s, Rudolph Schönheimer proposed the earliest statement emphasizing that proteins are in a dynamic state of synthesis and degradation, based on the radioisotopic tracing experiments (Ratner et al., 1940). This concept was pioneering but not widely accepted until the discovery of lysosomes.

1.1.4.1 Early discoveries of lysosomes and autophagy

Between 1949 and 1955, Christian René de Duve investigated the activity and subcellular distribution of acid phosphatase, which is now known as a ubiquitously expressed lysosomal enzyme. To maintain the structural integrity of subcellular organelles during fractionation, de Duve adopted a mild homogenization protocol

originally developed by Albert Claude (Sabatini and Adesnik, 2013). Previous studies utilizing intense mechanical homogenization showed that acid phosphatase is a soluble enzyme localized to the cytoplasmic supernatant. However, de Duve's gentler homogenization approach revealed an unexpected sedimentation profile, with enzymatic activity distributed across multiple subcellular fractions rather than only in the supernatant (de Duve et al., 1951). After unintentionally freezing and thawing samples, surprisingly, the activity of acid phosphatase increased in all fractions, suggesting the enzyme exists in a latent state prior to membrane disruption (Berthet and Deduve, 1951).

These observations led de Duve to hypothesize the existence of membrane-bound organelles containing acid hydrolases inside. Thus, the vigorous mechanical homogenization or freezing-thawing cycle breaks the membrane and releases latent enzymes. The following findings that four other acid hydrolases demonstrated similar properties as acid phosphatase further expanded the potential of these special organelles (Duve et al., 1955). Based on these biochemical and subcellular fractionation studies, de Duve conceived the concept of the lysosome, a membrane-bound organelle containing acid hydrolases with various specificities and the major function of lysosome was to digest intracellular macromolecules. In 1956, his collaborative work with Alex Novikoff provided the first electron microscopic images of lysosomes (Novikoff et al., 1956). This discovery established a morphological entity regulating protein degradation in cells. Nevertheless, a question arose: How are substrates transported into lysosomes?

Advancements in electron microscopy (EM) sample preparation during the mid-1950s facilitated the observation of an intracellular digestive system composed of lysosomes as well as certain related vacuole structures lacking hydrolases. For instance, Werner Straus introduced the term "phagosomes" to describe endocytic vacuoles that lack enzymes and form during the uptake of foreign proteins (Straus, 1958) (Straus, 1964). In 1962, Thomas Ashford and Keith Porter observed that glucagon, now recognized as

an autophagy inducer, increased lysosomes in the liver of rats (Ashford and Porter, 1962). They also found mitochondria which were embedded inside lysosomes and they hypothesized that lysosomes served as temporary storage sites for mitochondria prior to degradation (Ashford and Porter, 1962). Although this interpretation of autophagy biogenesis was unprecise, their pioneering observations laid the groundwork for refining the autophagy model. In 1963, studies on focal cytoplasmic degradation using EM proposed a three-step process: sequestration, formation of complex dense bodies, and construction of lysosome-like bodies (Hruban et al., 1963).

In 1966, de Duve and Robert Wattiaux summarized numerous studies about lysosomes in the last decade and proposed the existence of the “autophagosome” in autophagy, distinguishing it from the “heterophagosome” in endocytosis (Deduve and Wattiaux, 1966). Two years later, Trump and Arstila provided direct evidence that autophagosomes, in their double-membrane phase, lacked hydrolase activity and likely originated from the smooth endoplasmic reticulum (Arstila and Trump, 1968). They hypothesized that hydrolytic enzymes were delivered into the intermembrane space of the autophagosome through the fusion of its outer membrane with vesicles carrying these enzymes, followed by the degradation of the inner membrane (Arstila and Trump, 1968). Seeing is believing. Their foundational yet preliminary model was progressively refined through a series of detailed studies beginning in the 1980s, facilitated by advanced microscopy techniques such as immunoelectron microscopy and correlative light and electron microscopy (Eskelinen et al., 2011).

Although morphological studies based on EM highlighted the importance of lysosomal systems in cellular protein degradation, accumulating biochemical evidence gradually indicated the existence of non-lysosomal degradation (Ciechanover, 2005b). For example, individual proteins possessed various half-life ranging from about 10 min to more than 10 hours and their half-life did not change uniformly upon the same treatments such as starvation (Ciechanover, 2005b). These were difficult to be understood by the model of autophagic-lysosomal system because autophagy degraded

a bulky cytoplasm content (Ciechanover, 2005b). In the early 1980s, this dilemma was solved by the discovery of delicate molecular control during autophagy such as chaperone-mediated autophagy (CMA) (Backer et al., 1983) and another protein degradation pathway that is distinct from autophagy: the ubiquitin-proteasome system (UPS).

1.1.4.2 Early discovery of the ubiquitin-proteasome system (UPS)

To investigate the existence of other potential proteolysis systems, Avram Hershko and his graduate student Aaron Ciechanover utilized a terminally differentiating red blood cell model because these cells were believed to expel their lysosomes during maturation while continuing to degrade proteins by an ATP-dependent and unidentified mechanism (Etlinger and Goldberg, 1977). In 1980, employing gel electrophoresis, Hershko, Ciechanover, and Irwin Rose found that a small polypeptide formed a covalent bond with protease substrate. They named this polypeptide ATP-dependent proteolysis factor 1, which was later identified as ubiquitin, a previously isolated protein (Hershko et al., 1980). How was ubiquitin conjugated to its substrates? Over the following three years, through chromatographic techniques, Hershko and colleagues identified the E1, E2, and E3 enzymes and proposed an elegant stepwise model for their function (Hershko et al., 1983).

The earliest discovery of the proteasome can be traced back to 1968 when electron microscopy revealed a protein complex with a cylindrical shape (Harris, 1968). This complex was repeatedly discovered over the following decade, however, its function remained unknown (Baumeister et al., 1997). In the 1980s, this 600 kDa complex was found to possess proteolytic activity and was named the proteasome in 1988 (Arrigo et al., 1988). Subsequent studies confirmed that this 600 kDa proteasome was part of a larger complex, now recognized as the 20S and 26S proteasomes, respectively (Baumeister et al., 1997).

1.1.4.3 Current understanding of UPS and autophagy within proteostasis

The ubiquitin-proteasome system (UPS) serves as the primary pathway for protein degradation, accounting for approximately 80% of total protein turnover (Collins and Goldberg, 2017). Central to this system is the 26S proteasome, a multi-subunit protease complex responsible for recognizing and degrading substrates marked with ubiquitin. Ubiquitylation, a highly regulated and ATP-dependent process, involves a sequential cascade mediated by ubiquitin-activating enzymes (E1), ubiquitin-conjugating enzymes (E2), and ubiquitin ligases (E3). Among the approximately 2,000 components of the proteostasis network (PN), the UPS represents the largest subgroup, encompassing around 850 proteins, including nearly 600 distinct E3 ligases (Jayaraj et al., 2020).

The proteasome consists of two major complexes: the 20S core particle, which contains the proteolytic sites, and the 19S regulatory particle, which facilitates substrate recognition and processing (Arkinson et al., 2025). Access to the 20S core particle is restricted by a narrow entry channel, only allowing unfolded proteins to pass through for degradation (Bhattacharyya et al., 2014). Unfolding is carried out by the 19S regulatory particle, which caps the 20S core and utilizes ATP-driven mechanisms to prepare substrates for proteolysis (Dong et al., 2019). Additionally, the degradation of protein aggregates requires the disassembly function of chaperone systems (Jayaraj et al., 2020). Chaperones play a dual role by stabilizing misfolded proteins in a state suitable for ubiquitin tagging while also directing terminally misfolded substrates to the proteasome when refolding is unsuccessful. For instance, the E3 ligase carboxy terminus of HSP70-interacting protein functions with Hsp70 to ubiquitylate chaperone-bound proteins that fail to reach proper folding (Meacham et al., 2001).

Despite the efficiency of the UPS, stress conditions and protein misfolding can still lead to the formation of insoluble aggregates and larger inclusions (Jayaraj et al., 2020). Unlike the UPS, autophagy, in conjunction with lysosomal degradation, is capable of handling these aggregates. In this process, protein aggregates are usually sequestered

into double-membrane vesicles known as autophagosomes, which later fuse with lysosomes for degradation (Fleming et al., 2022). These aggregates often form ubiquitin-rich inclusions, which recruit autophagic components through chaperones in a process termed chaperone-assisted selective autophagy. Chaperone-assisted selective autophagy primarily involves proteins such as Hsp70, heat shock protein family B member 8 (HSPB8) and BCL2-associated athanogene 3 (BAG3) (Tedesco et al., 2023). Furthermore, under normal conditions, soluble proteins are degraded via chaperone-mediated autophagy (CMA), the first system to demonstrate that lysosome-based degradation could be selective (Backer et al., 1983; Kaushik and Cuervo, 2018). CMA recognizes substrates by specific KFERQ motifs, utilizes Hsp70 to unfold them, and translocates them across the lysosomal membrane via lysosome-associated membrane protein 2A, thus bypassing the formation of autophagosomes (Kaushik and Cuervo, 2018).

Although the UPS and Autophagy lysosomal pathway differed in their substrate specificity and mechanisms, they are functionally interconnected. These systems often compensate for each other when one pathway becomes overwhelmed or dysfunctional, reflecting the dynamic and cooperative nature of the proteostasis network (Li et al., 2022).

1.1.5 Compartmentalization of misfolded proteins

When efforts to refold, degrade, or prevent the accumulation of misfolded proteins fail, cells sequester these aberrant proteins into less harmful aggregate structures **(Figure 1.3)**.

In 1912, Frederick Lewy observed the existence of cellular inclusions as a characteristic feature of Parkinson's disease (Goedert et al., 2013; Lewy and Lewandowsky, 1912).

Around 1970, intracellular inclusions were widely reported, however, most of them were not mainly composed of proteins (Shively, 1974). One type of proteinaceous

inclusion is induced by canavanine, a structural analog of arginine (Schachtele et al., 1968). Later, research from Alfred Goldberg's laboratory demonstrated that these inclusions are less soluble (Prouty et al., 1975). Then they speculated such inclusions assemble from the spontaneous aggregation of aberrant proteins, particularly when the cellular degradation machinery is overwhelmed (Prouty et al., 1975). Under these conditions, misfolded proteins may accumulate, form inclusions and these inclusions may serve to promote their recognition by the degradative system (Prouty et al., 1975).

After the advent of recombinant DNA technology in the early 1970s, the expression of recombinant proteins was subsequently explored (Berg and Mertz, 2010). In 1982, recombinant human insulin was found to form dense, insoluble aggregates with reduced functionality in cells (Williams et al., 1982). The formation of inclusion bodies hindered recombinant protein production, urging biochemists to investigate methods for rescuing proteins from these aggregates. Around the mid-1990s, neuropathologists also identified the presence of protein aggregates in various neurodegenerative diseases (DiFiglia et al., 1997; Shibata et al., 1996).

In 1998, Ron Kopito and colleagues observed several types of inclusion bodies and misfolded proteins could be transported to these inclusion bodies in a microtubule-dependent manner. They used "aggresome" to term these microtubule-organizing center (MTOC)-localized inclusion bodies (Johnston et al., 1998). Kopito further proposed that these misfolded protein-enriched compartments might facilitate the degradation of toxic proteins via autophagy, a hypothesis confirmed in the 21st century (Fortun et al., 2003; Kopito, 2000). In addition to promoting degradation, these aggregates served to isolate misfolded proteins, protecting the cell from their toxic effects and creating an environment that minimized their interaction with functional cellular components (Kopito, 2000).

These compartments exhibited variation in localization and characteristics. In yeast, such compartments include the insoluble protein deposit (IPOD), intranuclear quality-

control compartment (INQ), juxtanuclear quality-control compartment (JUNQ), and CytoQ (formerly known as Q-bodies or quality control bodies) **(Figure 1.3A)** (Miller et al., 2015) (Sontag et al., 2023). In mammalian cells, similar structures are typically referred to as the aggresome, particularly for the juxtanuclear aggregates in the cytosol **(Figure 1.3B)** (Kopito, 2000) , although other less widely observed aggregates can be found in various subcellular locations such as the endoplasmic reticulum (Chambers et al., 2022). Notably, in dividing cells, such as the budding yeast and stem cells, inclusion bodies can be eliminated by being sequestered into the mother cell. This process helps to preserve the proteome quality in the daughter cell, suggesting a strong relationship between cell division and proteostasis maintenance (Miller et al., 2015) (Morrow et al., 2020).

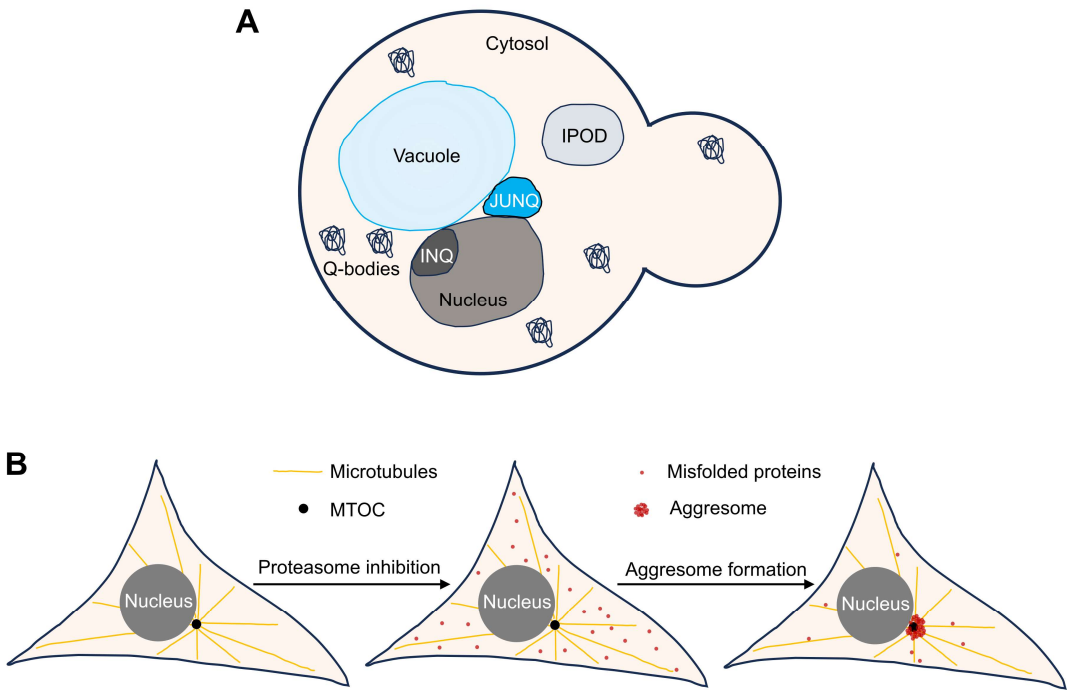


Figure 1.3: Compartmentalization of misfolded proteins. (A) Damaged protein compartmentalization in budding yeast. Misfolded proteins are systematically localized to specific deposition sites: cytoplasmic IPO, Q-bodies, JUNQ, and nuclear INQ. **(B)** The formation of an aggresome in mammalian cells. Proteostasis stress such as proteasome inhibition induces the accumulation of ubiquitinated and misfolded proteins, which are transported along with microtubules and deposited at the microtubule-organizing center (MTOC).

1.2 Proteostasis maintenance during cell division

1.2.1 General introduction of cell division

The early discoveries of cell division were primarily based on the observation of morphological changes in cells (McIntosh and Hays, 2016). Before the 1870s, chromosomes were observed incidentally, with limited focus on their significance (Baker, 1955). In the 1870s, cells exhibiting shapes characteristic of metaphase and anaphase were reported, however, the complete process of cell division remained unclear (Baker, 1955). It was around 1880 that Walther Flemming introduced an reliable cell fixation solution and other sample preparation methods (Paweletz, 2001). Flemming first described chromosome behaviour in a chronological order, distinguishing the various stages of the cell cycle, particularly during cell division (Flemming, 1879). However, molecular understanding of cell division only started from the 1970s.

In the 1970s, by direct injection or cell fusion, the cytoplasmic fraction in dividing cells was shown to trigger mitotic entry of interphase cells (Masui and Markert, 1971). To explain this, maturation promoting factor was hypothesized and started to be identified (Masui and Markert, 1971). During the 1970s and 1980s, by mutagenesis in yeast, geneticists including Lee Hartwell and Paul Nurse revealed several cell-cycle-progressing genes such as cell division cycle 28 (Cdc28) and cell division cycle 2 (Cdc2) (Hartwell, 1973; Nurse et al., 1976). Cdc2 in human cells was later discovered and named as cyclin-dependent kinase 1 (Cdk1), the main switch of mitosis (Lee and Nurse, 1987). Furthermore, Tim Hunt and colleagues discovered cyclins (Evans et al., 1983).

Cell cycle progression is regulated by the formation of complexes between cyclin-dependent kinases (Cdks) and their corresponding cyclin partners (Gavet and Pines, 2010b). In animal cells, Cdk1-cyclin B plays a central role in driving cell division (Gavet and Pines, 2010a). This complex is inhibited by the Wee family kinases and activated by the Cdc25 family phosphatases (Schmidt et al., 2017). Once activated, Cdk1-cyclin B can further enhance Cdc25 activity and suppress Wee kinase function,

creating a positive feedback loop (Schmidt et al., 2017). The activation of Cdk1 also depends on its association with cyclin B (Massacci et al., 2023). During the late G2 phase, the accumulation of cyclin B facilitates the assembly of active Cdk1-cyclin B complexes. The resulting high activity of the complex promotes further activation of Cdc25 and inhibition of Wee, reinforcing the shift toward full activation (Schmidt et al., 2017). Upon reaching a critical activation threshold, Cdk1-cyclin B initiates key mitotic processes such as nuclear envelope breakdown and chromatin condensation, thereby driving the cell into mitosis.

Cell division composes of mitosis and cytokinesis. Mitosis is the phase during which the replicated genetic material in a cell is divided into two genetically identical sets. Cytokinesis is the stage when the cytoplasm partitions to produce two daughter cells. In mammalian cells, the process of division can be divided into five major stages: prophase, prometaphase, metaphase, anaphase, and telophase.

Upon entry into mitosis, a series of morphologically distinct events occur, transitioning from prophase to metaphase **(Figure 1.4)**. These events include the disassembly of focal adhesions, leading to detachment from the adherent surface; the formation of a force-generating cortex primarily composed of actin and myosin beneath the plasma membrane to maintain high surface tension, allowing the cell to round up; chromatin condensation; breakdown of the nuclear envelope; remodeling of the endoplasmic reticulum (ER); disassembly of the Golgi into individual stacks; mitochondrial fission; and spindle assembly **(Figure 1.4)** (Carlton et al., 2020).

Once all chromosomes are bi-oriented in a metaphase cell, the spindle assembly checkpoint is silenced (McAinsh and Kops, 2023). Subsequently, the anaphase-promoting complex/cyclosome (APC/C), an E3 ubiquitin ligase, is activated, leading to the degradation of cyclin B, thus deactivating Cdk1-cyclin B and subsequently enabling mitotic exit (Nigg, 2001; Thornton and Toczyski, 2003). At this point, the cell enters anaphase and telophase when the following events occur: chromosome

segregation, cleavage furrow formation and ingression, ER remodeling, Golgi regeneration, mitochondrial fusion, chromosome recondensation, and nuclear envelope reassembly from the ER **(Figure 1.4)** (Carlton et al., 2020).

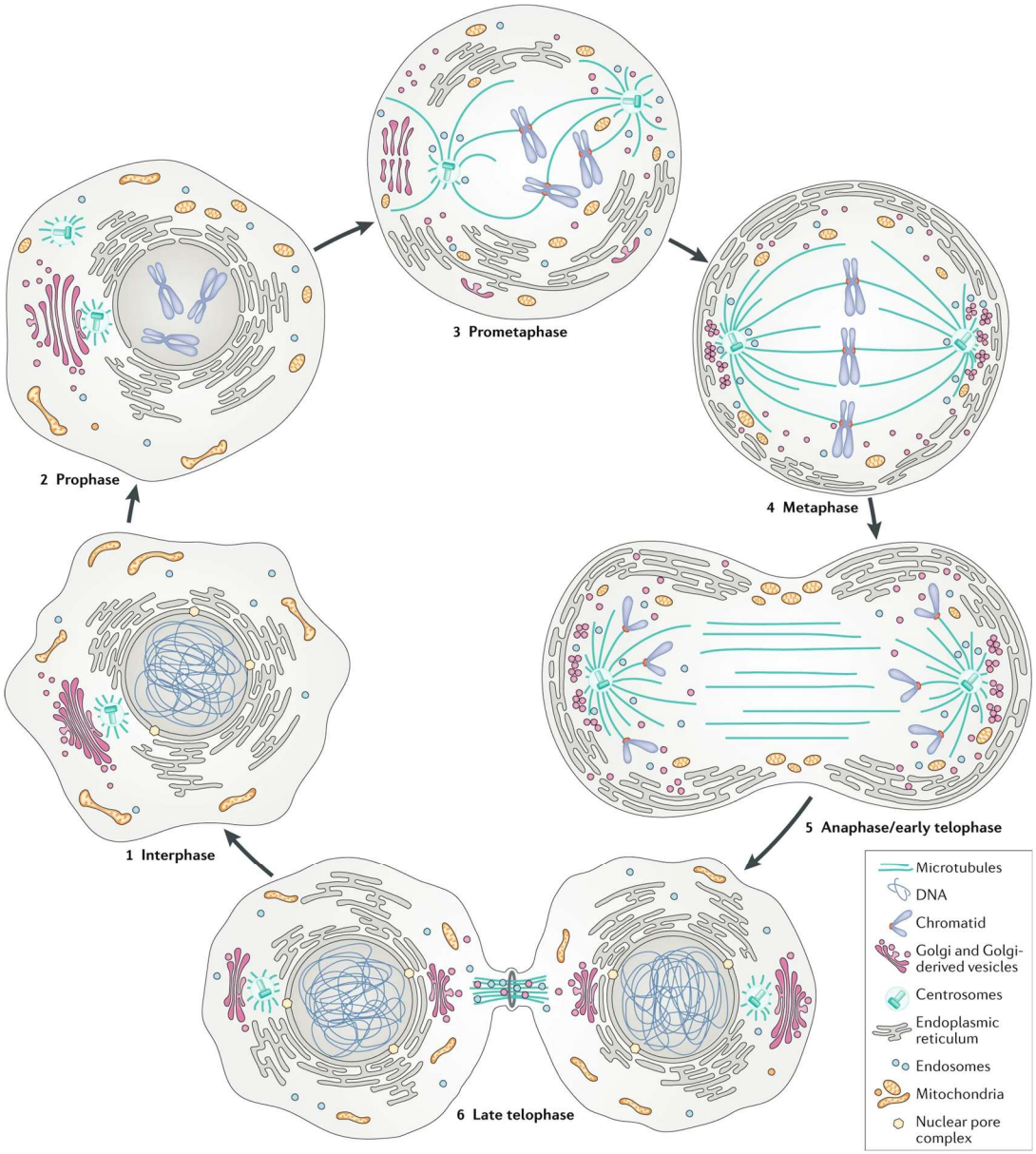


Figure 1.4: Reorganization of organelles during cell division. As cells transition from interphase to various cell division stages, significant rearrangements occur in membrane-associated structures. The plasma membrane undergoes dynamic shape changes, while the nuclear pore complex disassembles in prophase, allowing the nuclear envelope to detach and merge with the endoplasmic reticulum, which is then partitioned into daughter cells. During prometaphase, the Golgi disassembles into vesicles, which segregate in metaphase and reassemble in telophase, while mitochondria shift from a fused state in interphase to fragmentation in prophase and re-fusion in anaphase. The structure of ER goes through a transition from sheets to tubules during mitosis. This image was adapted (Carlton et al., 2020). The permission was acquired from Nature publishing group via CCC RightsLink for this thesis.

1.2.2 Proteostasis during cell division

1.2.2.1 Protein synthesis in dividing cells

Protein synthesis during various stages of cell division is finely regulated. Specifically, upon entry into mitosis, the rate of protein translation slightly increases during prophase, while it decreases around the metaphase-anaphase transition. This repression of synthesis is subsequently resumed during late cytokinesis. These regulatory processes were first demonstrated by autoradiography in the early 1960s and reconfirmed in recent years by more advanced techniques such as single-cell mass measurements (Konrad, 1963) (Miettinen et al., 2019). Previously, protein synthesis during cell division in human somatic cells occur at only ~ 30% of the rate in interphase (Fan and Penman, 1970; Sivan and Stein, 2008), but more recent studies suggest it reaches ~ 90% of the interphase rate (Miettinen et al., 2019; Stonyte et al., 2018). Next, protein synthesis during cell division is discussed separately by transcription and translation.

In classical models, mRNA transcription was considered inhibited during cell division due to chromatin condensation and the dissociation of transcription factors (Gottesfeld and Forbes, 1997). However, in the past decade, accumulating evidence has suggested that the genome is not entirely transcriptionally inactive during cell division. For instance, dozens of genes associated with extracellular regions are upregulated in synchronized dividing cells compared to unsynchronized populations (Palozola et al., 2017). Additionally, certain transcription factors remain bound to chromosomes in dividing cells (Ginno et al., 2018) (Kadauke et al., 2012). Moreover, chromatin accessibility increases at the metaphase-anaphase transition (Yu et al., 2023). Furthermore, inhibition of RNA polymerase II reduces centromeric satellite transcripts, leading to an increase in lagging chromosomes, which is a mitotic defect, suggesting the importance of mRNA transcription for cell division (Chan et al., 2012). Strikingly, genome-wide mRNA sequencing of mitotic cells reveals that overall mRNA abundance remains largely unchanged compared to G2-phase cells (Tanenbaum et al., 2015). These findings challenge the traditional view of transcriptional repression during cell division. Notably, similar debates extend beyond mRNA transcription to other aspects

of gene regulation, namely translation.

It is common sense that mRNA translation efficiency is largely repressed during cell division. The inhibition of translation elongation is mediated by Cdk1 (Sivan et al., 2011; Smith and Proud, 2008), however, the underlying mechanisms of translation initiation repression are still in a state of debate. The classical perspective is that 5′ cap-dependent translation initiation is inhibited in dividing cells, leading to a shift toward cap-independent initiation mediated by internal ribosome entry sites (IRES) (Pyronnet et al., 2001; Sivan and Stein, 2008; Wilker et al., 2007). However, recent studies challenged this view, arguing that mitotic translation repression observed in earlier studies may have been influenced by artifacts introduced by mitotic-arresting drugs such as nocodazole, which inhibits protein synthesis (Shuda et al., 2015). Instead, these studies reported that Cdk1, the master regulator of cell division, mediated phosphorylation of eIF4E-binding protein 1, highlighting the importance of 5′ cap-dependent translational initiation in dividing cells (Miettinen et al., 2019; Shuda et al., 2015).

Interestingly, a recent study identified a novel regulatory mechanism involving eukaryotic initiation factor 1, a translation initiation factor that is released from the nucleus upon mitotic entry. This release restricts start-codon selection during cell division, thereby modulating the translation of thousands of protein isoforms (Ly et al., 2024). This study provides additional perspective about how nuclear envelope disassembly, an organelle reorganization event during mitosis, unexpectedly orchestrates with proteostasis maintenance.

1.2.2.2 Protein folding and conformational maintenance in dividing cells

Protein folding highly depends on specific environmental factors, including salt concentration, molecular crowding and pH (Das et al., 2024; de Oliveira et al., 2018; Maity et al., 2018). Given the extensive reorganization of organelles and the changes in intracellular environments (such as the alterations of viscosity and pH) during cell

division (Hurst et al., 2021; Spear and White, 2023), it is reasonable to speculate that protein folding in dividing cells differs from that in interphase cells. However, studies closely concerning protein folding and conformation maintenance in dividing cells only started to emerge in the past two decades. This delay is likely due to the need for advanced microscopy and proteomics techniques capable of capturing these transient events with convincing resolution. Recent studies have primarily explored protein folding in dividing cells by analyzing solubility, thermal stability and the specialized functions of specific proteins, providing an emerging framework for understanding proteostasis during cell division.

For instance, a model protein transduced into U2OS cells exhibited higher thermal stability and faster folding kinetics in mitotic cells compared to interphase cells, a phenomenon originating from reduced molecular crowding in dividing cells (Wirth et al., 2013). This study also highlighted that such thermodynamic stabilization could be particularly relevant for proteins with intrinsically disordered regions. Indeed, several types of membraneless organelles, assembled via the phase separation of intrinsically disordered proteins, disassemble during mitosis and reassemble upon mitotic exit (Rai et al., 2018).

A proteomics-based study profiles the thermal stability and solubility of individual proteins in whole cells and reveals that a significant proportion of intrinsically disordered and mitotically phosphorylated proteins, including several mitotic spindle-associated and cytoskeleton-related proteins, exhibit increased stability and solubility during mitosis compared to the G1/S phase (Becher et al., 2018).

These global observations were further supported by functional studies investigating the roles of specific chaperones and co-chaperones during cell division. The activities of these molecular folding assistants were primarily associated with cytoskeletal components and other mitotic regulators. For instance, Hsp70 assists in microtubule nucleation and the maturation of functional mitotic centrosomes, facilitates centrosome

clustering in cancer cells, protects centrosomes from heat shock, and ensures kinetochore-microtubule stability and spindle integrity (Fang et al., 2019). Additionally, several subunits of chaperonin containing TCP1 (CCT) regulated mitotic checkpoint inactivation by disassembling mitotic checkpoint complex, ensured the correct localization of a dynactin subunit $p150^{Glued}$ thereafter avoiding mitotic defects, and potentially assisted in the folding of Polo-like kinase 1 (Plk1) (Córdoba-Beldad and Grantham, 2024; Kaisari et al., 2017; Vallin and Grantham, 2019). Moreover, the co-chaperone BAG3 undergoes hyperphosphorylation at mitotic entry and cooperates with a small heat shock protein HSPB8 in spindle positioning (Fuchs et al., 2015).

Critically summarizing current understandings of how chaperones and co-chaperones regulate cell division, most studies provide evidence supporting unconventional and previously unanticipated chaperone functions rather than classical protein folding. However, direct evidence demonstrating whether and how chaperones eliminate misfolded protein aggregates in mammalian dividing cells remains largely unexplored.

1.2.2.3 The ubiquitin-proteasome system (UPS) in dividing cells

In 1983, Tim Hunt and colleagues identified a set of proteins that were degraded each time cells divided, and they named them cyclins (Evans et al., 1983). The following year, two back-to-back papers from Alexander Varshavsky's laboratory described a mouse cell line that exhibited G2 arrest when cultured at a non-permissive temperature, and they also found that ubiquitin-protein conjugates in these cells decreased (Ciechanover et al., 1984; Finley et al., 1984). To explain this phenotype, they proposed that the impaired heat stability of the ubiquitin-activating enzyme led to defective cyclin degradation, ultimately causing G2 arrest (Ciechanover et al., 1984). This hypothesis was validated in 1991 by two independent studies demonstrating the essential role of ubiquitination in mitotic cyclin degradation, marking the beginning of research into how the ubiquitin-proteasome system (UPS) regulates mitosis (Glotzer et al., 1991; Hershko et al., 1991). It is now well established that the UPS plays a central role in mediating mitotic events. Specifically, Cdk1, Aurora kinases, and Plk1, three major

classes of mitotic kinases in eukaryotes, are regulated by the UPS, ensuring the stepwise progression of cell division and extensive organelle reorganization (Carlton et al., 2020; Nigg, 2001). Given the substantial demand placed on the UPS in dividing cells, it remains largely unknown whether misfolded proteins accumulate because the UPS becomes exhausted or the UPS remains powerful enough to clear them.

1.2.2.4 Autophagy and lysosomes in dividing cells

For a long time, the UPS was considered the primary pathway for protein degradation in dividing cells. In contrast, autophagic activity is largely suppressed from prometaphase to the onset of telophase (Eskelinen et al., 2002). This regulation was attributed to Cdk1-mediated phosphorylation of key autophagy machinery components (Furuya et al., 2010; Li et al., 2020; Lu et al., 2019; Odle et al., 2020). However, emerging evidence suggests that the functions of lysosomes, no matter autophagy-dependent or autophagy-independent, play a role in dividing cells, challenging the traditional view of autophagy suppression during division.

Among the three autophagy pathways (macroautophagy, microautophagy and chaperone-mediated autophagy), only macroautophagy is directly associated with mitotic regulation (Almacellas and Mauvezin, 2022). Specifically, macroautophagy maintains centrosome organization and stability by mediating the turnover of centriolar satellite components through pericentriolar material 1 (Holdgaard et al., 2019). It also ensures proper chromosome segregation by selectively degrading cohesion complexes and facilitates midbody ring remnant clearance after abscission (Almacellas et al., 2021; Pohl and Jentsch, 2009).

For the autophagy-independent function of lysosomes, chromatin-proximal lysosomes leak the protease cathepsin B during mitosis and thereafter facilitate chromosome segregation by the cleavage of histone H3 (Hämälistö et al., 2020). Furthermore, the knockdown of various autophagy-related genes leads to cell division defects although it remains unknown how they regulate cell division through protein degradation

(Almacellas and Mauvezin, 2022).

1.2.2.5 Protein aggregates in dividing cells

In 2003, it was observed that damaged proteins preferentially remained in the mother cell during asymmetric cell division in the budding yeast (Aguilaniu et al., 2003). Over the next several years, similar biased sequestration of protein aggregates was observed in various organisms ranging from *E. coli* to yeast and to, more importantly, metazoans such as stem cells (Erjavec et al., 2007; Lindner et al., 2008; Rujano et al., 2006). Currently, the most widely recognized fate of protein aggregates in dividing cells is their preferential sequestration into the short-lived mother cell, ensuring the rejuvenation of the long-lived daughter cell during asymmetric division (Miller et al., 2015). However, molecular-level insights into this asymmetric inheritance remain controversial in yeast. In the cytosol of the budding yeast, models explaining aggregate asymmetric inheritance are classified into two categories **(Figure 1.5A, 1.5B and 1.5C)**.

In the first theory, aggregate sequestration in the mother cell is an active transport process and majorly regulated by actin-related machinery **(Figure 1.5A)** (Liu et al., 2010; Liu et al., 2011; Tessarz et al., 2009). In this theory, misfolded proteins are attached to the actin cables and are transported from the daughter cell to the mother cell (Liu et al., 2010; Liu et al., 2011; Tessarz et al., 2009). However, the second model proposes that protein aggregates undergo random diffusion and the asymmetric inheritance originates from the unique geometry of the budding yeast, rather than being actively transported (Zhou et al., 2011). Interestingly, a following study shows that subcellular organelles, such as mitochondria and the ER, provide spatial constraints that limit the movement of aggregates from the mother cell to the daughter cell **(Figure 1.5C)** (Zhou et al., 2014). Moreover, small misfolded protein foci were observed to aggregate into large inclusion bodies, such as the intranuclear quality-control compartment (INQ) and the insoluble protein deposit (IPOD) in the mother cell. This spatial confinement of the narrow bud neck prevents the transmission of misfolded proteins to the daughter cell **(Figure 1.5B)** (Spokoini et al., 2012).

In addition to cytosolic protein aggregates, protein aggregates in the ER were also asymmetrically partitioned during cell division, which is regulated by the ER diffusion barrier and the ER stress surveillance (ERSU) pathway in the budding yeast **(Figure 1.5D and 1.5E)** (Clay et al., 2014) (Piña and Niwa, 2015). The ER diffusion barrier refers to a bud neck-localized and three-layer lateral diffusion barrier, primarily composed of septin proteins, Bud1 and sphingolipid **(Figure 1.5E)** (Clay et al., 2014). This structure restricts the movement of ER components between the mother and the daughter cell. The ER stress surveillance (ERSU) pathway, on the other hand, describes how ER stress induces the mislocalization of the septin ring at the bud neck, subsequently impeding the inheritance of stressed ER **(Figure 1.5D)** (Piña et al., 2018; Pina et al., 2023; Piña and Niwa, 2015).

In mammalian cells, inclusion bodies are also asymmetrically segregated during cell division. For instance, in various cell types, vimentin-enclosed JUNQ inclusion bodies are asymmetrically partitioned when vimentin is segregated during cell division, while IPOD, another type of inclusion body, is less tightly regulated (Morrow et al., 2020; Ogrodnik et al., 2014).

While asymmetric sequestration of protein aggregates in the mother cell during cell division is a widely observed phenomenon, several studies have reported equal partitioning of protein aggregates in cells undergoing symmetric division, such as in fission yeast. In fission yeast, protein aggregates are randomly distributed between the two daughter cells, which results in a combination of asymmetric and equal sequestration events **(Figure 1.5F)** (Coelho et al., 2013; Coelho et al., 2014). This suggests that the mechanism of aggregate partitioning during cell division may vary depending on the specific cellular context.

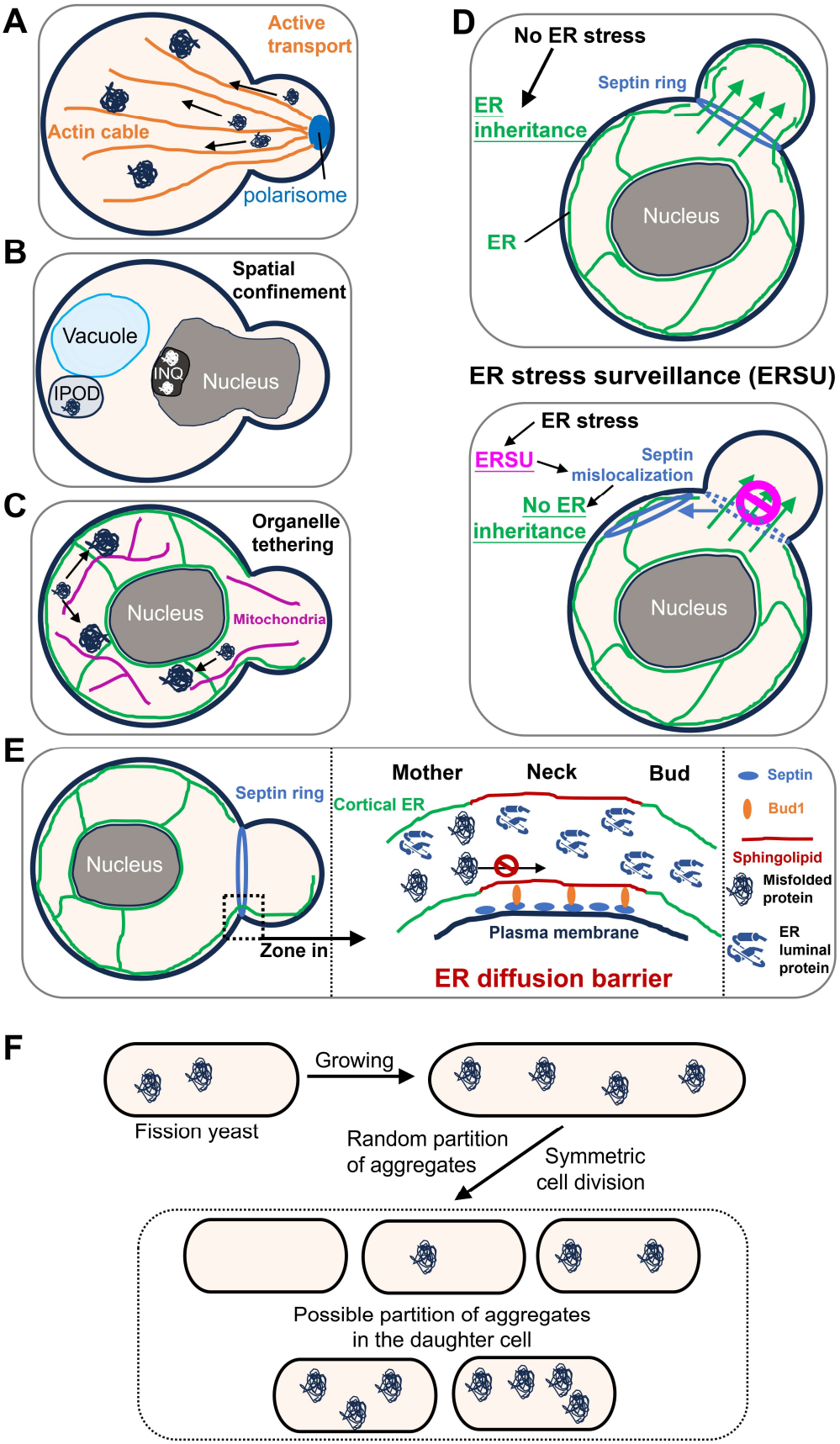


Figure 1.5: Protein aggregate inheritance during cell division. (A) to (C) Strategies of asymmetrically dividing cells coping with protein aggregates in the cytosol. **(D)** The

diagram of ER stress surveillance (ERSU) pathway. **(E)** The diagram of ER diffusion barrier. **(F)** The diagram of protein aggregates partition in fission yeast.

Are there alternative fates for protein aggregates during cell division? Ulrich Hartl, a molecular chaperone pioneer, proposes a model in which nuclear-localized protein aggregates are released into the cytosol upon nuclear envelope breakdown and subsequently degraded during mitosis (Hipp et al., 2014). However, the existence of this mechanism remains unknown. Assuming that protein aggregates are cleared during cell division, are they actually degraded, or are they simply disassembled due to extensive organelle reorganization?

1.3 The endoplasmic reticulum (ER)

1.3.1 The early discovery of the ER

Among all cellular organelles, the ER stands out for its extensive size, nevertheless, it is one of the latest large organelles described in the history of cell biology (Schuldiner and Schwappach, 2013). The early observations of the ER can be traced back to the era around 1900. From 1890 to 1894, both Romeo Fusari (a protégé of Golgi) and Santiago Ramón y Cajal used Golgi's silver chromate staining technique to examine muscle cells from a range of animals including insects and mammals (Mazzarello, 2002; Mazzarello et al., 2003). They identified reticular structures located either in intermediate regions of the sarcomere or aligned with the Z line. Although we know the reticulum described by Cajal and Fusari is exactly the ER of muscle cells, the sarcoplasmic reticulum, their works were widely questioned. For example, Pio Mingazzini, a histologist who pioneered the study of *Ciona* regeneration (Jeffery, 2015), argued that the silver staining method developed by Golgi was for central nervous system at first but not for muscle cells, thus "the alleged reticule" observed by Fusari was only the artifact originated from metallic precipitation in the sarcoplasm (Mazzarello et al., 2003).

The initial work of Cajal and Fusari was significantly advanced in the early 1900s by Emilio Veratti, who completed his doctoral thesis under the supervision of Fusari and later became an assistant of Golgi (Mazzarello, 2002). In 1902, employing Golgi's

staining method, Veratti carefully examined the reticulum in muscle cells by a light microscope and described it as “a true reticular apparatus made up of true filaments” (Veratti, 1961). Additionally, he observed “a very elegant reticulum with rounded meshes that winds around the nucleus and is continuous with the filaments in the trabeculae”, which firstly describing the continuity of the nuclear envelope and the ER (Veratti, 1961). In summary, Veratti’s fifty-nine-page study provided landmark evidence for the presence of a previously less recognized reticular organelle, the ER (Mazzarello et al., 2003). However, Veratti and other researchers of the same era did not notice the complicated structures of the ER: the lumen and the membrane. Additionally, the existence of the ER was met with considerable doubts. Many researchers regarded the muscle reticulum as merely the Golgi apparatus of muscle cells and some of them even went so far as to doubt the existence of the Golgi apparatus itself till the mid-1900s (Beams, 1929; Bentivoglio and Mazzarello, 1998). Thus, at the early 1900s, the reticulum was “a virtually forgotten component of muscle, or rather a component which was generally considered to be spurious” and the study of the ER was stuck at its existence (Mazzarello et al., 2003).

Facilitated by the invention of transmission electron microscope (Knoll and Ruska, 1932), Keith Porter, Albert Claude and Ernest Fullam reported the first electron micrograph of a cell and noticed a cytoplasmic "lace-like reticulum” extending throughout the cytoplasm (Porter et al., 1945). Then Porter further confirmed this reticular structure with a satisfactory resolution and named it “endoplasmic reticulum” (Porter, 1953). One year later, George Palade and Porter decently identified the tubule-like and fenestrated-cisternae structures of the ER (Palade and Porter, 1954), which remain valid from a modern perspective (Lu et al., 2023). Since the discovery of the ER, its properties were widely studied.

1.3.2 Protein folding in the ER

The ER is the largest membrane-bound organelle in eukaryotic cells and it processes one-third of the proteome, indicating its importance in the regulation of cellular

proteostasis (Baumann and Walz, 2001; Wright and Plate, 2021). Protein folding is regulated by local environment such as pH value, molecular crowding and salt concentration. The pH value in the ER is around 7.2, which is similar to the cytosol (Casey et al., 2010). Protein concentration in the ER is believed to reach 100 mg/mL (Gardner et al., 2013; Schröder and Kaufman, 2005; Stevens and Argon, 1999), which is a high concentration promoting protein aggregation and similar to the corresponding value in the cytoplasm of mammalian cells (Liu et al., 2022; Oh et al., 2022; Stevens and Argon, 1999).

Although the pH and protein concentration in the ER are similar to those in the cytosol, the viscosity of the ER lumen is higher than that of the cytosol (Chambers et al., 2018). Indeed, the diffusion coefficient of proteins in the ER is several-fold lower than that in the cytosol, indicating that proteins move more slowly in the ER than their cytosolic forms (Dayel et al., 1999). This can be interpreted as proteins in the ER having a higher risk of misfolding and aggregation, since the diffusion coefficient of aggregation-prone proteins is smaller than its wild-type (Guo et al., 2014). Additionally, because the diffusion coefficient of chaperones is lower than that of fluorescent proteins with the same molecular weight (Sadovsky et al., 2017), more chaperones required to refold misfolding-prone proteins in the ER will further make the ER lumen more “sticky” and subsequently slow down the diffusion (Guo et al., 2014). These arguments suggest the aggregation-prone nature of proteins in the ER lumen, however, the aggregation-prone protein expressed in the ER interestingly did not assemble into protein aggregates but they aggregated in the cytosol (Rousseau et al., 2004). Another study found that supersaturated amyloidogenic proteins formed protein aggregates in the cytosol but not in the ER (Vincenz-Donnelly et al., 2018). Strikingly, these soluble β-sheet proteins in the ER possessed a ~1,000-fold higher concentration contrasted to the corresponding concentration required for aggregation in vitro (Vincenz-Donnelly et al., 2018). This suggests that the ER has a very strong ability to maintain proteins in their soluble state. How does the ER achieve this?

An outstanding feature of the ER is its redox state. The ER maintains an inherently oxidizing environment, which is crucial for disulfide bond formation, a key step in stabilizing the tertiary and quaternary structures of many secreted and membrane-bound proteins (Cao and Kaufman, 2014). The initial evidence for oxidative protein folding in the ER was reported in 1963 when Christian Anfinsen reported a significant acceleration of the reoxidation of reduced RNase in a fractionated system containing microsomes (Goldberger et al., 1963). It is now known that oxidative folding in the ER is mediated by both enzymatic and nonenzymatic pathways **(Figure 1.6)**. Among these enzymatic pathways, protein disulfide isomerase (PDI) transfers disulfide bonds to substrate proteins by forming transient mixed disulfide intermediates with them (Wang et al., 2015). PDI then becomes reduced and must be reoxidized to continue catalysis. This reoxidation is primarily carried out by ER sulfhydryl oxidase 1 (Ero1), which restores oxidized PDI by transferring electrons to molecular oxygen, producing hydrogen peroxide (H_2O_2) as a byproduct (Wang and Wang, 2023). ER-localized peroxiredoxin (PRDX) and glutathione peroxidases (GPX) can subsequently consume H_2O_2 as an oxidizing equivalent to generate disulfide bonds in PDI or substrate proteins (Tavender et al., 2010; Wang et al., 2014). Nonenzymatic pathways of oxidative folding in the ER are mediated by small molecules such as glutathione, H_2O_2 and oxygen (Ruddock, 2012).

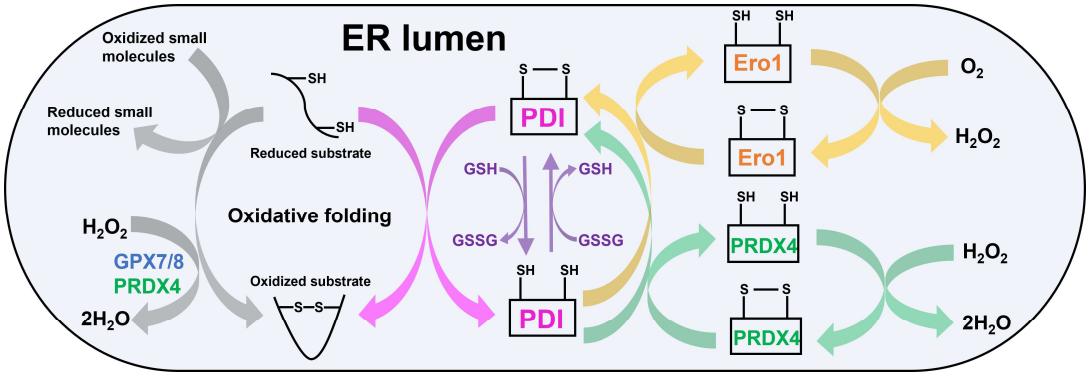


Figure 1.6: Diagram of oxidative protein folding in the ER. Oxidative folding of substrate proteins can be achieved by PDI, GPX (e.g. GPX7 and GPX8), PRDX (e.g. PRDX4), and some small molecules in their oxidized form. The reoxidation of PDI is primarily driven by Ero1 and PRDX. The oxidized form of glutathione (GSSG) and reduced form of glutathione (GSH) participate in these processes as the redox buffer.

It should be mentioned that the redox state of the ER is highly dependent on Ca^{2+} concentration (Avezov et al., 2013). Additionally, molecules responsible for oxidative folding in the ER are highly regulated by luminal Ca^{2+}. For example, one of the PDIs, PDIA6, can assemble into biomolecular condensates in a Ca^{2+}-dependent manner (Leder et al., 2025). These condensates recruit other chaperones, such as BiP, and act as protein-folding factories (Leder et al., 2025). Ca^{2+}-dependent pathways are supported by another outstanding feature of the ER: its Ca^{2+} concentration, which is about 1,000-fold higher than that in the cytosol (Bygrave and Benedetti, 1996; Rossi and Taylor, 2020).

It has long been speculated that the enrichment of Ca^{2+} in the ER lumen provides an environment comparable to extracellular Ca^{2+}, enabling client proteins to acquire conformational stability required for secretion (Araki and Nagata, 2011), however, direct and comprehensive evidence supporting this argument is largely missing. Instead, numerous studies have demonstrated that ER Ca^{2+} indirectly facilitates protein folding by ensuring the function of chaperones. Ca^{2+} binds to several abundant ER-resident chaperones, such as calreticulin, glucose-regulated protein 94 (GRP94), and binding immunoglobulin protein (BiP) (Araki and Nagata, 2011). Among these Ca^{2+}-binding chaperones, BiP is the most extensively studied. A high Ca^{2+} concentration keeps BiP in its monomeric rather than oligomeric state, thereby facilitating its substrate-binding function (Preissler et al., 2015). Additionally, high Ca^{2+} stabilizes the interaction between BiP and substrate proteins, ensuring sufficient time for unfolded substrates to fold before dissociating from BiP (Preissler et al., 2020). Upon ER stress induction by tunicamycin or overexpression of prion protein mutants, the Ca^{2+} concentration in the ER decreases (Torres et al., 2010; Zhang et al., 2020). Reduced Ca^{2+} concentration facilitates the deAMPylation of BiP, thus stabilizing BiP-ATP complexes and promoting the chaperone cycle (Preissler et al., 2017; Veyron et al., 2019).

Taking these features into account, the ER has a strong capacity to maintain proteostasis and prevent the formation of protein aggregates. Nevertheless, severe challenges to the

proteome can still cause the accumulation of misfolded proteins and protein aggregates, resulting in deleterious effects on cellular health.

1.3.3 The ER and protein misfolding in diseases

Misfolded proteins in the ER are central to the pathogenesis of several disorders such as α1-antitrypsin (AAT) deficiency, cystic fibrosis and neurodegenerative diseases.

In AAT deficiency, mutations in the SERPINA1 gene lead to conformational instability of the AAT protein, promoting aberrant folding and polymerization of AAT within the ER of hepatocytes (Strnad et al., 2020). Instead of being secreted into the circulation to inhibit neutrophil elastase in the lungs, the misfolded protein accumulates intracellularly, causing both a toxic gain of function in the liver and a loss of function in the lungs (Strnad et al., 2020). As a result, patients may develop chronic liver disease due to ER stress and hepatocyte injury, as well as early-onset emphysema due to unopposed proteolytic activity in structural proteins of the lung and innate immune proteins (Lawless et al., 2008; Strnad et al., 2020).

Cystic fibrosis arises primarily from mutations in the gene encoding the cystic fibrosis transmembrane conductance regulator (CFTR), a chloride and bicarbonate channel expressed at epithelial surfaces (Lukacs and Verkman, 2012). The most common mutation, Δ508F, disrupts the folding and assembly of CFTR, leading to its recognition as misfolded by the ER quality control machinery (Lukacs and Verkman, 2012). Instead of trafficking to the plasma membrane, the majority of mutant CFTR is targeted for degradation by the UPS (Ward et al., 1995). A fraction of CFTR mutants escapes the UPS and successfully reach the plasma membrane, however, these CFTR mutants are internalized by endocytosis and subsequently degraded in lysosomes (Ameen et al., 2007). These degradation events result in severely reduced chloride transport across epithelial surfaces, leading to the progressive decline of lung function because of dehydrated airway secretions, impaired mucociliary clearance and bacterial infections (Gibson et al., 2003).

Neurodegenerative diseases (NDD) are characterized by the collapse of neural network structure and function, accompanied by irreversible neuronal loss (Wilson et al., 2023). Owing to their terminally differentiated state, neurons cannot efficiently self-renew, leading to the disruption of core communication circuits and resulting in deficits in memory, cognition, behavior, sensory, and motor functions (Wilson et al., 2023). Misfolded protein aggregates are widely observed in post-mortem brain specimens from patients with NDD (Chiti and Dobson, 2017; Higuchi et al., 2025). Although there are numerous mechanisms underlying how misfolded proteins cause NDD through ER-associated pathways, these molecular understandings can be divided into two groups: the direct and the indirect.

Some misfolded species such as α-synuclein and the prion protein require processing in the ER and thus are able to accumulate in it (Colla et al., 2012; Harris, 2003). These misfolded proteins can directly induce ER stress and subsequent apoptosis, resulting in neuronal loss and NDD (Cooper et al., 2006; Hetz et al., 2003).

However, other neurodegenerative species such as tau, β-amyloid and huntingtin rarely accumulate in the ER. Instead, they and protein aggregates assembled from them preferentially enrich in extracellular regions, the cytoplasm and other parts of the secretion pathway (Annadurai et al., 2021; Chiti and Dobson, 2017). Indeed, the upregulation of ER stress-related markers has been found in post-mortem samples from patients with Alzheimer's disease, Parkinson's disease, Huntington's disease and amyotrophic lateral sclerosis (Carnemolla et al., 2009; Hoozemans et al., 2007; Hoozemans et al., 2005; Ito et al., 2009). Although these NDD-related aggregates are not localized in the ER, these misfolded species indirectly burden ER function and cause deleterious effects by ER-mediated pathways.

Although mechanisms associated with this indirect ER stress induction are largely missing, some studies revealed that this indirect induction can be attributed to the collapse of ER network resulting from disrupted connection between the ER and

microtubules (Lai et al., 2009), Ca^{2+} released from the ER (Ferreiro et al., 2006; Resende et al., 2008), impaired ER-associated degradation (Duennwald and Lindquist, 2008), and the potential perturbation on vesicular trafficking and autophagy biogenesis (Vidal et al., 2011). Notably, ER stress is not only a consequence of the accumulation of NDD-related misfolded proteins, perturbed ER homeostasis also acts as the reason why these misfolded proteins can further accumulate. For instance, ER stress induction facilitates the accumulation of toxic prion species and the conversion of normal prions to infectious prions, constructing a vicious loop accelerating prion replication (Hetz et al., 2007; Nunziante et al., 2011). This situation is not restricted to the prion disease. ER stress induction also inhibits the binding between tau and its ubiquitin E3 ligase, thus reducing its degradation and enabling its accumulation (Sakagami et al., 2013).

In sum, the ER plays a major role in the progression of protein misfolding diseases such as AAT deficiency, cystic fibrosis and NDD. Thus, mediating ER functions can prevent the deleterious effects of these diseases.

In the context of the ER, therapeutic strategies to treat protein misfolding diseases involve using chemical chaperones that help polypeptides to achieve native structure (Keene et al., 2002; Kraskiewicz and FitzGerald, 2012), manipulating endogenous chaperones such as BiP and PDI (Gorbatyuk et al., 2012; Hoffstrom et al., 2010), increasing Ca^{2+} concentration in the ER (Ong et al., 2010; Peng et al., 2012), the promotion of forward ER-to-Golgi transport (Cooper et al., 2006), the induction of mild ER stress (Fouillet et al., 2012), the manipulation on ER stress sensors (e.g. PERK, IRE1, ATF6) (Du et al., 2020; Lee et al., 2012; Moreno et al., 2013), and synergistic enhancement of multiple branches (Liu et al., 2024; Stojkovska et al., 2022). Interestingly, recent studies demonstrated that changes in ER morphology is able to mediate the fate of neurons (Beetz et al., 2013; Behrendt et al., 2019; Farías et al., 2019; Konno et al., 2024), enlightening a novel therapeutic strategy for ER-related protein misfolding diseases.

1.3.4 ER remodeling and cell division

The ER network comprises several morphological domains. Originating at the nuclear envelope (NE) as stacked sheets, the ER later changes to a peripheral network of tubules and sheets. The sheet formation is regulated by cytoskeleton-linking membrane protein 63 (CLIMP63) as the luminal spacer and sigma-1 receptor as the stabilizer of flat sheets (Sawyer et al., 2024), while the high membrane curvature required for assembling ER tubules and maintaining the edges of ER sheets is ensured by the reticulon (RTN) and receptor expression-enhancing (REEP) family proteins (Kors and Schlaitz, 2024; Xu et al., 2023). The atlastin family proteins mediate ER membrane fusion (Shi et al., 2024). Additionally, cytoskeleton proteins, especially microtubules, tether to ER membranes and facilitate ER dynamics (Nourbakhsh et al., 2021).

Upon entering mitosis, the nuclear envelope disassembles and the ER moves towards the cell periphery, vacating the inner spindle area. Previous studies demonstrated that the ER went through a tubule-to-sheet transition (Lu et al., 2009). However, recent evidence proposed that membrane curvature of the ER seems to increase in dividing cells, which is regulated by REEPs and Aurora kinase A (Kumar et al., 2019; Zhang et al., 2024). Currently, it's largely unknown how dividing cells achieve ER remodeling and even fewer studies focus on how ER remodeling mediates protein aggregates during cell division. To study this in live cells, tools to report proteostasis are needed.

1.4 Tools to report proteostasis in live cells

1.4.1 General introduction

There are two methods commonly used when measuring a live cell's capability to maintain its proteome stability (Owyong and Hong, 2022).

The first approach is examining the folding capacity of endogenous proteins. To achieve this, endogenous misfolding- or aggregation-prone proteins are expressed in cells and their aggregation profiles are observed. If cells can disassemble more protein aggregates, then they possess stronger ability to maintain proteostasis. However,

endogenous misfolding-prone proteins possess natural functions and interactors in cells, potentially rewiring proteostasis network and introduce artifact when studying how cells maintain proteostasis. Moreover, tissue-specific mutant may complicate the comparative analysis of different cell types and organs (Gupta et al., 2011). To eliminate the perturbation on cellular proteome, some small molecule-based probes are developed. Upon binding to hydrophobic areas or β-sheets structures or other residues exposed from endogenous misfolded proteins, these probes alter their emission properties such as the intensity and lifetime of fluorescence, thus reporting how robust a cell can fold its proteins (Biancalana and Koide, 2010; Owyong and Hong, 2022). However, these small molecule probes rely on the precise recognition of particular structures, limiting their application on reporting a general protein folding landscape in cells.

The second approach to report cellular proteome stability is by expressing exogenous proteins such as the thermally unstable mutant of retroaldolase, misfolding-prone mutants of haloalkane dehydrogenase (Halo) and firefly luciferase (Fluc) (Gupta et al., 2011; Liu et al., 2015; Melo et al., 2022). These proteins can assemble into protein aggregates upon the challenge on proteome stability. When tagging with fluorescent proteins or incorporating with other probes, these aggregates can be observed as the readout of cellular proteome stress. Due to the exogenous nature, these recombinant proteins have few biologically roles, minimizing the perturbation on intrinsic proteome (Gupta et al., 2011; Melo et al., 2022). Thus, in my study, these type-two proteostasis reporters are employed.

1.4.2 Firefly luciferase mutants as proteostasis reporters

Among all these type-two probes, Fluc-based proteostasis reporters have been widely utilized in diverse contexts, from cellular models to whole mice, and across various subcellular compartments since its initial development (Blumenstock et al., 2021; Gupta et al., 2011; Sanchón et al., 2021). Firefly luciferase is a multidomain protein and relies on chaperone-mediated folding and refolding in mammalian cells. By introducing double point mutations, the resulting Fluc with double mutations (FlucDM)

exhibited decreased conformational stability and an increased propensity to misfold and aggregate. Moreover, when FlucDM was fused to fluorescent proteins such as eGFP, the FlucDM-eGFP construct assembled into visible aggregates in live cells upon proteostasis stress such as heat shock **(Figure 1.7)**. Thus, under conditions that compromise proteome balance during cell division, the aggregation of FlucDM-eGFP serves as a readout of cellular proteome stress.

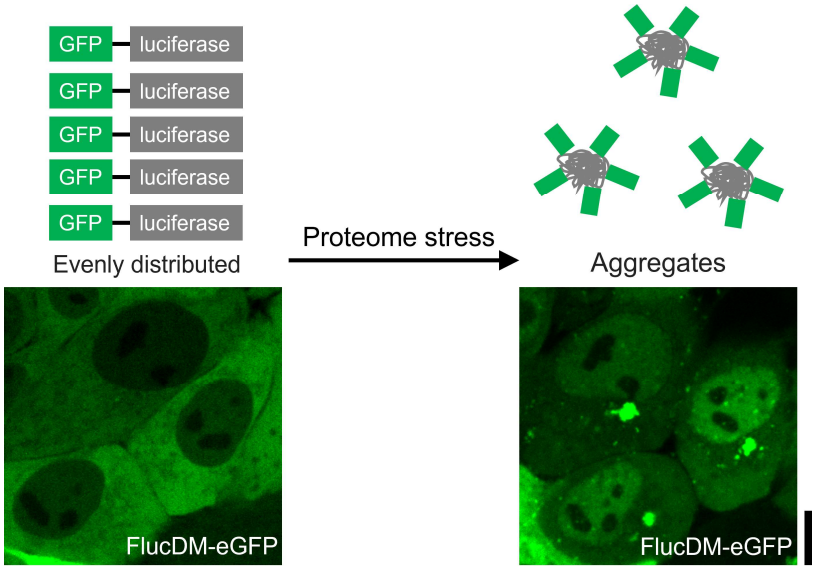


Figure 1.7: Diagram of the proteostasis reporter system. MCF10A cells expressing FlucDM-eGFP were treated with 5 μM MG132 for 7 hours. The signal of FlucDM-eGFP was evenly distributed while some aggregates appeared upon the treatment of MG132. Single Z-slice images were shown. Scale bar, 10 μm.

1.5 Aims of this thesis

Despite a substantial body of evidence and an evolving understanding in the proteostasis field, its regulation in dividing cells remains poorly characterized. This is particularly true in mammalian cells and those undergoing symmetric division. Moreover, how cells employ the fourth type of proteostasis maintenance mechanism (i.e. misfolded protein aggregation) has started to be revealed mainly after entering the 21st century **(Figure 1.2)**, suggesting the existence of numerous undiscovered mechanisms regulating protein aggregation and disaggregation. Given that the proteostasis network co-evolves with the proteome to sustain cellular health and respond to diverse stressors (Powers and Balch, 2013), I hypothesize that novel regulatory mechanisms exist in the proteostasis networks of mammalian cells undergoing symmetric division.

For these cells, this thesis aims to answer the following research questions:

1. Which molecules are responsible for eliminating misfolded protein aggregates in dividing cells?
2. What is the fate of protein aggregates in the ER during cell division?

To address these questions, this thesis employed the following technical strategies:

1. FlucDM-eGFP was expressed in cells, and key components of the proteostasis network such as Hsp70 and the proteasome were inhibited in dividing cells. Aggregation dynamics were then profiled using live-cell imaging.
2. FlucDM-eGFP was specifically enriched in the ER, and its aggregation was induced by disrupting ER proteostasis. The dynamics of the resulting aggregates during cell division were subsequently characterized.

Chapter 2 Materials and Methods

2.1 Plasmids and cloning

2.1.1 Plasmid list

Table 2.1: Plasmid information

Plasmid ID	Plasmid name	Source
pTGL0081 (LV007)	pHBLV-CMV-MCS-EF1-puro	Synthesis from HanBio Technology (Shanghai, China)
pTGL0257 (257)	pCDH-CMV-MCS-EF-1a-Hygromycin	Synthesis from Youze Biotechnology (Changsha, China)
pTGL0386 (386)	Lenti-(BB)-EF1a-KRAB-dCas9-P2A-BlastR	From Addgene
pTGL0483	LV007+laminVHH-tagGFP	This study, WM
pTGL0561	LV007-FlucWT-eGFP	This study
pTGL0562	LV007-FlucSM-eGFP	This study
pTGL0563	LV007-FlucDM-eGFP	This study
pTGL0645	LV007-FlucDM-eGFP-ER targeting	This study, S
pTGL0662	LV007-NLS-FlucDM-eGFP	This study, C
pTGL0673	LV007-FlucDM-mCherry-ER targeting	This study, C
pTGL0698	LV007-FlucWT-eGFP-ER targeting	This study, C
pTGL0703	LV007-HTaggr (M21K, F86L of HaloTag)-eGFP-ER	This study
pTGL0707	LV007-HaloTag-eGFP-ER	This study
pTGL0737	LV007-CFTR (WT)-eGFP	This study
pTGL0738	LV007-CFTR (Δ508F)-eGFP	This study
pTGL0739	LV007-SERPINA1 (WT) -eGFP	This study

Continue Table 2.1

Plasmid ID	Plasmid name	Source
pTGL0740	LV007-SERPINA1 (Glu264Val, S variant) -eGFP	This study
pTGL0740	LV007-SERPINA1 (Glu264Val, S variant) -eGFP	This study
pTGL0741	LV007-SERPINA1 (Glu342Lys, Z variant) -eGFP	This study
pTGL0743	LV007-FlucDM-eGFP-Plasma Membrane (FSHR)	This study, C
pTGL0828	PL07-72-mGreenLantern-hGeminin (degron)	From Chan Kuan Yoow's lab
pTGL0891	LV007-empty	This study
pTGL0894	257-CLIMP63-mCherry	This study
pTGL0914	257-mStayGold-Sec61β	This study, WYH
pTGL0955	257-ER-FlucDM-mCherry	This study
pTGL0959	257-BiP-mCherry-KDEL	This study
pCRI 0207	386(CRISPRi)-HSPA5 sgRNA1	This study
pCRI 0209	386(CRISPRi)-HSPA1A sgRNA1	This study
pCRI 0211	386(CRISPRi)-HSPA8 sgRNA1	This study
pCRI 0249	386(CRISPRi)-ATL2 (atlastin 2) sgRNA 1	This study
pCRI 0252	386(CRISPRi)-ATL3 (atlastin 3) sgRNA 2	This study

WYH indicates that this plasmid is constructed with help from Yuhan Wang. C indicates that this plasmid is constructed with help from Bowen Chen. WM indicates that this plasmid is constructed by Yuyang Miao and Chao Wang. S indicates that this plasmid is constructed with help from undergraduates from Ting Gang Lab. pTGL0828 was constructed by Shuangshuang Xie in Chan Kuan Yoow's lab. The construct containing wild-type Fluc was a gift from Dr. Mikael Bjorklund.

2.1.2 Molecular cloning methods

All plasmids in this study were constructed by following methods:

2.1.2.1 Vector preparation

Vectors used in cloning were prepared first by cutting plasmids with restriction enzymes (New England Biolabs) according to manufacturer's instructions. Then these enzyme-digested products were separated in agarose gel (1% w/v agarose in TAE buffer) to separate bands. Targeted bands, which revealed by DNA gel marker, were cut and purified by FastPure Gel DNA Extraction Mini Kit (Vazyme, DC301-01) to obtain vectors. Vectors were stored in -20°C.

2.1.2.2 DNA fragments preparation before Gibson assembly

Table 2.2: The recipe for DNA fragments preparation

Reagents	Volume (μl)
Forward primer (10 nM)	0.6
Reverse primer (10 nM)	0.6
Templates	0.6
ddH_2O	5.7
Mix (with Taq polymerase)	7.5

2 × Phanta Flash Master Mix Dye plus (Vazyme) was used in this context. These PCR products were separated in agarose gels and purified by FastPure Gel DNA Extraction Mini Kit (Vazyme, DC301-01) before being stored in -20°C.

2.1.2.3 Gibson assembly

Table 2.3: The recipe for Gibson assembly

Reagents	Volume (μl)
Fragments	0.5 each fragment
Vectors	0.5
ddH_2O	To complement to 5
2 × Seamless Mix	2.5

2 × Seamless Mix used in this study were supplied by Beyotime or TransGen Bio.

2.1.2.4 Short DNA fragments annealing

Table 2.4: The recipe for DNA fragments annealing

Reagents	Volume (μl)
Forward primer (100 nM)	1
Reverse primer (100 nM)	1
10 × Ligation Buffer	1
ddH_2O	7

The above system was incubated at 37°C for 30 min and subsequent 95°C for 5 min and then ramp down to 25°C at 5°C per minute. Products were diluted 200 times in ddH_2O and freeze at -20°C.

2.1.2.5 T4 ligation

Table 2.5: The recipe for T4 ligation

Reagents	Volume (μl)
Diluted products in 2.1.2.4	1
Vector	1
T4 ligation buffer (Beyotime)	1
T4 ligase (Beyotime)	0.2
ddH_2O	0.8

Ligation system would be kept at 20 to 25°C for at least 1 h. The products were stored in -20°C.

2.1.2.6 Plasmid transformation

Following methods were used during transformation:

1. 4 μl Gibson assembly, T4 ligation products or plasmids were gently mixed with 33 μl defreezed DH5α competent *E. coli* on ice for 20 min.
2. Samples were heat-shocked at 42°C for 90 s.

3. Mixture was put back on ice for 3 min.
4. 500 µl LB medium without antibiotics was added.
5. Samples were incubated at 37°C with shaking for at least 30 min,
6. Bacteria were centrifuged down and spread on LB plates with specific antibiotics.
7. Plates were incubated at 37°C for 12-18 h.
8. Clones were picked and transferred to fresh LB medium antibiotics.

2.1.2.7 Colony PCR

Table 2.6: The recipe for colony PCR

Reagents	Volume (µl)
Forward primer (10 nM)	0.6
Reverse primer (10 nM)	0.6
LB solution containing bacteria	0.6
ddH_2O	5.7
Mix (with Taq polymerase)	7.5

2 × Phanta Flash Master Mix Dye plus (Vazyme) was used in this context. These PCR products were separated in agarose gels and positive clones were sent for sequencing.

2.1.2.8 DNA sequencing of cloning products

Sanger sequencing was performed by ABI 3730XL via Sangon Biotech (Shanghai) Co., Ltd. or Tsingke Biotech Co., Ltd.

2.1.2.9 Plasmids extraction

Successfully sequenced bacteria were grown in fresh LB medium with antibiotics overnight at 37°C with 220 rpm shaking. Plasmids extraction was realized by EasyPure® HiPure MiniPrep Kit (TranGen, EM111), Endo-Free Plasmid Mini Kit (Omega Bio-tek, D6950) or EZgene EndoFree Maxiprep Kit (BioMIGA, PD2568).

2.2 Cell line culture and preparation

2.2.1 General cell culture conditions

MCF10A cells were cultured in DMEM F-12 (Sigma) with 1% (v/v) Glutamax (Gibco), 5% (v/v) horse serum (Biological Industries), 20 ng/ml EGF (Gibco), 0.5 mg/ml Hydrocortisone (MedChemExpress), 100 ng/ml Cholera toxin (Sigma), 10 μg/ml Insulin (Biological Industries), and 1% (v/v) Pen/Strep (Biological Industries).

HEK293Ta, U2OS, A549 and HepG2 cells were cultured in DMEM (Sigma) with 1% (v/v) Glutamax (Gibco), 6% (v/v) fetal bovine serum (Biological Industries), and 1% (v/v) Pen/Strep (Biological Industries). MDA-MB-231 cells were cultured in DMEM F-12 (Sigma) with 10% (v/v) fetal bovine serum (Biological Industries) 1% (v/v) Glutamax (Gibco) and 1% (v/v) Pen/Strep (Biological Industries).

Cells were maintained at 37°C with 5% CO_2 in a humidified incubator except in the case of heat shock experiments.

2.2.2 Chemical transfection

HEK293Ta cells were chemically transfected via GeneTwin transfection reagent (Biomed, TG101) or polyetherimide (1 mg/mL). For a 10 cm-dish supplied by 10 mL culture medium, a mixture of solution A and solution B was used.

Solution A was 12 μg plasmids diluted into DMEM to a total volume of 250 μL. Solution B was either 60 μL polyetherimide supplied with 190 μL DMEM or 40 μL GeneTwin supplied with 210 μL DMEM. After separately preparing A and B solutions, B was added to A and the mixture was kept at room temperature for at least 20 min before adding to newly changed fresh culture medium.

2.2.3 Lentivirus transduction

Lentivirus transduction was achieved by following two steps:

2.2.3.1 Lentivirus packaging

Using a third-generation lentiviral packaging system, lentiviral particles were generated by following protocols:

1. The packaging plasmids (pRSV-Rev, pMDLg/pRRE, and pMD2.G, generously provided by Didier Trono) along with the transfer plasmid were transfected into HEK293Ta packaging cells (Genecopoeia, LT008) by the chemical transfection method mentioned above.
2. After 48 hours, the cell culture medium was collected, followed by filtration through a 0.45 μm membrane.
3. The filtrate was then concentrated by overnight precipitation with a 5 X solution consisting of 250 g/L PEG 8,000 and 43.83 g/L NaCl in distilled water.
4. Solutions went through centrifugation at 4,000 × g for 25 minutes at 4°C.
5. The precipitated viral particles were resuspended in phosphate-buffered saline (PBS) and stored at -80°C.

2.2.3.2 Transduction

Lentivirus in PBS were directly introduced into the culture medium, which was supplemented with 1 μg/mL polybrene (HanBio). Unless otherwise stated, after lentivirus infection for 2 days, transduced cells were passaged and medium with antibiotics would be used for selection.

2.2.3.3 CRISPRi knockdown

Cells were transduced with lentivirus containing CRISPRi plasmids for four or five days. Cell lysates were collected and the knockdown (KD) efficiency was confirmed by quantitative real-time polymerase chain reaction (qRT-PCR). Following single guide RNA (sgRNA) was used in this thesis:

Table 2.7: The sequence of single guide RNA

Gene	Sequence of sgRNA
HSPA5	5'- GGCGACGGTGAGGTCGACGC -3'
HSPA1A	5'- GTCACTCTCGAAAAAGGTAG -3'
HSPA8	5'- GCAGGCGAGTTCAATGAGAC -3'
ATL2	5'- GAGGGCAGCAACCGCACCAG -3'
ATL3	5'- GAGCAGGGGTGCAGAGGAGA -3'

2.2.4 Fluorescence-activated cell sorting (FACS)

In this study, lentiviral transduction was used to generate MCF10A cells co-expressing ER-FlucDM-eGFP and ER-FlucDM-mCherry for FRAP, or ER-FlucDM-mCherry and mGreenLantern-hGeminin (degron), or ER-FlucDM-mCherry and NLS-FlucDM-eGFP. After transduction, cells underwent selection with 5 μg/mL puromycin for at least 2 days. Then cell suspension for FACS was prepared by 10-minutes trypsin digestion, centrifugation, PBS rinsing and filtration through a 40 μm cell strainer (Biosharp). BD Influx cell sorter was used to identify and enrich double-positive cell populations from cell suspension.

2.2.5 Mitotic cell preparation

In order to enrich dividing cells, cells were first seeded on chamber slides (ibidi, 80826) or 2-well chambers (Cellvis, C2-1.5H-N) for one day before employing 7.5 μM RO-3306 to synchronize cells to the G2/M boundary by treating them for 16 to 20 hours. Cells were released to enter into mitosis synchronously by washing once with pre-warmed fresh medium.

2.2.6 Drug list

The following drugs were used to treat cells:

Table 2.8: Drugs used

Drugs	Manufacturer
Apcin	Sigma, SML1503
Calcimycin	MCE, HY-N6687
Cycloheximide	AbMole, M4879
MG132	CSN Pharm, CSN11436
MLN-8237	TargetMol, T2241
Nocodazole	Beyotime, S1765
proTAME	Cayman Chemical, 25835
RO-3306	Selleckchem, S7747
Thapsigargin	Abcam, ab120286
Tunicamycin	GlpBio, GC16738
VER-155008	CSN Pharm, CSN13116
YUM70	Aladdin, Y413413

2.3 Biochemistry methods

2.3.1 Western blots (WB)

2.3.1.1 General WB workflow

General protein immunoblotting methods used in this thesis were provided below:

1. Cells were lysed by a lysis buffer containing NP-40 or LDS.
2. Lysates were boiled at 95°C for 8 to 10 min.
3. Samples were separated by pre-cast SDS-PAGE gels (from GenScript or Tsingke) and transferred to a PVDF membrane (EMD Millipore).
4. Blots were blocked with 5% (w/v) skim milk for 1 h or Quick Block buffer supplied by Beyotime for at least 20 min at room temperature.
5. Blocked blots were incubated at 4°C overnight with the primary antibody.
6. Primary antibodies were removed and blots were rinsed by TBST for more than three times (totally more than 15 min).
7. Blots were incubated at room temperature with diluted secondary antibodies

for one to two hours before washed with TBST.

Odyssey CLX was employed for blots exposure and LI-COR Image Studio software was used to quantify the bands intensities on blots. To incubate different primary antibodies at the same blot, blot was vigorously rinsed by stripping buffer from CWBio and washed with TBST for three times. Then blot was blocked and incubated with primary antibody again as methods mentioned before. The molecular weight marker used in WB was PageRuler™ Prestained Protein Ladder (10 to 180 kDa, Thermo Scientific, 26616).

2.3.1.2 Supernatant and pellet fraction preparation

To differentiate supernatant and pellet fractions of ER-FlucDM-eGFP, cells in 12-well were first washed with 1 mL PBS and lysed by 100 μL 0.2%, 0.5% or 1.0% (v/v) NP-40 lysis buffer (NP-40 diluted in dilution buffer) supplied with 1% (v/v) protease inhibitor cocktail (Lablead, C0101). After peeling cells by scraping, the lysate was collected and centrifuged at 14,000 × g for 10 min at 4°C. About 90 μL of the supernatant was transferred to another Eppendorf tube and 30 μL 1 × LDS sample buffer was added. Meanwhile, pellet was further lysed by 120 μL 1 × LDS on ice for at least 30 min with vigorous shaking intermittently.

2.3.1.3 List of reagents used in WB

Buffers used in WB were prepared by following recipes:

Table 2.9: Buffers used in western blot

Buffer names	Compositions	Application
10 × TBS	8 g KCl + 120 g Tris + 320 g NaCl in ddH_2O (4 L totally)	To prepare 1 × TBST
1 × TBST	4.5 L ddH_2O + 0.5 L 10 × TBS + 2.5 mL Tween-20	To wash blots
Dilution buffer	100 mM Tris-HCl (pH 7.4)	To dilute lysis buffer
4 × LDS	900 μL LDS buffer (Beyotime) + 100 μL β-mercaptoethanol	To prepare 1 × LDS
1 × LDS	300 μL 4 × LDS + 900 μL dilution buffer	As lysis buffer

Table 2.10: Antibodies used in western blot

1st antibodies	Dilution ratio	Corresponding 2nd antibody
GFP (Huabio, ET1601-13)	1:3000	1:5000
β-actin (Genscript, A00702)	1:5000	1:20000
Cyclin B1 (Proteintech, 55004-1-AP)	1:1000	1:5000
p53 (Huabio, ET1601-13)	1:1000	1:5000

All antibodies listed above were diluted in 1 × TBST and stored at 4°C. The 2nd anti-rabbit and anti-mouse antibodies were Goat anti-Rabbit IgG (H+L) Highly Cross-Adsorbed Secondary Antibody, Alexa Fluor™ Plus 800 (Invitrogen, A32735) and Goat anti-Mouse IgG (H+L) Highly Cross-Adsorbed Secondary Antibody, Alexa Fluor™ Plus 680 (Invitrogen, A32729), respectively. Both primary and secondary antibodies were reused. All primary antibodies have the corresponding specific second antibodies to evade cross-incubation issues.

2.3.2 Immunofluorescence staining

For BiP staining, the following protocol was executed:

1. MCF10A cells expressing ER-FlucDM-eGFP were seeded in 8-well ibidi plates for 24 hours.
2. Cells were fixed in 100% methanol for 10 minutes.
3. Fixed samples were permeabilized with 0.5% (v/v) Triton X-100 for 15 minutes.
4. Permeabilized cells were blocked with 5% (v/v) FBS (fetal bovine serum) in PBS for 30 minutes.
5. Samples were incubated overnight at 4°C with a 1:200 dilution of mouse anti-BiP antibody (HuaBio, HA601076) in 1% (v/v) FBS.
6. After removing primary antibodies, samples were washed with TBST for three times.
7. Secondary antibody, Donkey Anti-Mouse IgG H&L (Alexa Fluor® 568, ab175472, Abcam), was applied at a 1:2000 dilution for one hour.
8. After removing secondary antibodies, samples were washed with TBST for three times.
9. Imaging by confocal microscopy.

For tubulin and DAPI staining, following methods were used:

1. Cells were fixed with 4% (w/v) paraformaldehyde for 20 minutes.
2. Fixed cells were permeabilized using 0.5% (v/v) Triton X-100 for 15 minutes.
3. Permeabilized samples were blocked with 5% (v/v) FBS in PBS for 30 minutes.
4. Cells were incubated with a 1:200 dilution of mouse anti-α-tubulin monoclonal antibody (Proteintech, 66031-1-IG).
5. After removing primary antibodies, samples were washed with TBST for three times.
6. The secondary antibody, Donkey Anti-Mouse IgG H&L (Alexa Fluor® 568, ab175472, Abcam), was again applied at a 1:2000 dilution for one hour.
7. After removing secondary antibodies, samples were washed with TBST for

three times.

8. Cells were treated with DAPI Staining Solution (Sangon Biotech, E607303, 5 mg/L) diluted in PBS to 50 ng/mL for 10 minutes.
9. After the removal of the DAPI solution, cells were washed twice with PBS.
10. Cells were imaged by confocal microscopy.

2.3.3 Luciferase activity test

A total of 10,000 cells in 100 μL of medium were seeded into each well of 96-well plates (Biosharp, BS-MP-96W for luminescence and BS-MP-96B for fluorescence). After 18 hours of incubation, 5 μM MG132 was added to the MG132 + FlucDM-eGFP group, while the remaining untreated wells were left unchanged. Six hours later, the cells were washed once with PBS.

For luminescence detection, 50 μL of Steady-Glo Luciferase Assay System buffer (Promega, E2510) was added to each well to lyse the cells, followed by a 15-minute incubation at room temperature. Luminescence from each well was measured three times over a 5-minute interval using the Spark® Multimode Microplate Reader (Tecan, 1000 ms exposure). The luminescence intensity was calculated by normalizing the three measurements and subtracting the background signal from the empty wells.

To determine relative specific luciferase activities, 100,000 MCF10A cells were seeded in 12-well and went through corresponding treatments done in luminescence experiments. These cells were lysed by LDS buffer and went through general protein blotting protocol described before. β-actin was used to normalize GFP intensity first. Then relative GFP intensity was used to normalize corresponding luminescence to acquire final luciferase activity.

2.3.4 Quantitative real-time PCR (qRT-PCR)

Total RNA was extracted from the cells using the RNA isolation kit (Vazyme, RC112-01). The extracted RNA was then reverse transcribed into complementary DNA (cDNA) using HiScript II Q RT SuperMix for qRT-PCR (Vazyme, R223-01). qRT-PCR was

performed to quantify cDNA levels, employing the ChamQ Universal SYBR qPCR Master Mix (Vazyme, Q711-02). The PCR reaction mixture was set up in a hard-shell PCR plate (Bio-Rad, HSP9655), sealed with Microseal 'B' seals (Bio-Rad, MSB1001), and run on the CFX96 Touch Real-Time PCR Detection System (Bio-Rad, C1000). To determine relative expression levels, the CT value for glyceraldehyde-3-phosphate dehydrogenase (GAPDH) was used for normalization. Primers used in qRT-PCR were listed below:

Table 2.11: Primers used in quantitative real-time PCR

Gene name	Primers
GAPDH	5'- CAGGAGGCATTGCTGATGAT -3'
	5'- GAAGGCTGGGGCTCATTT -3'
HSPA1A	5'- CAAGACTTTGCATTTCCTAG -3'
	5'- GGCCTGAGTTAAGTGTATT -3'
HSPA5	5'- CACAGTGGTGCCTACCAAGA -3'
	5'- TGTCTTTTGTCAGGGGTCTTT -3'
HSPA8	5'- CCTACACCCCAGCAACCAT -3'
	5'- TCAGTGTCCGTAAAGGCGAC -3'
CALR	5'- ATAAAGGTTTGCAGACAAGC -3'
	5'- CCACAGTCGATGTTCTGCTC -3'
HSP90B1	5'- TCCAGCAGAAAAGAGGCTGA -3'
	5'- CAAATTCGGGAAGGGCCTGA -3'
CANX	5'- GCACCTATTCTGGAGGCGAG -3'
	5'- ACAGCAACCACTTCCCTTCC -3'
P4HB	5'- TTCAGGAATGGAGACACGGC -3'
	5'- TCCACGTCCTTGAAGAAGCC -3'

2.4 Microscopy imaging techniques

2.4.1 Transmission electron microscopy (TEM)

For TEM sample preparation, MCF10A cells expressing ER-FlucDM-eGFP were

synchronized at the G2/M boundary by treating them with RO-3306 for 16 to 20 hours. Cells were then released into mitosis by removing the RO-3306. Forty-five minutes after release, the cells were trypsinized for 10 minutes and centrifuged. The resulting cell pellet was initially fixed with 2.5% (w/v) paraformaldehyde at room temperature for 30 minutes and then kept overnight at 4°C. The following sample preparation and TEM observation were performed at the Center of Cryo-Electron Microscopy (CCEM), Zhejiang University. The pellet was further fixed with 1% (w/v) osmium tetroxide followed by 2% (w/v) uranium acetate. Dehydration was performed using ethanol and acetone before embedding the samples in epoxy resin. Finally, the sectioned samples were observed using a Tecnai G2 Spirit 120kV transmission electron microscope (Thermo FEI).

2.4.2 Live-cell staining

The live-cell staining dyes used in this study included 100 nM SiR-Tubulin (Cytoskeleton, CY-SC002), 1 μM ER-Tracker Red (Beyotime, C1041S), and 10 μM Thioflavin T (ThT). These dyes were added to the medium, and cells were incubated for approximately 30 minutes before imaging. For ThT staining, about 10% of aggregates in ER-FlucDM-mCherry cells were detectable.

2.4.3 Spinning-disk confocal microscopy methods

The spinning-disk confocal microscopy setup included a Nikon Eclipse Ti2-E inverted microscope, equipped with a Nikon 60 × oil-immersion objective lens (N.A. 1.40, Plan Apochromat Lambda), a Nikon 100 × oil-immersion objective lens (N.A. 1.45, Plan Apochromat Lambda), and a Yokogawa Electric Corporation CSU-W1 spinning-disk system. The imaging system also featured a Photometrics Prime 95B sCMOS camera, a PiezoZ stage (Physik Instrumente), and a live-cell stage top chamber with humidified CO_2 (Okolab). Fluorescence recovery after photobleaching (FRAP) was facilitated by the iLAS2 FRAP system (Gataca).

Imaging was performed with a z-step size of 0.5 μm, while the x-y plane pixel size was

183.3 nm/pixel for the 60 × lens and 110 nm/pixel for the 100 × lens. Fluorophores were excited using laser lines at 405, 488, 561, or 640 nm wavelengths.

For FRAP movie acquisition, images were captured using the 488 nm and 561 nm laser lines through the 100 × lens. The procedure involved acquiring three pre-bleach images at 30-second intervals, followed by bleaching the mCherry signal with the 561 nm laser. After bleaching, one image was immediately acquired, followed by ten more images at 30-second intervals. A total of fourteen time-point images were collected over a 6.5-minute FRAP experiment.

2.4.4 Image analysis and processing

Fiji was used to process images. In addition to common image processing techniques, which will be mentioned in figure legend, following specially processing methods were used in this thesis.

To quantify aggregates, projected images were classified by Trainable Weka Segmentation (Arganda-Carreras et al., 2017), a method combining machine learning algorithms and image features to reach pixel-level segmentation (Fiji/Plugins/Segmentation/Trainable Weka Segmentation). Then segmented images were processed using following ImageJ Macro commands **(Figure 2.1)**:

1. run("8-bit");
2. setOption("BlackBackground", true);
3. run("Convert to Mask");
4. run("Watershed");
5. Analyze Particles (Fiji/Analyze/Analyze Particles)

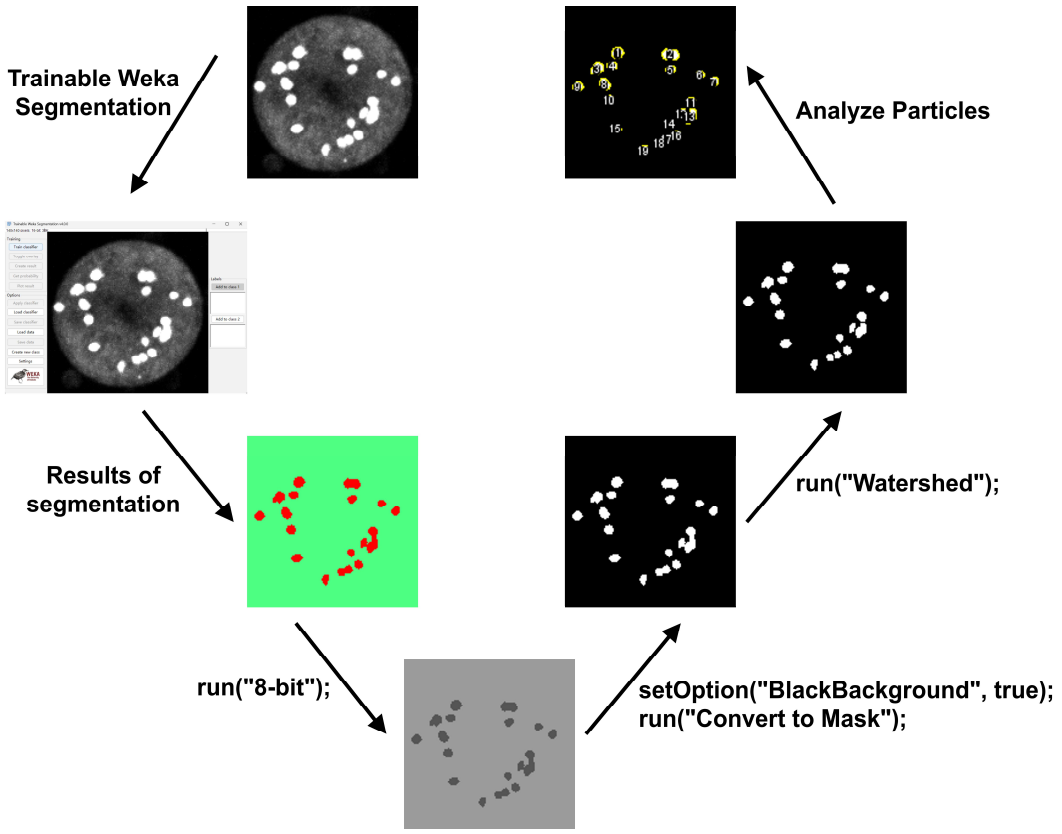


Figure 2.1: Quantifying aggregates by Trainable Weka Segmentation.

To quantify total GFP fluorescence signals in a live cell, a Z-stack image was captured and projected using the "Sum Slices" method. The cell in the projected image was segmented by polygon selection in Fiji. Then, the total GFP fluorescence intensity in this segmented cell is measured. This intensity was corrected by subtracting a background value calculated as:

$$\text{Background} = \text{B_mean (a.u./pixel)} \times \text{N_slices} \times \text{A_cell (pixels)}$$

where B_mean is the mean background intensity per pixel, N_slices is the number of Z slices in the stack and A_cell is the segmented cell area.

In my experiments, background mean intensities ranged from 95 to 100 a.u./pixel. The background-subtracted signal was regarded as the GFP intensity of this segmented cell.

Except images from FRAP, other segmented images from time-lapse movies were processed by using ImageJ Macro commands:

1. run("8-bit");

2. setThreshold(0, 120);
3. run("Make Binary", "method=Default background=Light black");
4. run("InvertLUT");
5. run("Watershed", "stack");
6. Analyze Particles (Fiji/Analyze/Analyze Particles)

For FRAP analysis of ER-eGFP and ER-HaloDM-eGFP, the average fluorescence intensity from manually selected regions of interest (ROI) in projected images was measured in Fiji.

For FRAP analysis of aggregates in cells co-expressing ER-FlucDM-eGFP and ER-FlucDM-mCherry, Weka Segmentation was employed to segment aggregates first to localize their dynamics. The resulting segmentation masks were applied to the corresponding mCherry images, which were then processed with the Analyze Particles (Fiji/Analyze/Analyze Particles) to quantify photobleaching and recovery. For fluorescence intensity quantification, the mean background intensity per pixel in all FRAP experiments were 100 a.u. per pixel and subtracted by the aforementioned method.

To quantify aggregates in Chapter 3, cells were captured first and Z-stacks were projected by the “Max Intensity” method. A significant proportion of aggregates in these cells was too small to be segmented precisely by Trainable Weka Segmentation or by conventional intensity-thresholding method. Furthermore, FlucDM-eGFP in nearby interphase cells also assembled into protein aggregates, increasing the difficulty to distinguish aggregates in dividing cells. Thus, I manually counted aggregates in each cell and classified cells into three categories: cells with no visible aggregates, cells with 1-20 aggregates and cells with more than 20 aggregates.

2.5 Heat shock treatment

Heat shock was executed in the stage-top chamber mentioned before. After adjusting Okolab temperature controller to the specified temperature and waiting for more than 30 min to equilibrate, the adherent cells seeded in wells were placed on the metal part of live-cell chamber for heat shock treatment. Temperature of live-cell chamber metal basis was confirmed by handheld infrared temperature detector. Heat shock treatment was executed as following protocol **(Figure 2.2)**.

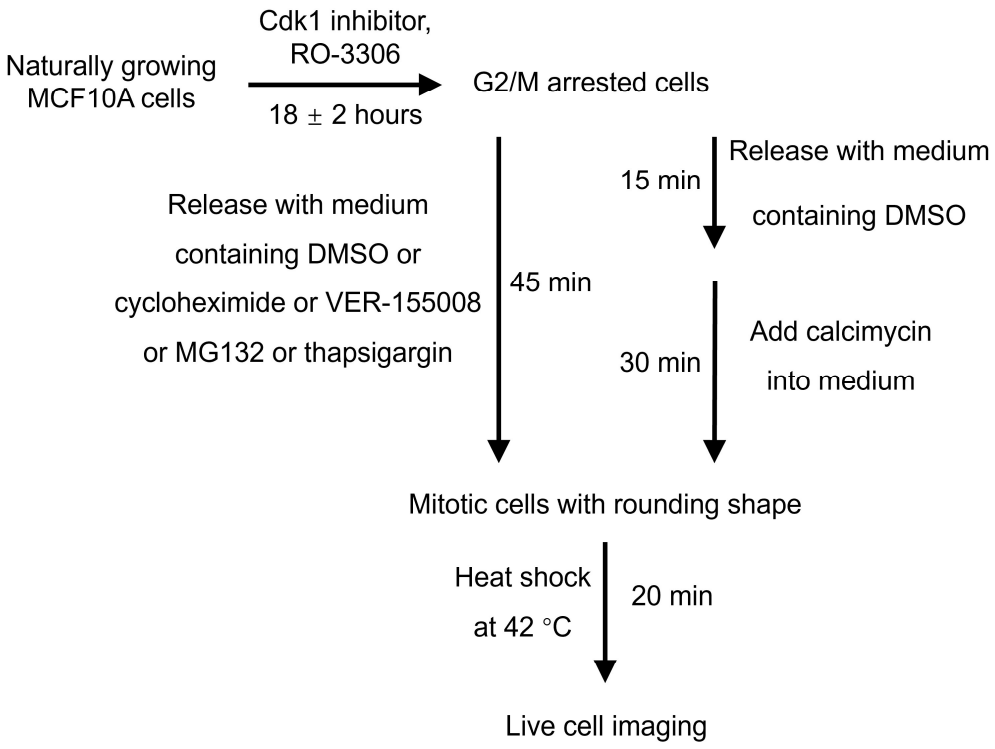


Figure 2.2: Workflow of heat shock treatment in dividing cells.

2.6 Proteomics methods

The following protocol was used when prepared samples for proteomics analysis.

1. MCF10A cells were transduced with pTGL0891 (empty vector) or pTGL0645 (ER-FlucDM-eGFP) for six days.
2. Cells were digested by trypsin, centrifuged, and washing twice with ice-cold PBS.
3. Pellets were rapidly frozen in liquid nitrogen and sent to Tsingke (Wuhan, China).

4. Pellets were lysed using a buffer containing 8 M urea, 1 mM phenylmethylsulfonyl fluoride (PMSF), and 2 mM ethylenediaminetetraacetic acid (EDTA).
5. Samples underwent ultrasound sonication on ice for five minutes.
6. Samples were centrifuged at 15,000 × g for 10 minutes.
7. Supernatants were collected, and protein concentrations were determined using the BCA method (Beyotime).
8. A 100 μg aliquot was adjusted to a final volume of 200 μl with 8 M urea, and DTT (final concentration 5 mM).
9. Samples were incubated at 37°C for 45 minutes.
10. Proteins were alkylated with iodoacetamide (final concentration 11 mM) in the dark at room temperature for 15 minutes.
11. Samples underwent trypsin digestion.
12. Samples were analyzed via LC-MS/MS. MS/MS data processing was performed using DIA-NN (v1.8.1), with protein quantification carried out through the MaxLFQ algorithm.

Steps 3 to 12 were performed by Tsingke (Wuhan, China). Fold changes were calculated by averaging protein quantification and division. p-value for volcano plot was calculated by t-test.

2.7 Statistics

Student's t-test or Mann-Whitney test was used to analysis datasets. Prism 8 (GraphPad) was used for the statistical analysis and data plotting. Statistical details are indicated in the figure legends.

Chapter 3 Proteostasis Maintenance in Mammalian Cells during Mitosis

3.1 Introduction

Protein folding is influenced by several key environmental factors, including salt concentration, macromolecular crowding, and pH values (Das et al., 2024; de Oliveira et al., 2018; Maity et al., 2018). During cell division, significant changes occur in the organization of organelles and intracellular conditions such as viscosity and pH, which intuitively suggests that protein folding dynamics in dividing cells may differ from those in interphase cells (Hurst et al., 2021; Spear and White, 2023). Proteins exhibited greater thermal stability and faster folding kinetics in mitotic cells compared to interphase cells (Wirth et al., 2013). Furthermore, a significant proportion of intrinsically disordered proteins, along with mitotically phosphorylated proteins such as mitotic spindle-binding proteins and cytoskeletal proteins, displayed increased stabilization and solubility during mitosis (Becher et al., 2018). These findings are further supported by functional studies focusing on specific chaperones. These protein folding helpers are predominantly associated with cytoskeletal and mitosis-related proteins (Fang et al., 2019; Fuchs et al., 2015; Vallin and Grantham, 2019). For example, Hsp70 is involved in microtubule nucleation, maturation of functional mitotic centrosomes, and centrosome clustering in cancer cells (Fang et al., 2019). It also protects centrosomes during heat shock and ensures the stability of kinetochore-microtubule and the integrity of the mitotic spindle (Fang et al., 2019).

Protein synthesis is delicately regulated during cell division. For instance, transcription of certain genes remains active while others are repressed (Palozola et al., 2017). In addition, translation is generally attenuated in dividing cells (Tanenbaum et al., 2015), leading to a slightly overall decrease in protein synthesis during mitosis (Miettinen et al., 2019). Although the mechanisms by which dividing cells adjust their protein synthesis rates have been increasingly elucidated, it remains unclear whether these regulatory adaptations support or compromise proteostasis. Although cells are known

to attenuate protein synthesis in response to stress, such as endoplasmic reticulum (ER) stress (Acosta-Alvear et al., 2025; Wiseman et al., 2022), it has been less thoroughly investigated whether similar mechanisms operate during cell division.

It has become increasingly evident that the ubiquitin-proteasome system (UPS) is crucial for regulating key mitotic processes. Specifically, research indicates that the UPS modulates three principal classes of mitotic kinases in eukaryotes, namely Cdk1, Aurora, and Plk1 (Carlton et al., 2020; Nigg, 2001). These regulations are essential for the orderly progression of cell division and the extensive reorganization of cellular organelles. Given the significant demand on the UPS during mitosis, it is conceivable that additional misfolded proteins induced by external stressors, such as heat shock, could overwhelm the system, which is a possibility that remains underexplored in dividing mammalian cells.

If critically summarizing current understanding about studies concerning proteostasis regulation in mitotic cells, these studies majorly provided evidence about unconventional and suspicious functions of elements in proteostasis networks. However, the specific roles of these elements in eliminating misfolded protein aggregates in dividing mammalian cells remain largely unexplored, as does the distinction between proteostasis maintenance in interphase versus mitotic cells.

To address these gaps, I employed a firefly luciferase (Fluc) proteostasis reporter system, in which misfolding-prone Fluc mutants were tagged with a fluorescent protein and expressed in human cells (Gupta et al., 2011). Fluc aggregation was then profiled to elucidate how cellular proteostasis machineries eliminate misfolded proteins during mitosis.

3.2 Results

3.2.1 Validation of FlucDM reporter system in MCF10A cells

To examine whether Fluc system could report proteostasis in live cells, I generated fusion constructs of enhanced green fluorescent protein (eGFP) with firefly luciferase in three variants: wild-type (FlucWT), single-mutant (FlucSM), and double-mutant (FlucDM). FlucSM is more prone to misfolding compared to FlucWT, and FlucDM exhibits an higher propensity for misfolding than FlucSM (Gupta et al., 2011). These constructs were stably expressed in human breast epithelial MCF10A cells.

To test which constructs were more prone to aggregate, cells were treated with the proteasome inhibitor MG132 to inhibit protein degradation and disrupt proteome stability. Upon inhibition of proteasomes, misfolded Fluc formed aggregates in cells. Indeed, FlucSM-eGFP and FlucDM-eGFP assembled into bright green aggregates while eGFP signals from FlucWT-eGFP were still evenly distributed after 7 h of MG132 treatment **(Figure 3.1)**. Moreover, strong GFP signals were detected at perinuclear dot structures **(Figure 3.1)**, which were similar to the centrosome, a deposition site for misfolded proteins (Johnston et al., 1998; Kopito, 2000). Since FlucDM was more likely to misfold than FlucSM (Gupta et al., 2011), FlucDM was used in the following experiments of this chapter to ensure high sensitivity of detection.

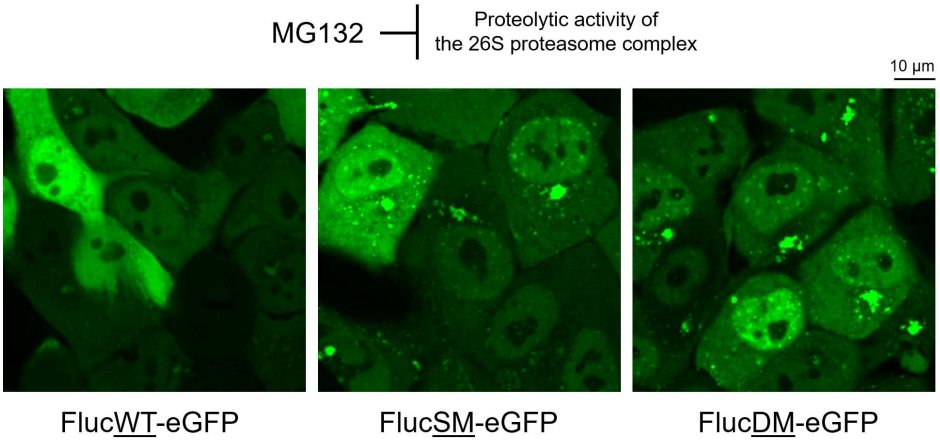


Figure 3.1: The Fluc proteostasis reporter in MG132-treated cell. MCF10A cells expressing three Fluc constructs. Cells were treated by 5 μM MG132 for 7 hours. Single Z-slice images were shown.

3.2.2 Aggregation of FlucDM-eGFP in dividing cells under heat shock

To further test whether the FlucDM-eGFP system was able to report proteostasis upon short-term proteostasis stress, cells were subjected to heat shock to perturb proteome stability. Upon heat shock, dividing cells accumulated FlucDM-eGFP aggregates **(Figure 3.2)**. Taken together, FlucDM-eGFP reliably reported the proteome stability in dividing cells and was used to study how protein synthesis, folding and degradation machineries are involved in protein aggregation during mitosis.

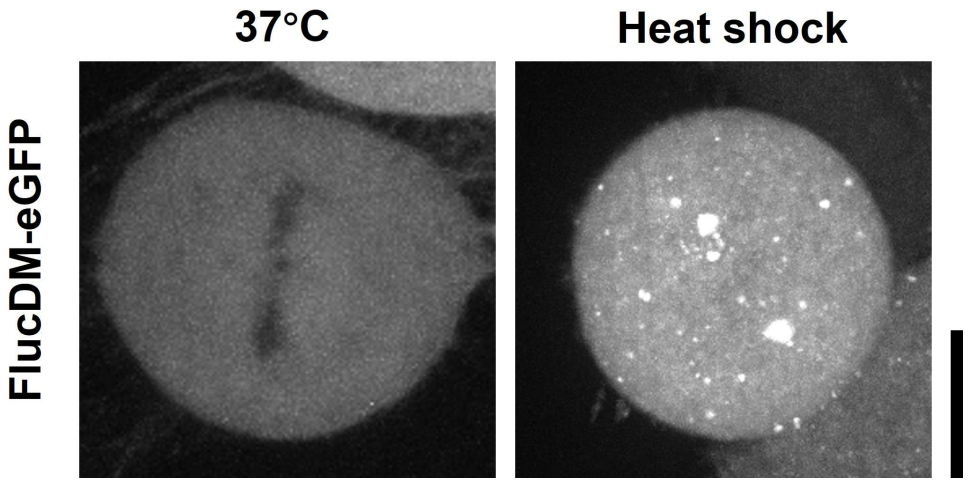


Figure 3.2: Mitotic MCF10A cells expressing FlucDM-eGFP upon heat shock. Left, cells cultured at 37°C; Right, cells upon exposure to 42°C for 20 min. Maximum projected images were shown. Scale bar, 10 μm.

3.2.3 Inhibition of protein translation decreases protein aggregation in dividing cells upon heat shock

Although the proteome in mitotic cells is more thermally stable than in interphase cells (Becher et al., 2018; Wirth et al., 2013), protein aggregation still happens upon heat shock **(Figure 3.2)**. It is unknown whether newly synthesized proteins in mitotic cells contribute to aggregations. To test this, cells synchronized at the G2/M boundary were released into medium containing either DMSO or cycloheximide (CHX), which inhibited protein translation in dividing cells. Upon entry into mitosis, cells expressing FlucDM-eGFP were subjected to heat shock at 42°C for 20 min to induce protein aggregation. Then, the aggregates were counted in dividing cells. Upon heat shock, cells accumulated fewer aggregates in the presence of CHX, suggesting that protein aggregation during mitosis involves newly synthesized proteins **(Figure 3.3)**.

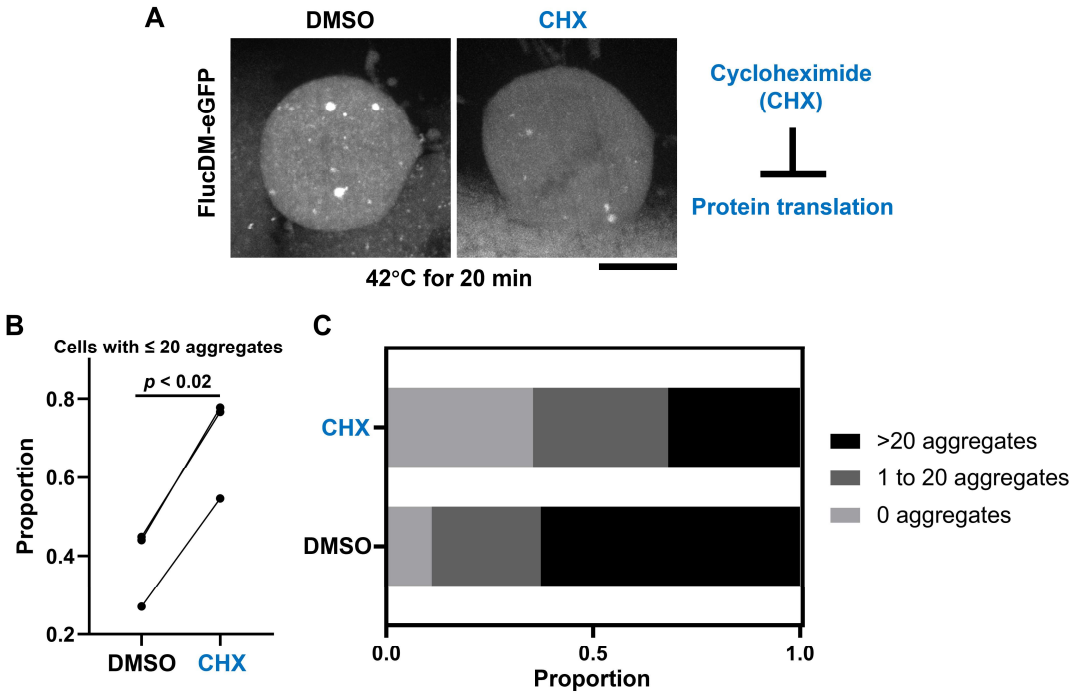


Figure 3.3: Effects of cycloheximide on protein aggregation in dividing cells. (A) Representative images of dividing MCF10A cells treated with DMSO or 200 μM CHX upon heat shock at 42°C for 20 min. Maximum projected images were shown. Scale bar, 10 μm. **(B)** Proportion of cells with less than twenty protein aggregates upon heat shock. Data were collected from three independent experiments. Statistical significance was measured by t-test. DMSO, 66 cells; CHX, 74 cells. **(C)** Distribution of dividing cells assembling different amounts of protein aggregates upon heat shock. DMSO, 66 cells; CHX, 74 cells.

3.2.4 Hsp70 ATPase inhibition increases protein aggregation in heat-shocked mitotic cells

Heat shock protein 70 (Hsp70) family members assist in refolding misfolded proteins and disassembling protein aggregates (Radons, 2016). Thus, Hsp70 might also function in mitotic cells to regulate the aggregation of FlucDM. To determine this, VER-155008 (VER), an Hsp70 ATPase inhibitor, was used to treat mitotic cells. Results demonstrated that there were more aggregates in cells treated with both VER-155008 and heat shock compared to cells treated only with heat shock **(Figure 3.4)**. Thus, Hsp70 prevented the aggregation of FlucDM-eGFP in mitotic cells.

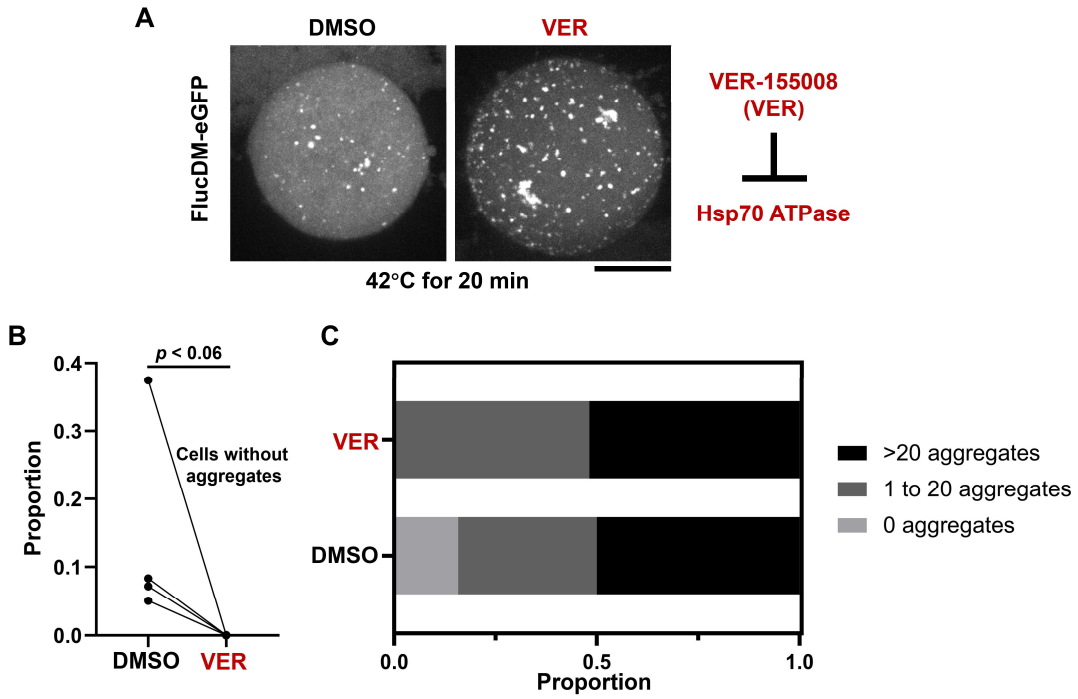


Figure 3.4: Effects of VER-155008 on protein aggregation in dividing cells. (A) Representative images of dividing cells treated with DMSO or 50 μM VER upon heat shock at 42°C for 20 min. Maximum projected images were shown. Scale bar, 10 μm. **(B)** Proportion of cells without protein aggregates upon heat shock. Data were collected from four independent experiments. Statistical significance was measured by t-test. DMSO, 76 cells; VER, 108 cells. **(C)** Distribution of dividing cells assembling different amounts of protein aggregates upon heat shock. DMSO, 76 cells; VER, 108 cells.

3.2.5 26S proteasome inhibition by MG132 increases protein aggregation in heat-shocked mitotic cells but only MG132 does not induce protein aggregation in mitotic cells

The proteasome is the master regulator of protein degradation (Li et al., 2022). Also, it regulates the sequential progression of cell division (Carlton et al., 2020; Nigg, 2001). However, it remains unclear whether the elimination of misfolded proteins requires proteasomes in mitotic cells. To examine this, MG132, a proteasome inhibitor, was employed to treat mitotic cells expressing FlucDM-eGFP. MG132 is known to arrest dividing cells in metaphase by inhibiting the degradation of several key metaphase-anaphase transition proteins (such as cyclin B1 for mitotic exit and securin for chromatid separation). As expected, all dividing cells observed were arrested with the round shape at metaphase in MG132 group, suggesting MG132 successfully inhibits

proteasome activity **(Figure 3.5)**. Interestingly, the GFP signal in these cells was more homogeneous than that in interphase cells and no visible aggregates were detected under confocal microscopy **(Figure 3.5)**.

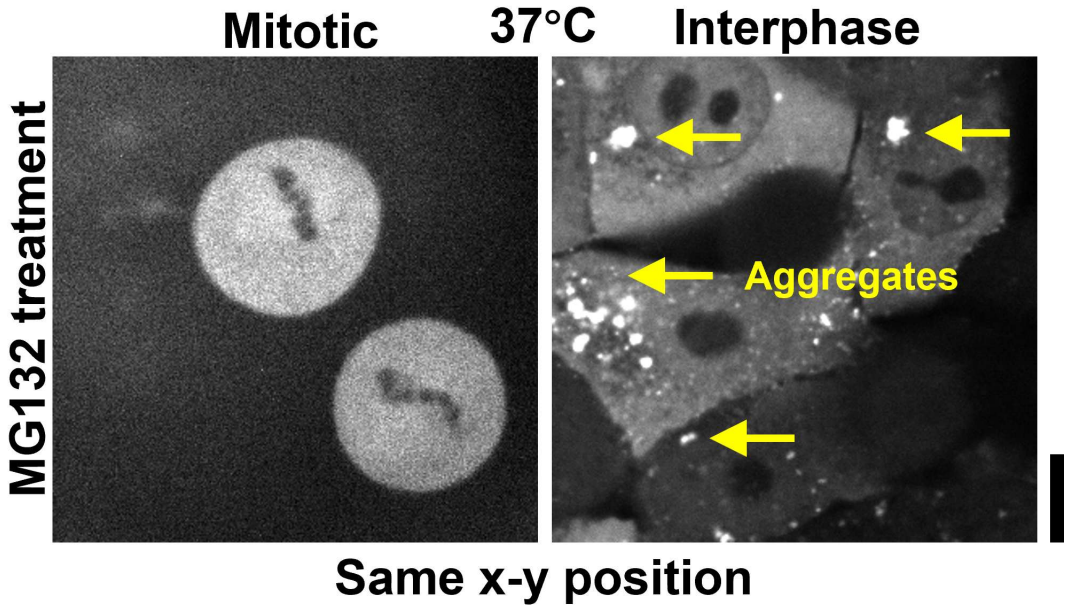


Figure 3.5: MG132 induces protein aggregation in interphase cells but not in mitotic cells. Representative images of MCF10A cells expressing FlucDM-eGFP treated with 5 μM MG132 for 4 hours. The phenotypes of all cells are similar to those shown in this image. Single Z-slice images were shown. Scale bar, 10 μm.

This unexpected observation could be explained by the fact that proteasome inhibition also attenuates protein synthesis through regulating protein translation (Liu et al., 2013). Thus, it is speculated that few misfolded proteins were synthesized upon the treatment of MG132. This active response led to a challenge in studying the role of the proteasome in the elimination of misfolded protein aggregates because the attenuation of protein synthesis limits the occurrence of protein aggregation.

To overcome this, heat shock was employed to induce global protein misfolding in MG132-arrested cells. Upon heat shock, there were more aggregates in dividing cells treated with MG132 than in cells treated with DMSO, suggesting that the proteasome assists in eliminating misfolded proteins in dividing cells **(Figure 3.6)**.

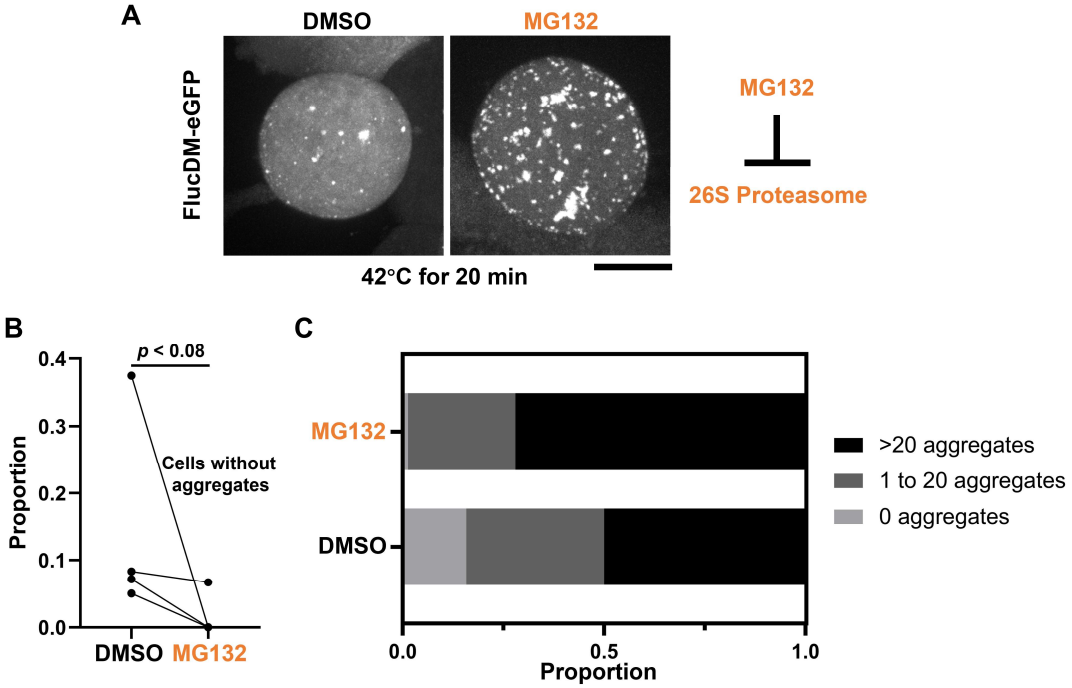


Figure 3.6: Effects of MG132 on protein aggregation in mitotic cells upon heat shock. (A) Representative images of dividing cells treated with DMSO or 5 μM MG132 upon heat shock at 42°C for 20 min. Cells were released with medium containing DMSO or MG132 before heat shock treatment. Maximum projected images were shown. Scale bar, 10 μm. **(B)** Proportion of cells without protein aggregates upon heat shock. Data were collected from four independent experiments. Statistical significance was measured by t-test. DMSO, 76 cells; MG132, 75 cells. **(C)** Distribution of dividing cells assembling different amounts of protein aggregates upon heat shock. DMSO, 76 cells; MG132, 75 cells.

To further exclude the participation of protein synthesis in dividing cells, G2/M-arrested cells were released in medium containing CHX or a combination of CHX and MG132 prior to heat shock. Similar to the only MG132 treatment, there were more FlucDM-eGFP aggregates in cells simultaneously treated with CHX and MG132 **(Figure 3.7)**. This indicated that the proteasome indeed participates in the elimination of misfolded proteins and subsequently decreased their aggregation in dividing cells.

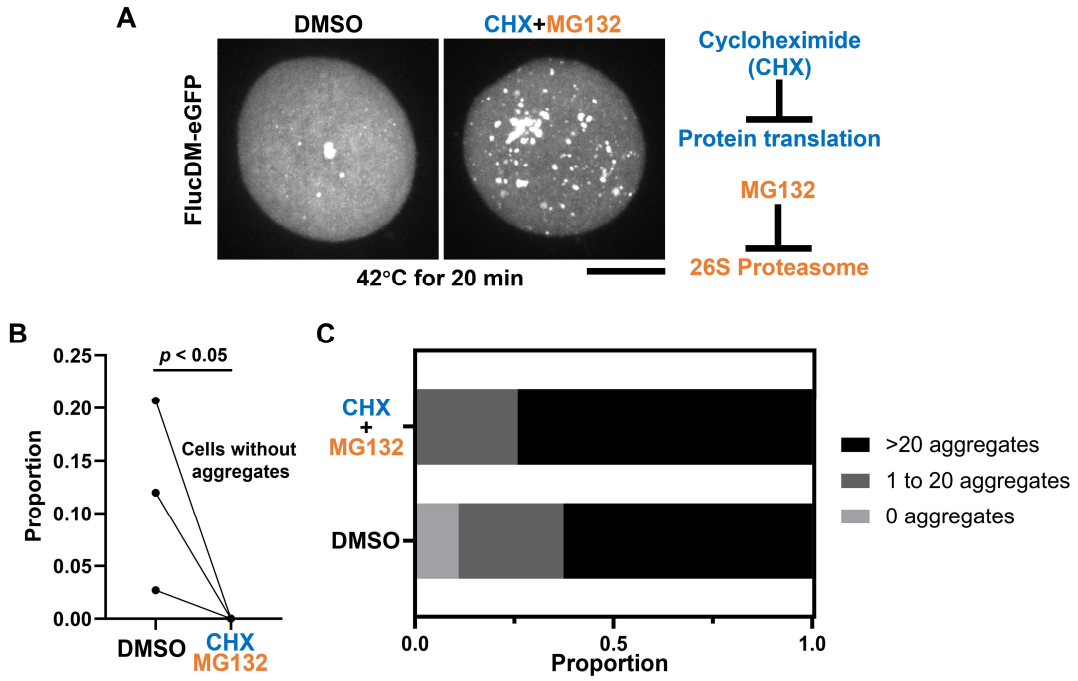


Figure 3.7: Effects of combined MG132 and CHX treatment on protein aggregation in mitotic cells upon heat shock. (A) Representative images of dividing cells treated with DMSO or 5 µM MG132 with 200 µM CHX upon heat shock at 42°C for 20 min. Cells were released with medium containing DMSO or MG132 with CHX before heat shock treatment. Maximum projected images were shown. Scale bar, 10 µm. **(B)** Proportion of cells without protein aggregates upon heat shock. Data were collected from three independent experiments. Statistical significance was measured by t-test. DMSO, 76 cells; CHX + MG132, 61 cells. **(C)** Distribution of dividing cells assembling different amounts of protein aggregates upon heat shock. DMSO, 76 cells; CHX + MG132, 61 cells.

3.2.6 ER stress inducers relieve protein aggregation in heat-shocked mitotic cells

Previous studies demonstrated that ER stress induced by calcium ion depletion attenuates protein translation (Hetz et al., 2020; Karagöz et al., 2019). However, whether a similar mechanism exists in dividing cells remains less explored. To examine this, thapsigargin (Thaps) and calcimycin (Cal) were employed to induce ER stress. Upon heat shock, fewer protein aggregates were found in dividing cells treated with Thaps and Cal **(Figure 3.8)**. Thus, as in interphase, cells might also attenuate protein synthesis upon ER stress induction during mitosis.

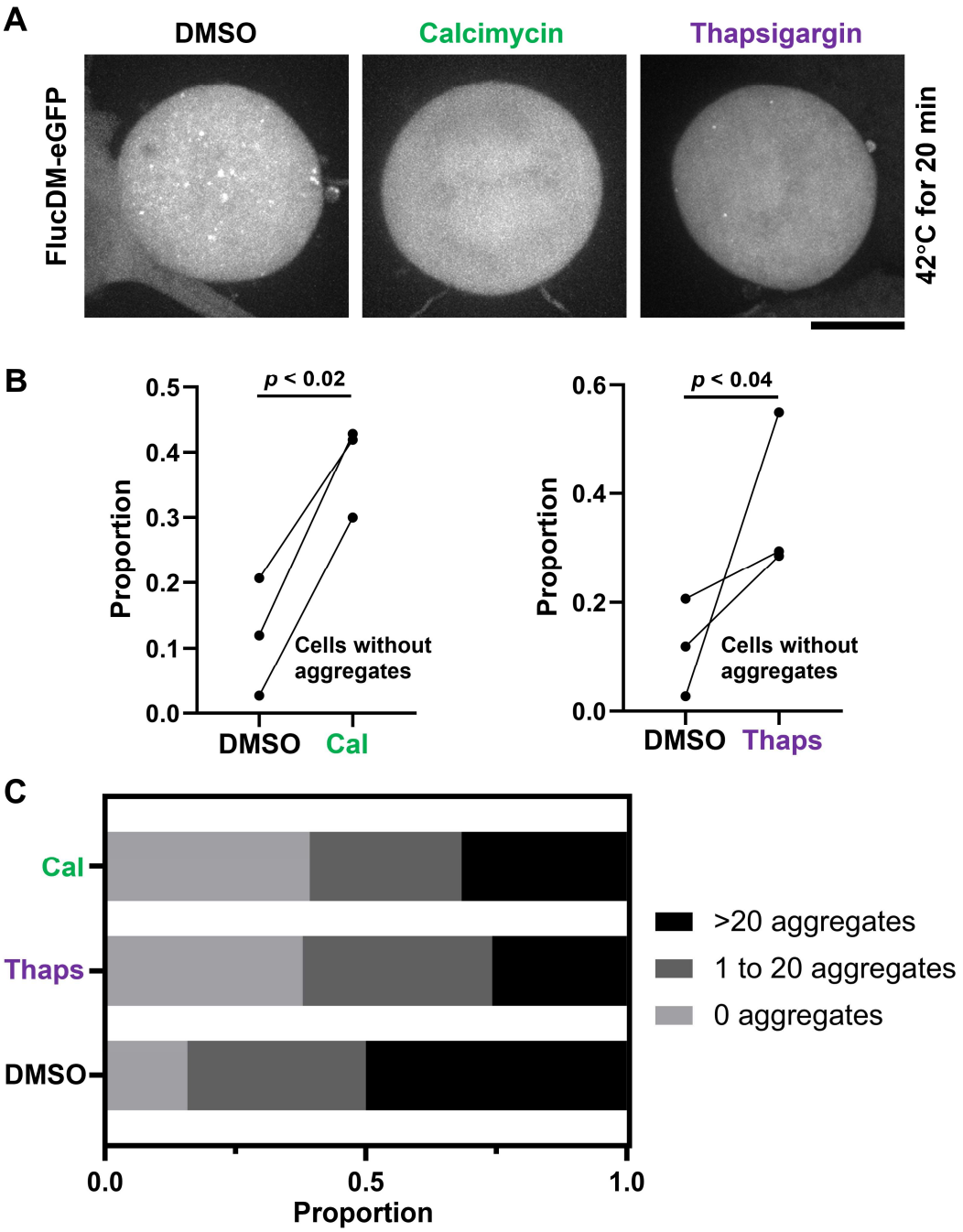


Figure 3.8: Effects of ER stress inducers, calcimycin or thapsigargin, on protein aggregation in mitotic cells upon heat shock. (A) Representative images of dividing cells treated with DMSO or 1 μM Cal or 1 μM Thaps upon heat shock at 42°C for 20 min. Cells were released with medium containing DMSO or Thap. Cal was added into medium 15 min after release because cells were arrested if releasing with Cal. Maximum projected images were shown. Scale bar, 10 μm. **(B)** Proportion of cells without protein aggregates upon heat shock. Data were collected from three independent experiments. Statistical significance was measured by t-test. DMSO, 74 cells; Cal, 79 cells; Thaps, 44 cells. **(C)** Distribution of dividing cells assembling different amounts of protein aggregates upon heat shock. DMSO, 74 cells; Cal, 79 cells; Thaps, 44 cells.

3.3 Discussion

3.3.1 Summary of results in this chapter

The regulation of proteostasis (protein homeostasis) in mammalian cells undergoing symmetric division is largely unknown. In this chapter, there are two aims. The first aim is to verify if Fluc proteostasis reporter is able to correctly monitor proteostasis stress in dividing cells. The second aim is to preliminarily study how mammalian cells maintain proteostasis during mitosis.

To achieve the first aim, Fluc reporter constructs were expressed in the MCF10A cell line to monitor proteostasis. Aggregation of FlucDM-eGFP occurred in mitotic cells upon heat shock, indicating that the FlucDM system correctly reports proteostasis stress in symmetrically dividing cells. To achieve the second aim, small-molecule drugs were utilized to inhibit protein translation, chaperone function or protein degradation in cells subjected to heat shock. The inhibition of protein translation with cycloheximide and the induction of ER stress with thapsigargin or calcimycin both reduced FlucDM-eGFP aggregation. Furthermore, inhibiting protein degradation by proteasome inhibitor MG132 and suppressing chaperone activity by the Hsp70 ATPase inhibitor VER-155008 increased the quantity of FlucDM-eGFP aggregates upon heat shock. Therefore, mitotic cells utilize similar components to regulate their proteostasis as interphase cells do.

Unexpectedly, upon the treatment of MG132, mitotic cells did not exhibit any visible FlucDM-eGFP aggregates, while obvious aggregation was observed in adjacent interphase cells. For this surprising observation, there were two points worth discussing: how to validate it, and how to explain it? The discussion of the second point leads to the focus of the next two chapters.

3.3.2 How to further verify only MG132 does not induce visible protein aggregates in mitotic cells?

In my study, FlucDM-eGFP was used as a reporter for proteostasis in live cells. More

protein aggregates of FlucDM-eGFP indicates that cells experience a higher level of proteome stress. While proteasome inhibition is known to induce proteome stress, it can also promote the assembly of stress granules (Mazroui et al., 2007), which are morphologically similar to misfolded protein aggregates. Furthermore, stress granules are able to co-aggregate with misfolding-prone proteins (Mateju et al., 2017; Wu et al., 2024). Is it possible that the aggregation of FlucDM-eGFP is the consequence of stress granule assembly in my study? It is unlikely because ER stress inducers such as thapsigargin also induce the formation of stress granules (Wheeler et al., 2016). However, in my study, thapsigargin did not facilitate the aggregation of FlucDM-eGFP. On the contrary, ER stress inducers in my study decrease the quantity of protein aggregates induced by heat shock in mitotic cells. Thus, it is highly possible that the aggregation of FlucDM-eGFP in my study solely results from the accumulation of misfolded proteins and the exhaustion of protein quality control factors in mitotic cells. To further validate this, other misfolding-prone proteins such as destabilizing retro-aldolase could be expressed in cells prior to MG132 treatment during mitosis (Liu et al., 2015).

3.3.3 How to explain why MG132 does not induce protein aggregates in mitotic cells?

There are two potential interpretations to explain why MG132 fails in causing the aggregation of FlucDM-eGFP in mitotic cells:

Firstly, the reduced accumulation of misfolded protein aggregates may be explained by the intertwined regulations in the proteostasis network. To be specific, stress imposed on the protein degradation system can regulate the rate of protein synthesis. Previous studies reported that ubiquitin-proteasome system inhibition attenuated global translation by undermining initiation and pausing elongation in cells globally (Jiang and Wek, 2005; Liu et al., 2013). This explains why MG132 alone fails to induce the aggregation of FlucDM-eGFP in mitotic cells, however, this can’t explain why MG132 induces protein aggregates in nearby interphase cells. To explain this difference, it is

possible that the suppression of protein synthesis is more pronounced in mitotic cells upon proteasome inhibition, resulting in fewer aggregates. How do mitotic cells realize this delicate control?

A recent study demonstrated that microtubule disassembly or inhibition of anaphase promoting complex/cyclosome (APC/C) decreases protein synthesis rate to about 40% in mitotic cells but has neglectable effects in interphase cells (Miettinen et al., 2019). Similar treatment that causes mitotic arrest is shown to decrease protein translation rate (Stonyte et al., 2018). This suggests the lack of protein aggregation in MG132-treated mitotic cells might result from the attenuation of protein synthesis upon metaphase arrest. However, protein synthesis attenuation caused by metaphase arrest is less studied and the underlying mechanisms are largely unknown.

Phosphorylation of the α subunit of eukaryotic initiation factor 2 (eIF2α) increases upon nocodazole-induced mitotic arrest (Coldwell et al., 2013; Stonyte et al., 2018). The phosphorylation of eIF2α inhibits global protein translation (Preissler and Ron, 2019). Thus, is it possible that mitotic-arrested cells decrease protein synthesis by increasing the phosphorylation of eIF2α? It is unlikely. Mitotic arrest induced by S-Trityl-L-cysteine attenuates protein synthesis (Miettinen et al., 2019), however, it does not increase the phosphorylation level of eIF2α (Ly et al., 2024). Additionally, upon similar treatment of microtubule disassembly, elevated phosphorylation of eIF2α is reported in studies that do not distinguish between interphase and mitotic cells (Balsamo et al., 2022; Senovilla et al., 2012). In my study, ER stress induction decreased the aggregation of FlucDM-eGFP in both mitotic and interphase cells. Therefore, the failure of MG132 to induce protein aggregation in mitotic cells cannot be solely attributed to metaphase arrest-induced eIF2α phosphorylation and the subsequent attenuation of translation.

The second interpretation to explain why MG132 does not induce the aggregation of FlucDM-eGFP in mitotic cells is that mitotic cells are intrinsically less likely to

assemble misfolded protein aggregates. Protein aggregation requires locally enriched misfolded proteins (Majid and Khan, 2023), however, this enrichment might be difficult to achieve during cell division. Previous studies proposed that cells absorb water and ions upon entering mitosis, subsequently diluting the cytoplasm (Son et al., 2015; Stewart et al., 2011). Indeed, the viscosity of the cytoplasm decreases while its fluidity increases upon entering mitosis (Hurst et al., 2021). Given these alterations in the physical properties of the cytoplasm, it is speculated that less protein aggregation would occur. A previous study proposed that morphological deformation in migrating cells increase cytoplasmic flow and organelle movement (Koslover et al., 2017). During mitosis, the morphology of cells drastically changes and extensive organelle reorganization events occur (Carlton et al., 2020), thereby potentially facilitating the homogenization of cytoplasmic contents and subsequently mitigating protein aggregation.

3.3.4 The speculation on protein aggregates in the ER during cell division

MG132 does not induce misfolded protein aggregates in mitotic cells, which can potentially be explained by organelle remodeling during mitosis. Is it possible that this hypothetical explanation can be applied to other situations? The size of protein condensates in the ER is limited by ER tubules (Parashar et al., 2021). During mitosis, the structure of the ER preferentially changes from sheets to tubules (Kors and Schlaitz, 2024). Thus, it is speculated that less protein aggregation also occurs in the ER of mammalian dividing cells. This hypothesis will be examined in the next two chapters.

Chapter 4 ER-Targeted Proteins Form Aggregates in the Nucleus

4.1 Introduction

The endoplasmic reticulum (ER) participates in the post-translational modification, folding and transport of secretory proteins such as cytokines and hormones in cells (Wiseman et al., 2022). Approximately one-third of the proteome in cells is processed in the ER (Wright and Plate, 2021). To maintain a functional proteome, cells employ a specialized proteostasis network known as ER quality control (ERQC) (Vincenz-Donnelly and Hipp, 2017). Similar to the global proteostasis network, ERQC is also classified into four categories: protein synthesis, protein folding and conformational maintenance, protein degradation, and the compartmentalization of misfolded proteins. The following section briefly introduces these four categories.

During protein synthesis, the signal sequence from newly synthesized polypeptides or the non-coding elements in their mRNA is recognized by the signal recognition particle (SRP) (Akopian et al., 2013; Chartron et al., 2016). Then SRP decreases translation speed (Walter and Blobel, 1981) and directs polypeptides to the translocon in the ER membrane. Once the SRP arrives at the translocon, translation is rescued and these polypeptides start to be imported into the luminal space of the ER (Akopian et al., 2013).

In the ER lumen, four dominant categories of molecular chaperones assist in the posttranslational modification and correct folding. Firstly, N-glycosylation determines most secretory proteins and is one of the major functions of the ER (Aebi, 2013). For these nascent glycoproteins, the calnexin/calreticulin (CANX/CRT) chaperone system recognizes their glycans, assists in correct folding, retains unfolded species in the ER, avoids their aggregation and premature ER exit (Rutkevich and Williams, 2011). Secondly, the folding of non-glycosylated proteins is majorly facilitated by binding immunoglobulin protein (BiP) with the help of ERdj proteins (ERdj is the Hsp40 in the ER and co-chaperones for BiP) (Pobre et al., 2019). Thirdly, disulfide bonds formation

is critical for the correct folding of numerous proteins (Wang and Wang, 2023). In the ER, disulfide bonds-dependent protein folding is facilitated by ER-localized oxidoreductases including the family of protein disulfide isomerases (PDI) and ER sulfhydryl oxidase 1 (Wang and Wang, 2023). Fourthly, glucose response protein 94 (GRP94) assists in the folding of a tiny fraction (fewer than twenty) of proteins in the ER, acting as the Hsp90 in the ER (Marzec et al., 2012).

Misfolded proteins are identified and removed from the ER by ER-assisted degradation (ERAD) and ER-phagy (Wiseman et al., 2022). For ERAD, substrate proteins are identified, transported to the ER membrane, transferred to the cytosol by retro-translocation channels, polyubiquitinated and finally degraded by the proteasome (Wu and Rapoport, 2018). As a parallel misfolded protein degradation system, ER-phagy takes the responsibility for the removal of misfolded proteins and their aggregates. During ER-phagy, misfolded proteins are sequestered into specific subdomains in the ER, allowing ER-phagy receptors to deliver them to the lysosome for degradation (Mochida and Nakatogawa, 2022).

The ER from dividing budding yeast cells hinders the diffusion of misfolded proteins from the mother cell to the daughter cell by regulating the septin ring at the bud neck. These strategies are known as ER stress surveillance (ERSU) and ER diffusion barrier (Clay et al., 2014; Piña and Niwa, 2015). Furthermore, the ER also actively responds to stress by the unfolded protein response (UPR). UPR is a signal transduction pathway which decreases global protein translation to ameliorate protein folding problems, upregulates specific genes to enhance protein folding and degradation capability, and induces apoptosis if UPR is overwhelmed (Acosta-Alvear et al., 2025).

It is well established how cells respond to ER stress. However, the fate of protein aggregates during cell division, especially in cells that undergo symmetric division, remains largely unknown. In this chapter, FlucDM-eGFP is targeted to the ER (ER-FlucDM-eGFP). Unexpectedly, ER-FlucDM-eGFP assembles into protein aggregates

in the cell nucleus and these aggregates are encapsulated by the ER membrane. The studies in this chapter mainly examine the properties of these aggregates. Additionally, the dynamics of these aggregates are higher in mitotic cells than in interphase cells, prompting a detailed investigation of the fate of these aggregates during cell division in the Chapter 5.

4.2 Results

4.2.1 ER-FlucDM-eGFP is largely soluble as revealed by western blot

To study how the endoplasmic reticulum (ER) maintains proteostasis during cell division, the FlucDM-eGFP reporter was fused with an N-terminal ER targeting sequence (amino acid sequence: MGWSCIILFFVATAT) and a C-terminal ER-resident protein retro-transport sequence (amino acid sequence: KDEL) (Sharma et al., 2018) **(Figure 4.1A)**.

For FlucDM without specific targeting sequences, its solubility decreases upon heat shock treatment, ensuring its role as a proteostasis reporter (Gupta et al., 2011). To measure the solubility of ER-FlucDM-eGFP in cells, MCF10A cells expressing the reporter were lysed using buffers with various concentrations of NP-40 (v/v). After centrifugation, the supernatant was collected as the soluble fraction. The remaining pellet was then treated with the lysis buffer containing the stronger detergent lithium dodecyl sulfate (LDS), and was regarded as the insoluble fraction.

Unexpectedly, in cells growing at 37°C, ER-FlucDM-eGFP was only detected in the soluble pool regardless of the concentration of NP-40 **(Figure 4.1B and 4.1C)**. This suggested that ER-FlucDM-eGFP in cells is mainly soluble. Previous studies reported that the ER possesses high capability to maintain the solubility of proteins (Rousseau et al., 2004; Vincenz-Donnelly et al., 2018). In my study, the percentage of soluble ER-FlucDM-eGFP was more than 98% (98.5% for 0.2% NP-40; 98.4% for 0.5% NP-40; 98.7% for 1% NP-40), which is intuitively too high for misfolding-prone proteins. This raises a question of whether this lysis buffer system based on NP-40 and LDS correctly differentiates soluble and insoluble fractions of ER-FlucDM-eGFP. To address this, heat shock treatment was used to induce ER-FlucDM-eGFP misfolding. Upon heat shock treatment at 45°C, the insoluble fraction of ER-FlucDM-eGFP increased **(Figure 4.1B)**. Moreover, insoluble fraction of ER-FlucDM-eGFP increased with the decrease of NP-40 concentration **(Figure 4.1C)**. This indicated that the lysis buffer with lower concentration of NP-40 has a reduced ability to dissolve misfolded proteins and

subsequently leaves more undissolved ER-FlucDM-eGFP in the insoluble fraction before being dissolved by the LDS lysis buffer.

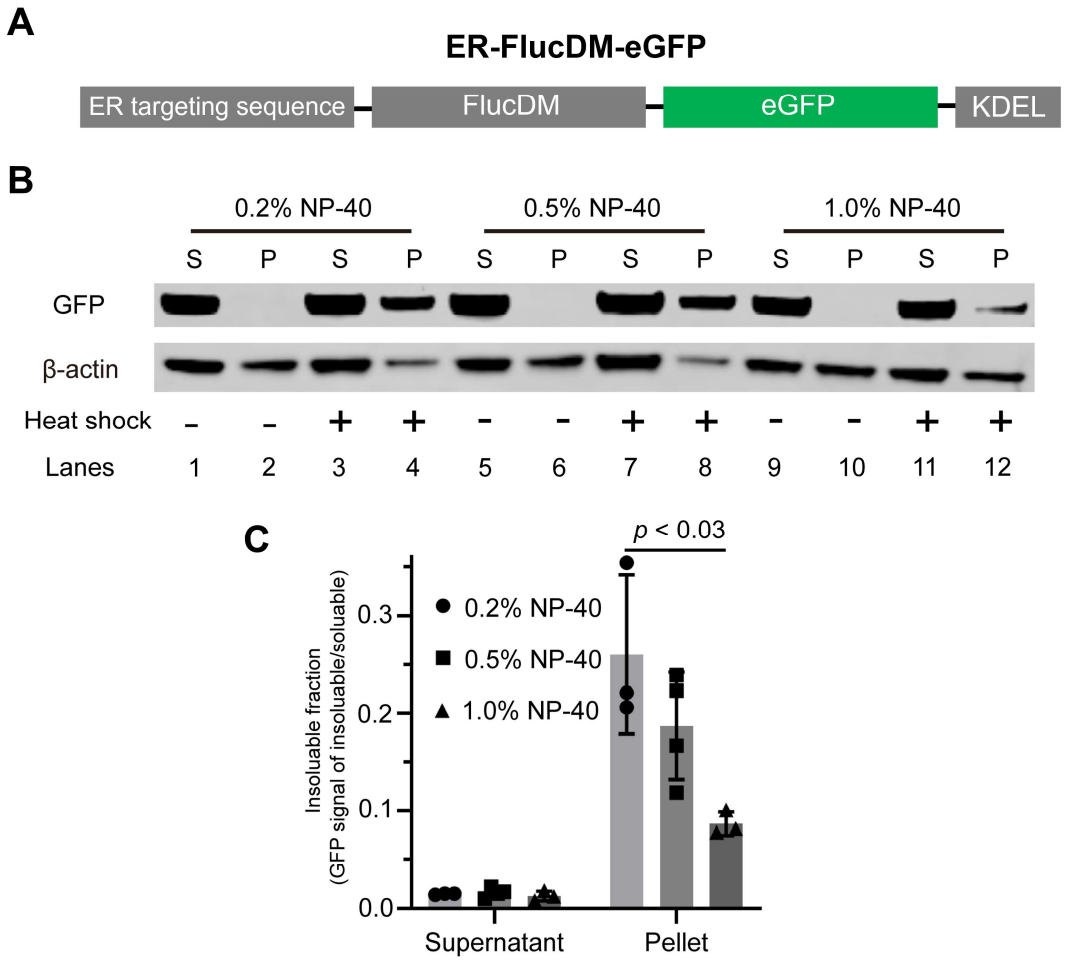


Figure 4.1: ER-FlucDM-eGFP is largely soluble, as revealed by protein immunoblotting. (A) The construct details of ER-FlucDM-eGFP. **(B)** Protein immunoblotting to profile the solubility of ER-FlucDM-eGFP in diverse concentrations (v/v) of NP-40. In heat shock experiments, MCF10A cells expressing ER-FlucDM-eGFP were exposed to 45 °C for 1 h, followed by cell lysate collection. **(C)** Quantification of the insoluble fractions from supernatant or pellet were quantified and plotted. Data were collected from at least three independent experiments and represented as the mean ± SD. Unpaired t-test was used.

4.2.2 ER-FlucDM-eGFP is less functional proved by luciferase activity test

Luciferase enzymatic activity of FlucDM is lower than FlucWT (firefly luciferase wild-type) because of the double destabilizing mutations (Gupta et al., 2011). This decreased luciferase activity indicates the misfolding-prone state of FlucDM, guaranteeing its role as a proteostasis reporter.

To further test the properties of ER-FlucDM-eGFP in my system, luciferase activity test was employed (Gupta et al., 2011). Before measuring luciferase activity of ER-FlucDM-eGFP, this method was first validated by treating cells expressing FlucDM-eGFP with DMSO or the proteasome inhibitor MG132. Results showed that MG132 treatment significantly decreased the luciferase activity of FlucDM-eGFP as previously reported **(Figure 4.2)** (Gupta et al., 2011). After validating this method, luciferase activities of ER-FlucWT-eGFP and ER-FlucDM-eGFP were compared. Luciferase activity of ER-FlucDM-eGFP was significantly lower than ER-FlucWT-eGFP **(Figure 4.2)**. This indicated that FlucDM in ER-FlucDM-eGFP is less functional than FlucWT, suggesting ER-FlucDM-eGFP is prone to misfolding in MCF10A cells.

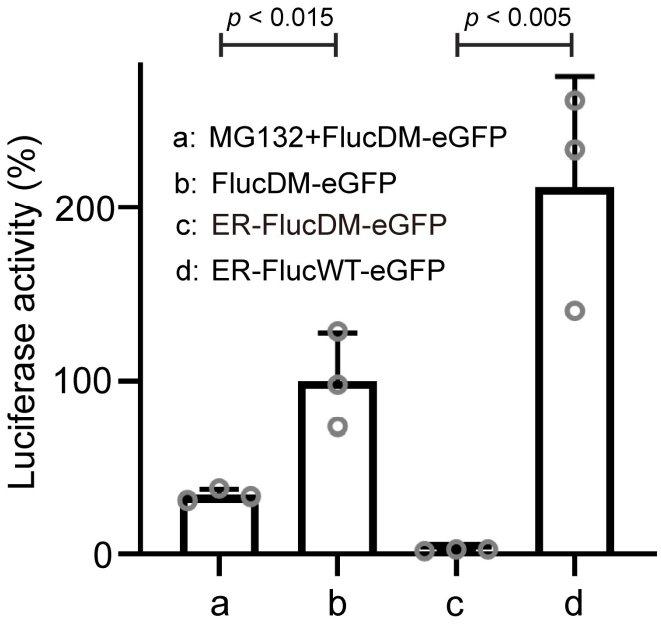


Figure 4.2: ER-FlucDM-eGFP is less functional revealed by luciferase activity test. Relative luciferase activity in MCF10A cells expressing various constructs. The expression level of GFP-fused proteins was determined using protein blotting and was used to normalize the relative activity of luciferase. Unpaired t-test was used. Data were collected from three independent experiments and represented as the mean + SD.

4.2.3 ER-FlucDM-eGFP forms protein aggregates in the cell nucleus while being surrounded by ER membranes

Interestingly, when stably expressed in mammary epithelial MCF10A cells, ER-FlucDM-eGFP spontaneously assembled into visible protein aggregates in the cell nucleus **(Figure 4.3A)**, although the ER network portions of ER-FlucDM colocalized with an ER membrane marker **(Figure 4.3B)**. These aggregates started to appear in the first 1.5 days after lentivirus transduction and gradually accumulated in cells before achieving equilibrium several days after transduction.

To examine whether these aggregates were indeed in the nucleus, transmission electron microscopy (TEM) was utilized to observe sectioned cells. Several single membrane-encapsulated electron dense areas were found in the nucleus and they were close to the nuclear envelope, indicating aggregates assembled by ER-FlucDM-eGFP indeed invaginate into the cell nucleus **(Figure 4.3B)**.

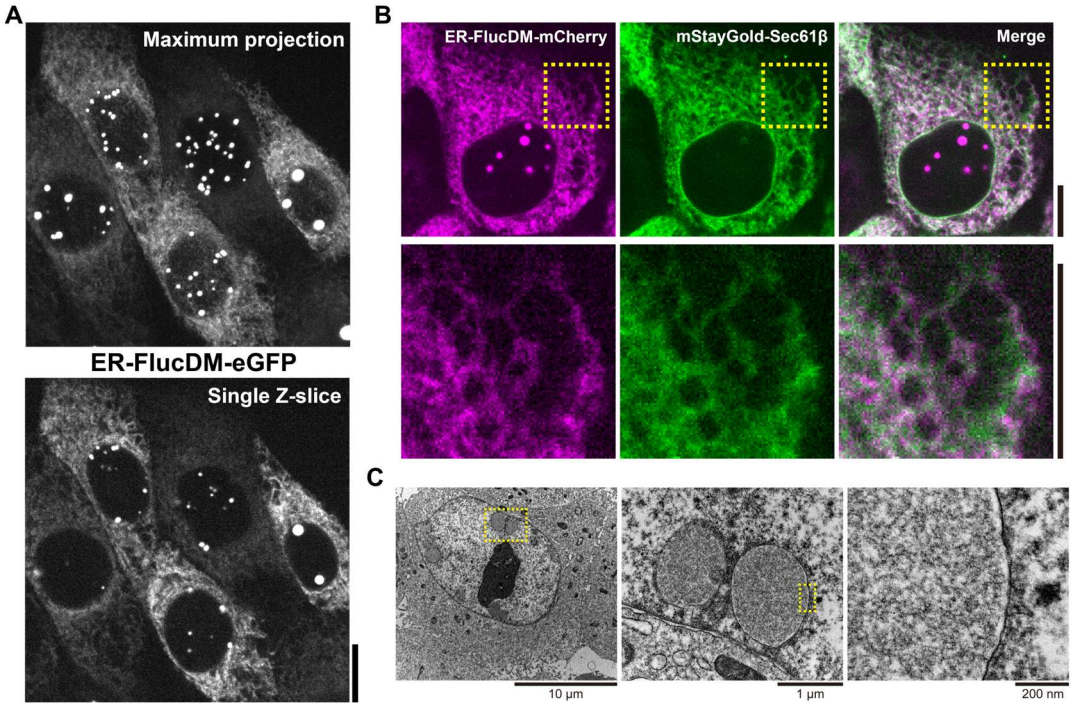


Figure 4.3: ER-FlucDM-eGFP assembles into protein aggregates in the cell nucleus. (A) ER-FlucDM-eGFP expressed in MCF10A cells. GFP signals were acquired by confocal microscopy. Scale bar, 10 μm. **(B)** Microscopy images of cells expressing ER-FlucDM-mCherry and mStayGold-Sec61β. Single Z-slice images were shown. Scale bar, 10 μm. **(C)** TEM images of sectioned MCF10A interphase cells expressing ER-FlucDM-eGFP.

The appearance of ER structures inside the nucleus is not a totally novel observation. Previous studies also identified some ER structures invaginating into the nucleus and these structures are termed the nucleoplasmic reticulum (NR) (Fricker et al., 1997; McPhee et al., 2024).

Given this invagination occurs from the ER to the cell nucleus, the NR membrane is commonly labelled by ER-membrane markers and also marked by compositions from nuclear lamina such as lamins (Malhas et al., 2011). To test whether ER-FlucDM-eGFP aggregates were NR-like structures, Sec61β and ER-Tracker were used to label ER membranes. Results demonstrated all aggregates were surrounded by these two markers, indicating ER-FlucDM-eGFP aggregates are packed inside ER membranes **(Figure 4.4A and 4.4B)**. Next, nuclear lamina was labelled by laminVHH, a nanobody of the lamin. It could be observed that some of these aggregates were indeed surrounded by laminVHH **(Figure 4.4C)**.

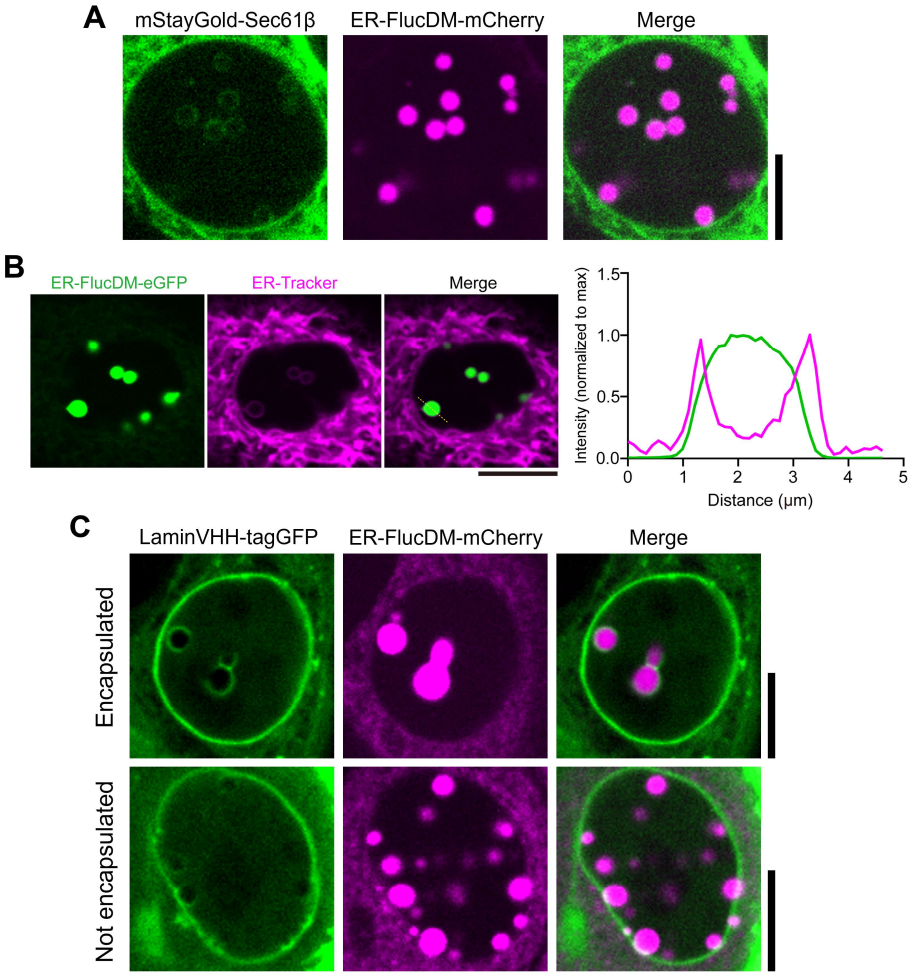


Figure 4.4: ER-FlucDM protein aggregates in the nucleus are encapsulated by the ER membrane. (A) Representative images of MCF10A cells co-expressing mStayGold-Sec61β and ER-FlucDM-mCherry. Scale bar, 10 μm. **(B)** Representative images of MCF10A cells expressing ER-FlucDM-eGFP stained by ER-Tracker. Scale bar, 10 μm. **(C)** Representative images of MCF10A cells co-expressing LaminVHH-tagGFP and ER-FlucDM-mCherry. Scale bar, 10 μm.

4.2.4 NLS-FlucDM-eGFP alone does not induce protein aggregates

ER-FlucDM-eGFP assembled into protein aggregates in the cell nucleus, leading to a hypothesis, which is, nuclear-targeting FlucDM-eGFP might assemble into protein aggregates as well. To examine this, FlucDM-eGFP was enriched in the cell nucleus by fusing it with a nuclear localization signal (NLS).

NLS-FlucDM-eGFP was successfully expressed and enriched in the nucleus **(Figure 4.5A)**. However, different from ER-FlucDM-eGFP, no visible protein aggregates were found upon the expression of NLS-FlucDM-eGFP **(Figure 4.5A)**. When co-expressing ER-FlucDM-mCherry and NLS-FlucDM-eGFP in cells, ER-FlucDM-mCherry aggregated successfully while NLS-FlucDM-eGFP was majorly excluded from the aggregates **(Figure 4.5B)**. Protein immunoblotting indicated that FlucDM expressed in the ER is more abundant than in the cell nucleus **(Figure 4.5C and 4.5D)**. To exclude the possibility that NLS-FlucDM-eGFP was not able to aggregate, MG132 was used to inhibit the 26S proteasome, thereby allowing the accumulation of misfolded NLS-FlucDM-eGFP. Upon the treatment of MG132, NLS-FlucDM-eGFP assembled into protein aggregates in the cell nucleus **(Figure 4.5E)**. This indicated that NLS-FlucDM-eGFP still possesses the ability to aggregate. Surprisingly, when co-expressing NLS-FlucDM-eGFP and ER-FlucDM-mCherry, NLS-FlucDM-eGFP was found to aggregate close to ER-FlucDM-mCherry aggregates, suggesting that the misfolded proteins in the ER potentially regulate the proteome in the nucleus **(Figure 4.5E)**.

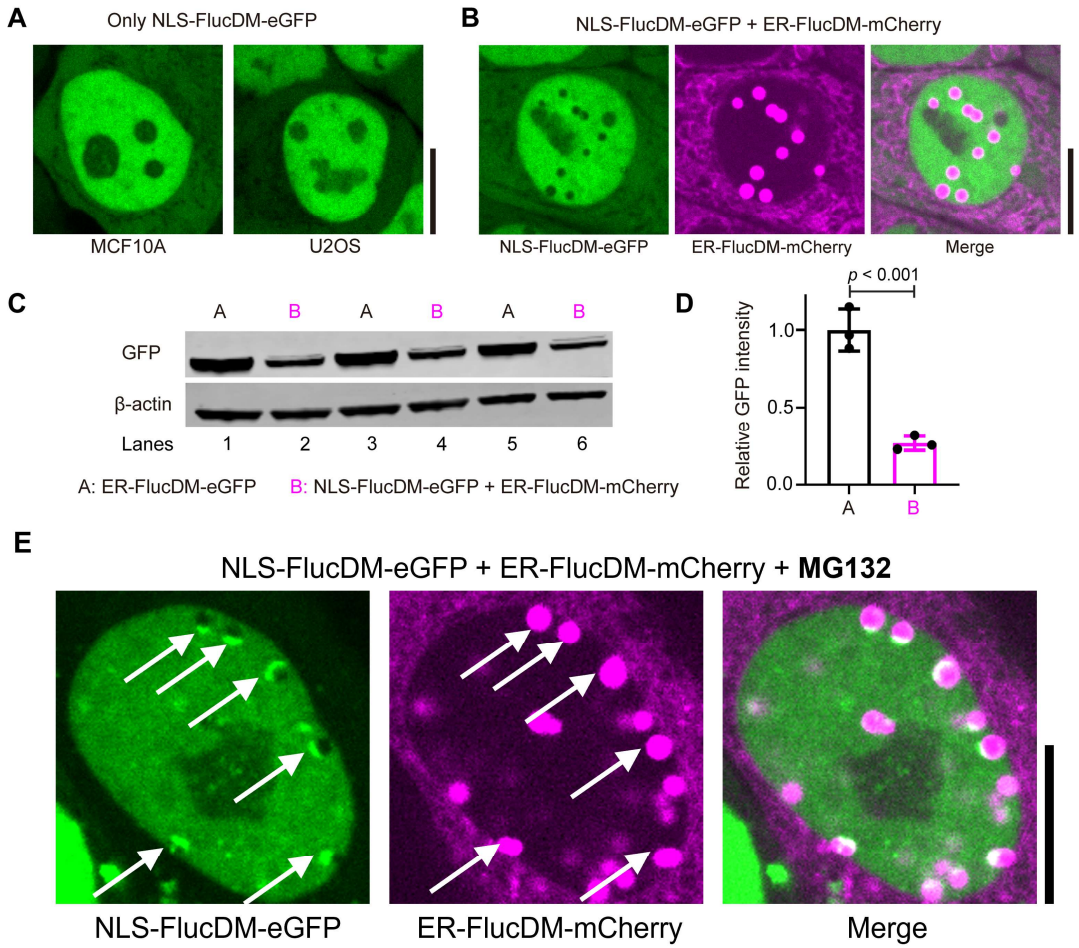


Figure 4.5: The expression of NLS-FlucDM-eGFP in cells. (A) Confocal microscope images of cells expressing NLS-FlucDM-eGFP in MCF10A and U2OS. **(B)** Confocal microscope images of MCF10A cells simultaneously expressing ER-FlucDM-mCherry and NLS-FlucDM-eGFP. **(C)** Protein blots of samples from cells expressing ER-FlucDM-eGFP (lanes 1, 3 and 5) and cells co-expressing NLS-FlucDM-eGFP and ER-FlucDM-mCherry (lanes 2, 4 and 6). **(D)** Quantification of relative GFP protein intensity in (C). The abundance of β-actin was employed during normalization. Student's t-test was used to calculate the statistical significance. Data were collected from three independent experiments and represented as the mean ± SD. **(E)** Microscopy images of cells expressing ER-FlucDM-mCherry and NLS-FlucDM-eGFP were treated with 5 μM MG132 for 4 hours. Single-layer images along the Z-axis are shown. The scale bar is 10 μm.

4.2.5 ER-FlucDM-eGFP protein aggregates are stained by Thioflavin T

To test the properties of ER-FlucDM-eGFP aggregates, the antibody of GFP was employed to confirm that they were protein aggregates instead of auto-fluorescent non-protein aggregates. The results showed that these aggregates colocalized with anti-GFP antibody signals, indicating ER-FlucDM-eGFP aggregates are indeed protein

aggregates **(Figure 4.6A)**.

To examine whether ER-FlucDM-eGFP aggregates consisted of misfolded proteins, Thioflavin T (ThT) was employed. ThT is a small molecule dye and exhibits strong fluorescence when binding to amyloid fibrils (Biancalana and Koide, 2010). Results demonstrated that ThT colocalized with ER-FlucDM-eGFP **(Figure 4.6B)**. It should be mentioned that only a small percentage (less than 10%) of aggregates was successfully stained by ThT and most aggregates showed very little colocalization with it. To explain this, it should be mentioned that only 'late' soluble amyloid aggregates demonstrate obviously stronger fluorescence upon binding with ThT, however, these 'early' aggregates do not (De et al., 2019). Given that ER-FlucDM-eGFP was largely soluble, it could be speculated that most of the aggregates ER-FlucDM-eGFP assembled might be a mixture of small 'early' aggregates.

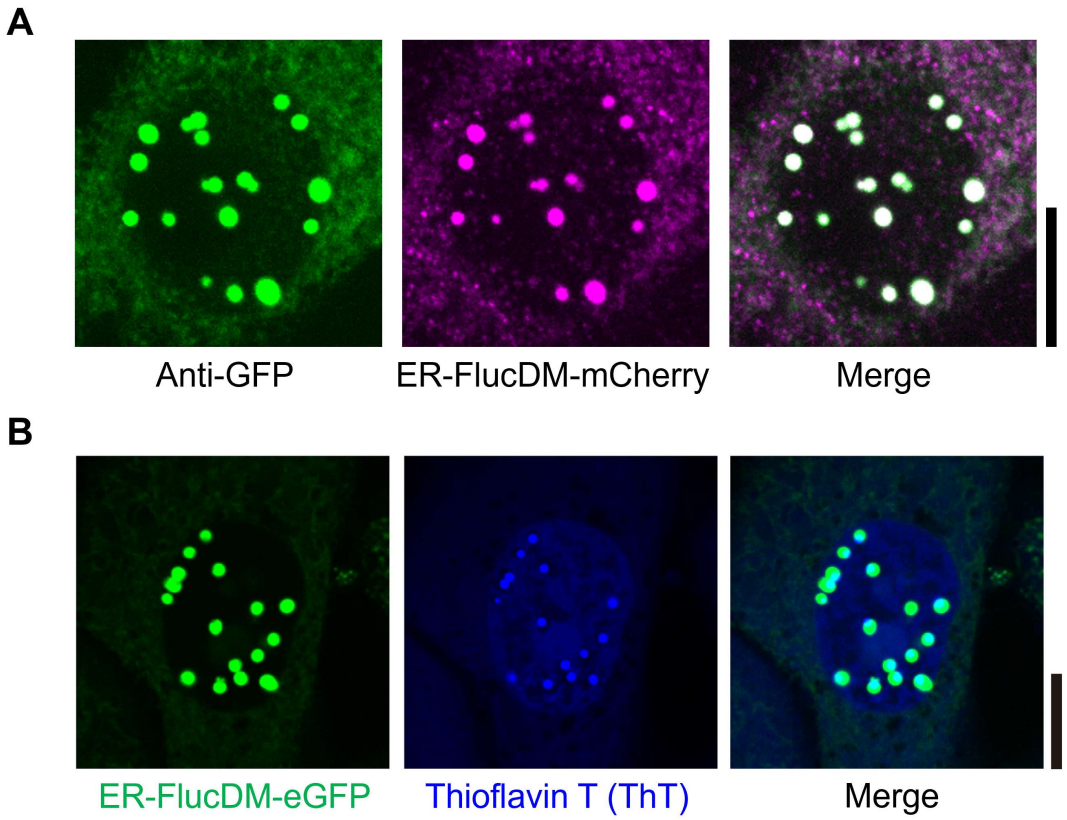


Figure 4.6: ER-FlucDM colocalizes with anti-GFP and Thioflavin T. (A) Immunofluorescence staining of anti-GFP antibodies in cells expressing ER-FlucDM-mCherry. Single Z-slice images were shown. Scale bar, 10 μm. **(B)** Colocalization of ER-FlucDM-eGFP and Thioflavin T (ThT), a marker for protein aggregates. Single-

layer images along the Z-axis are shown. The scale bar is 10 μm.

4.2.6 BiP is involved in ER-FlucDM-eGFP aggregation

Binding immunoglobulin protein (BiP) was previously reported to facilitate the folding of luciferase (Amankwah et al., 2022; Jin et al., 2008). Moreover, previous study demonstrated that BiP overexpression induced visible protein aggregates (Morris et al., 1997). Therefore, although BiP, as a molecular chaperone, is widely accepted to disassemble protein aggregates, it may also facilitate the aggregation of ER-FlucDM-eGFP to relieve cellular proteome. To examine this, CRISPR interference (CRISPRi) was employed to achieve BiP knockdown (KD). The KD efficiency was confirmed by quantitative real-time PCR (qRT-PCR) **(Figure 4.7A)**.

Results demonstrated that BiP (HSPA5 in figure) knockdown led to the disappearance of ER-FlucDM-eGFP protein aggregates in the cell nucleus **(Figure 4.7B and 4.7C)**. Moreover, knockdown of two other members from Hsp70 family (HSPA1A and HSPA8) barely changed protein aggregation **(Figure 4.7B and 4.7C)**. This suggests BiP, as the Hsp70 in the ER, specifically mediates the aggregation of ER-FlucDM-eGFP. Additionally, by immunofluorescence staining, BiP was observed to colocalize with ER-FlucDM-eGFP protein aggregates, further indicating the involvement of BiP on aggregation **(Figure 4.7D)**.

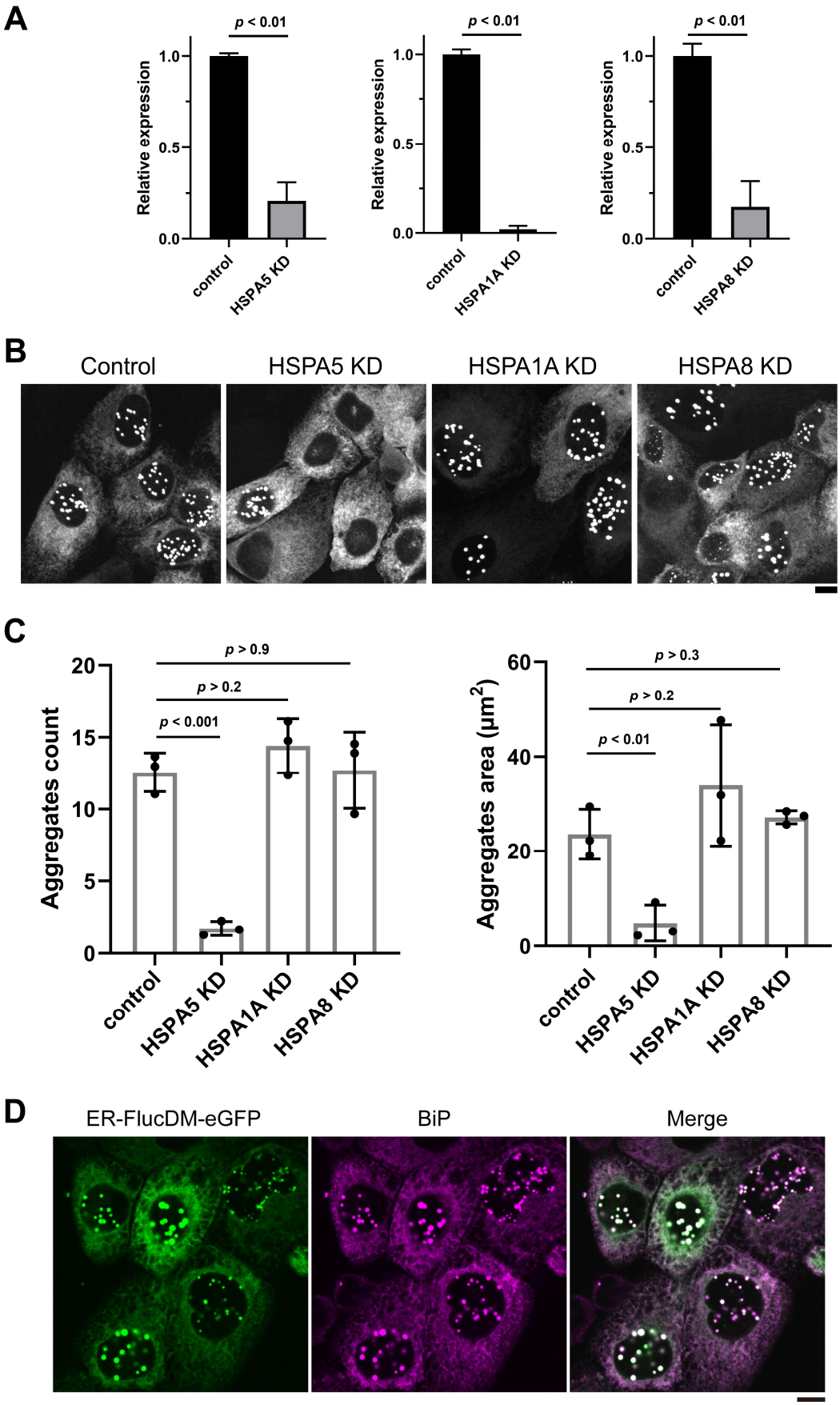

A
p < 0.01
Relative expression
1.0
0.5
0.0
control
HSPA5 KD
p < 0.01
Relative expression
1.0
0.5
0.0
control
HSPA1A KD
p < 0.01
Relative expression
1.0
0.5
0.0
control
HSPA8 KD
B
Control
HSPA5 KD
HSPA1A KD
HSPA8 KD
C
p > 0.9
p > 0.2
p < 0.001
Aggregates count
20
15
10
5
0
control
HSPA5 KD
HSPA1A KD
HSPA8 KD
p > 0.3
p > 0.2
p < 0.01
Aggregates area (μm2)
60
40
20
0
control
HSPA5 KD
HSPA1A KD
HSPA8 KD
D
ER-FlucDM-eGFP
BiP
Merge

Figure 4.7: Correlation between BiP and protein aggregates. (A) CRISPRi knockdown of Hsp70 was validated by qRT-PCR. Unpaired t-test. Data were collected from three independent experiments and represented as the mean + SD. **(B)** Representative images of cells expressing ER-FlucDM-eGFP upon the knockdown of Hsp70 family members. Images were acquired four days after knockdown. Maximum projected images along the Z-axis are shown. The scale bar is 10 μm. **(C)** Quantification of (B). Aggregates count and area meant aggregates per cells. Unpaired t-test. Data were collected from three independent experiments. Data represent the mean ± SD. **(D)** Representative images of BiP and ER-FlucDM-eGFP in interphase cells from immunofluorescence staining. Single-layer images along the Z-axis are shown. The scale bar is 10 μm.

4.2.7 Protein aggregates induced by ER-FlucDM-eGFP in the cell nucleus are independent of cell lines

To test whether these aggregates were only assembled in MCF10A cells, ER-FlucDM-eGFP was also transduced into other cell lines such as U2OS, A549 and MDA-MB-231. Results showed that ER-FlucDM-eGFP in all four cell lines formed aggregates **(Figure 4.8A)**. Moreover, the quantity and the size of these aggregates varied in different cell lines, suggesting that the ability of assembling ER-FlucDM-eGFP to protein aggregates depends on the cell type **(Figure 4.8B)**.

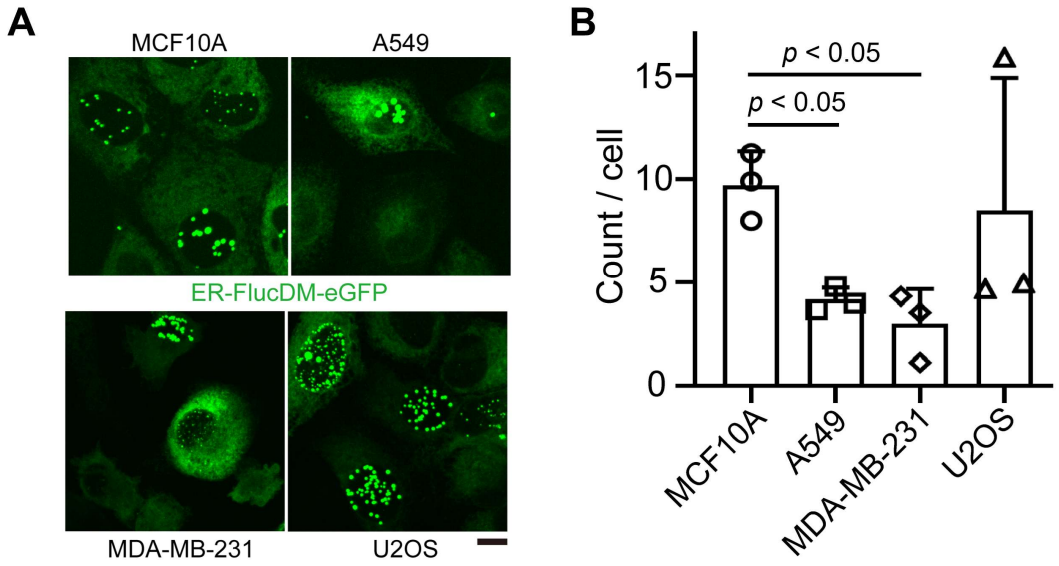


Figure 4.8: ER-FlucDM-eGFP assembles into protein aggregates in various cell lines. (A) Representative images of ER-FlucDM-eGFP expressed in various cell lines. Maximum projected images along the Z-axis are shown. The scale bar is 10 μm. **(B)** Quantification of ER-FlucDM-eGFP aggregate number of individual cells in different cell lines. MCF10A, 516 cells; A549, 395 cells; MDA-MB-231, 369 cells; U2OS, 528 cells. Data were collected from three independent experiments and represented as the

mean ± SD. Unpaired t-test was used.

4.2.8 Various ER targeted proteins induce protein aggregates

Next, I tested whether other constructs expressing in the ER induced aggregates similar to ER-FlucDM-eGFP. It could be found that ER-FlucDM-eGFP composed of an N-terminal ER targeting sequence, FlucDM and eGFP. In this section, these three units were replaced one by one to see whether protein aggregation still occurred.

A previous study reported that eGFP is intrinsically transported into the cell nucleus (Seibel et al., 2007), which potentially facilitates the assembly of ER-FlucDM-eGFP into the nucleus. To examine this, eGFP was replaced with mCherry and the results showed that same aggregates were also induced by ER-FlucDM-mCherry **(Figure 4.9A)**.

To test whether the ER targeting sequence used in constructing ER-FlucDM-eGFP alone could induce protein aggregation, another predicted N-terminal signal peptide sequence (He et al., 2019) from the follicle stimulating hormone receptor (FSHR) was fused to FlucDM-eGFP (ER^{FSHR}-FlucDM-eGFP) and expressed in MCF10A cells. Results showed that ER^{FSHR}-FlucDM-eGFP also assembled into protein aggregates, similar to the previously tested ER-FlucDM-eGFP **(Figure 4.9A)**.

To test whether FlucDM was the key to induce protein aggregation, another misfolding-prone protein, Halo tag with double mutations (HaloDM) was linked to an ER targeting sequence and eGFP (Melo et al., 2022). Although the quantity of aggregates assembled from ER-HaloDM-eGFP was smaller than those induced by ER-FlucDM-eGFP, protein aggregation was still observed **(Figure 4.9A and 4.9B)**. Next, eGFP was directly fused with an ER targeting sequence (ER-eGFP). Results showed that similar aggregates were found in a small fraction of cells **(Figure 4.9A)**.

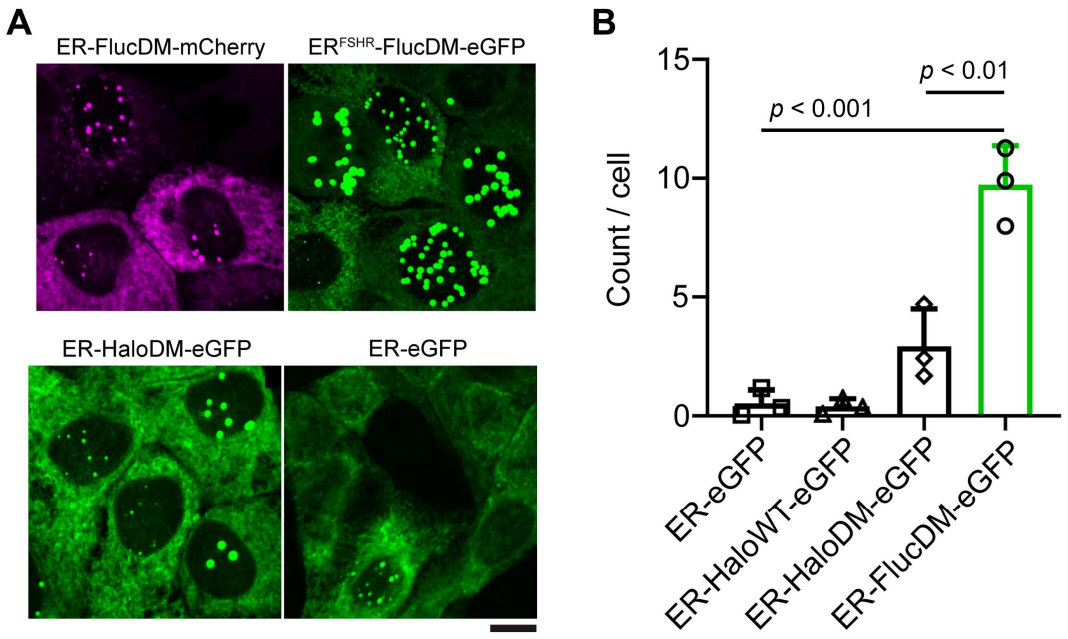


Figure 4.9: Various ER-targeted proteins induce protein aggregates. (A) Representative images showing MCF10A cells expressing ER-FlucDM-mCherry, ER^{FSHR}-FlucDM-eGFP, ER-HaloDM-eGFP or ER-eGFP. Maximum projected images along the Z-axis are shown. The scale bar is 10 μm. **(B)** Quantification of aggregate number in cells expressing ER-eGFP, ER-HaloWT-eGFP, ER-HaloDM-eGFP or ER-FlucDM-eGFP. ER-eGFP, 612 cells; ER-HaloWT-eGFP, 405 cells; ER-HaloDM-eGFP, 759 cells; ER-FlucDM-eGFP, 516 cells. Data were collected from three independent experiments. Unpaired t-test was used.

4.2.9 Pathologically misfolded proteins expressed in the ER do not induce protein aggregates in the cell nucleus

Next, I explored whether similar protein aggregates could be induced by other physiological or pathological conditions. Because protein aggregation in my study was achieved by overexpressing misfolding-prone proteins in the ER, it could be hypothesized that other misfolded proteins accumulated in the ER might also assemble similar aggregates. To test this, two misfolded mutants of α-1 antitrypsin (Pérez, 2024), Glu264Val (the S allele) and Glu342Lys (the Z allele) were overexpressed in MCF10A cells. Results showed that these two mutants could not assemble into aggregates in the cell nucleus in all cell lines tested **(Figure 4.10A and 4.10B)**. In addition to antitrypsin mutants, a cystic fibrosis transmembrane conductance regulator (CFTR) mutant, CFTR Δ508 (with a deletion of an amino acid at position 508) was also tested because this mutant is misfolding-prone and retained in the ER while the wild-type of CFTR is

supposed to reach the plasma membrane (Lukacs and Verkman, 2012). Results showed that CFTRΔ508-eGFP was excluded from the plasma membrane and retained in the ER network, suggesting its misfolded state. However, unlike ER-FlucDM-eGFP, it did not assemble into any visible protein aggregates in the cell nucleus **(Figure 4.10C)**.

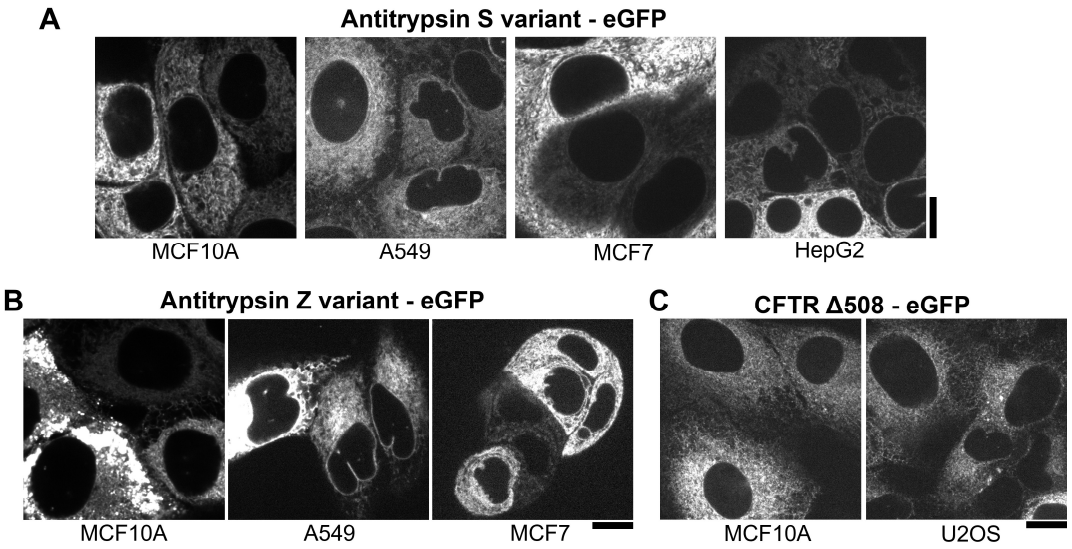


Figure 4.10: Expression of α-1 antitrypsin and CFTR mutants in cells. (A) Representative images of various cell lines expressing eGFP-tagged α-1 antitrypsin S variant. **(B)** Representative images of various cell lines expressing eGFP-tagged α-1 antitrypsin Z variant. **(C)** Representative images of two cell lines expressing eGFP-tagged CFTR Δ508 mutant. All scale bars in this figure are 10 μm.

4.2.10 Proteostasis perturbations by small molecules treatment do not induce protein aggregates in the cell nucleus

The expression of misfolded proteins in the ER induces ER stress (Karagöz et al., 2019). The ER stress also causes the aggregation of proteins (Hamdan et al., 2017). Therefore, it can be speculated that ER-FlucDM-eGFP induces ER stress, subsequently causing aggregates in the nucleus. Previous studies demonstrated that MG132 (26S proteasome inhibitor), bafilomycin A1 (lysosome acidification inhibitor), thapsigargin (an inhibitor of the sarco/endoplasmic reticulum Ca^{2+}-ATPase pump), tunicamycin (a N-linked glycosylation inhibitor) and A23187 (also known as calcimycin, a Ca^{2+} chelator) all induce ER stress (Deniaud et al., 2008; Kawaguchi et al., 2011; Melo et al., 2022; Nakajima et al., 2011; Verwilst et al., 2019). To test whether chronic ER stress induction led to aggregates assembly in the cell nucleus, several ER stress inducers were

employed to treat wild-type MCF10A cells at various dosages. Then, ER-tracker was used to label the ER membrane to observe the existence of NR structures in the nucleus. Results demonstrated that no NR-like structures were found in the nucleus upon any ER stress inducer treatment **(Figure 4.11A to 4.11E)**. However, the ER membrane with round shape was observed in cells expressing ER-FlucDM-eGFP **(Figure 4.11F)**. This suggests the nuclear aggregation of ER-FlucDM-eGFP may not originate from chronic ER stress induction.

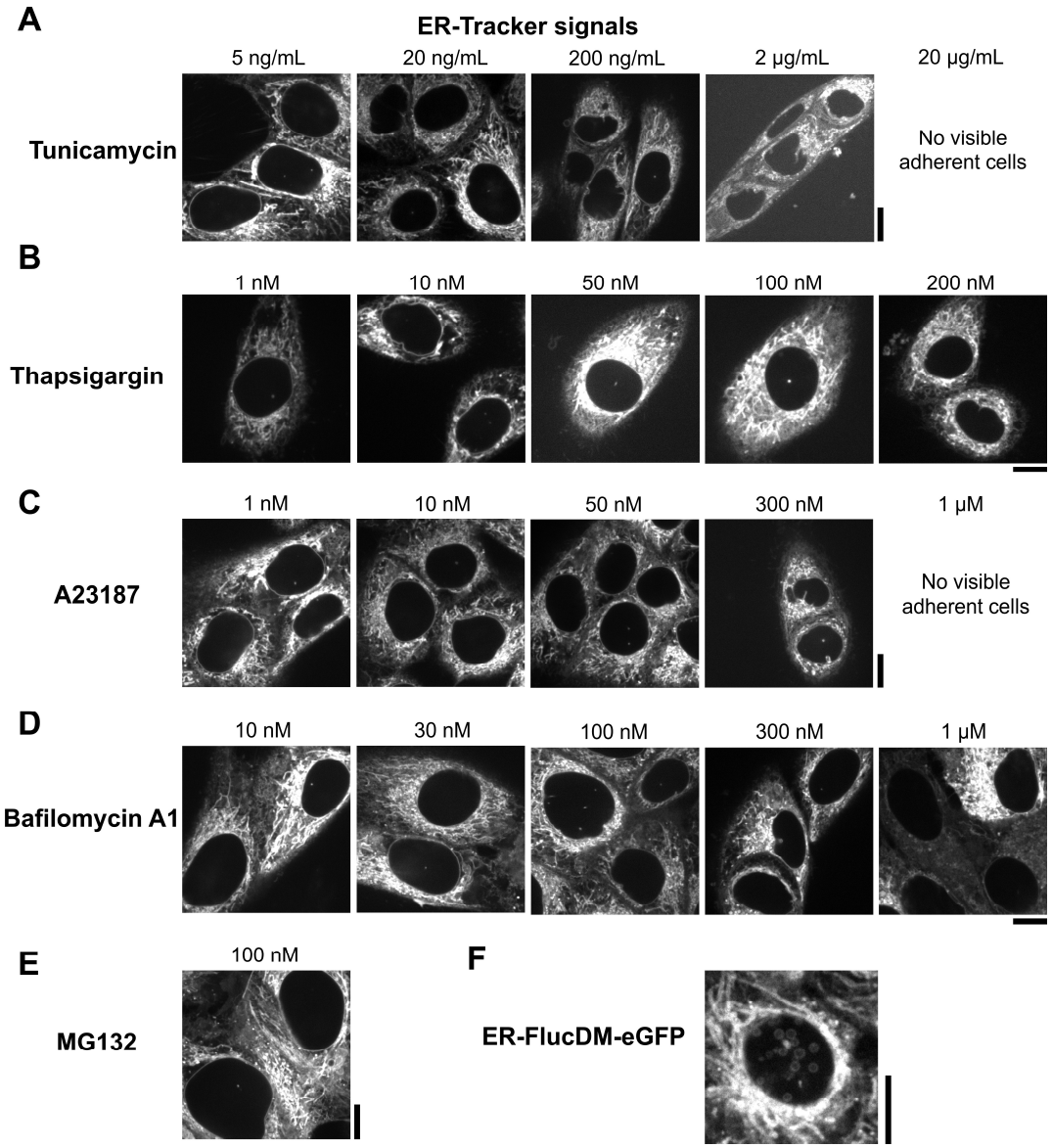


Figure 4.11: Proteostasis perturbation by small molecules does not induce ER membrane appearance in the cell nucleus. (A) to (E) Representative images of wild-type MCF10A cells stained by ER-Tracker. Cells were treated with various inhibitors with specific dosages for 72 hours before passaging into imaging chamber. **(F)** Representative image of a MCF10A cell expressing ER-FlucDM-eGFP stained by ER-

Tracker. All images in this figure are single-layer images along the Z-axis. All scale bars are 10 μm.

4.2.11 Differential aggregate dynamics in cells at interphase and mitosis

Although protein aggregates in the nucleus were not found by expressing pathological misfolded proteins or by small molecule treatment, similar protein aggregates might assemble upon currently unknown stimulations. Given their striking phenotype, it is still worth exploring their properties.

Next, the turnover dynamics of ER-FlucDM-eGFP aggregates were tested by fluorescence recovery after photobleaching (FRAP). To achieve this, ER-FlucDM-eGFP and ER-FlucDM-mCherry were simultaneously expressed in cells. Given that the mCherry signal is bleached when bleaching GFP signal using the 488 nm laser, the signal from ER-FlucDM-mCherry was bleached to probe the recovery dynamics while the ER-FlucDM-eGFP signal served as a tracker to locate aggregates.

In interphase cells, the fluorescent intensity from ER-FlucDM-mCherry aggregates barely recovered after 4.5 min post-bleaching **(Figure 4.12A and 4.12B)**. Analogously, aggregates of ER-HaloDM-eGFP in the nucleus also demonstrated minimal recovery after photobleaching **(Figure 4.12C)**. When testing the turnover dynamics of condensates assembled by ER-eGFP, the fluorescence signal recovery speed was faster than that of ER-HaloDM-eGFP and ER-FlucDM-mCherry **(Figure 4.12D)**. ER-eGFP does not contain any misfolding-prone elements, therefore, condensates it assembled may not be misfolded protein aggregates and therefore do not follow the dynamics of ER-FlucDM-eGFP and ER-HaloDM-eGFP.

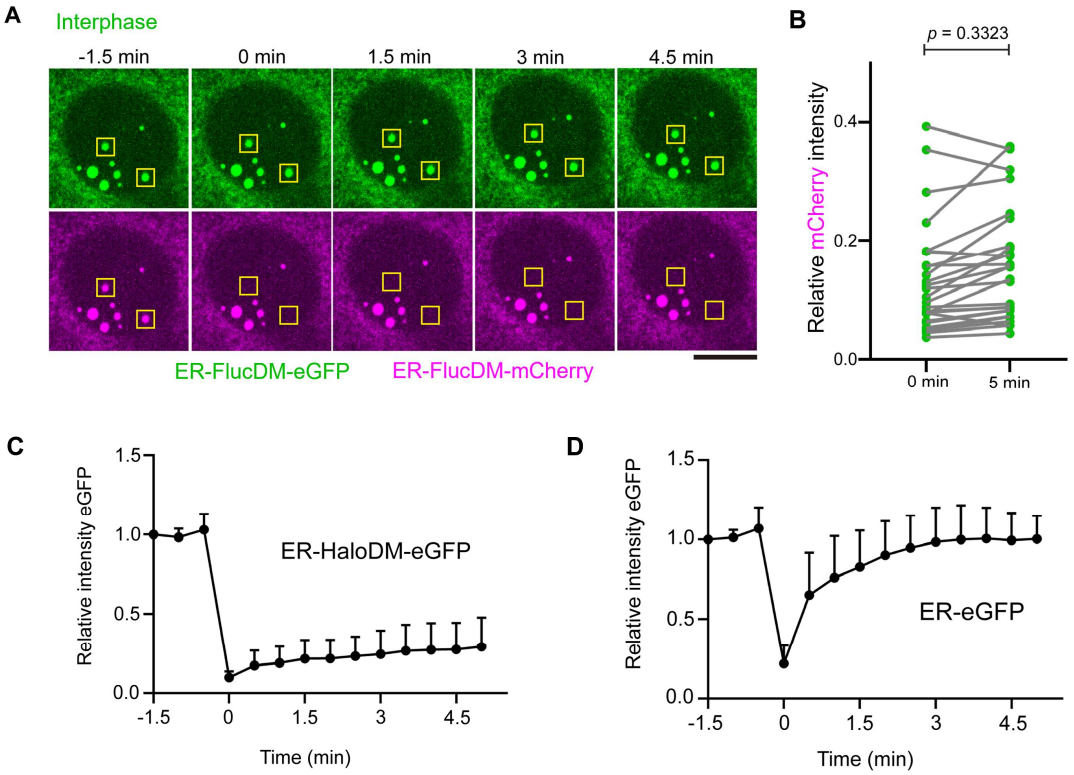


Figure 4.12: Fluorescence recovery after photobleaching (FRAP) of protein aggregates in the cell nucleus. (A) Representative images of interphase cells simultaneously expressing ER-FlucDM-eGFP and ER-FlucDM-mCherry before and after photobleaching. Bleached aggregates were highlighted by yellow rectangles. Maximum projected images along the Z-axis are shown. The scale bar is 10 μm. **(B)** Quantification of the intensity of bleached ER-FlucDM-mCherry aggregates instantly after bleaching (0 min) and after 5 min of recovery (5 min). Paired t-test was used to process the data from three independent experiments. **(C)** Fluorescence recovery curve of ER-HaloDM-eGFP before and after photobleaching. Seven interphase cells from three independent experiments were captured. Data were represented as the mean + SD. **(D)** Recovery curve of ER-eGFP before and after bleaching. Seven interphase cells from three independent experiments were captured. Data were represented as the mean + SD.

Next, turnover dynamics of ER-FlucDM-mCherry aggregates in dividing cells was examined. Results demonstrated that their recovered intensity was also much lower than the ER networks regions of ER-FlucDM-mCherry **(Figure 4.13A to 4.13D)**. However, the fluorescence recovery was faster in mitotic cells than that in interphase cells **(Figure 4.12B, and Figure 4.13B to 4.13D)**. Overall, these results indicated that ER-FlucDM-mCherry aggregates in the nucleus exhibit low turnover, with slightly higher dynamics observed during mitosis.

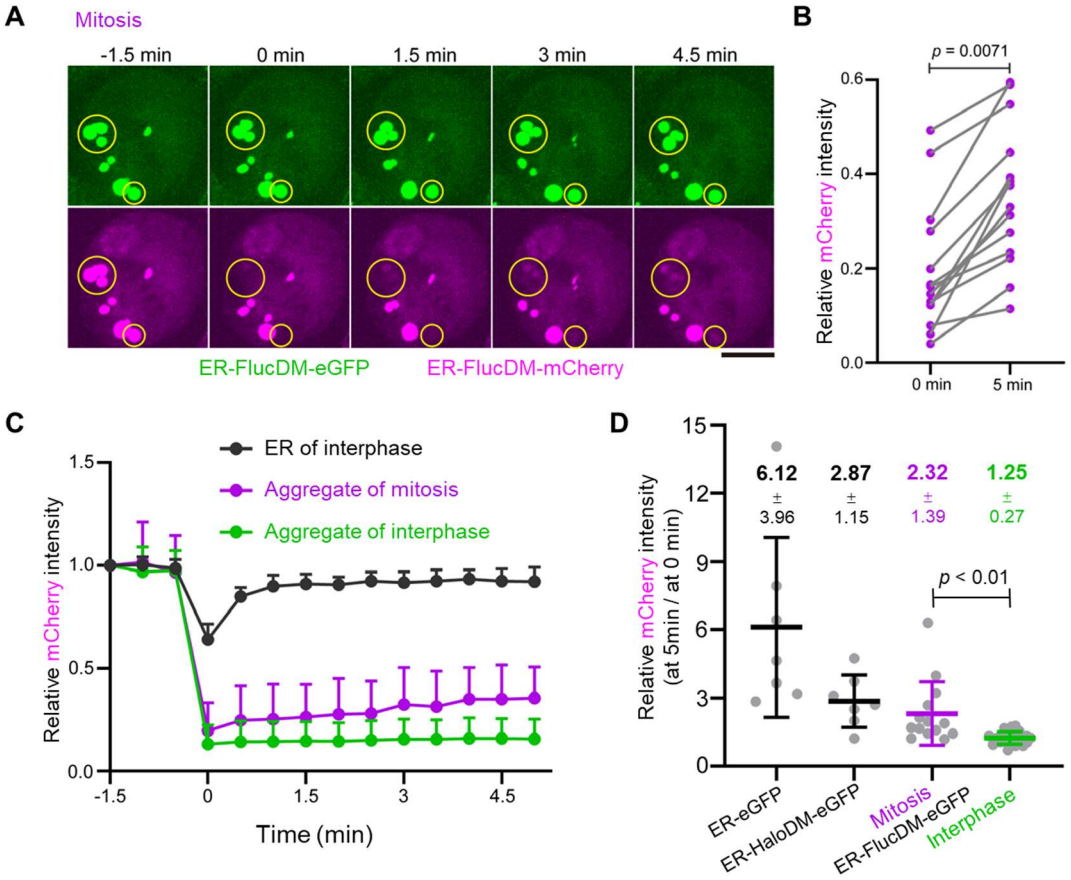


Figure 4.13: Differential aggregate dynamics in interphase and mitosis. (A) Representative images of mitotic cells simultaneously expressing ER-FlucDM-mCherry and ER-FlucDM-eGFP before and after photobleaching. Bleached aggregates were indicated by yellow circles. Maximum projected images along the Z-axis are shown. The scale bar is 10 μm. **(B)** Quantification of the ER-FlucDM-mCherry intensity of bleached aggregates instantly after bleaching (0 min) and after 5 min of recovery (5 min). Paired t-test was used to calculate the statistical significance. **(C)** Fluorescence recovery curves of ER-FlucDM-mCherry intensity after bleaching. The ER of interphase, 14 ROIs; Aggregates of mitosis, 14 aggregates; Aggregates of interphase, 26 aggregates. Data were represented as the mean + SD. A small region of ER-FlucDM-mCherry in the ER network was chosen as a control for photobleaching. Data were collected from three independent experiments. **(D)** Quantification of protein fluorescence intensity of different constructs instantly after photobleaching and 5 min after recovery. 0 min is the fluorescence signal instantly after photobleaching. 5 min is the fluorescence signal after a 5-min recovery since photobleaching. Cells were collected from at least three independent experiments and represented as the mean ± SD.

4.3 Discussion

4.3.1 Summary of results in this chapter

In this chapter, ER-FlucDM-eGFP was overexpressed in MCF10A cells as a proteostasis reporter. ER-FlucDM-eGFP remained largely soluble while the functionality of FlucDM was lower than its wild-type version, suggesting ER-FlucDM-eGFP is misfolded in cells. It was expected to be homogeneously distributed in the ER when expressed in cells, as described for FlucDM-eGFP in Chapter 3 prior to additional proteome stress. Surprisingly, ER-FlucDM-eGFP assembled into visible protein aggregates in the absence of any additional proteostasis perturbation. Interestingly, these aggregates appeared to localize to the cell nucleus while still being encapsulated by the ER membrane. These aggregates colocalized with BiP, the Hsp70 in the ER. The aggregation of ER-FlucDM-eGFP was inhibited upon the knockdown of BiP instead of the other two Hsp70s, suggesting BiP facilitates this aggregation.

In previous studies, misfolded proteins expressed in the ER assembled into protein aggregates in the ER or membrane-encapsulated inclusion bodies in the cytosol (Cunningham et al., 2019; Granell et al., 2008). Additionally, several types of protein aggregates in the ER seemed to form at juxtanuclear spaces (Melo et al., 2022; Morris et al., 1997). However, to the best of my knowledge, direct evidence demonstrating their nuclear localization and whether these aggregates are encapsulated by the ER membrane remain unknown. On the other hand, although protein aggregates can form in the cell nucleus, these aggregates are not encapsulated by the ER membrane (Frottin et al., 2019). This suggests that the protein aggregates in my study may represent a novel and previously uncharacterized category of protein aggregates. Interestingly, these aggregates demonstrated differential recovery speeds after photobleaching in interphase and mitotic cells.

Before further profiling their dynamics during cell division in the next chapter, I discuss three key topics related to this novel type of protein aggregates in this chapter's discussion. The first topic is the material properties of ER-FlucDM-eGFP protein

aggregates. Secondly, how ER-expressed proteins assemble into aggregates in the cell nucleus is speculated. Finally, this thesis anticipates the physiological situations in which protein aggregates assemble in the cell nucleus while being encapsulated by the ER membrane.

4.3.2 The properties of ER-FlucDM-eGFP protein aggregates

When testing the properties of ER-FlucDM-eGFP in MCF10A cells, BiP, the Hsp70 in the ER lumen, colocalized with ER-FlucDM-eGFP aggregates, indicating these aggregates are protein aggregates still in the ER lumen and these aggregates may contain other components in the ER lumen. What is the function of BiP?

BiP assists in the disaggregation of protein aggregates (Melo et al., 2022). Strikingly, in my study, BiP knockdown caused the disappearance of ER-FlucDM-eGFP protein aggregates, suggesting that BiP, as a molecular chaperone, unexpectedly facilitates the aggregation of ER-FlucDM-eGFP. Previous reports demonstrated that purified BiP tends to form natural oligomers (Preissler et al., 2020) and that the overexpression of BiP solely induces protein aggregates similar to my study (Morris et al., 1997). Additionally, chaperones in the ER are immobilized in misfolded protein aggregates and these chaperones stiffen aggregates (Chambers et al., 2022). Therefore, although BiP possesses the widely accepted disaggregation function, it might also facilitate the assembly of protein aggregates. This sequestration may be a cellular strategy to relieve proteome stress when proteins are overexpressed in the ER.

Interestingly, when expressing native Fluc in the ER (namely ER-FlucWT-eGFP), it also assembled into protein aggregates, which was similar to ER-FlucDM-eGFP. Furthermore, the luciferase activity of FlucDM from ER-FlucDM-eGFP was lower than FlucWT of ER-FlucWT-eGFP, suggesting FlucDM in these aggregates is majorly less-functional and misfolded while FlucWT remains functional and folded. Given that the correctly folded FlucWT also assembled into aggregates in the ER, FlucDM in aggregates might be at least partially folded into its functional structure. As shown by

western blot, ER-FlucDM-eGFP possessed correct band size as predicted, indicating it is fully expressed in cells instead of being partially degraded. Moreover, the strong green fluorescence suggested that eGFP from ER-FlucDM-eGFP is also correctly folded into its 3D structure. Taken together, it is highly possible that ER-FlucDM-eGFP possesses partially or even majorly correct folding structures rather than being fully intertwined with BiP instantly after translocation from the cytosol prior to aggregation.

Additionally, ER-FlucDM-eGFP protein aggregates demonstrated limited recovery rate after photobleaching in interphase cells. This implies its solid-like state, which is similar to that of pathologically misfolded protein aggregates. One might argue that the ER membrane tightly encapsulates aggregates and subsequently limits protein turnover. This statement was unlikely because signals from the condensates assembled by ER-eGFP recovered quickly after photobleaching and these condensates were embedded in the ER membrane, indicating protein transport from the ER lumen to aggregates is not totally abolished.

Notably, ER-FlucDM-eGFP in MCF10A cells was largely soluble even in 0.2% (v/v) NP-40, a very weak lysis buffer recipe. This raises the possibility that ER-FlucDM-eGFP aggregates are composed of soluble proteins, although they are misfolded. In a previous study, based on evidence from molecular simulation, misfolded and less-functional proteins possessed a native-like surface while maintaining an entangled internal structure, enabling them to remain soluble while partially losing function (Nissley et al., 2022). In this way, it is speculated that the native-like surface might be the reason why ER-FlucDM-eGFP and its FlucWT version aggregate. BiP might recognize the surface of Fluc via its corresponding co-chaperones (i.e., J-domain proteins) to facilitate this aggregation.

Thioflavin T, an amyloid marker, was occasionally rather than predominantly found to colocalize with ER-FlucDM-eGFP aggregates. This incomplete colocalization might result from the specificity of Thioflavin T for amyloid fibril structures, a terminal and

stable form of protein aggregates. However, aggregates formed by ER-FlucDM-eGFP might be more preliminary and more polymorphic (i.e., composed of multiple structures), allowing them to evade the detection of Thioflavin T (De Giorgi et al., 2020; De et al., 2019).

In sum, ER-FlucDM-eGFP in this study was composed of less dynamic and partially misfolded elements bound to BiP, forming detergent-soluble and structurally polymorphic protein aggregates encapsulated in the ER membrane.

4.3.3 How do the aggregates assemble in the cell nucleus while being embedded in the ER membrane?

Protein aggregates induced by ER-FlucDM-eGFP started to visibly accumulate from about 1.5 days after transduction in interphase cells. During this time, no additional external stimuli were applied, suggesting that the aggregation in the cell nucleus originates solely from the cells' own ability. A previous study reported that mutant Huntingtin polyglutamine preferentially aggregates around the periphery of the cell nucleus (Choi et al., 2024). Although this study does not provide any speculations to explain the tendency of aggregation near the cell nucleus, their observation indicated that the preference of perinuclear aggregation may be ubiquitous, spanning from polyglutamine in the cytosol to ER-FlucDM-eGFP in the ER. Therefore, before asking how aggregates enter the cell nucleus, a question might worth discussing first: why does misfolding-prone proteins in the ER form aggregates close to the cell nucleus rather than in the cytoplasm? There are several possible interpretations:

Firstly, a previous study showed that the junction between the nuclear envelope (NE) and the major fraction of the ER is significantly restricted (7 to 20 nm) in interphase cells (Bragulat-Teixidor et al., 2024). However, the luminal width of ER sheets is about 50 nm (Xu et al., 2023). Thus, misfolded proteins translocated from the cytosol into the NE are less likely to be transported out because of the narrow junctions between the NE and other fractions of the ER, subsequently causing their accumulation around the

cell nucleus. Secondly, a previous study reported that the temperature of the cell nucleus is higher than the cytoplasm (Okabe et al., 2012). This hyperthermia might also facilitate protein aggregation close to the nucleus, which is similar to heat shock-induced aggregation. Thirdly, ER-to-lysosome-associated degradation was reported to eliminate misfolded polymers (Fregno et al., 2018). It is widely accepted that autophagy machineries have limited access to the cell nucleus (Hipp et al., 2014), which undermines the clearance of invaginated misfolded protein aggregates.

After stating several reasons why proteins expressed in the nuclear envelope, a specialized subdomain of the ER, are more likely to form aggregates, three possible mechanisms for how protein aggregates invaginate into the cell nucleus are proposed next:

Firstly, a previous study demonstrated that BiP translocated into the cell nucleus via its nuclear localization sequence (NLS) upon ER stress induction (Liu et al., 2023). Moreover, misfolded proteins accumulated in the ER cause ER stress (Acosta-Alvear et al., 2025). Given the colocalization of ER-FlucDM-eGFP and BiP, it is possible that the accumulation of ER-FlucDM-eGFP induces ER stress and subsequently forces BiP to enter the cell nucleus. Alternatively, BiP also might coerce ER-FlucDM-eGFP to the nucleus. This model can be supported by the disappearance of aggregation upon BiP knockdown in my study. However, this model is also challenged. BiP is predominantly expressed in the ER lumen and on the cell surface (Wang et al., 2017). NLS facilitates protein transport from the cytoplasm to the nucleus rather than from the ER to the nucleus (Lu et al., 2021). Therefore, it is elusive about how BiP in the ER enters the cell nucleus through its NLS sequence.

Secondly, proteins in the ER invaginating into the nucleus might rely on a category of less-reported ER structures. The nuclear envelope is not merely a smooth and continuous boundary enclosing the nucleus (Malhas et al., 2011; McPhee et al., 2024). Instead, it contains invaginations that extend deeply into the nucleoplasm and, in some

cases, even traverse the nucleus entirely. These structures are the nucleoplasmic reticulum (NR). The invagination of type one NR originates from the inner nuclear membrane alone (Malhas et al., 2011), consistent to the feature of ER-FlucDM-eGFP protein aggregates in my study. Interestingly, upon oleate induction, lipid droplets form in the ER and invaginate into the nucleus (Mosquera et al., 2021; Soltysik et al., 2019). Thus, similar to lipid droplets, ER-FlucDM-eGFP aggregates in the NR might also invaginate into the cell nucleus.

Next, the third speculative mechanism will be discussed. A previous study reported that liquid-like biomolecular condensates naturally associated with membranes and drive intraluminal vesicle formation without any active transport regulators (Wang et al., 2024). Furthermore, accumulating evidence provided the possibility that the nucleation step of misfolded protein aggregation originates from their liquid-like properties (Mukherjee et al., 2024). Therefore, misfolded proteins in the ER might drive inner nuclear membrane invagination during their nucleation step. How do these small aggregate seeds grow? It could be imagined that these preliminary misfolded protein seeds are trapped inside. Therefore, luminal transport of this invaginated area is slower than other places in the ER, and these seeds act as templates for other misfolded proteins to co-aggregate, finally causing visible protein aggregates. The invagination theory also helps to explain the following two points: (1) the reason that ER-FlucDM-eGFP aggregates are partially encapsulated by lamins and (2) potential crosstalk among misfolded proteins in the ER, the inner nuclear envelope, and the cell nucleus.

4.3.4 Why are ER-FlucDM-eGFP aggregates partially encapsulated by the lamin?

When employing the nanobody of lamins, laminVHH, to label nuclear lamina and using ER-Tracker to label ER membranes, all aggregates were embedded inside the ER membrane, however, not every aggregate was surrounded by the marker of lamins.

To explain these two subtypes, one can imagine a game between the invagination force from the ER to the nucleus and the tension generated by the nuclear lamina to balance

invagination force. If the nuclear lamina tension is strong enough to resist invagination, the invagination might not break the local lamina. This situation was represented by these aggregates surrounded by the marker of lamins. In another situation, when the force generated by invagination is sometimes too strong or the local curvature is too high for the nuclear lamina to resist, invagination might break through the nuclear lamina and these breached lamins will leave the invagination front, resulting in aggregates that are only packed inside ER membranes. Indeed, previous studies proposed that the localized high curvature of membranes depleted local lamins (Nmezi et al., 2019; Pfeifer et al., 2022). This case is represented by those aggregates not surrounded by the marker of lamins.

It should be mentioned how the force generated by these aggregates during invagination still remains an open question to be explored and answers to address this might be an important direction for further research. The invagination hypothesis proposed here not only explains why ER-FlucDM-eGFP aggregates are partially encapsulated by lamins, but also explains why NLS-FlucDM-eGFP forms protein aggregates near ER-FlucDM-mCherry.

4.3.5 Potential crosstalk among misfolded proteins in the ER, the inner nuclear envelope, and the cell nucleus

Interestingly, when NLS-FlucDM-eGFP and ER-FlucDM-mCherry were co-expressed in MCF10A cells, NLS-FlucDM-eGFP assembled small protein aggregates closely near ER-FlucDM-mCherry aggregates. This unexpected adjacent aggregation could be understood by a complex interaction between ER-FlucDM-mCherry, lipids of the inner nuclear envelope, and NLS-FlucDM-eGFP. It is known that protein aggregation is regulated by physico-chemical properties of the lipid membrane surface, such as membrane curvature, surface charge, and hydrophobicity (Grigolato and Arosio, 2021). Furthermore, protein aggregates on the surface of lipids inversely regulate the lipid membrane (Hellstrand et al., 2013). Thus, ER-FlucDM-mCherry aggregates might alter the material properties of the lipid membrane when invaginating because of the high

curvature demanded, and these altered lipids would facilitate the aggregation of NLS-FlucDM-eGFP as feedback. Therefore, NLS-FlucDM-eGFP aggregates spontaneously assemble close to the aggregates of ER-FlucDM-mCherry.

If boldly extending this interaction, it could be speculated that protein aggregates in the ER or even other membrane-bound organelles might mediate extra-organelle events such as biomolecular condensation by regulating local membrane properties.

4.3.6 Under which conditions do protein aggregates invaginate into the cell nucleus?

Several exogenous proteins tested also induced similar aggregates when expressed in MCF10A cells, suggesting the ability of overexpressed proteins in the ER to assemble into protein aggregates in the nucleus is not limited to a specific protein. However, either overexpressing pathologically misfolded proteins in the ER (two antitrypsin mutants and one CFTR mutant) or chronic ER stress induction by small molecules failed to reconstruct visible aggregates in the cell nucleus, undermining the ubiquitousness of these novel aggregates. In the literature, the most similar aggregates were observed by overexpressing BiP in Chinese hamster ovary (CHO) cells (Morris et al., 1997). Although my study did not provide evidence demonstrating in which situations similar aggregates occurred, which was one of the major limitations of this study, the following probable scenarios were imagined.

Firstly, virus infection and replication in the ER might cause similar protein aggregation in the nucleus. Previous studies reported that BiP interacted and colocalized with various viral proteins such as the viral envelope composition, glycoproteins (Kohli et al., 2021). Moreover, BiP knockdown was shown to decrease the production of viruses (Kohli et al., 2021). This indicates that viral proteins may act similarly to FlucDM: being overexpressed in the ER and able to bind to BiP. Interestingly, virus infection was reported to remodel the ER (Bagchi, 2020), potentially causing the less reported ER structures in my study.

Secondly, when aggregates invaginate into the cell nucleus, the local inner nuclear membrane (INM) should expand to accommodate the extra volume required by the aggregates. This could be realized by INM component synthesis, especially lipids. Oleate-induced lipid synthesis of the INM causes ER membrane expansion and invagination into the nucleus, forming the NR (Niu et al., 2024). In their study, the number of induced NR structures per cell is similar to the quantity of aggregates in my study although their size is obviously smaller. It could be speculated that these small oleate-induced NR structures could expand when overexpressing proteins in the ER. Therefore, it could be speculated that INM expansion and protein overexpression in the ER possibly collaborate to induce protein aggregates in the cell nucleus.

Chapter 5 Clearance of Protein Aggregates during Cell Division

5.1 Introduction

Newly synthesized polypeptides adopt three-dimensional conformations to carry out their biological roles (Hipp et al., 2019). Misfolded proteins tend to expose their hydrophobic residues and lead to protein aggregation (Hartl et al., 2011). Misfolded proteins and their aggregates not only undermine their own function but can also disrupt the activity of other proteins through co-aggregation (Olzscha et al., 2011; Woerner et al., 2016). This compromises protein homeostasis (proteostasis) and induces proteostatic stress in cells, a key factor in cellular aging and neurodegenerative diseases (Labbadia and Morimoto, 2015).

To maintain proteostasis, cells develop multiple protein quality control (PQC) mechanisms, which assist in folding, degradation, and spatial confinement into specific cellular compartments (Jayaraj et al., 2020). Molecular chaperones play a central role in these PQC systems. They assist in the folding of nascent polypeptides, target misfolded proteins for degradation via the ubiquitin-proteasome system or autophagy, and facilitate the dissolution of protein aggregates (Tyedmers et al., 2010). In eukaryotic cells, misfolded proteins and smaller aggregates are compartmentalized into distinct deposition sites, limiting their harmful interactions with the proteome (Kaganovich et al., 2008). These sites include the aggresome or aggresome-like induced structures near the centrosomes, intranuclear quality control compartment (INQ) in the nucleus, cytosolic CytoQ, and the perivacuolar insoluble protein deposit (IPOD) (Kaganovich et al., 2008). Sequestering protein aggregates into these compartments aids in retaining them in the short-lived mother cell during asymmetric division (Coelho et al., 2014; Lindner et al., 2008; Ogrodnik et al., 2014; Rujano et al., 2006; Spokoini et al., 2012; Zhou et al., 2014).

The endoplasmic reticulum (ER), responsible for processing about one-third of the cellular proteome, demonstrates high capacity to maintain aggregation-prone proteins in a non-toxic state due to its specialized molecular chaperone environment (Vincenz-Donnelly et al., 2018). ER-resident chaperones such as binding immunoglobulin protein (BiP) regulate the unfolded protein response (UPR) (Preissler and Ron, 2019). UPR inhibits immediate protein synthesis and activates the transcription of PQC-related genes (Preissler and Ron, 2019). Furthermore, proteostasis stress in the ER induces ER-associated degradation (ERAD) and ER-phagy to eliminate misfolded proteins (Mochida and Nakatogawa, 2022; Wu and Rapoport, 2018).

Despite high capacity of the ER to maintain proteostasis (Rousseau et al., 2004; Vincenz-Donnelly et al., 2018), excessive misfolding-prone proteins can still accumulate and assemble into protein aggregates in the ER (Chambers et al., 2022; Melo et al., 2022). To counteract this, BiP acts as a disaggregase, promoting the solubilization of ER protein aggregates (Melo et al., 2022). In organisms that undergo asymmetric division such as the budding yeast, the ER diffusion barrier and the ER stress surveillance (ERSU) pathway ensure that ER protein aggregates remain in the short-lived mother cell (Clay et al., 2014; Piña and Niwa, 2015). However, the regulation of ER protein aggregates in symmetrically dividing cells remains less understood.

In mammalian cells undergoing symmetric division, the structure of the ER preferentially changes from sheets to tubules (Kors and Schlaitz, 2024). In interphase cells, the size of protein condensates in the ER is restricted by ER tubules (Parashar et al., 2021). Thus, it is possible that the size of protein aggregates in the ER is eliminated during cell division. Based on the aggregates characterized in Chapter 4, this chapter further examines their fate during cell division and identifies a clearance mechanism that eliminates these aggregates. This clearance depends on ER remodeling during cell division.

5.2 Results

5.2.1 The quantity and area of protein aggregates depend on the cell stages in naturally dividing cells

Aggregates in dividing cells demonstrated slight turnover while aggregates in interphase cells showed almost no turnover **(Figure 4.13)**. Next, the behavior of aggregates during cell division was further profiled. To achieve this, MCF10A cells expressing ER-FlucDM-eGFP were stained with SiR-Tubulin to differentiate dividing cells at various stages according to microtubule structure. These naturally growing cells were categorized into interphase and prophase, prometaphase, metaphase, anaphase, telophase and early G1 cells. Next, the 3D-stack images were projected onto 2D planes based on their maximum intensity along the Z-axis **(Figure 5.1A)**. Then the number and area of aggregates in cells were analyzed.

Interestingly, the number and area of aggregates in telophase and early G1 cells were significantly lower than in interphase cells **(Figure 5.1A and 5.1B)**. Moreover, the number and area of aggregates were found to continuously decrease from interphase to telophase and early G1, suggesting that aggregates are gradually cleared when cells progress through mitosis and cytokinesis **(Figure 5.1B)**.

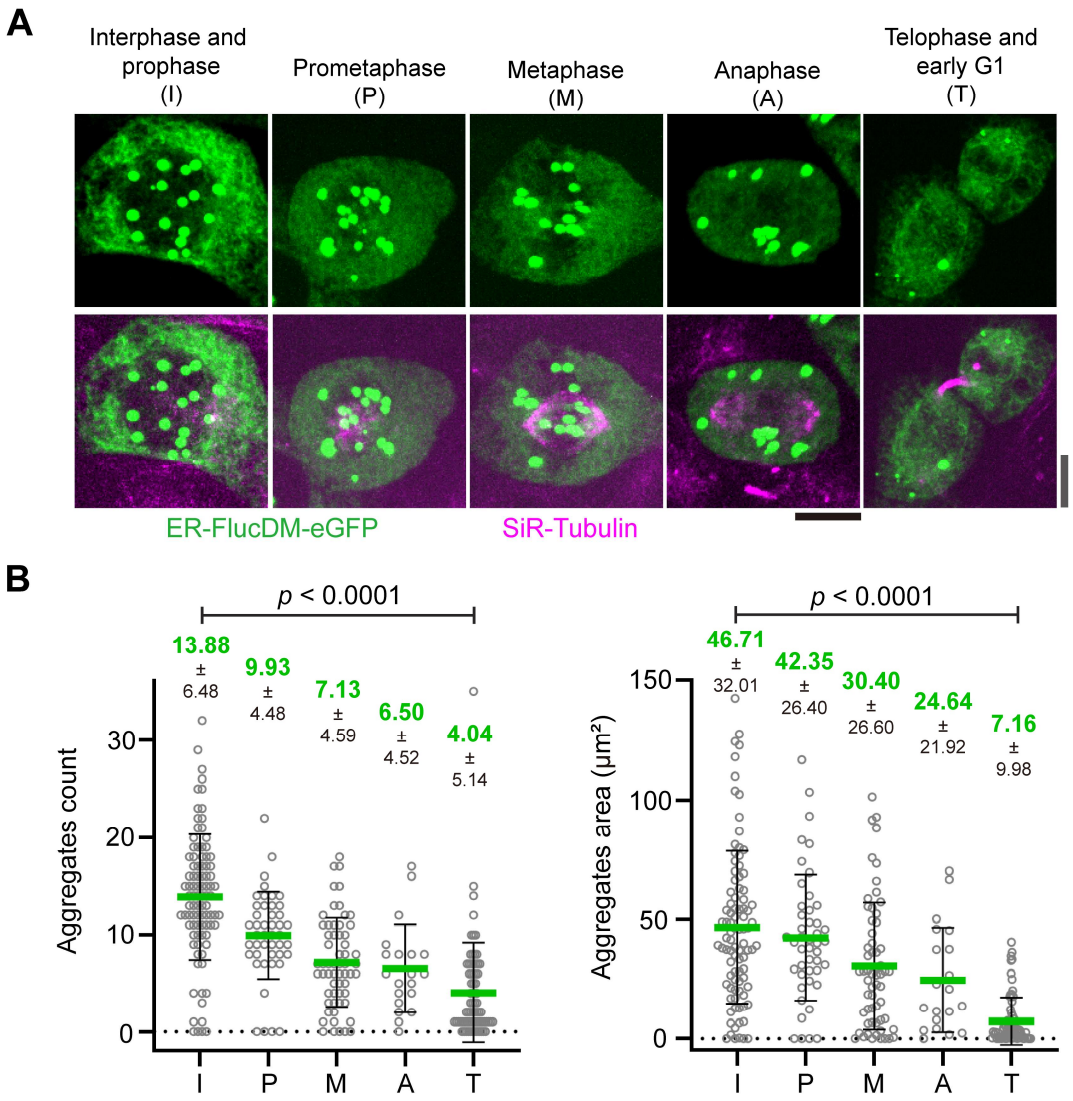


Figure 5.1: The quantity and area of aggregates correlate with stages of cell division. (A) Representative images of dividing cells expressing ER-FlucDM-eGFP at various cell cycle phases. Grey bar was used to scale telophase and early G1 cells. Black bar was used to scale interphase and prophase, prometaphase, metaphase and anaphase. All scale bars are 10 µm. Maximum projected images along the Z-axis are shown. **(B)** Count and areas of ER-FlucDM-eGFP aggregates in dividing cells at different cell cycle phases. Each grey ring represents aggregates from one cell. Interphase and prophase (I), 91 cells; Prometaphase (P), 45 cells; Metaphase (M), 60 cells; Anaphase (A), 20 cells; Telophase and early G1 (T), 73 cells. Data were collected from three independent experiments and represented as the mean ± SD. Unpaired two side Mann-Whitney U-test was used to calculate statistical significance.

5.2.2 Live-cell imaging reveals ER-FlucDM-eGFP aggregates are cleared during cell division

It was previously reported that fixation might introduce artifact to ER structures and

result in unconvincing observations (Wang et al., 2016). Next, to further confirm the clearance of ER-FlucDM-eGFP aggregates, time-lapse imaging was utilized to profile aggregates in cells undergoing division. Because the population of dividing cells in naturally growing MCF10A cells is less than 10%, it is difficult to find dividing cells by random capture. Additionally, naturally dividing cells that could be identified are always post-metaphase, leading to insufficient profiling of whole cell division. Therefore, to enrich dividing cells when imaging, cells were synchronized by RO-3306 at the G2/M boundary and released into mitosis before being observed by microscopy.

Time-lapse imaging results demonstrated that ER-FlucDM-eGFP protein aggregates were released from the nucleus during nuclear envelope breakdown upon mitosis entry **(Figure 5.2A)**. Furthermore, the number and area of these aggregates gradually decreased as cells were progressing through mitosis and cytokinesis **(Figure 5.2B)**. There were essentially no detectable aggregates in the majority of early G1 cells **(Figure 5.2)**. In contrast, the quantity and area of aggregates hardly changed in interphase cells **(Figure 5.2)**. Thus, ER-FlucDM-eGFP aggregates were cleared during cell division but maintained in interphase cells.

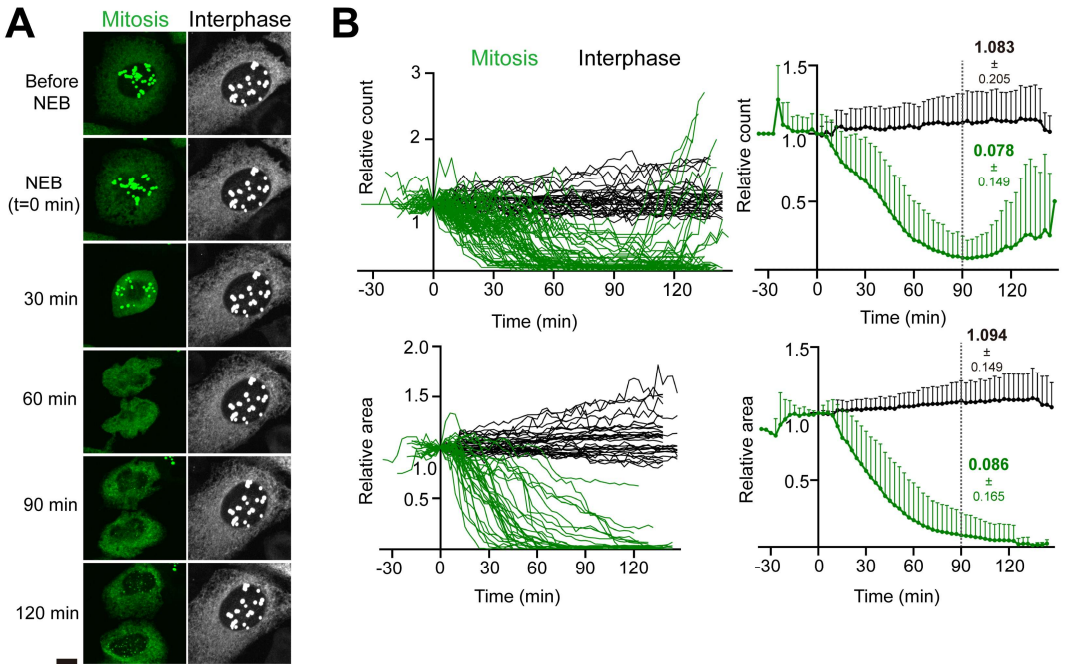


Figure 5.2: Protein aggregates are cleared during cell division. (A) Representative time-lapse images of cells expressing ER-FlucDM-eGFP released from the G2/M

boundary. The moment of nuclear envelope breakdown (NEB) is designated as t = 0 min. Maximum projected images along the Z-axis are shown. The scale bar is 10 μm. **(B)** Quantification of aggregate number and area of dividing cells expressing ER-FlucDM-eGFP. The left panel presents quantification for individual cells. The right panel displays the mean + SD. For each cell, the time corresponding to NEB is set at 0 min. The aggregate counts and total area at each time point were normalized to their respective values at t = 0 min. Data for aggregate counts were collected from 61 interphase and 73 dividing cells across four independent experiments, and aggregate area measurements were obtained from 32 interphase and 34 dividing cells in two independent experiments.

5.2.3 ER-FlucDM-eGFP aggregates in dividing cells are surrounded by the ER membrane

As mentioned previously, ER-FlucDM-eGFP aggregates in interphase cells were surrounded by the ER membrane **(Figure 4.3 and 4.4)**. Next, whether this structure was same in dividing cells was tested by labelling the ER membrane with ER-Tracker. Clearly, these large aggregates were still packaged inside the ER membrane in metaphase, anaphase and telophase cells **(Figure 5.3)**.

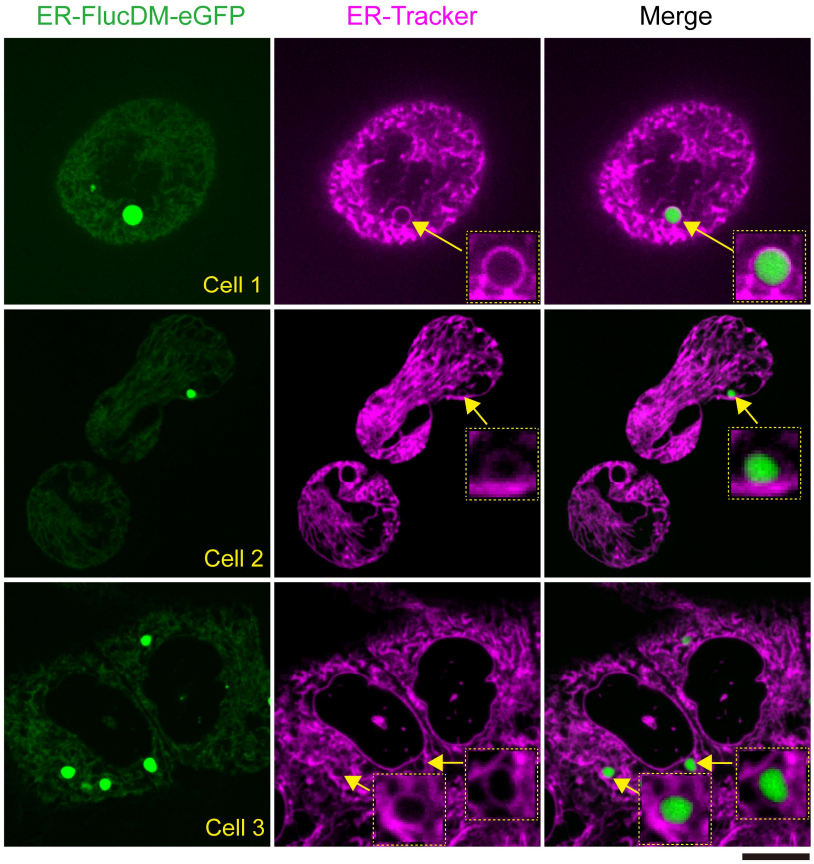


Figure 5.3: Protein aggregates are encapsulated by the ER membrane in dividing

cells. Images to show ER-FlucDM-eGFP aggregates of dividing cells were surrounded by the membrane stained by the ER-Tracker. The scale bar is 10 μm. Single-layer images along the Z-axis are shown.

5.2.4 ER-HaloDM-eGFP aggregates are also cleared during cell division

To test whether aggregate clearance only happened for ER-FlucDM-eGFP aggregates, the dynamics of ER-HaloDM-eGFP aggregates was profiled. Time-lapse movies demonstrated that similar aggregate clearance happened in MCF10A cells expressing ER-HaloDM-eGFP **(Figure 5.4)**.

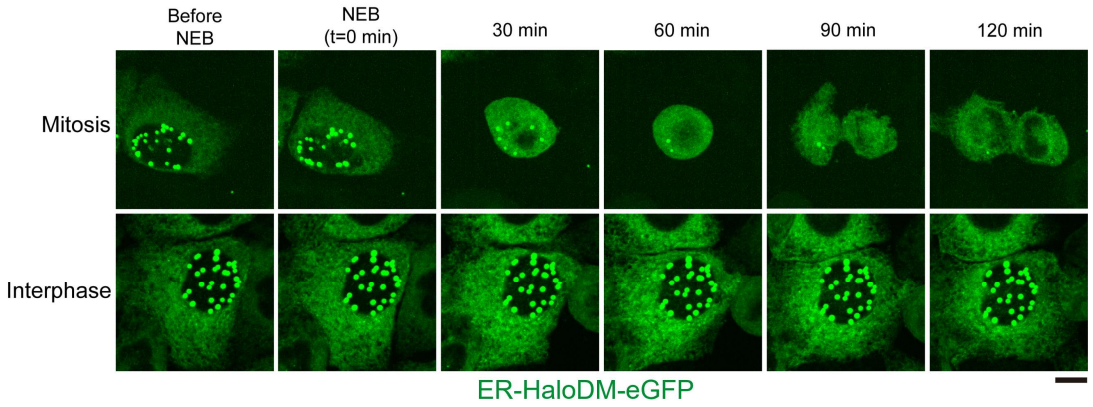


Figure 5.4: Protein aggregates of ER-HaloDM-eGFP are also cleared during cell division. Time-lapse images of cells expressing ER-HaloDM-eGFP released at the G2/M transition. The onset of nuclear envelope breakdown (NEB) is designated as t = 0 min. Maximum projected images along the Z-axis are shown. Scale bar, 10 μm.

5.2.5 Proteasome inhibition undermines aggregate clearance

The proteasomes assist in the degradation of protein aggregates in cells (Li et al., 2022). To investigate whether proteasome activity is involved in aggregate clearance during cell division, I treated dividing cells expressing ER-FlucDM-eGFP with the proteasome inhibitor MG132. Cells released from the G2/M transition were exposed to either low or high concentrations of MG132 for 55 minutes, resulting in most mitotic cells becoming arrested at metaphase and showing a marked increase in aggregate accumulation compared to DMSO-treated controls **(Figure 5.5A and 5.5B)**. Furthermore, when cells in late anaphase or telophase were treated with MG132 and analyzed 35 minutes later, those that had completed cytokinesis displayed significantly higher aggregate numbers than cells treated with DMSO **(Figure 5.5C to 5.5H)**.

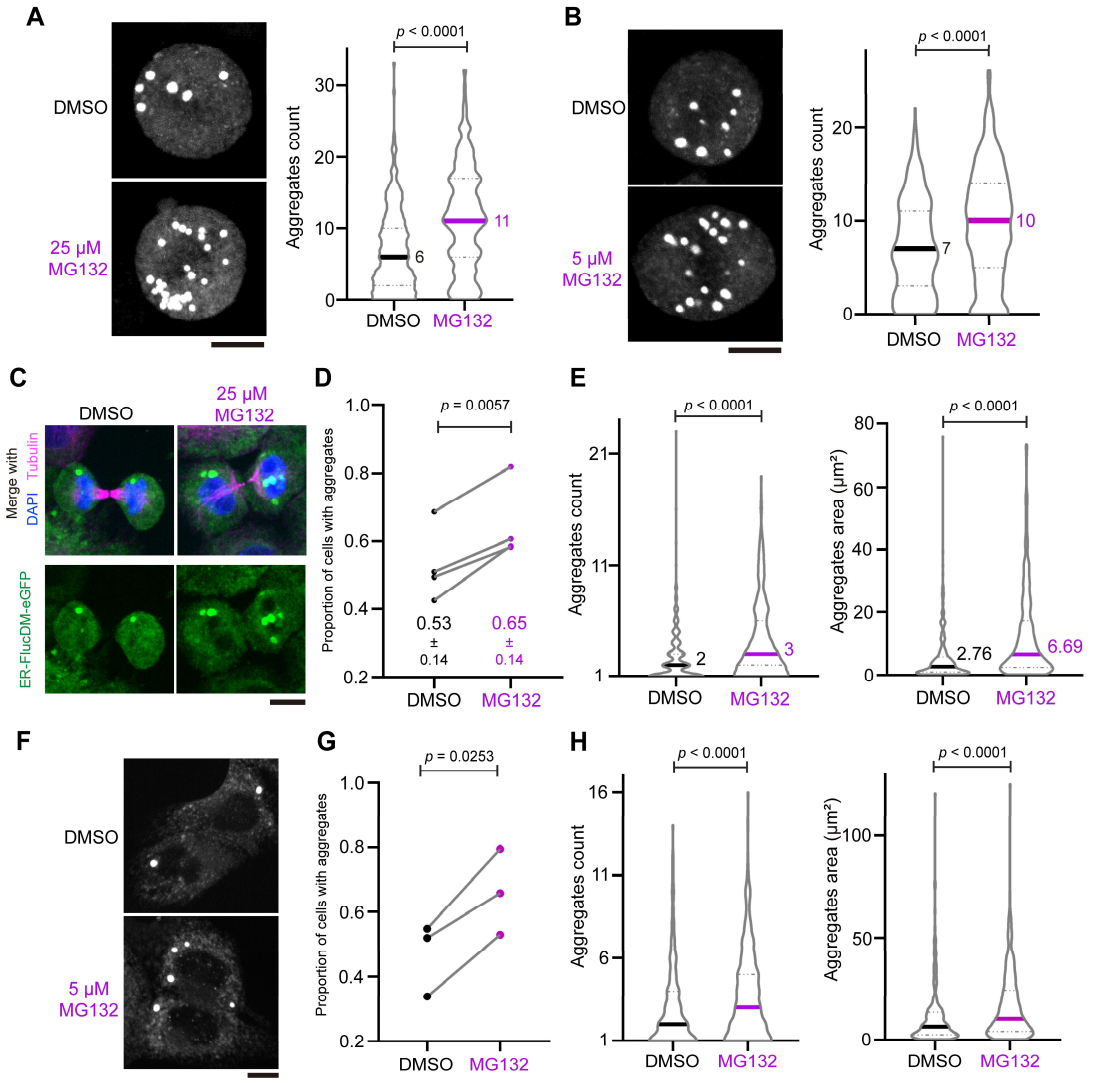


Figure 5.5: MG132 inhibits protein aggregate clearance during cell division. (A) Representative images and quantification of cells expressing ER-FlucDM-eGFP treated with DMSO or 25 μM MG132 and fixed at 55 min after release from the G2/M boundary. DMSO, 293 cells; MG132, 350 cells. **(B)** Representative images and quantification of cells expressing ER-FlucDM-eGFP treated with DMSO or 5 μM MG132 and fixed 55 min after release. DMSO, 295 cells; MG132, 436 cells. **(C)** Representative images of cells at telophase or newly divided cells following treatment with DMSO or 25 μM MG132 for 35 min. **(D)** Telophase cells or newly divided cells that have aggregates upon treatment of 25 μM MG132 were counted. DMSO, 455 cells; MG132, 393 cells. **(E)** The number and area of aggregates were counted in cells at telophase or in newly divided cells after treatment with DMSO or 25 μM MG132. Only those cells that had aggregates were counted. DMSO, 294 cells; MG132, 339 cells. **(F)** Images of cells at telophase and newly divided cells after treatment with DMSO or 5 μM MG132 for 35 min. **(G)** Cells at telophase or newly divided cells that have aggregates upon treatment of DMSO or 5 μM MG132. DMSO, 676 cells; MG132, 646 cells. **(H)** Aggregates number and area were counted in cells at telophase or in newly divided cells after treatment with DMSO or 5 μM MG132. Only cells with aggregates were included in the quantification. DMSO, 227 cells; MG132, 297 cells. Only

maximum projected images along the Z-axis are shown in this figure. All scale bars are 10 μm. Data were collected from at least three independent experiments and analysed by unpaired two side Mann-Whitney U-test (A, B, E and H) and paired t-test (D and G).

5.2.6 APC/C is not involved in aggregate clearance during cell division

It was established that the clearance of aggregates during cell division requires proteasomes **(Figure 5.5)**. It is possible that the anaphase promoting complex/cyclosome (APC/C), as an E3 ubiquitin ligase regulating mitotic exit, contributes to aggregate clearance. To investigate this, I inhibited APC/C activity in dividing cells expressing ER-FlucDM-eGFP using a cocktail of inhibitors (APC/Ci), composed of Apcin and proTAME (Sackton et al., 2014).

Interestingly, APC/C inhibition did not alter aggregate clearance because APC/Ci-treated cells that had arrested at metaphase had comparable number of aggregates as in DMSO-treated cells **(Figure 5.6A and 5.6B)**. Likewise, when APC/Ci was applied to cells in late anaphase or telophase, the resulting newly divided cells showed aggregate counts comparable to control cells **(Figure 5.6C to 5.6E)**. Furthermore, the efficacy of APC/C inhibition was confirmed using an APC/C reporter derived from the degron of human Geminin (hGeminin). APC/Ci treatment prevented the removal of the reporter in newly divided cells, demonstrating effective inhibition of APC/C at the used concentration **(Figure 5.6F and 5.6G)**. Taken together, while the clearance of ER-FlucDM-eGFP aggregates during mitotic exit relies on proteasomal activity, it does not appear to require the E3 ligase APC/C.

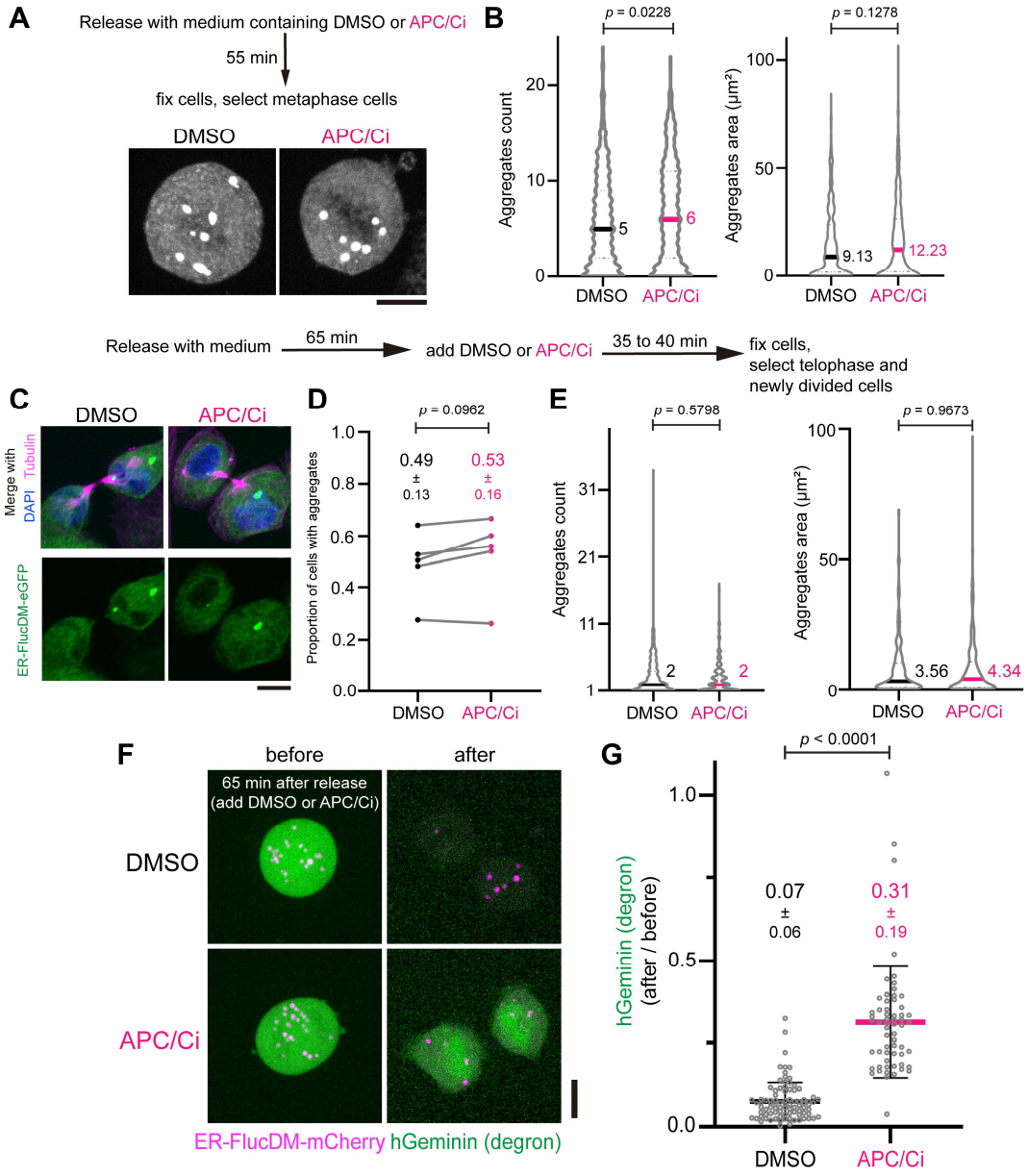


Figure 5.6: APC/C is not involved in aggregate clearance during cell division. (A) Representative images of cells expressing ER-FlucDM-eGFP treated with DMSO or APC/Ci (a combination of 20 μM proTAME and 300 μM Apcin) and fixed at 55 min after released from the G2/M boundary. **(B)** Quantifications of cells expressing ER-FlucDM-eGFP treated with DMSO or APC/Ci. DMSO, 450 cells; APC/Ci, 549 cells. **(C)** Representative images of cells either at telophase or newly divided after exposure to DMSO or APC/Ci for 35 to 40 minutes. **(D)** Cells at telophase or newly divided cells that have aggregates upon treatment of DMSO or APC/Ci were counted. **(E)** Aggregates number and area were counted in cells at telophase or newly divided cells after treatment with DMSO or APC/Ci. Only cells with aggregates were included in the quantification. DMSO, 297 cells; APC/Ci, 319 cells. **(F)** Representative images of cells simultaneously expressing ER-FlucDM-mCherry and mGreenLantern-hGeminin (degron). Left panel: cells were treated with DMSO or APC/Ci after 65 min post-release from the G2/M. Right panel: cells were treated with DMSO or APC/Ci for 40 minutes

using live-cell imaging after a 65-minute release from G2/M. **(G)** Quantification of mGreenLantern-hGeminin (degron) fluorescence intensity in cells treated with DMSO or APC/Ci for 40 min. DMSO, 87 cells; APC/Ci, 60 cells. All representative images are maximum projected images along the Z-axis in this figure. All scale bars are 10 μm. Data are from at least three independent experiments and analyzed by unpaired two side Mann-Whitney U-test (B and E), paired t-test (D) or unpaired t-test (G).

5.2.7 Lysosome acidification inhibition hinders aggregate clearance

Lysosomes participate in the degradation of protein aggregates (Johnston and Samant, 2021). To test whether lysosomes involved in aggregate clearance in dividing cells, bafilomycin A1 (Baf), a lysosome acidification inhibitor, was employed. G2/M-arrested cells were released with Baf or were pretreated with Baf for 3 hours before being released into mitosis. Releasing with Baf demonstrated the neglectable effect on aggregate clearance **(Figure 5.7A and 5.7B)**. However, cells pretreated with Baf remained more aggregates at 65 min after release, suggesting lysosomes may be involved in aggregate clearance **(Figure 5.7C and 5.7D)**.

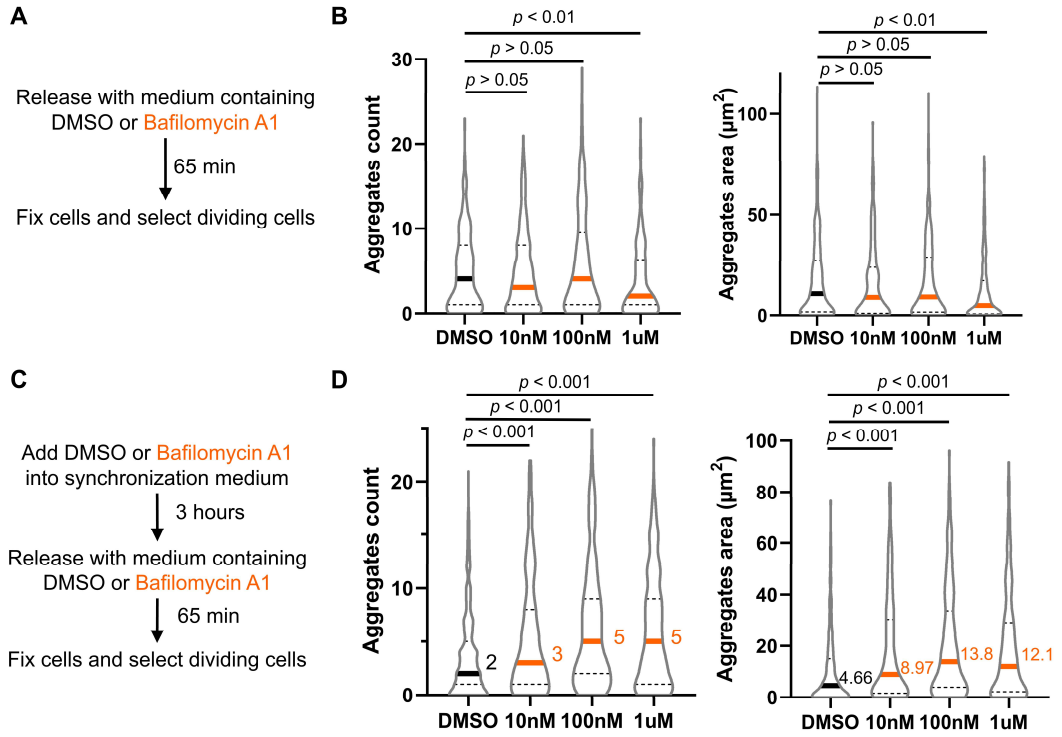


Figure 5.7: Effects of bafilomycin A1 on protein aggregate clearance during cell division. (A) The procedure of bafilomycin A1 short treatment. **(B)** Quantifications of dividing cells expressing ER-FlucDM-eGFP treated with DMSO or bafilomycin A1. DMSO, 364 cells; 10 nM, 225 cells; 100 nM, 265 cells; 1 μM, 230 cells. **(C)** The procedure of bafilomycin A1 pretreatment. **(D)** Quantifications of remaining aggregates in cells expressing ER-FlucDM-eGFP pretreated with DMSO or bafilomycin A1.

DMSO, 372 cells; 10 nM, 249 cells; 100 nM, 231 cells; 1 μM, 262 cells. The specific number in figure is the median. Data are collected from three independent experiments and analyzed by unpaired two side Mann-Whitney U-test.

5.2.8 Total GFP levels barely change along with aggregate clearance

Knowing that both proteasome and lysosome perturbation inhibited aggregate clearance, next, if aggregate clearance originated from degradation was tested. Ideally, the convincing technique to profile their degradation in a live cell is using ER-FlucDM tagged with photoactivatable fluorescent proteins. By activating the fluorescent protein in the aggregates and monitoring the intensity of fluorescence during cell division, whether aggregate clearance results from degradation can be addressed. However, this method is difficult to achieve because of several technical reasons. A cell typically contains about twenty aggregates in my study and these aggregates move rapidly within a Z-stack of about 20 μm. Furthermore, it is not easy to precisely activate the fluorescent proteins in an aggregate with the diameter of about 1 μm without activating nearby proteins. These concerns all increased the difficulties in precisely photoactivating aggregates within a realistic timescale.

In my study, to profile the degradation of ER-FlucDM-eGFP, cycloheximide (CHX) chase experiments were employed. To be specific, cells expressing ER-FlucDM-eGFP were arrested at G2/M and released into mitosis with DMSO or CHX, an inhibitor of protein translation. At several time points after release, cell lysates were collected. The degradation of ER-FlucDM-eGFP was profiled by quantifying the remaining GFP in the lysate because new protein synthesis was blocked by CHX **(Figure 5.8A)**. The degradation of cyclin B1 along with mitotic progression was used to demonstrate mitotic cell enrichment **(Figure 5.8B)** (Kucharski et al., 2017). A short half-life protein, p53, was employed to validate the inhibition efficiency **(Figure 5.8B)** (Li et al., 2021). Surprisingly, the abundance of GFP from ER-FlucDM-eGFP did not significantly decrease along with the progression of cell division in both DMSO and CHX groups, suggesting ER-FlucDM-eGFP is not significantly degraded during cell division **(Figure 5.8C)**. Interestingly, the GFP intensity in DMSO group decreased slightly before

increasing **(Figure 5.8C)**, which is similar to the consensus about protein synthesis during cell division (Konrad, 1963; Miettinen et al., 2019). This tendency further solidates our method, namely, profiling the degradation of ER-FlucDM-eGFP by CHX chase experiments.

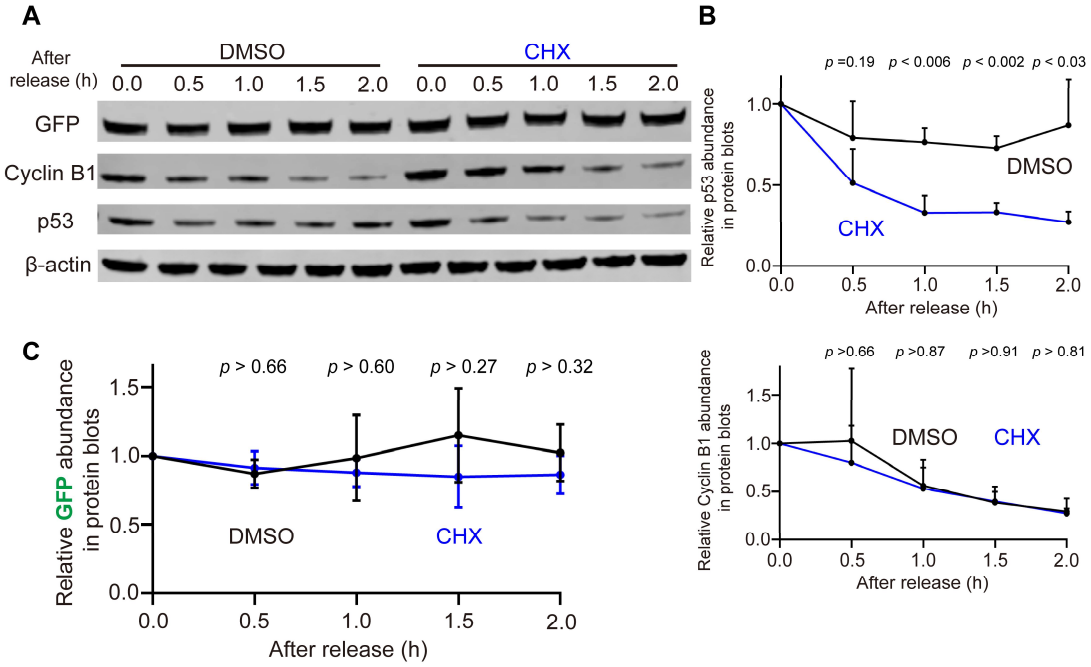


Figure 5.8: Cycloheximide chase experiments of cells expressing ER-FlucDM-eGFP. (A) Protein blots of ER-FlucDM-eGFP, cyclin B1, p53 and β-actin following treatment with either DMSO or 200 μM CHX. Cells were synchronized at the G2/M boundary and released into medium containing DMSO or CHX. At several designated time points, lysates were harvested. **(B)** Quantification and plotting of p53 and cyclin B1 protein levels at various time points after DMSO or CHX treatment, with β-actin serving as the normalization control. **(C)** Quantification and plotting of ER-FlucDM-eGFP protein levels over time after DMSO or CHX treatment, normalized to β-actin. Data were collected from three independent experiments and represented as the mean + SD (B) or mean ± SD (C). All data were analysed by unpaired t-test.

To further examine whether ER-FlucDM-eGFP was degraded during cell division, I profiled the fluorescent intensity of GFP in dividing cells. To be specific, cells were arrested at G2/M and released into mitosis. At 25 min or 90 min after release, Z-stacked images containing dividing cells were randomly captured. After subtracting the background, GFP fluorescence signals at two different time points were compared. If ER-FlucDM-eGFP aggregates are obviously degraded during cell division, GFP intensity at 90 min should be significantly lower than that at 25 min. However,

negligible difference was observed at these two time points, indicating that the ER-FlucDM-eGFP signal was largely maintained during cell division **(Figure 5.9)**.

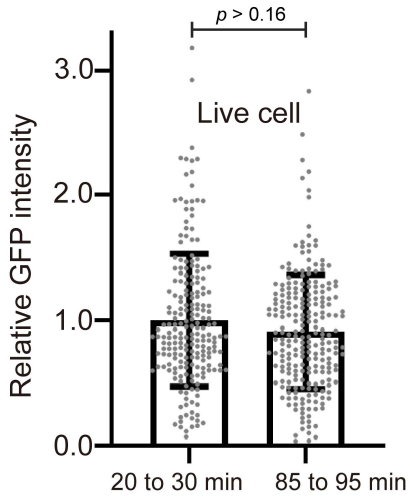


Figure 5.9: Relative intensity of ER-FlucDM-eGFP in early versus late dividing cells. Mean ± SD of three independent experiments. 20 to 30 min, 208 cells; 85 to 95 min, 232 cells. Data were analyzed by unpaired t-test.

Taken together, the clearance of ER-FlucDM-eGFP protein aggregates in dividing cells unexpectedly originates from disassembly instead of degradation.

5.2.9 The expression of ER-FlucDM-eGFP induces the unfolded protein response

To explore how dividing cells disassembled protein aggregates, proteomics was employed to profile cells' response upon the expression of ER-FlucDM-eGFP. An empty plasmid transduction group was utilized to exclude potential artefacts resulted from the transduction of lentivirus and the selection of puromycin.

Compared to the empty plasmid, ER stress-related genes such as HSPA5 (BiP, the Hsp70 in the ER), HSP90B1 (an Hsp90 in the ER), MANF (mesencephalic astrocyte-derived neurotrophic factor, a protein recently considered to facilitate protein folding in the ER), several PDIs (protein disulfide isomerases, which assisted in protein folding) and two lectin chaperones (CALR and CANX) were upregulated upon the overexpression of ER-FlucDM-eGFP **(Figure 5.10A)**. These upregulated genes were enriched in the ER stress and unfolded protein response (UPR) (Wiseman et al., 2022;

Yan et al., 2019), indicating that misfolding-prone FlucDM induces ER stress and that cells utilize the UPR to relieve this stress. Additionally, quantitative real-time PCR (qRT-PCR) revealed that mRNA levels of several ER stress response genes were upregulated upon the expression of ER-FlucDM-eGFP **(Figure 5.10B)**.

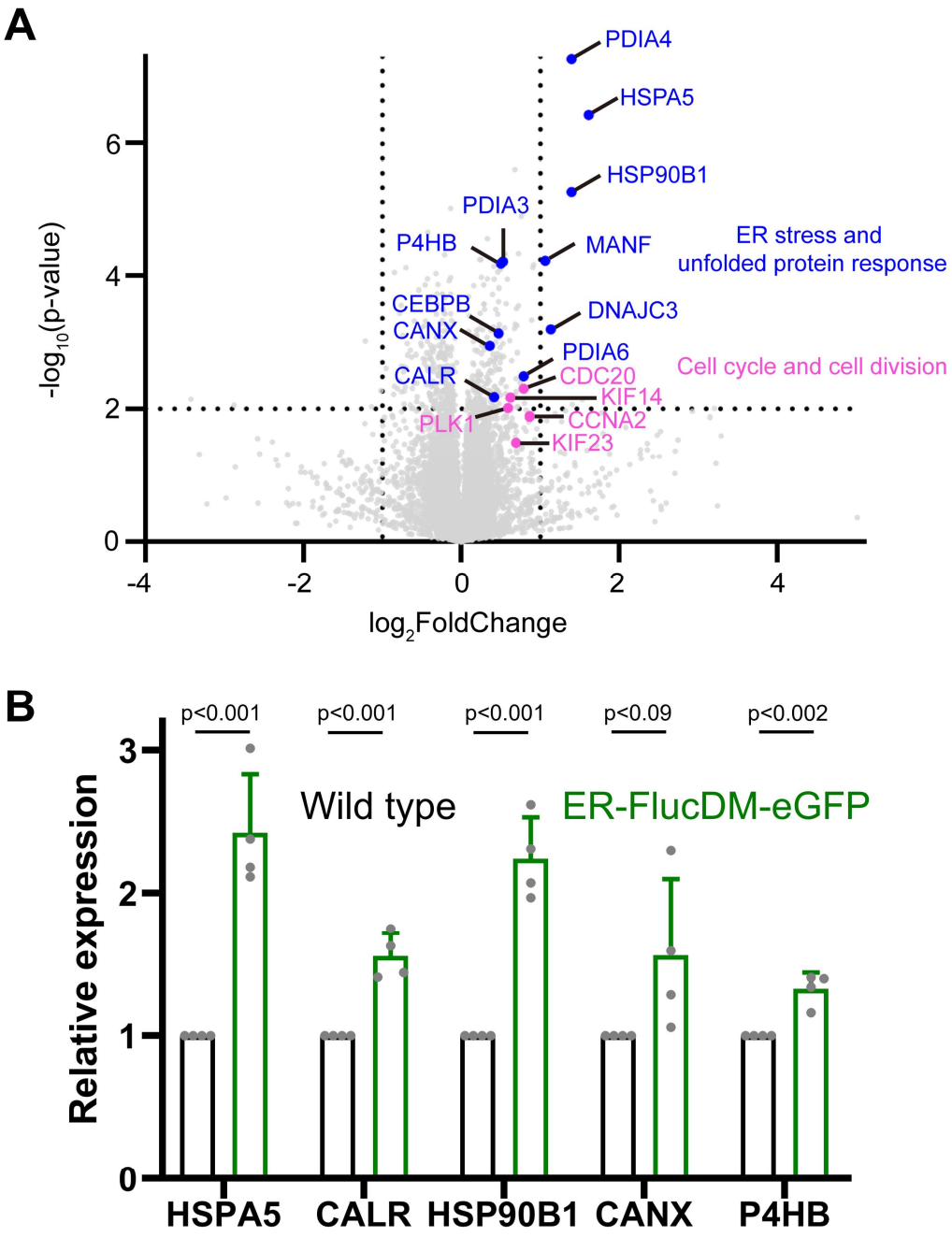


Figure 5.10: Volcano plot of proteomics analysis and the validation by qRT-PCR. (A) Volcano plot illustrating the proteomic profiling of cells expressing ER-FlucDM-eGFP. Data were collected from three independent replicas. Proteins associated with ER stress and the unfolded protein response are marked in blue, while those related to

cell cycle regulation and division are highlighted in pink. **(B)** qRT-PCR analysis of several ER stress induced genes. Five days after the transduction of ER-FlucDM-eGFP in wild-type MCF10A cells, lysates were collected. Relative expressions of each gene were normalized to GAPDH first. Mean + SD of four independent experiments. Unpaired t-test was used.

5.2.10 Effects of ER stressors on aggregate clearance

5.2.10.1 Thapsigargin inhibits aggregate clearance

Proteomics profiling revealed that multiple ER stress response proteins were upregulated **(Figure 5.10A)**, suggesting ER proteostasis facilitate the clearance of protein aggregates. Therefore, it is assumed that additional ER stress during cell division might inhibit aggregate clearance. To test this, thapsigargin (Thaps), an inhibitor of sarco-endoplasmic reticulum Ca^{2+} ATPases, was used to deplete calcium ions in the ER and subsequently induced ER stress (Melo et al., 2022). MCF10A cells expressing ER-FlucDM-eGFP were synchronized and released into mitosis with medium containing either DMSO or 1 μM Thaps. 35 min or 65 min after release, cells were fixed. Then the number and area of aggregates in dividing cells were calculated.

The results indicated that in cells at prometaphase and metaphase (35 minutes post-release), both the number and area of aggregates demonstrated no significant differences **(Figure 5.11A and 5.11B)**. However, at the late stage of cell division (65 minutes post-release), cells treated with Thaps retained a significantly higher number of aggregates compared to those treated with DMSO **(Figure 5.11A and 5.11B)**. In addition to fixed cells, time-lapse microscopy consistently showed that ER-FlucDM-eGFP aggregates were largely remained in Thaps-treated cells even after cytokinesis, whereas these aggregates were primarily cleared in control cells **(Figure 5.11C and 5.11D)**. In sum, ER stress inducer thapsigargin inhibited the clearance of ER-FlucDM-eGFP aggregates in dividing cells.

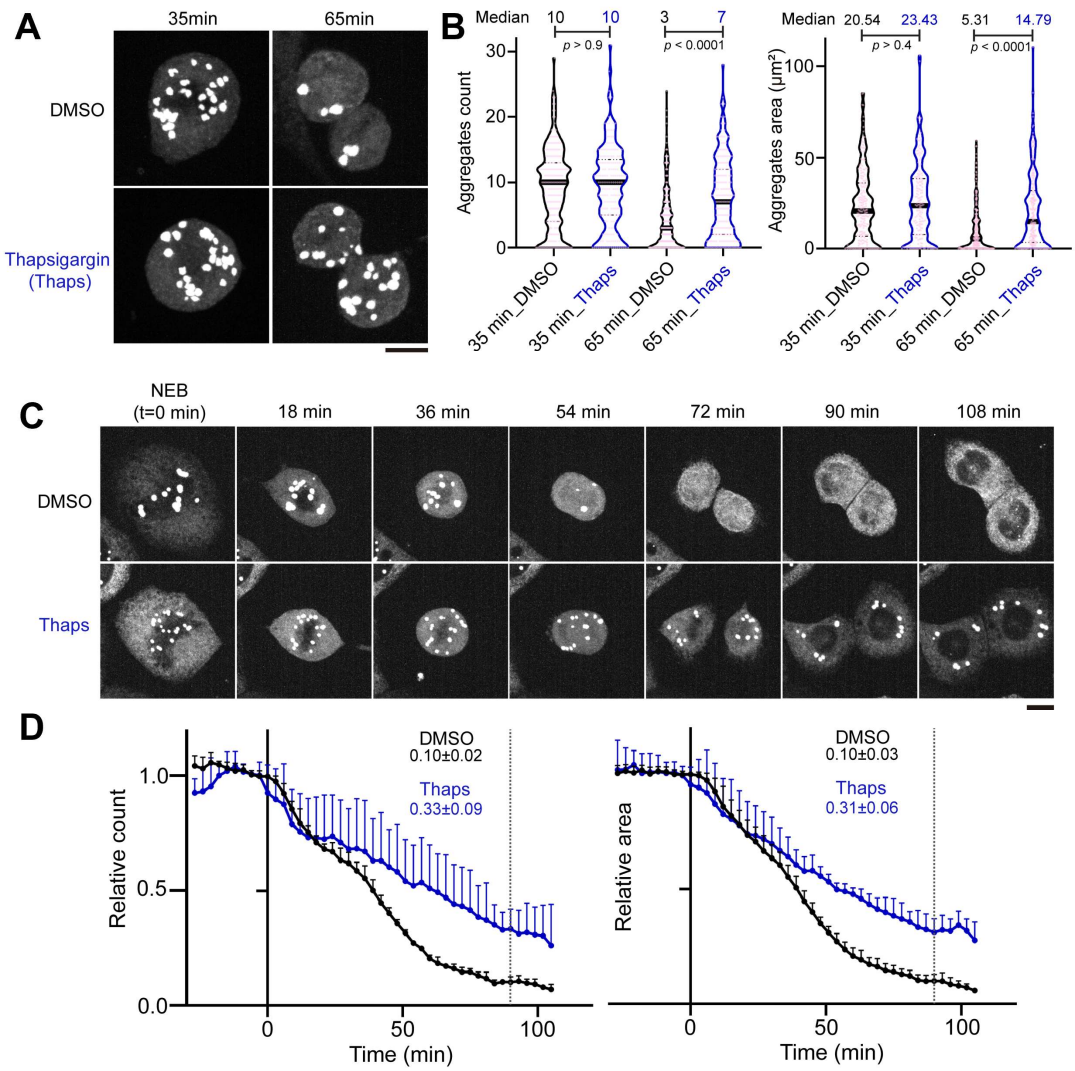


Figure 5.11: Thapsigargin inhibits protein aggregate clearance during cell division. **(A)** Representative images of MCF10A cells expressing ER-FlucDM-eGFP treated with DMSO or 1 µM Thaps and fixed at 35 min or 65 min after release from the G2/M boundary. **(B)** Quantification of cells treated with DMSO or 1 µM Thaps and fixed at 35 min or 65 min after release from the G2/M boundary. 35 min_DMSO, 207 cells; 35 min_Thaps, 173 cells; 65min_DMSO, 244 cells; 65 min_Thaps, 209 cells. Unpaired two side Mann-Whitney U-test was used to calculate statistical significance. In the violin plot, the solid black line represents the median, gray dotted lines indicate quartiles, and each light pink circle represents an individual cell measurement. **(C)** Representative time-lapse images of cells expressing ER-FlucDM-eGFP treated with either DMSO or 1 µM Thaps following release from the G2/M boundary. **(D)** Quantification of cells expressing ER-FlucDM-eGFP treated with DMSO or 1 µM Thaps, with the time of nuclear envelope breakdown (NEB) set as t = 0 min for each cell. Aggregate counts and total aggregate areas were normalized to their respective values at t = 0 min. Black dotted lines mark 90 minutes post-NEB. The data include 89 cells for the DMSO group and 65 cells for the Thaps group. Representative images in this figure are maximum projected images along the Z-axis. All scale bars are 10 µm. Data were collected from three (C and E) or four (A) independent experiments.

5.2.10.2 Tunicamycin short treatment does not inhibit aggregate clearance while its pretreatment accelerates aggregate clearance

To test if other ER stress inducers had the same inhibitory effect on aggregate clearance during cell division, tunicamycin (Tuni), an inhibitor of glycosylation, was used to treat cells (Melo et al., 2022). Results demonstrated that there was no significant difference between DMSO-treated and Tuni-treated cells at the late stage of cell division **(Figure 5.12A and 5.12B)**.

A previous study demonstrated that the treatment of Thaps or Tuni promoted the clearance of protein aggregates after several hours (Melo et al., 2022). To investigate whether prolonged Tuni treatment cleared aggregates in cells, I pretreated G2/M-arrested cells with various concentrations of Tuni for 3 hours before releasing them into mitosis. Interestingly, Tuni pretreatment before mitosis facilitated aggregate clearance in dividing cells **(Figure 5.12C and 5.12D)**. Next, Thaps was also used to pretreat cells, however, almost no cells entered mitosis after pretreatment with 100 nM Thaps for 3 hours. In summary, Tuni short treatment did not inhibit aggregate clearance while extended pretreatment promoted aggregate clearance.

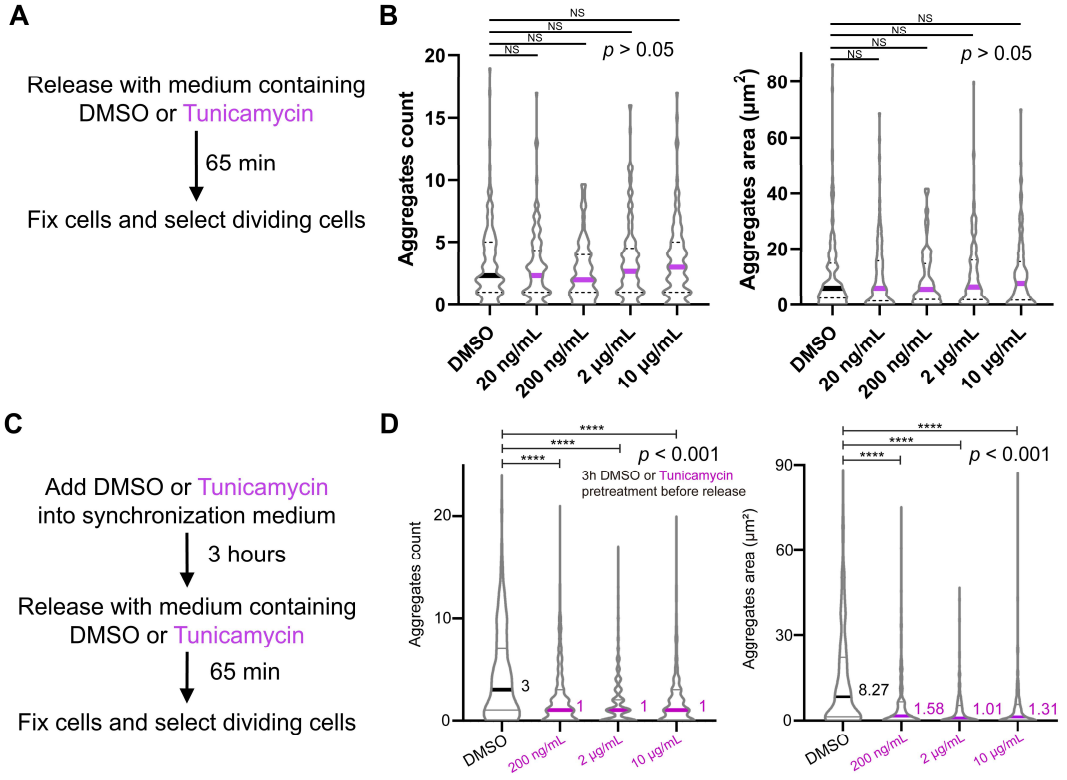


Figure 5.12: Effects of tunicamycin on protein aggregate clearance during cell division. (A) The procedure of tunicamycin short treatment. **(B)** Quantification of aggregate number and total area of dividing cells expressing ER-FlucDM-eGFP pretreated with DMSO or Tunicamycin. DMSO, 169 cells; 20 ng/mL, 131 cells; 200 ng/mL, 98 cells; 2 μg/mL, 173 cells; 10 μg/mL, 145 cells. **(C)** The procedure of Tunicamycin short treatment. **(D)** Quantification of aggregate number and total area of dividing cells expressing ER-FlucDM-eGFP pretreated with DMSO or Tunicamycin. DMSO, 542 cells; 200 ng/mL, 385 cells; 2 μg/mL, 471 cells; 10 μg/mL, 439 cells. The specific number in figure is the median. Data were acquired from three (B) or four (D) independent experiments. Unpaired two side Mann-Whitney U-test.

5.2.11 Inhibition of either Hsp70 or its family member BiP prevents aggregate clearance

The heat shock protein 70 (Hsp70) family, a group of ATP-dependent molecular chaperones, was widely reported to assist in the disaggregation of firefly luciferase protein aggregates and this disaggregation capacity depended on its ATPase activity (Amankwah et al., 2022; Jin et al., 2008). Therefore, Hsp70 might play a major role in aggregate clearance during cell division in my study. To examine this, VER-155008 (VER), an ATPase inhibitor of Hsp70, was utilized to treat dividing cells (Massey et al., 2010). MCF10A cells expressing ER-FlucDM-eGFP were synchronized at G2/M boundary and released into mitosis in the presence of DMSO or VER. 65 min after release, cells were fixed. Results showed that dividing cells retained significantly more aggregates upon VER treatment **(Figure 5.13A and 5.13B)**. Moreover, live-cell time-lapse microscopy also demonstrated that ER-FlucDM-eGFP aggregates were not cleared effectively upon VER treatment **(Figure 5.13C)**.

The human Hsp70 family consists of thirteen members (Radons, 2016). In this work, upon the overexpression of ER-FlucDM-eGFP, the upregulation of binding immunoglobulin protein (BiP), the major Hsp70 in the ER, was confirmed by proteomics **(Figure 5.10)**. Meanwhile, the ER stress inducer thapsigargin also hindered aggregate clearance **(Figure 5.11)**. Therefore, it is speculated that BiP might be involved in the disaggregation process. Results demonstrated that YUM70, a BiP ATPase specific inhibitor (Samanta et al., 2021), indeed abolished aggregate clearance

in dividing cells in a dose-dependent manner **(Figure 5.13D and 5.13E)**.

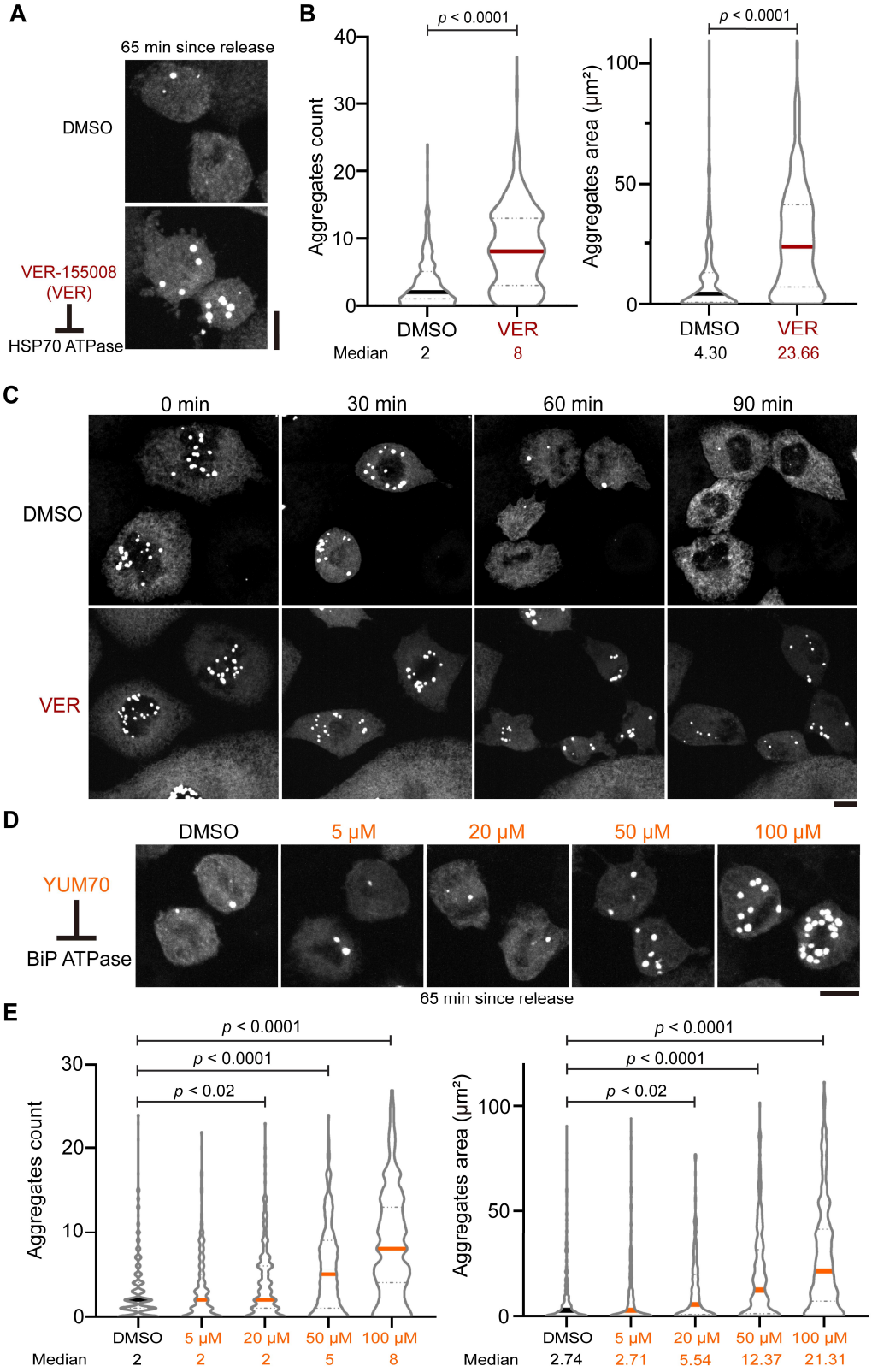


Figure 5.13: Inhibition of Hsp70 and BiP abolishes aggregate clearance. (A) Representative images of cells expressing ER-FlucDM-eGFP treated with either DMSO or 50 µM VER and fixed at 65 min after release from the G2/M boundary. **(B)** Quantification of cells expressing ER-FlucDM-eGFP treated with DMSO or 50 µM

VER and fixed at 65 min post-release from the G2/M boundary. DMSO, 357 cells; VER, 465 cells. **(C)** Time-lapse images of dividing cells expressing ER-FlucDM-eGFP treated with DMSO or 50 μM VER. **(D)** Representative images of cells expressing ER-FlucDM-eGFP treated with DMSO or various dosages of YUM70. **(E)** Quantification of cells expressing ER-FlucDM-eGFP treated with DMSO or YUM70 and fixed 65 min post release. DMSO, 310 cells; 5 μM YUM70, 258 cells; 20 μM YUM70, 215 cells; 50 μM YUM70, 209 cells; 100 μM YUM70, 287 cells. All representative images in this figure are maximum projected images along the Z-axis. All scale bars are 10 μm. Unpaired two side Mann-Whitney U-test.

5.2.12 ER structure remodeling ensures aggregate clearance

5.2.12.1 ER membrane structures are perturbed upon BiP inhibition in mitotic cells

ER stress induction by Thaps, VER or YUM70 all inhibited aggregate clearance **(Figure 5.11 and Figure 5.13)**. Furthermore, aggregates were encapsulated by the ER membrane **(Figure 5.3)**. Previous studies demonstrated that ER stress changed ER structures such as the induction of ER dilation and ER whorls (Xu et al., 2021; Xu and Wang, 2024). Thus, the ER structure alteration introduced by ER stress might explain aggregate clearance. To test whether ER stress induction by BiP inhibition changed ER structures in mitotic cells, Sec61β tagged with a fluorescent protein was used to label the ER membrane of dividing cells (Zhao et al., 2024). Upon YUM70 treatment, visible alterations of ER membrane structures occurred **(Figure 5.14)**. Therefore, ER structure perturbation correlated with the abolishment of aggregate clearance.

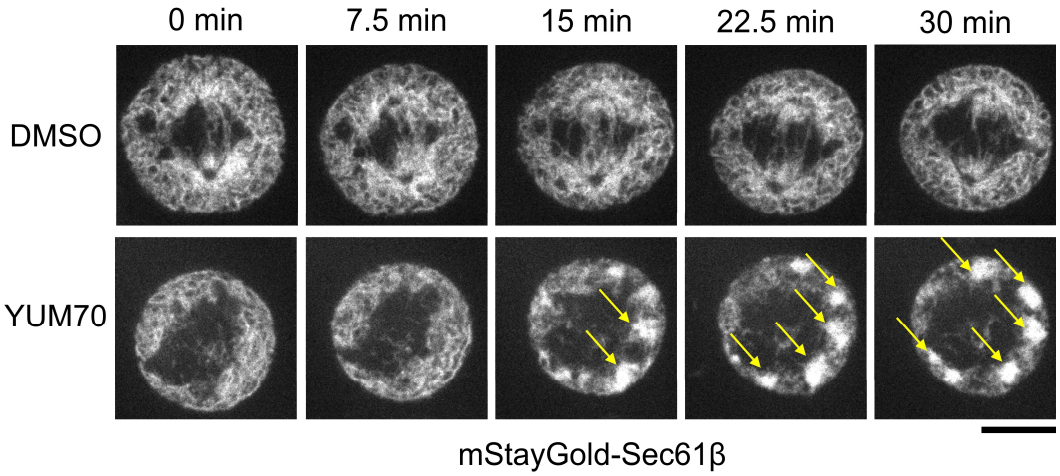


Figure 5.14: BiP inhibition alters ER structure in dividing cells. Cells were transduced by lentivirus to express mStayGold-Sec61β. Within 72 hours after

transduction, naturally dividing cells were monitored. The scale bar is 10 μm. The imaging start time was set to 0 min.

5.2.12.2 Nocodazole, a microtubules depolymerizer, inhibits aggregate clearance

Previous studies demonstrated that microtubules participated in ER remodeling during cell division (Diaz et al., 2019; Schlaitz et al., 2013; Zhang et al., 2024). Therefore, if the clearance of aggregates depends on ER remodeling, it should be inhibited upon the disassembly of microtubules. To examine this, nocodazole was employed to induce the depolymerization of microtubules in dividing cells. G2/M-arrested cells were released with DMSO or nocodazole for 65 minutes before fixation. Results showed that cells from the nocodazole group remained more aggregates than DMSO group, suggesting the efficient assembly of microtubule facilitates aggregate clearance **(Figure 5.15)**.

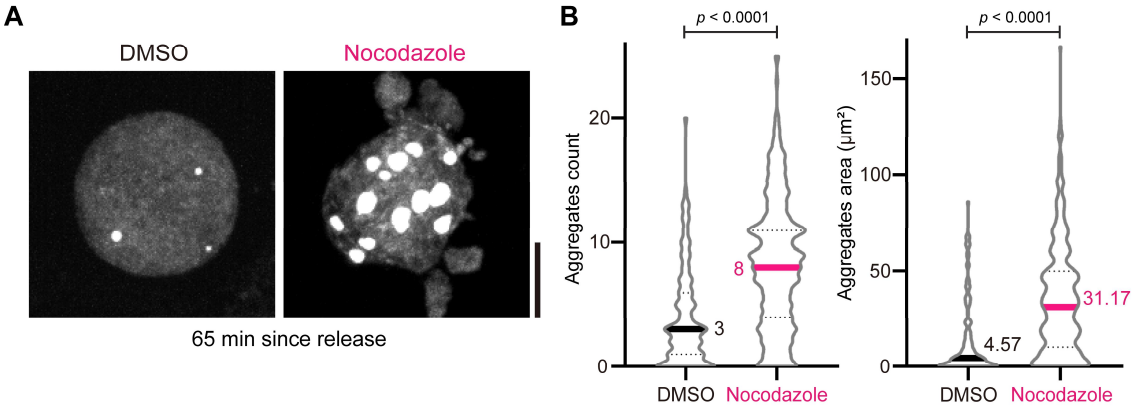


Figure 5.15: Nocodazole inhibits aggregate clearance during cell division. (A) Representative images of cells expressing ER-FlucDM-eGFP treated with DMSO or 331 nM nocodazole and fixed at 65 min post-release from the G2/M boundary. **(B)** Quantification of cells expressing ER-FlucDM-eGFP treated with DMSO or 331 nM nocodazole and fixed at 65 min post-release. Only round mitotic cells were counted during quantification. DMSO, 122 cells; Nocodazole, 320 cells. All representative images in this figure are maximum projected images along the Z-axis. The scale bar is 10 μm. Data were from three independent experiments and analysed by unpaired two side Mann-Whitney U-test. The specific number in figure is the median.

5.2.12.3 RO-3306, a Cdk1 inhibitor, accelerates aggregate clearance in metaphase-arrested cells

Previous studies demonstrated that cyclin-dependent kinase 1 (Cdk1) was involved in the ER reorganization during cell division (Bergman et al., 2015; Gatta et al., 2021). In this study, protein aggregates were eliminated as cells progressed through mitosis and cytokinesis, stages of the cell cycle characterized by low Cdk1 activity. This suggests that Cdk1 inactivation may promote the clearance of ER-FlucDM-eGFP aggregates. To investigate this, cells were released into mitosis and treated with MG132 for 55 minutes to induce metaphase arrest, followed by RO-3306 treatment to inhibit Cdk1 activity. Notably, ER-FlucDM-eGFP aggregates were cleared in cells treated by RO-3306, whereas they persisted in DMSO-treated controls **(Figure 5.16A and 5.16B)**. Consistently, live-cell imaging confirmed that Cdk1 inhibition accelerated aggregate removal **(Figure 5.16C and 5.16D)**. These findings indicate that Cdk1 inactivation facilitates aggregate clearance.

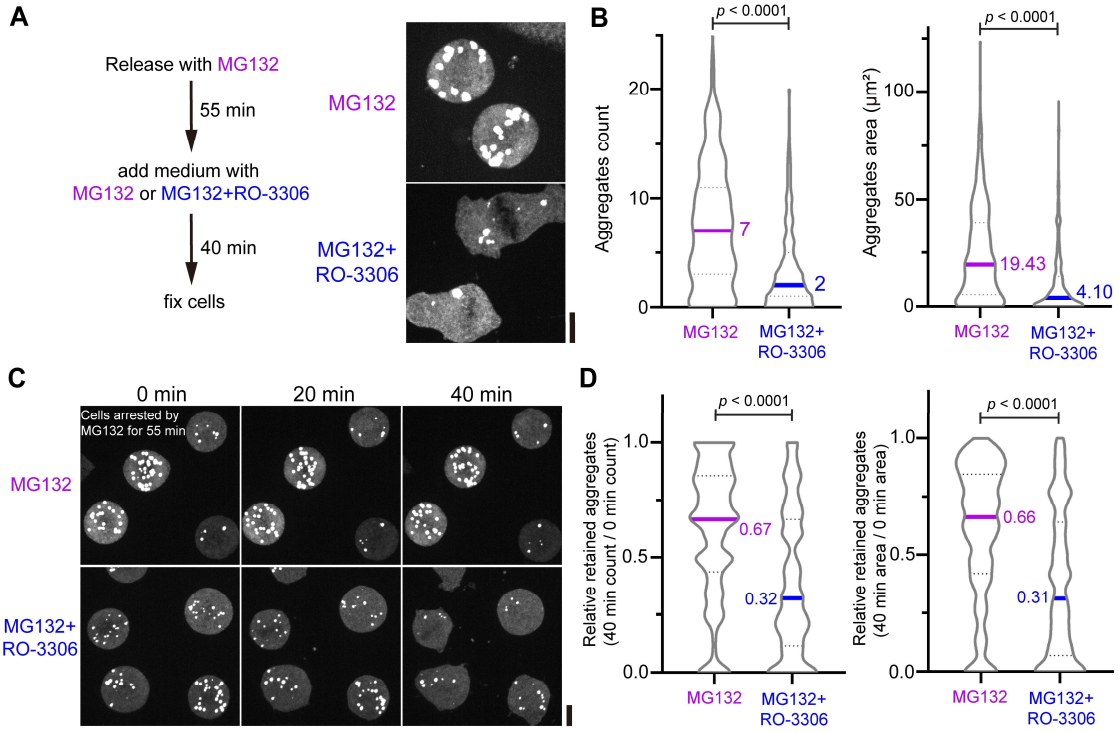


Figure 5.16: Cdk1 inhibition in MG132-arrested cells accelerates aggregate clearance. (A) Representative images of cells expressing ER-FlucDM-eGFP arrested at mitosis by MG132 and further treated with the Cdk1inhibitor to induce mitotic exit. Cells were initially exposed to 25 µM MG132 for 55 minutes, after which mitotically arrested cells were further treated with either 25 µM MG132 alone or a combination of

25 μM MG132 and 10 μM RO-3306. Fixation was performed 40 minutes after the second treatment. **(B)** Quantification of (A). MG132 only, 442 cells; MG132 + RO-3306, 374 cells. **(C)** Time-lapse images of cells expressing ER-FlucDM-eGFP arrested at mitosis by MG132 and further treated with RO-3306 to induce mitotic exit. Cells were treated with 25 μM MG132 for 55 min, and further treated with 25 μM MG132 plus 10 μM RO-3306 or 25 μM MG132 before imaging. **(D)** The number and area of remaining aggregates at 40 minutes were assessed and compared to those at 0 min. MG132 only, 125 cells; MG132 + RO-3306, 134 cells. All representative images in this figure are maximum projected images along the Z-axis. All scale bars are 10 μm. Data were collected from three independent experiments and analysed using unpaired two side Mann-Whitney U-test. The specific number in figure is the median value.

5.2.12.4 Nocodazole inhibits the accelerated aggregate clearance induced by Cdk1 inactivation

In my study, microtubule disassembly inhibited aggregate clearance while Cdk1 inactivation facilitate it **(Figure 5.15 and Figure 5.16)**. Previous studies reported that Cdk1 ensured microtubules dynamics in dividing cells (Fourest-Lieuvin et al., 2006; Serpico et al., 2022). Therefore, Cdk1 inactivation might accelerate aggregate clearance by mediating microtubules. To test this, MG132-arrested metaphase cells were treated with RO-3306 (RO) supplemented with DMSO or RO supplemented with nocodazole (Noco) **(Figure 5.17A)**. Results demonstrated that cells treated with both RO and Noco remained more aggregates than only RO group **(Figure 5.17B)**. This indicated proper microtubule assembly may facilitate Cdk1-mediated acceleration of aggregate clearance.

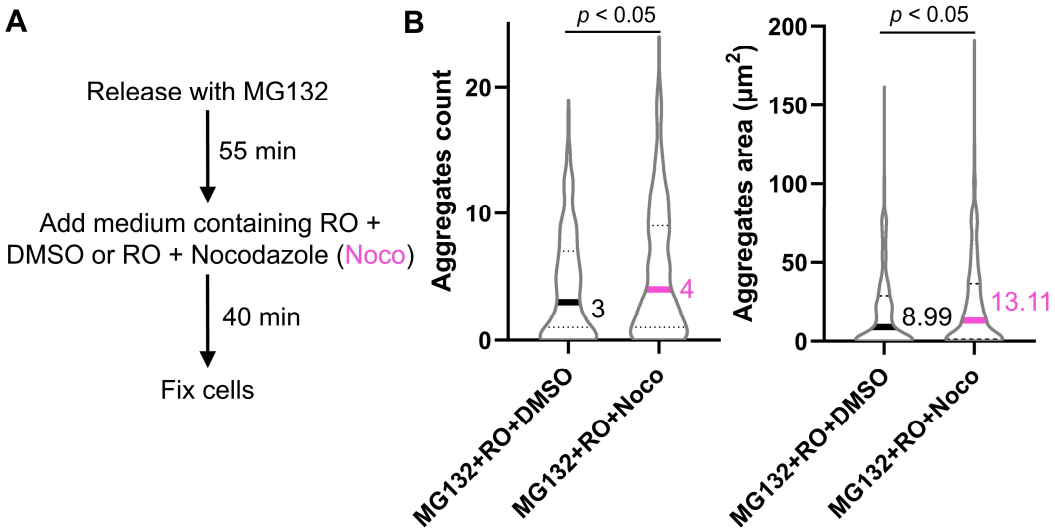


Figure 5.17: Nocodazole inhibits the acceleration of aggregate clearance induced

by Cdk1 inactivation. (A) The procedure of how mitotic cells were treated with nocodazole and RO-3306 simultaneously. **(B)** Quantification of (A). MG132 + RO + DMSO, 378 cells; MG132 + RO + Noco, 385 cells. The concentrations of MG132, RO and Noco are 25 μM, 10 μM, and 331 nM, respectively. Data are from three independent experiments and analysed by unpaired two side Mann-Whitney U-test. The specific number in figure is the median value.

5.2.12.5 CLIMP63 overexpression accelerates aggregate clearance

Previous studies demonstrated that cytoskeleton linking membrane protein 63 (CLIMP63) connected the ER and microtubules (Klopfenstein et al., 1998; Vedrenne et al., 2005). Additionally, CLIMP63 is also the "spacer" of the ER lumen, expanding luminal width of the ER (Xu et al., 2023). Therefore, it is speculated that CLIMP63 facilitates microtubule-dependent dynamics of the ER and provides additional ER luminal volume to accommodate disaggregated protein aggregates. To test this, an empty plasmid or a plasmid to express CLIMP63-mCherry was transduced in MCF10A cells with ER-FlucDM-eGFP aggregates. These cells were synchronized to G2/M and released into mitosis. After 65 minutes, cells were fixed and the successful CLIMP63 expression was verified by mCherry signal **(Figure 5.18A)**. Remaining aggregates were profiled in these cells. Results demonstrated that CLIMP63 overexpression decreased the remaining of ER-FlucDM-eGFP aggregates **(Figure 5.18B)**, suggesting CLIMP63 facilitates aggregate clearance.

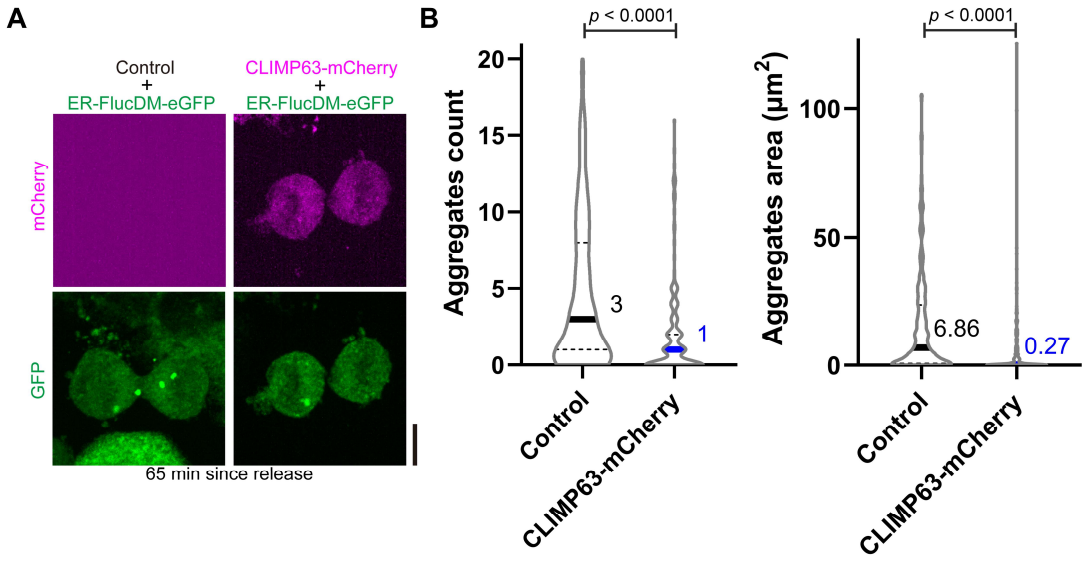


Figure 5.18: CLIMP63 overexpression accelerates aggregate clearance. (A) Representative images of cells expressing ER-FlucDM-eGFP and CLIMP63-mCherry

or a control plasmid. The plasmid used to express CLIMP63-mCherry was construct by inserting CLIMP63-mCherry into control plasmid. Co-transduced cells were fixed after released from G2/M boundary for 65 min. All representative images in this figure are maximum projected images along the Z-axis. The scale bar is 10 μm. **(B)** Quantification of (A). Cells expressing CLIMP63 were confirmed by mCherry signals. Data are from three independent experiments and analysed by unpaired two side Mann-Whitney U-test. The specific number in figure is the median value.

5.2.12.6 Atlastin 2 and 3 knockdown inhibits aggregate clearance

Atlastins shape and maintain ER networks by fusing ER tubules (Hu et al., 2009). To test whether atlastins were involved in aggregate clearance, atlastin 2 (ATL2) and atlastin 3 (ATL3) were knocked down simultaneously because of their compensatory functions (Liang et al., 2018). In dividing cells, more aggregates remained in the knockdown group, indicating ATL2 and ATL3 assist in aggregate clearance in dividing cells **(Figure 5.19)**.

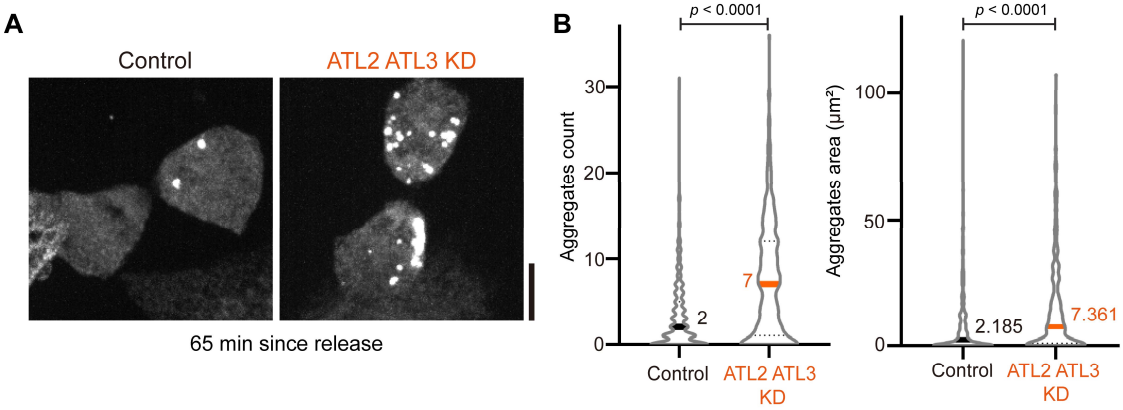


Figure 5.19: Simultaneous knockdown of atlastin 2 and 3 inhibits aggregate clearance. (A) Representative images of cells expressing ER-FlucDM-eGFP following the depletion of atlastin 2 and atlastin 3 and fixed at 65 min post-release from the G2/M boundary. **(B)** Quantification of cells expressing ER-FlucDM-eGFP after atlastin 2 and atlastin 3 depletion and fixed at 65 min post release. Control, 396 cells; ATL2 ATL3 KD, 362 cells. All representative images in this figure are maximum projected images along the Z-axis. The scale bar is 10 μm. Data were analysed by unpaired two side Mann-Whitney U-test. The median value is indicated in the figure.

5.2.12.7 Aurora kinase A inhibition by MLN-8237 inhibits aggregate clearance

A previous study reported that Aurora kinase A mediated ER remodeling in mitotic cells (Zhang et al., 2024). To test whether Aurora kinase A facilitated aggregate clearance, its inhibitor, MLN-8237, was employed to treat mitotic cells. MCF10A cells expressing ER-FlucDM-eGFP were arrested at G2/M and released into mitosis with the medium containing DMSO or MLN-8237. 65 minutes after release, remaining aggregates were counted. Results demonstrated that MLN-8237 treatment caused more aggregates remaining in cells **(Figure 5.20)**. Therefore, Aurora kinase A activity regulated aggregate clearance.

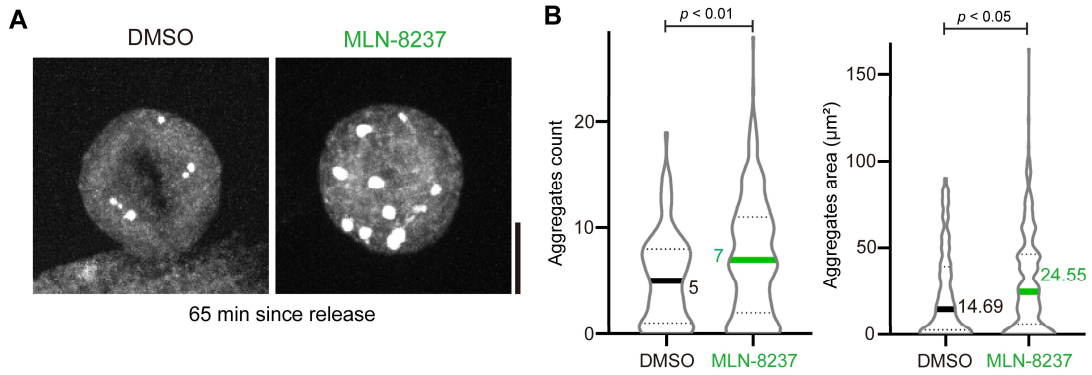


Figure 5.20: Aurora kinase A inhibition abolishes aggregate clearance. (A) Representative images of cells expressing ER-FlucDM-eGFP treated with either DMSO or 100 nM MLN-8237 and fixed 65 minutes post-release from the G2/M boundary. **(B)** Quantification of round mitotic cells expressing ER-FlucDM-eGFP following treatment with DMSO or 100 nM MLN-8237 and fixed 65 minutes post-release. Only round mitotic cells were counted. DMSO, 102 cells; MLN-8237, 288 cells. All representative images in this figure are maximum projected images along the Z-axis. The scale bar is 10 μm. Data were collected from three independent experiments and analysed by unpaired two side Mann-Whitney U-test. The median value is indicated in the figure.

5.3 Discussion

5.3.1 Summary of results in this chapter

In Chapter 4, the turnover speed of aggregates was different between interphase and mitotic cells. In this chapter, the dynamics of ER-FlucDM-eGFP aggregates were further profiled. Surprisingly, these aggregates were cleared during cell division but maintained in interphase cells. Next, dividing cells were found to retain more aggregates upon the inhibition of proteasome by MG132 or the inhibition of lysosome acidification by bafilomycin A1, suggesting that aggregate clearance may originate from the degradation of ER-FlucDM-eGFP. However, evidence from western blot and live-cell imaging revealed that total GFP levels didn't change significantly during cell division, indicating aggregate clearance is more likely due to the disassembly of aggregates rather than their degradation. To explore how cells clear aggregates, proteomics was employed to understand cellular responses to the misfolded protein aggregates induced by ER-FlucDM-eGFP. Results showed that ER-FlucDM-eGFP induced ER stress, and cells utilized the unfolded protein response to ameliorate this proteostasis stress. Therefore, it was hypothesized that the perturbation of ER protein homeostasis might inhibit aggregate clearance.

ER stress induction by thapsigargin inhibited aggregate clearance in dividing cells. Additionally, although short exposure to tunicamycin had negligible effects on aggregate clearance, cells pretreated with tunicamycin during interphase exhibited faster aggregate clearance during cell division. Meanwhile, both the Hsp70 inhibitor VER-155008 and the BiP-specific inhibitor YUM70 abolished aggregate clearance. Correspondingly, YUM70 treatment altered the ER structures in dividing cells. Considering the close relationship between the ER structures and aggregate clearance, ER remodeling during cell division might facilitate this clearance.

Previous studies reported that Cdk1 is involved in ER reorganization in dividing cells (Bergman et al., 2015). In my study, indeed, Cdk1 inactivation facilitated aggregate clearance in MG132-arrested cells, further suggesting aggregate clearance does not

depend on the activity of proteasomes. However, enforcing cells to exit mitosis by APC/C inhibition had negligible effects on remaining aggregates, suggesting that aggregate clearance in this study may be mediated by the kinase activity of Cdk1 specifically rather than the degradation of cyclin B. As another key kinase in mitotic cells, Aurora kinase A increases the ER complexity and facilitates ER remodeling in dividing cells (Zhang et al., 2024). Indeed, in my study, inhibiting Aurora kinase A by MLN-8237 abolished aggregate clearance, indicating that mitotic ER remodeling plays a pivotal role. Overexpressing the ER luminal spacer CLIMP63 facilitated aggregate clearance, suggesting that adequate ER luminal volume contributes to successful aggregate clearance. When inhibiting microtubule assembly by nocodazole, aggregate clearance was also abolished. Interestingly, nocodazole also abolished the acceleration of aggregate clearance upon Cdk1 inactivation, further suggesting the involvement of microtubules in aggregate clearance. Next, when decreasing ER tubule fusion events by simultaneous knockdown of atlastin 2 and atlastin 3, aggregates were found to be maintained in the knockdown group, suggesting that proper ER tubule network construction assists in aggregate clearance.

It should be noted that while most of the evidence above directly demonstrates how aggregate clearance is regulated by ER structure remodeling during cell division, there remains a possibility that aggregate clearance in this study is due to degradation. Therefore, before proposing a speculative model for how aggregate clearance is achieved, the degradation-supporting evidence will be discussed first and possibly integrated into the following disassembly-dominated model.

5.3.2 Evidence supporting degradation is incorporated into a disassembly model

In this study, the inhibition of proteasome by MG132 or the perturbation of lysosome acidification by bafilomycin A1 abolished aggregate clearance in dividing cells. Considering the typical functions of proteasomes and lysosomes in protein degradation, aggregate clearance reported here might originate from degradation. However, Cdk1 inactivation in MG132-arrested cells strikingly accelerated aggregate clearance, which

is difficult to explain by the degradation hypothesis.

It should be mentioned that MG132 treatment alters microtubule architecture and dynamics (Sengupta et al., 2025; Tipton and Gorbsky, 2022). Furthermore, microtubules are known to regulate dynamics of the ER in mitotic cells (Schlaitz, 2014). Indeed, proteasome inhibition affects ER network formation and the assembly of the cell nucleus (Sengupta et al., 2025). Therefore, in my study, MG132 might inhibit aggregate clearance by altering organelle dynamics rather than undermining degradation. Moreover, previous studies also reported that MG132 induces ER stress (Nakajima et al., 2011; Prieto-Garcia et al., 2024). In my study, ER stress induction inhibited aggregate clearance. Therefore, MG132 might abolish aggregate clearance via ER stress induction.

Additionally, similar to proteasomes, previous studies reported the active regulation of lysosomes on ER structures (Gubas and Dikic, 2022; Lu et al., 2020). Lysosome inhibition also induced ER stress (Kawaguchi et al., 2011). Therefore, in my study, the reason why proteasome and lysosome inhibition abolished aggregate clearance might originate from ER stress induction and the alteration of organelle dynamics, instead of the degradation of misfolded proteins.

Before proposing the disassembly-based hypothetical model to explain aggregate clearance during cell division, it should be noticed that several evidences supporting disassembly also can be combined into a degradation model. However, this degradation hypothesis is challenged by several observations in my study.

5.3.3 Evidence supporting the disassembly model is difficult to integrate into a degradation model

Protein degradation in cells is majorly achieved by proteasomes and lysosomes (Jayaraj et al., 2020). For a degradation model dominantly based on proteasomes, it seems unlikely. Proteasome inhibition by MG132 successfully arrested mitotic cells in

metaphase, however, Cdk1 inactivation in these cells obviously accelerated aggregate clearance while these mitotic cells remained arrested at rounding shape. This indicated that aggregate clearance can be achieved without sufficient activity of the proteasome.

For degradation models majorly based on lysosomes and autophagy, they are also unlikely. Previous studies reported that microtubule disassembly and CLIMP63 knockout hindered the transport of autophagy machineries and the progression of ER-phagy, respectively (Mackeh et al., 2013) (Li et al., 2024). Additionally, ATLs act as receptors or the downstream of receptors during ER-phagy (Chen et al., 2019; Liang et al., 2018). Thus, in my study, aggregate clearance inhibition upon microtubule disassembly or ATL knockdown might originate from the inhibition of autophagy. Furthermore, in my study, aggregate clearance acceleration achieved by CLIMP63 overexpression might result from the alteration of autophagy. However, this autophagy-based aggregate clearance model might be unlikely because of three reasons. First, no visible autophagosomes were observed in my study under either optical or electron microscopy. Second, ER stress induction, such as thapsigargin treatment, is widely reported to increase ER-phagy flux (Reggio et al., 2021; Tao et al., 2019). Thus, if ER-phagy is the mechanism of aggregate clearance, thapsigargin should accelerate aggregate clearance. However, in my study, thapsigargin clearly inhibited aggregate clearance. Thirdly, Cdk1 activation assists in the maintenance of autophagy in mitotic cells (Li et al., 2020). Thus, if autophagy is the mechanism of aggregate clearance, Cdk1 inactivation should inhibit autophagy and consequently hinder aggregate clearance. However, in my study, Cdk1 inactivation accelerated aggregate clearance.

Taken together, degradation-supporting evidences are more likely to be incorporated into a disassembly-dominated aggregate clearance model in my study.

5.3.4 Why are protein aggregates cleared only during cell division?

ER remodels both morphologically and compositionally during cell division (Kors and Schlaitz, 2024). In a previous study, lipid droplets in the nucleoplasmic reticulum disappeared at anaphase but reappeared after cell division (Soltysik et al., 2019), which was similar to the aggregate clearance during cell division that I reported. In my study, misfolded protein aggregates assembled by ER-FlucDM-eGFP were only cleared during cell division while remaining intact in interphase cells. This clearance was speculated to originate from ER remodeling as aforementioned. However, ER remodeling also exists in interphase cells. Why does aggregate clearance happen only in dividing cells? There might be two major reasons:

Firstly, in interphase cells, it can be imagined that ER-FlucDM-eGFP protein aggregates are "clamped" by nuclear components after invagination into the cell nucleus. Upon entering mitosis, these nuclear-trapped aggregates are released because of the disengagement of the nuclear envelope from nuclear components (Carlton et al., 2020; Champion et al., 2017). Thus, these inner nuclear envelope-encapsulated aggregates could freely participate in ER remodeling in dividing cells. Additionally, a previous study demonstrated that the junctions between the outer nuclear membrane (ONM) and the ER exhibited a constricted neck shape with a width of 7 to 20 nm in interphase cells (Bragulat-Teixidor et al., 2024). Interestingly, ER-ONM junctions in anaphase cells are about 60 nm and these hourglass-shaped junctions only started to narrow after anaphase (Bragulat-Teixidor et al., 2024). Therefore, aggregates assembled between INM and ONM in interphase cells are less likely to be disaggregated potentially because the luminal transport is restricted by these constrained ER-ONM junctions.

Secondly, the dynamics of ER remodeling in dividing cells might be higher than interphase cells for disaggregation although this statement currently lacks direct and comprehensive evidences in both my study and literatures. A previous study reported that organelle movement is enhanced in migrating cells because their morphological

deformation generate cytoplasmic flow and mixing (Koslover et al., 2017). Therefore, ER remodeling might also be enhanced during cell division because of the tremendous reorganization and deformation events in dividing cells (Carlton et al., 2020; Champion et al., 2017). During mitosis, the ER undergoes significant changes in both its distribution and morphology. In interphase, the ER extends outward from the nuclear envelope toward the plasma membrane, forming a dense network in the perinuclear region (Kors and Schlaitz, 2024). However, as the cell enters metaphase, the ER network shifts toward the cell periphery and largely clears from the inner spindle area (Kors and Schlaitz, 2024). This spatial enrichment might facilitate ER remodeling and luminal transport. Additionally, a previous study reported that ER contraction facilitates its luminal transport (Htet et al., 2024). In my study, it should be noted that the aggregates were released from the inner nuclear membrane, suggesting these aggregates may still be close to the mitotic spindle. Astral microtubules and related motors from the spindle might directly exert mechanical force to enhance ER contraction and this potentially facilitates the luminal transport in the ER, subsequently accelerating aggregate clearance.

5.3.5 The proposed model of aggregate clearance

Based on aforementioned results in my study and several related concepts in literatures, the following hypothetical model is proposed to explain the clearance of protein aggregates during cell division.

Upon entering cell division, hyperphosphorylated Cdk1 causes nuclear envelope breakdown and subsequently releases aggregates that were clamped by nuclear components, allowing the major fraction of the ER to approach these aggregates. Then, BiP, acting as a disaggregase, assists in the disaggregation and subsequent clearance. The robust clearance is ensured by another mitotic kinase, Aurora kinase A, regulating ER remodeling by phosphorylating Rab1A. This phosphorylation is also might be co-regulated by Cdk1 because Rab1A is a potential target of Cdk1 (Massacci et al., 2023). Furthermore, ER tubule fusion achieved by atlastins, ER volume expansion regulated

by CLIMP63, and ER dynamics facilitated by microtubules all potentially contribute to the disaggregation by replenishing disaggregation machinery and providing adequate volume to accommodate disaggregated components.

The figure illustrating this model will be combined with Chapter 4 and summarized in the next chapter. It should be noticed that this model aims to explain how microscopically visible protein aggregates are cleared during cell division instead of how misfolded proteins from these disaggregated aggregates are cleared. For the latter, conventional protein degradation pathways such as proteasomes and lysosomes might be involved in.

5.3.6 Future studies to elucidate the mechanism of protein aggregate clearance during cell division

In my study, perturbations of ER remodeling all demonstrated some effects on the clearance of protein aggregates. However, this study still lacks an in-depth understanding of how these elements regulate aggregate clearance.

The overexpression of CLIMP63, a linker protein of microtubules and the ER, facilitated aggregate clearance. However, CLIMP63 also facilitates the formation of ER sheets (Shibata et al., 2010) and increases the width of ER tubules (Wang et al., 2022), potentially increasing the volume of the ER lumen and providing more space to accommodate proteins from disassembled aggregates. Thus, my study did not answer how CLIMP63 regulated aggregate clearance. Phosphorylation of CLIMP63 occurs in mitosis and causes disassociation of the ER from microtubules (Vedrenne et al., 2005). Thus, in my study, overexpressed CLIMP63 might not tether the ER to microtubules. Therefore, the role of CLIMP63 in aggregate clearance was most likely dependent on its function of ER volume expansion. To further explore this, a mutant of CLIMP63 containing only its luminal domain could be expressed in cells (Shen et al., 2019). This dominant-negative mutant binds to endogenous CLIMP63 and disrupts its dimerization, thus narrowing the width of the ER lumen (Shen et al., 2019). If CLIMP63 facilitates

aggregate clearance by expanding the ER lumen, this mutant should diminish the clearance of protein aggregates during cell division.

Microtubule disassembly by nocodazole obviously abolished aggregate clearance. Furthermore, in MG132-arrested cells, Cdk1 inactivation facilitated the clearance of protein aggregates. However, this acceleration was inhibited by microtubule disassembly, further suggesting that microtubules play a major role in aggregate clearance. In my study, it was unknown why efficient microtubule assembly ensured the clearance of protein aggregates. ER reorganization is microtubule-dependent (Diaz et al., 2019). Therefore, it could be speculated that microtubule assembly facilitates aggregate clearance via controlling ER remodeling during cell division. To examine this, another ER-microtubule tether, the thousand and one amino acid kinase 2 (TAOK2) is worth testing. In mitotic cells, TAOK2 knockout decreases ER-microtubule tethering and weakens the association between the ER and the mitotic spindle (Nourbakhsh et al., 2021). If microtubules mediate aggregate clearance through regulating ER remodeling, aggregate clearance in TAOK2 knockdown cells should be inhibited.

During mitosis, Aurora kinase A phosphorylates Rab1A (Zhang et al., 2024). Rab1A induces the oligomerization of ER-shaping proteins and increases the complexity of the ER by shortening the length of ER elements (Zhang et al., 2024). In my study, the inhibition of Aurora kinase A caused more aggregates remaining in mitotic cells. Thus, it is speculated that shorter ER elements (less ER complexity) during cell division facilitates the clearance of aggregates. Similarly, in my study, the knockdown of atlastins, which induced unbranched ER (longer ER elements contrasted to well-interconnected tubules), also inhibited aggregate clearance. Therefore, it is possible that a well-interconnected ER tubule network facilitates aggregate clearance. Is it possible that an excessively interconnected ER network inhibits this clearance? To test this, the overexpression of membrane curvature-stabilizing proteins such as reticulons and atlastins might deepen our understanding of this process.

5.3.7 The significance and limitations of this study

In recent two decades, microscopy-based studies found that protein aggregates can be partially segregated into the mother cell while being excluded from the rejuvenated daughter cell during asymmetric division (Miller et al., 2015). Furthermore, in fission yeast, protein aggregates are randomly partitioned between daughter cells during symmetric division (Coelho et al., 2013; Coelho et al., 2014). It is speculated that misfolded protein aggregates might be cleared upon cell division (Hipp et al., 2014), however, direct evidence has not been reported. To the best of my knowledge, this work is the first observation describing the clearance of protein aggregates during cell division.

Organelle remodeling during cell division is widely reported previously (Carlton et al., 2020; Champion et al., 2017). Meanwhile, in recent years, emerging evidence started to demonstrate how organelle remodeling cooperated with proteome stability maintaining (Gubas and Dikic, 2022). In my study, the clearance of protein aggregates during cell division was ensured by organelle dynamics-driven disaggregation, providing a novel perspective on how organelle dynamics orchestrate the regulation of proteostasis. However, similar clearance under physiological or pathological conditions was not identified, which is the major limitation of this study and worth further exploration.

Chapter 6 Conclusions and General Discussion

6.1 Summary of this thesis

The proteostasis network maintains proteins in their native state and prevents the accumulation of misfolded proteins. The intracellular proteostasis network, involving the regulation of protein synthesis, folding, degradation, and sequestration of protein aggregates, has been widely studied (Hipp et al., 2019). However, how dividing cells regulate proteostasis remains largely unknown, especially in mammalian cells undergoing symmetric division. Given that the proteostasis network co-evolves with the cellular proteome (Powers and Balch, 2013), I speculate that the proteostasis network in these cells might differ from that in other cell types. When examining this assumption, my work discovered several proteostasis maintenance strategies.

Chapter 3: Mitotic cells utilized several protein quality control factors previously characterized in studies that did not differentiate interphase and mitosis. However, mitotic cells assembled fewer protein aggregates upon proteasome inhibition compared to interphase cells. The discussion of this observation leads to a hypothesis that protein aggregates in the endoplasmic reticulum (ER) are eliminated during cell division, inspiring the study in Chapter 4 and Chapter 5.

Chapter 4: Misfolding-prone proteins expressed in the endoplasmic reticulum (ER) formed protein aggregates and invaginated into the cell nucleus through the inner nuclear membrane. This aggregation depended on binding immunoglobulin protein (BiP) **(Figure 6.1)**. The protein turnover rate in these aggregates was higher in mitosis than that in interphase, encouraging the study in Chapter 5.

Chapter 5: Protein aggregates in the ER were maintained in interphase but cleared during cell division. This clearance resulted from the disintegration rather than the degradation of aggregates. This clearance depended on ER proteostasis, heat shock protein 70 (Hsp70), cyclin-dependent kinase 1 (Cdk1), Aurora kinase A, microtubule assembly and ER remodeling during cell division **(Figure 6.1)**.

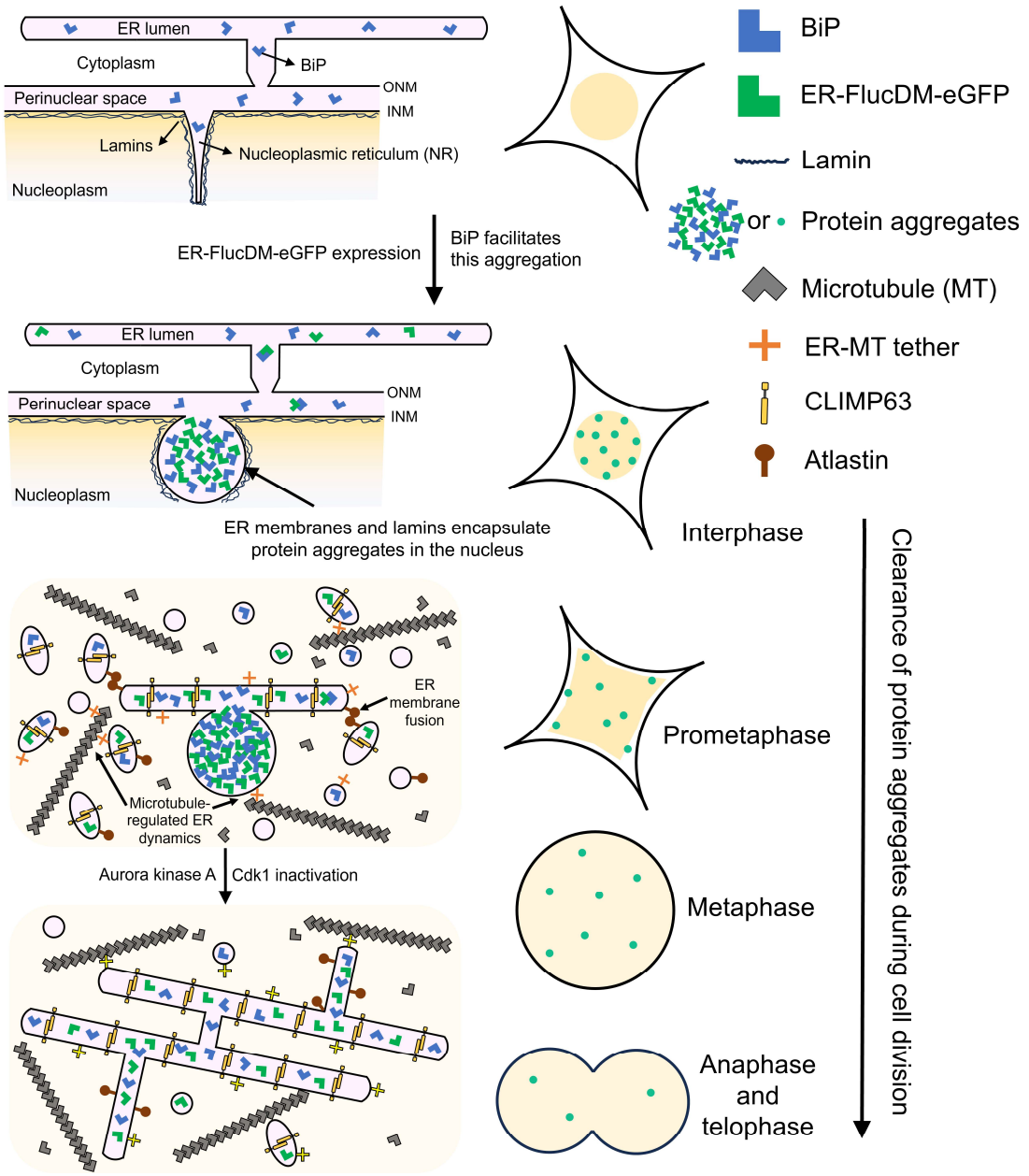


Figure 6.1: A summary of working models in Chapter 4 and Chapter 5. ER-FlucDM-eGFP assembled into protein aggregates in the cell nucleus. These aggregates were encapsulated by the ER membrane and lamins. The aggregation process depended on a molecular chaperone, binding immunoglobulin protein (BiP). Unexpectedly, these aggregates were cleared during cell division. Clearance of protein aggregates depended on ER stress induction, the proteasome, the ATPase activity of heat shock protein (Hsp70), lysosome acidification, cyclin-dependent kinase 1 (Cdk1), Aurora kinase A, the assembly of microtubules, cytoskeleton-linking membrane protein 63 (CLIMP63) and atlastins. This clearance was independent on the anaphase promoting complex/cyclosome (APC/C).

6.2 Crosstalk of proteostasis across subcellular compartments

Misfolding-prone proteins expressed in the endoplasmic reticulum (ER-FlucDM-eGFP) unexpectedly assembled into protein aggregates in the cell nucleus and these aggregates were encapsulated by the ER membrane and nuclear lamina **(Figure 6.1)**. Transmission electron microscopy revealed that these aggregates were surrounded by a single-layer membrane, which was the inner nuclear membrane (INM). However, nuclear-targeting misfolding-prone proteins (NLS-FlucDM-eGFP) did not assemble into any visible protein aggregates in the nucleus. Interestingly, when co-expressing ER-FlucDM-mCherry and NLS-FlucDM-eGFP, NLS-FlucDM-eGFP preferentially concentrated near the protein aggregates of ER-FlucDM-mCherry. This suggests that the proteome in the ER regulates the proteome in the cell nucleus although the inner nuclear membrane is in the middle of them. This regulation might occur directly by leaking the components of aggregates into the nucleoplasm or indirectly by mediating the structure of the local lipid membrane.

The invagination of ER components into the cell nucleus was termed the nucleoplasmic reticulum (NR) (McPhee et al., 2024). Upon ER stress, lipid droplets are transported from the ER to the NR and then to the nucleus to increase phosphatidylcholine synthesis and relieve ER stress (Soltysik et al., 2019). In Chapter 4, protein aggregates assembled by ER-FlucDM-eGFP invaginated into the nucleus. These aggregates contained binding immunoglobulin protein (BiP), a member of the Hsp70 family in the ER lumen. A recent study reported that BiP translocated from the ER lumen to the cell nucleus upon ER stress and acted as a transcriptional regulator, which allowed cancer cells to adopt an invasive phenotype (Liu et al., 2023). In Chapter 4, BiP, which was translocated from the ER lumen to the cell nucleus, might also regulate transcription. In Chapter 5, the overexpression of ER-FlucDM-eGFP in non-tumorigenic human epithelial cell line MCF10A induced the upregulation of multiple ER stress related proteins and surprisingly several proteins related to cell division and cell cycle progression. It is possible that BiP and other components from protein aggregates that have invaginated into the cell nucleus are released into the nucleoplasm and mediate

the upregulation of proteins related to cell division and cell cycle progression.

Protein aggregates in the cytoplasm disrupt the transport of protein and RNA between the cytoplasm and the nucleus (Woerner et al., 2016). Aggregation-prone proteins in the cytosol are imported into mitochondria for degradation (Ruan et al., 2017). ER-misfolded proteins are sequestered with mitochondria (Sanchón et al., 2021). Together with my findings, it is worth further exploring proteostasis maintenance by studying the communication between subcellular compartments. These regulations might provide multilevel protective strategies for cells dealing with proteome stress.

6.3 Aggregation and disaggregation of protein aggregates in the ER

Misfolded proteins accumulated in the ER triggered ER stress, and ER stress in turn promotes the accumulation of misfolded proteins (Hetz et al., 2020; Verwilst et al., 2019). Cells employ an adaptive unfolded protein response (UPR) to counteract ER stress and misfolded proteins by attenuating protein synthesis, upregulating genes related to protein folding and degradation, and triggering apoptosis if the UPR is exhausted (Hetz et al., 2020). ER-FlucDM-eGFP expressed in cells upregulated UPR-related proteins including multiple molecular chaperones such as BiP. Although the ER had high capacity to prevent protein aggregation (Vincenz-Donnelly et al., 2018), the consequence of UPR in my study was the assembly of protein aggregates in the ER with the assistance from BiP. Misfolded proteins in protein aggregates are less toxic and the aggregation of misfolded proteins is cytoprotective (Arrasate et al., 2004; Walther et al., 2015). Thus, BiP-assisting protein aggregation in my study might be a protective strategy for cells relieving proteostasis stress.

The ER has a strong ability to maintain misfolding-prone proteins in a soluble state and prevent their aggregation (Rousseau et al., 2004; Vincenz-Donnelly et al., 2018). My findings indicate that the ER even has the ability to sequester misfolding-prone proteins into the nucleus as temporary confinement sites, rather than allowing them to aggregate within the ER network. Thus, it is possible to retranslocate pathological misfolded

proteins into the ER to avoid their detrimental effects on cellular homeostasis, which may represent a potential therapeutic strategy.

ER stress induction promoted the disaggregation of protein aggregates in the ER (Melo et al., 2022). Stress-induced disaggregation is realized by BiP, which exhibits higher activity upon ER stress induction (Melo et al., 2022). In my study, cell division ensured the disaggregation of similar protein aggregates and this clearance was promoted by pretreatment with the ER stress inducer. Thus, previously observed stress-induced disaggregation might happen during cell division. ER stress induction before cell division accelerated protein aggregate clearance and subsequently caused fewer protein aggregates in daughter cells.

6.4 Organelle dynamics and proteostasis during cell division.

In the budding yeast, mitochondria frequently capture protein aggregates that initially form on the ER, limiting their movement in cells (Zhou et al., 2014). During cell division, these aggregates remain attached to the stationary mitochondria in the mother cell, while the mitochondria that are passed to the bud stay largely aggregate-free (Zhou et al., 2014). When the connection between aggregates and mitochondria is disrupted, their mobility increases, allowing aggregates that would typically remain in the mother cell to disperse into the bud (Zhou et al., 2014). In my study, protein aggregates were encapsulated in the ER membrane in dividing cells. The perturbation of ER tubule fusion, the alteration of ER complexity and the disassembly of microtubules inhibited aggregate clearance. The overexpression of ER luminal spacer CLIMP63 accelerated the clearance. Thus, the clearance of protein aggregates is ensured by ER remodeling during cell division.

Although my study focuses on the protein aggregates in the ER and their dynamics during cell division, it is possible that protein aggregates in other organelles also demonstrate differential dynamics in dividing cells. Accumulation of mitochondrial misfolded proteins facilitates mitochondrial fission, which is mediated by dynamin-

related protein 1 (Drp1) (Burman et al., 2017). Isolated and dysfunctional mitochondria are subsequently degraded by mitophagy (Burman et al., 2017). After entering mitosis, Cdk1 phosphorylates Drp1 and promotes Drp1-dependent mitochondrial fission (Taguchi et al., 2007). Thus, it is possible that mitochondria possess higher capacity to facilitate the sequestration of their misfolded proteins-enriched portions during cell division.

My findings and arguments above indicate that the dynamics of organelles regulate the proteostasis network. Indeed, typical organelle-reshaping factors have been shown to contribute to cellular proteostasis (Parashar et al., 2021), indicating that targeting organelle dynamics is a therapeutic avenue for protein-misfolding diseases.

6.5 Leave the protein aggregates to be dealt with during cell division

The work in Chapter 3 demonstrated that mitotic cells employ Hsp70 and the 26S proteasome to eliminate misfolded protein aggregation induced by heat shock. Furthermore, both inhibition of protein synthesis and ER stress induction decreased protein aggregation. These findings are consistent with current knowledge about proteostasis (Hetz et al., 2020; Jayaraj et al., 2020). Unexpectedly, proteasome inhibition did not induce any visible protein aggregates in mitotic cells, suggesting mitotic cells possess a stronger ability to restrict the aggregation of misfolded proteins than interphase cells.

During cell division, the budding yeast and stem cells preferentially confine protein aggregates in the mother cell, thus rejuvenating the daughter cell (Miller et al., 2015). In fission yeast, protein aggregates are randomly partitioned (Coelho et al., 2013). In my study, protein aggregates assembled in the cell nucleus were maintained in interphase cells, however, they were cleared during cell division **(Figure 6.1)**, suggesting protein aggregates in dividing cells are more likely to be disintegrated. Taken together, it is speculated that mammalian cells undergoing symmetric division have a stronger ability to eliminate protein aggregation and clear protein aggregates

than interphase cells. In human self-renewing tissues, cell division rates decrease with age (Tomasetti et al., 2019). It has been proposed that the reason why postmitotic cells such as neurons are particularly susceptible to protein aggregation-related pathologies is that they do not undergo division (Hipp et al., 2019). My findings suggest a novel therapeutic strategy to disassemble protein aggregates and potentially restore cellular proteostasis by inducing cells to enter mitosis.

6.6 The inheritance and maintenance of cellular materials during division

The basic material components of the cell such as proteins, lipids and carbohydrates fulfill their biological functions by assembling into various microdomains. These include organelles, chromosomes, glycogen granules, lipid rafts, membrane contact sites, cytoskeletal structures, liquid-like droplets and other specialized subcellular compartments. Although the mechanisms governing chromosome segregation have been extensively characterized, how other cellular compartments are inherited and maintained during division is still less understood.

The size of mitochondria and Golgi decrease upon the entry of cell division (Liao et al., 2024; Taguchi et al., 2007; Tang et al., 2012). Lipid droplets in the NR disappear in dividing cells (Soltysik et al., 2019). Membraneless organelles such as stress granules and splicing speckles are dissolved during cell division (Rai et al., 2018). In my study, protein aggregates are cleared in dividing cells. Taken together, mammalian cells prefer to disintegrate visibly large cellular entities during division. Additionally, mitochondrial disassembly is accompanied by actin-mediated mixing (Moore et al., 2021). In my study, efficient microtubule assembly promoted the disassembly of protein aggregates. Thus, successful inheritance of organelles is ensured by cytoskeletal function.

Organelle remodeling during mitosis is accompanied by extensive molecular exchange. For example, upon mitotic entry, the ER absorbs proteins and lipids from the inner nuclear envelope and from the Golgi apparatus (Ellenberg et al., 1997; Sengupta et al.,

2015; Zaal et al., 1999). This redistribution of components directs other important mitotic events. For example, the mitotic ER takes up lamin B receptors from the inner nuclear envelope (Ellenberg et al., 1997). These re-localized lamin B receptors facilitate the formation of mitochondria-ER contact sites, thereby boosting mitochondrial Ca^{2+} uptake, which fuels the metaphase–anaphase transition (Zhao et al., 2024). In my study, protein aggregates that were sequestered at the nuclear periphery were released into the cytoplasm upon nuclear envelope disassembly as cells entered mitosis. This allows aggregates to mix with the ER network, potentially facilitating their disaggregation. Taken together, mitotic mixing facilitates redistribution of cellular material and enables cellular renewal during division.

It should be emphasized that disassembly and intermixing of cellular compartments are not the only strategies cells use during division. The formation of biomolecular condensates driven by phase separation in mitotic cells ensures the precise spatiotemporal control of mitotic progression (Jiang et al., 2015; Liu et al., 2020; Ong and Torres, 2020). A recent study reported BiP-containing multichaperone condensates in the ER that facilitate protein folding and display liquid-like properties (Leder et al., 2025). Whether similar condensates or other proteostasis-related droplets exist in dividing cells and how they coordinate with cell division processes remain unknown. Moreover, how dividing cells manage other compartments such as lipid rafts and glycogen granules is poorly understood.

The inheritance and maintenance of the cellular materials discussed above are not yet fully elucidated, particularly in terms of their functional consequences. These processes may contribute to faithful division and to the preservation of cellular health in daughter cells.

Reference

Acosta-Alvear, D., J.M. Harnoss, P. Walter, and A. Ashkenazi. 2025. Homeostasis control in health and disease by the unfolded protein response. *Nat Rev Mol Cell Bio*. 26:193-212.

Aebi, M. 2013. N-linked protein glycosylation in the ER. *Bba-Mol Cell Res*. 1833:2430-2437.

Aguilaniu, H., L. Gustafsson, M. Rigoulet, and T. Nyström. 2003. Asymmetric inheritance of oxidatively damaged proteins during cytokinesis. *Science*. 299:1751-1753.

Akopian, D., K. Shen, X. Zhang, and S.O. Shan. 2013. Signal Recognition Particle: An Essential Protein-Targeting Machine. *Annual Review of Biochemistry*. 82:693-721.

Albanèse, V., A.Y.W. Yam, J. Baughman, C. Parnot, and J. Frydman. 2006. Systems analyses reveal two chaperone networks with distinct functions in eukaryotic cells. *Cell*. 124:75-88.

Almacellas, E., and C. Mauvezin. 2022. Emerging roles of mitotic autophagy. *J Cell Sci*. 135:jcs255802.

Almacellas, E., J. Pelletier, C. Day, S. Ambrosio, A. Tauler, and C. Mauvezin. 2021. Lysosomal degradation ensures accurate chromosomal segregation to prevent chromosomal instability. *Autophagy*. 17:796-813.

Amankwah, Y.S., P. Collins, Y. Fleifil, E. Unruh, K.J.R. Márquez, K. Vitou, and A.N. Kravats. 2022. Grp94 Works Upstream of BiP in Protein Remodeling Under Heat Stress. *J Mol Biol*. 434:167762.

Ameen, N., M. Silvis, and N.A. Bradbury. 2007. Endocytic trafficking of CFTR in health and disease. *J Cyst Fibros*. 6:1-14.

Annadurai, N., J.B. De Sanctis, M. Hajdúch, and V. Das. 2021. Tau secretion and propagation: Perspectives for potential preventive interventions in Alzheimer's disease and other tauopathies. *Exp Neurol*. 343:113756.

Araki, K., and K. Nagata. 2011. Protein Folding and Quality Control in the ER. *Csh Perspect Biol*. 3:a007526.

Arganda-Carreras, I., V. Kaynig, C. Rueden, K.W. Eliceiri, J. Schindelin, A. Cardona, and H.S. Seung. 2017. Trainable Weka Segmentation: a machine learning tool for microscopy pixel classification. *Bioinformatics*. 33:2424-2426.

Arkinson, C., K.C. Dong, C.L. Gee, and A. Martin. 2025. Mechanisms and regulation of substrate degradation by the 26S proteasome. *Nat Rev Mol Cell Bio*. 26:104-122.

Arrasate, M., S. Mitra, E.S. Schweitzer, M.R. Segal, and S. Finkbeiner. 2004. Inclusion body formation reduces levels of mutant huntingtin and the risk of neuronal death. *Nature*. 431:805-810.

Arrigo, A.P., K. Tanaka, A.L. Goldberg, and W.J. Welch. 1988. Identity of the 19s Prosome Particle with the Large Multifunctional Protease Complex of Mammalian Cells (the Proteasome). *Nature*. 331:192-194.

Arstila, A.U., and B.F. Trump. 1968. Studies on Cellular Autophagocytosis. The Formation of Autophagic Vacuoles in Liver after Glucagon Administration. *Am J Pathol*. 53:687-733.

Ashford, T.P., and K.R. Porter. 1962. Cytoplasmic Components in Hepatic Cell

Lysosomes. *J Cell Biol*. 12:198-202.

Avezov, E., B.C.S. Cross, G.S.K. Schierle, M. Winters, H.P. Harding, E.P. Melo, C.F. Kaminski, and D. Ron. 2013. Lifetime imaging of a fluorescent protein sensor reveals surprising stability of ER thiol redox. *J Cell Biol*. 201:337-349.

Backer, J.M., L. Bourret, and J.F. Dice. 1983. Regulation of Catabolism of Microinjected Ribonuclease-a Requires the Amino-Terminal 20 Amino-Acids. *P Natl Acad Sci-Biol*. 80:2166-2170.

Bagchi, P. 2020. Endoplasmic reticulum in viral infection. *Int Rev Cel Mol Bio*. 350:265-284.

Baker, J.R. 1955. The Cell-theory : a Restatement, History, and Critique: Part V. The Multiplication of Nuclei. *Q J Microsc Sci*. 96:449-481.

Balchin, D., M. Hayer-Hartl, and F.U. Hartl. 2016. In vivo aspects of protein folding and quality control. *Science*. 353:aac4354.

Balsamo, J.A., K.E. Penton, Z.H. Zhao, M.J. Hayes, S.M. Lima, J.M. Irish, and B.O. Bachmann. 2022. An immunogenic cell injury module for the single-cell multiplexed activity metabolomics platform to identify anti-cancer natural products. *J Biol Chem*. 298:102300.

Baumann, O., and B. Walz. 2001. Endoplasmic reticulum of animal cells and its organization into structural and functional domains. *Int Rev Cytol*. 205:149-214.

Baumeister, W., Z. Cejka, M. Kania, and E. Seemuller. 1997. The proteasome: A macromolecular assembly designed to confine proteolysis to a nanocompartment. *Biol Chem*. 378:121-130.

Beams, H.W. 1929. Studies on the 'Golgi apparatus' of insect muscle. *Anat Record*. 42:323-333.

Becher, I., A. Andrés-Pons, N. Romanov, F. Stein, M. Schramm, F. Baudin, D. Helm, N. Kurzawa, A. Mateus, M.T. Mackmull, A. Typas, C.W. Müller, P. Bork, M. Beck, and M.M. Savitski. 2018. Pervasive Protein Thermal Stability Variation during the Cell Cycle. *Cell*. 173:1495-1507.

Beetz, C., N. Koch, M. Khundadze, G. Zimmer, S. Nietzsche, N. Hertel, A.K. Huebner, R. Mumtaz, M. Schweizer, E. Dirren, K.N. Karle, A. Irintchev, V. Alvarez, C. Redies, M. Westermann, I. Kurth, T. Deufel, M.M. Kessels, B. Qualmann, and C.A. Hübner. 2013. A spastic paraplegia mouse model reveals REEP1-dependent ER shaping. *J Clin Invest*. 123:4273-4282.

Behrendt, L., I. Kurth, and C. Kaether. 2019. A disease causing ATLASTIN 3 mutation affects multiple endoplasmic reticulum-related pathways. *Cell Mol Life Sci*. 76:1433-1445.

Bentivoglio, M., and P. Mazzarello. 1998. The pathway to the cell and its organelles: one hundred years of the Golgi apparatus. *Endeavour*. 22:101-105.

Berg, P., and J.E. Mertz. 2010. Personal Reflections on the Origins and Emergence of Recombinant DNA Technology. *Genetics*. 184:9-17.

Bergman, Z.J., J.D. Mclaurin, A.S. Eritano, B.M. Johnson, A.Q. Sims, and B. Riggs. 2015. Spatial Reorganization of the Endoplasmic Reticulum during Mitosis Relies on Mitotic Kinase Cyclin A in the Early Embryo. *Plos One*. 10:e0117859.

Berthet, J., and C. Deduve. 1951. Tissue Fractionation Studies .1. The Existence of a Mitochondria-Linked, Enzymically Inactive Form of Acid Phosphatase in Rat-Liver Tissue. *Biochem J*. 50:174-181.

Bhattacharyya, S., H.Q. Yu, C. Mim, and A. Matouschek. 2014. Regulated protein

turnover: snapshots of the proteasome in action. *Nat Rev Mol Cell Bio*. 15:122-133.

Biancalana, M., and S. Koide. 2010. Molecular mechanism of Thioflavin-T binding to amyloid fibrils. *Bba-Proteins Proteom*. 1804:1405-1412.

Blumenstock, S., E.K. Schulz-Trieglaff, K. Voelkl, A.L. Bolender, P. Lapios, J. Lindner, M.S. Hipp, F.U. Hartl, R. Klein, and I. Dudanova. 2021. Fluc-EGFP reporter mice reveal differential alterations of neuronal proteostasis in aging and disease. *Embo J*. 40:e107260.

Boivin, A., and R. Vendrely. 1947. Sur Le Role Possible Des Deux Acides Nucleiques Dans La Cellule Vivante. *Experientia*. 3:32-34.

Bracher, A., and J. Verghese. 2015. The nucleotide exchange factors of Hsp70 molecular chaperones. *Front Mol Biosci*. 2:10.

Bragulat-Teixidor, H., K. Ishihara, G.M. Szücs, and S. Otsuka. 2024. The endoplasmic reticulum connects to the nucleus by constricted junctions that mature after mitosis. *Embo Rep*. 25:3137-3159.

Brandman, O., and R.S. Hegde. 2016. Ribosome-associated protein quality control. *Nat Struct Mol Biol*. 23:7-15.

Brenner, S., M. Meselson, and F. Jacob. 1961. An Unstable Intermediate Carrying Information from Genes to Ribosomes for Protein Synthesis. *Nature*. 190:576-581.

Bross, P., R. Magnoni, and A.S. Bie. 2012. Molecular Chaperone Disorders: Defective Hsp60 in Neurodegeneration. *Curr Top Med Chem*. 12:2491-2503.

Burman, J.L., S. Pickles, C.X. Wang, S. Sekine, J.N.S. Vargas, Z. Zhang, A.M. Youle, C.L. Nezich, X.F. Wu, J.A. Hammer, and R.J. Youle. 2017. Mitochondrial fission facilitates the selective mitophagy of protein aggregates. *J Cell Biol*. 216:3231-3247.

Bygrave, F.L., and A. Benedetti. 1996. What is the concentration of calcium ions in the endoplasmic reticulum? *Cell Calcium*. 19:547-551.

Campbell, P.N., and T.S. Work. 1953. Biosynthesis of Proteins. *Nature*. 171:997-1001.

Cao, S.S., and R.J. Kaufman. 2014. Endoplasmic Reticulum Stress and Oxidative Stress in Cell Fate Decision and Human Disease. *Antioxid Redox Sign*. 21:396-413.

Carlton, J.G., H. Jones, and U.S. Eggert. 2020. Membrane and organelle dynamics during cell division. *Nat Rev Mol Cell Bio*. 21:151-166.

Carnemolla, A., E. Fossale, E. Agostoni, S. Michelazzi, R. Calligaris, L. De Maso, G. Del Sal, M.E. MacDonald, and F. Persichetti. 2009. Rrs1 Is Involved in Endoplasmic Reticulum Stress Response in Huntington Disease. *J Biol Chem*. 284:18167-18173.

Carra, S., S. Alberti, P.A. Arrigo, J.L. Benesch, I.J. Benjamin, W. Boelens, B. Bartelt-Kirbach, B.J.J.M. Brundel, J. Buchner, B. Bukau, J.A. Carver, H. Ecroyd, C. Emanuelsson, S. Finet, N. Golenhofen, P. Goloubinoff, N. Gusev, M. Haslbeck, L.E. Hightower, H.H. Kampinga, R.E. Klevit, K. Liberek, H.S. Mchaourab, K.A. McMenimen, A. Poletti, R. Quinlan, S.V. Strelkov, M.E. Toth, E. Vierling, and R.M. Tanguay. 2017. The growing world of small heat shock proteins: from structure to functions. *Cell Stress Chaperon*. 22:601-611.

Casey, J.R., S. Grinstein, and J. Orlowski. 2010. Sensors and regulators of intracellular pH. *Nat Rev Mol Cell Bio*. 11:50-61.

Cavaillon, J.M. 2020. Andre Boivin: A pioneer in endotoxin research and an amazing

visionary during the birth of molecular biology. *Innate Immun-London*. 26:165-171.

Chambers, J.E., M. Kubánková, R.G. Huber, I. López-Duarte, E. Avezov, P.J. Bond, S.J. Marciniak, and M.K. Kuimova. 2018. An Optical Technique for Mapping Microviscosity Dynamics in Cellular Organelles. *Acs Nano*. 12:4398-4407.

Chambers, J.E., N. Zubkov, M. Kubánková, J. Nixon-Abell, I. Mela, S. Abreu, M. Schwiening, G. Lavarda, I. López-Duarte, J.A. Dickens, T. Torres, C.F. Kaminski, L.J. Holt, E. Avezov, J.A. Huntington, P. St George-Hyslop, M.K. Kuimova, and S.J. Marciniak. 2022. Z-α-antitrypsin polymers impose molecular filtration in the endoplasmic reticulum after undergoing phase transition to a solid state. *Sci Adv*. 8:eabm2094.

Champion, L., M.I. Linder, and U. Kutay. 2017. Cellular Reorganization during Mitotic Entry. *Trends Cell Biol*. 27:26-41.

Chan, F.L., O.J. Marshall, R. Saffery, B.W. Kim, E. Earle, K.H.A. Choo, and L.H. Wong. 2012. Active transcription and essential role of RNA polymerase II at the centromere during mitosis. *P Natl Acad Sci USA*. 109:1979-1984.

Chartron, J.W., K.C.L. Hunt, and J. Frydman. 2016. Cotranslational signal-independent SRP preloading during membrane targeting. *Nature*. 536:224-228.

Chen, Q.Z., Y. Xiao, P.Y. Chai, P.L. Zheng, J.L. Teng, and J.G. Chen. 2019. ATL3 Is a Tubular ER-Phagy Receptor for GABARAP-Mediated Selective Autophagy. *Curr Biol*. 29:846-855.

Chen, Y.C., K.K. Bose, C.L. Woodley, and N.K. Gupta. 1972. Protein-Synthesis in Rabbit Reticulocytes: The Characteristics of a Met-tRNA fMet Binding Factor. *Biochem Bioph Res Co*. 48:1-9.

Cheng, M.Y., F.U. Hartl, J. Martin, R.A. Pollock, F. Kalousek, W. Neupert, E.M. Hallberg, R.L. Hallberg, and A.L. Horwich. 1989. Mitochondrial Heat-Shock Protein Hsp60 Is Essential for Assembly of Proteins Imported into Yeast Mitochondria. *Nature*. 337:620-625.

Chirico, W.J., M.G. Waters, and G. Blobel. 1988. 70k Heat-Shock Related Proteins Stimulate Protein Translocation into Microsomes. *Nature*. 332:805-810.

Chiti, F., and C.M. Dobson. 2017. Protein Misfolding, Amyloid Formation, and Human Disease: A Summary of Progress Over the Last Decade. *Annual Review of Biochemistry, Vol 86*. 86:27-68.

Choi, C.H., D.S.W. Lee, D.W. Sanders, and C.P. Brangwynne. 2024. Condensate interfaces can accelerate protein aggregation. *Biophys J*. 123:1404-1413.

Ciechanover, A. 2005a. Intracellular protein degradation: From a vague idea, through the lysosome and the ubiquitin-proteasome system, and onto human diseases and drug targeting (Nobel lecture). *Angew Chem Int Edit*. 44:5944-5967.

Ciechanover, A. 2005b. Proteolysis: from the lysosome to ubiquitin and the proteasome. *Nat Rev Mol Cell Bio*. 6:79-86.

Ciechanover, A., D. Finley, and A. Varshavsky. 1984. Ubiquitin Dependence of Selective Protein-Degradation Demonstrated in the Mammalian-Cell Cycle Mutant Ts85. *Cell*. 37:57-66.

Clay, L., F. Caudron, A. Denoth-Lippuner, B. Boettcher, S.B. Frei, E.L. Snapp, and Y. Barral. 2014. A sphingolipid-dependent diffusion barrier confines ER stress to the yeast mother cell. *Elife*. 3:e01883.

Clerico, E.M., J.M. Tilitsky, W.L. Meng, and L.M. Gierasch. 2015. How Hsp70

Molecular Machines Interact with Their Substrates to Mediate Diverse Physiological Functions. *J Mol Biol*. 427:1575-1588.

Cobb, M. 2015. Who discovered messenger RNA? *Curr Biol*. 25:R526-R532.

Cobb, M. 2017. 60 years ago, Francis Crick changed the logic of biology. *Plos Biol*. 15:e2003243.

Coelho, M., A. Dereli, A. Haese, S. Kühn, L. Malinovska, M.E. DeSantis, J. Shorter, S. Alberti, T. Gross, and I.M. Tolić-Nørrelykke. 2013. Fission yeast does not age under favorable conditions, but does so after stress. *Curr Biol*. 23:1844-1852.

Coelho, M., S.J. Lade, S. Alberti, T. Gross, and I.M. Tolic. 2014. Fusion of Protein Aggregates Facilitates Asymmetric Damage Segregation. *Plos Biol*. 12:e1001886.

Coldwell, M.J., J.L. Cowan, M. Vlasak, A. Mead, M. Willett, L.S. Perry, and S.J. Morley. 2013. Phosphorylation of eIF4GII and 4E-BP1 in response to nocodazole treatment A reappraisal of translation initiation during mitosis. *Cell Cycle*. 12:3615-3628.

Colla, E., P.H. Jensen, O. Pletnikova, J.C. Troncoso, C. Glabe, and M.K. Lee. 2012. Accumulation of Toxic α-Synuclein Oligomer within Endoplasmic Reticulum Occurs in α-Synucleinopathy. *J Neurosci*. 32:3301-3305.

Collins, G.A., and A.L. Goldberg. 2017. The Logic of the 26S Proteasome. *Cell*. 169:792-806.

Cooper, A.A., A.D. Gitler, A. Cashikar, C.M. Haynes, K.J. Hill, B. Bhullar, K.N. Liu, K.X. Xu, K.E. Strathearn, F. Liu, S.S. Cao, K.A. Caldwell, G.A. Caldwell, G. Marsischky, R.D. Kolodner, J. LaBaer, J.C. Rochet, N.M. Bonini, and S. Lindquist. 2006. α-synuclein blocks ER-Golgi traffic and Rab1 rescues neuron loss in Parkinson's models. *Science*. 313:324-328.

Córdoba-Beldad, C.M., and J. Grantham. 2024. The CCTδ subunit of the molecular chaperone CCT is required for correct localisation of p150Glued to spindle poles during mitosis. *Eur J Cell Biol*. 103:151430.

Crick, F. 1970. Central Dogma of Molecular Biology. *Nature*. 227:561-563.

Crick, F.H. 1958. On protein synthesis. *Symp Soc Exp Biol*. 12:138-163.

Cunningham, C.N., J.M. Williams, J. Knupp, A. Arunagiri, P. Arvan, and B. Tsai. 2019. Cells Deploy a Two-Pronged Strategy to Rectify Misfolded Proinsulin Aggregates. *Mol Cell*. 75:442-456.

Das, N., T. Khan, B. Halder, S. Ghosh, and P. Sen. 2024. Macromolecular crowding effects on protein dynamics. *Int J Biol Macromol*. 281:136248.

Dayel, M.J., E.F.Y. Hom, and A.S. Verkman. 1999. Diffusion of green fluorescent protein in the aqueous-phase lumen of endoplasmic reticulum. *Biophys J*. 76:2843-2851.

de Duve, C., J. Berthet, L. Berthet, and F. Appelmans. 1951. Permeability of Mitochondria. *Nature*. 167:389-390.

De Giorgi, F., F. Laferrière, F. Zinghirino, E. Faggiani, A. Lends, M. Bertoni, X. Yu, A. Grélard, E. Morvan, B. Habenstein, N. Dutheil, E. Doudnikoff, J. Daniel, S. Claverol, C. Qin, A. Loquet, E. Bezard, and F. Ichas. 2020. Novel self-replicating α-synuclein polymorphs that escape ThT monitoring can spontaneously emerge and acutely spread in neurons. *Sci Adv*. 6:eabc4364

de Oliveira, V.M., V.D. Contessoto, F.B. da Silva, D.L.Z. Caetano, S.J. de Carvalho, and V.B.P. Leite. 2018. Effects of pH and Salt Concentration on Stability of a

Protein G Variant Using Coarse-Grained Models. *Biophys J*. 114:65-75.

De, S., D.C. Wirthensohn, P. Flagmeier, C. Hughes, F.A. Aprile, F.S. Ruggeri, D.R. Whiten, D. Emin, Z.J. Xia, J.A. Varela, P. Sormanni, F. Kundel, T.P.J. Knowles, C.M. Dobson, C. Bryant, M. Vendruscolo, and D. Klenerman. 2019. Different soluble aggregates of Aβ42 can give rise to cellular toxicity through different mechanisms. *Nat Commun*. 10:1541.

Deduve, C., and R. Wattiaux. 1966. Functions of Lysosomes. *Annu Rev Physiol*. 28:435-492.

Deniaud, A., O.S. el Dein, E. Maillier, D. Poncet, G. Kroemer, C. Lemaire, and C. Brenner. 2008. Endoplasmic reticulum stress induces calcium-dependent permeability transition, mitochondrial outer membrane permeabilization and apoptosis. *Oncogene*. 27:285-299.

Deshaies, R.J., B.D. Koch, M. Wernerwashburne, E.A. Craig, and R. Schekman. 1988. A Subfamily of Stress Proteins Facilitates Translocation of Secretory and Mitochondrial Precursor Polypeptides. *Nature*. 332:800-805.

Diaz, U., Z.J. Bergman, B.M. Johnson, A.R. Edington, M.A. de Cruz, W.F. Marshall, and B. Riggs. 2019. Microtubules are necessary for proper Reticulon localization during mitosis. *Plos One*. 14:e0226327.

DiFiglia, M., E. Sapp, K.O. Chase, S.W. Davies, G.P. Bates, J.P. Vonsattel, and N. Aronin. 1997. Aggregation of huntingtin in neuronal intranuclear inclusions and dystrophic neurites in brain. *Science*. 277:1990-1993.

Dill, K.A., and J.L. MacCallum. 2012. The Protein-Folding Problem, 50 Years On. *Science*. 338:1042-1046.

Dong, Y.C., S.W. Zhang, Z.L. Wu, X.M. Li, W.L. Wang, Y.A. Zhu, S. Stoilova-McPhie, Y. Lu, D. Finley, and Y.D. Mao. 2019. Cryo-EM structures and dynamics of substrate-engaged human 26S proteasome. *Nature*. 565:49-55.

Dounce, A.L. 1952. Duplicating mechanism for peptide chain and nucleic acid synthesis. *Enzymologia*. 15:251-258.

Dounce, A.L. 1953. Nucleic Acid Template Hypotheses. *Nature*. 172:541-541.

Drummond, D.A., and C.O. Wilke. 2009. The evolutionary consequences of erroneous protein synthesis. *Nat Rev Genet*. 10:715-724.

Du, Y.Y., X.L. Liu, X.L. Zhu, Y. Liu, X.R. Wang, and X.P. Wu. 2020. Activating transcription factor 6 reduces Aβ1-42 and restores memory in Alzheimer's disease model mice. *Int J Neurosci*. 130:1015-1023.

Duennwald, M.L., and S. Lindquist. 2008. Impaired ERAD and ER stress are early and specific events in polyglutamine toxicity. *Gene Dev*. 22:3308-3319.

Duve, C.D., B.C. Pressman, R. Gianetto, R. Wattiaux, and F. Appelmans. 1955. Tissue Fractionation Studies .6. Intracellular Distribution Patterns of Enzymes in Rat-Liver Tissue. *Biochem J*. 60:604-617.

Edsall, J.T. 1995. Wu,Hsien and the First Theory of Protein Denaturation (1931). *Advances in Protein Chemistry*. 46:1-5.

Eilers, M., and G. Schatz. 1986. Binding of a Specific Ligand Inhibits Import of a Purified Precursor Protein into Mitochondria. *Nature*. 322:228-232.

Ellenberg, J., E.D. Siggia, J.E. Moreira, C.L. Smith, J.F. Presley, H.J. Worman, and J. LippincottSchwartz. 1997. Nuclear membrane dynamics and reassembly in living cells: Targeting of an inner nuclear membrane protein in interphase and mitosis. *J Cell Biol*. 138:1193-1206.

Erjavec, N., L. Larsson, J. Grantham, and T. Nyström. 2007. Accelerated aging and failure to segregate damaged proteins in Sir2 mutants can be suppressed by overproducing the protein aggregation-remodeling factor Hsp104p. *Gene Dev*. 21:2410-2421.

Eskelinen, E.L., A.R. Prescott, J. Cooper, S.M. Brachmann, L.J. Wang, X.W. Tang, J.M. Backer, and J.M. Lucocq. 2002. Inhibition of autophagy in mitotic animal cells. *Traffic*. 3:878-893.

Eskelinen, E.L., F. Reggiori, M. Baba, A.L. Kovács, and P.O. Seglen. 2011. Seeing is believing The impact of electron microscopy on autophagy research. *Autophagy*. 7:935-956.

Etlinger, J.D., and A.L. Goldberg. 1977. Soluble Atp-Dependent Proteolytic System Responsible for Degradation of Abnormal Proteins in Reticulocytes. *P Natl Acad Sci USA*. 74:54-58.

Evans, T., E.T. Rosenthal, J. Youngblom, D. Distel, and T. Hunt. 1983. Cyclin: a Protein Specified by Maternal Messenger-RNA in Sea-Urchin Eggs That Is Destroyed at Each Cleavage Division. *Cell*. 33:389-396.

Fan, H., and S. Penman. 1970. Regulation of Protein Synthesis in Mammalian Cells. II. Inhibition of Protein Synthesis at Level of Initiation during Mitosis. *J Mol Biol*. 50:655-670.

Fang, C.T., H.H. Kuo, S.C. Hsu, and L.H. Yih. 2019. HSP70 is required for the proper assembly of pericentriolar material and function of mitotic centrosomes. *Cell Div*. 14:4.

Farías, G.G., A. Freal, E. Tortosa, R. Stucchi, X.X. Pan, S. Portegies, L. Will, M. Altelaar, and C.C. Hoogenraad. 2019. Feedback-Driven Mechanisms between Microtubules and the Endoplasmic Reticulum Instruct Neuronal Polarity. *Neuron*. 102:184-201.

Farrell, P.J., K. Balkow, T. Hunt, R.J. Jackson, and H. Trachsel. 1977. Phosphorylation of initiation factor elF-2 and the control of reticulocyte protein synthesis. *Cell*. 11:187-200.

Ferreiro, E., R. Resende, R. Costa, C.R. Oliveira, and C.M.F. Pereira. 2006. An endoplasmic-reticulum-specific apoptotic pathway is involved in prion and amyloid-beta peptides neurotoxicity. *Neurobiol Dis*. 23:669-678.

Finley, D., A. Ciechanover, and A. Varshavsky. 1984. Thermolability of Ubiquitin-Activating Enzyme from the Mammalian-Cell Cycle Mutant Ts85. *Cell*. 37:43-55.

Fleming, A., M. Bourdenx, M. Fujimaki, C. Karabiyik, G.J. Krause, A. Lopez, C. Puri, A. Scrivo, J. Skidmore, S.M. Son, E. Stamatakou, L. Wrobel, Y. Zhu, A.M. Cuervo, and D.C. Rubinsztein. 2022. The different autophagy degradation pathways and neurodegeneration. *Neuron*. 110:935-966.

Flemming, W. 1879. Ueber das Verhalten des Kerns bei der Zelltheilung, und über die Bedeutung mehrkerniger Zellen. *Archiv für pathologische Anatomie und Physiologie und für klinische Medicin*. 77:1-29.

Fortun, J., W.A. Dunn, S. Joy, J. Li, and L. Notterpek. 2003. Emerging role for autophagy in the removal of aggresomes in Schwann cells. *J Neurosci*. 23:10672-10680.

Fouillet, A., C. Levet, A. Virgone, M. Robin, P. Dourlen, J. Rieusset, E. Belaidi, M. Ovize, M. Touret, S. Nataf, and B. Mollereau. 2012. ER stress inhibits neuronal

death by promoting autophagy. *Autophagy*. 8:915-926.

Fourest-Lieuvin, A., L. Peris, V. Gache, I. Garcia-Saez, C. Juillan-Binard, V. Lantez, and D. Job. 2006. Microtubule regulation in mitosis: Tubulin phosphorylation by the cyclin-dependent kinase Cdk1. *Mol Biol Cell*. 17:1041-1050.

Fregno, I., E. Fasana, T.J. Bergmann, A. Raimondi, M. Loi, T. Soldà, C. Galli, R. D'Antuono, D. Morone, A. Danieli, P. Paganetti, E. van Anken, and M. Molinari. 2018. ER-to-lysosome-associated degradation of proteasome-resistant ATZ polymers occurs via receptor-mediated vesicular transport. *Embo J*. 37:e99259.

Fricker, M., M. Hollinshead, N. White, and D. Vaux. 1997. Interphase nuclei of many mammalian cell types contain deep, dynamic, tubular membrane-bound invaginations of the nuclear envelope. *J Cell Biol*. 136:531-544.

Frottin, F., F. Schueder, S. Tiwary, R. Gupta, R. Körner, T. Schlichthaerle, J. Cox, R. Jungmann, F.U. Hartl, and M.S. Hipp. 2019. The nucleolus functions as a phase-separated protein quality control compartment. *Science*. 365:342-347.

Fuchs, M., C. Luthold, S.M. Guilbert, A.A. Varlet, H. Lambert, A. Jetté, S. Elowe, J. Landry, and J.N. Lavoie. 2015. A Role for the Chaperone Complex BAG3-HSPB8 in Actin Dynamics, Spindle Orientation and Proper Chromosome Segregation during Mitosis. *Plos Genet*. 11:e1005582.

Furuya, T., M. Kim, M. Lipinski, J.Y. Li, D. Kim, T. Lu, Y. Shen, L. Rameh, B. Yankner, L.H. Tsai, and J.Y. Yuan. 2010. Negative Regulation of Vps34 by Cdk Mediated Phosphorylation. *Mol Cell*. 38:500-511.

Gamow, G. 1954. Possible Relation between Deoxyribonucleic Acid and Protein Structures. *Nature*. 173:318-318.

Gardner, B.M., D. Pincus, K. Gotthardt, C.M. Gallagher, and P. Walter. 2013. Endoplasmic Reticulum Stress Sensing in the Unfolded Protein Response. *Csh Perspect Biol*. 5:a013169.

Gatta, A.T., Y. Olmos, C.L. Stoten, Q. Chen, P.B. Rosenthal, and J.G. Carlton. 2021. CDK1 controls CHMP7-dependent nuclear envelope reformation. *Elife*. 10:e59999.

Gavet, O., and J. Pines. 2010a. Activation of cyclin B1-Cdk1 synchronizes events in the nucleus and the cytoplasm at mitosis. *J Cell Biol*. 189:247-259.

Gavet, O., and J. Pines. 2010b. Progressive Activation of CyclinB1-Cdk1 Coordinates Entry to Mitosis. *Dev Cell*. 18:533-543.

Geiger, T., A. Wehner, C. Schaab, J. Cox, and M. Mann. 2012. Comparative Proteomic Analysis of Eleven Common Cell Lines Reveals Ubiquitous but Varying Expression of Most Proteins. *Mol Cell Proteomics*. 11:M111.014050.

Gibson, R.L., J.L. Burns, and B.W. Ramsey. 2003. Pathophysiology and management of pulmonary infections in cystic fibrosis. *Am J Resp Crit Care*. 168:918-951.

Ginno, P.A., L. Burger, J. Seebacher, V. Iesmantavicius, and D. Schübeler. 2018. Cell cycle-resolved chromatin proteomics reveals the extent of mitotic preservation of the genomic regulatory landscape. *Nat Commun*. 9:4048.

Glotzer, M., A.W. Murray, and M.W. Kirschner. 1991. Cyclin Is Degraded by the Ubiquitin Pathway. *Nature*. 349:132-138.

Goedert, M., M.G. Spillantini, K. Del Tredici, and H. Braak. 2013. 100 years of Lewy pathology. *Nat Rev Neurol*. 9:13-24.

Goldberger, R.F., C.J. Epstein, and C.B. Anfinsen. 1963. Acceleration of Reactivation of Reduced Bovine Pancreatic Ribonuclease by a Microsomal System from Rat

Liver. *J Biol Chem*. 238:628-635.
Goldschmidt, R. 1935. Gen und Außeneigenschaft (Untersuchungen an Drosophila). i, ii. *Zeitschrift für induktive Abstammungs- und Vererbungslehre*. 69:37-131.
Gorbatyuk, M.S., A. Shabashvili, W.J. Chen, C. Meyers, L.F. Sullivan, M. Salganik, J.H. Lin, A.S. Lewin, N. Muzyczka, and O.S. Gorbatyuk. 2012. Glucose Regulated Protein 78 Diminishes α-Synuclein Neurotoxicity in a Rat Model of Parkinson Disease. *Mol Ther*. 20:1327-1337.
Gottesfeld, J.M., and D.J. Forbes. 1997. Mitotic repression of the transcriptional machinery. *Trends Biochem Sci*. 22:197-202.
Granell, S., G. Baldini, S. Mohammad, V. Nicolin, P. Narducci, B. Storrie, and G. Baldini. 2008. Sequestration of mutated α1-antitrypsin into inclusion bodies is a cell-protective mechanism to maintain endoplasmic reticulum function. *Mol Biol Cell*. 19:572-586.
Grigolato, F., and P. Arosio. 2021. The role of surfaces on amyloid formation. *Biophys Chem*. 270:106533.
Gros, F., C.G. Kurland, H. Hiatt, J.D. Watson, W. Gilbert, and R.W. Risebrough. 1961. Unstable Ribonucleic Acid Revealed by Pulse Labelling of Escherichia Coli. *Nature*. 190:581-585.
Gu, J., Y. He, C. He, Q. Zhang, Q. Huang, S. Bai, R. Wang, Q. You, and L. Wang. 2025. Advances in the structures, mechanisms and targeting of molecular chaperones. *Signal Transduct Target Ther*. 10:84.
Gubas, A., and I. Dikic. 2022. ER remodeling via ER-phagy. *Mol Cell*. 82:1492-1500.
Guo, M.H., H. Gelman, and M. Gruebele. 2014. Coupled Protein Diffusion and Folding in the Cell. *Plos One*. 9.
Gupta, R., P. Kasturi, A. Bracher, C. Loew, M. Zheng, A. Villella, D. Garza, F.U. Hartl, and S. Raychaudhuri. 2011. Firefly luciferase mutants as sensors of proteome stress. *Nat Methods*. 8:879-884.
Guzman, I., and M. Gruebele. 2014. Protein Folding Dynamics in the Cell. *J Phys Chem B*. 118:8459-8470.
Haber, E., and C.B. Anfinsen. 1961. Regeneration of Enzyme Activity by Air Oxidation of Reduced Subtilisin-Modified Ribonuclease. *J Biol Chem*. 236:422-424.
Hämälistö, S., J.L. Stahl, E. Favaro, Q. Yang, B. Liu, L. Christoffersen, B. Loos, C.G. Boldú, J.A. Joyce, T. Reinheckel, M. Barisic, and M. Jäättelä. 2020. Spatially and temporally defined lysosomal leakage facilitates mitotic chromosome segregation. *Nat Commun*. 11:229.
Hamdan, N., P. Kritsiligkou, and C.M. Grant. 2017. ER stress causes widespread protein aggregation and prion formation. *J Cell Biol*. 216:2295-2304.
Harris, D.A. 2003. Trafficking, turnover and membrane topology of PrP. *Brit Med Bull*. 66:71-85.
Harris, J.R. 1968. Release of a Macromolecular Protein Component from Human Erythrocyte Ghosts. *Biochim Biophys Acta*. 150:534-537.
Hartl, F.U. 1996. Molecular chaperones in cellular protein folding. *Nature*. 381:571-580.
Hartl, F.U., A. Bracher, and M. Hayer-Hartl. 2011. Molecular chaperones in protein folding and proteostasis. *Nature*. 475:324-332.
Hartwell, L.H. 1973. 3 Additional Genes Required for Deoxyribonucleic Acid Synthesis in Saccharomyces-Cerevisiae. *J Bacteriol*. 115:966-974.

He, W.B., J. Du, X.W. Yang, W. Li, W.L. Tang, C. Dai, Y.Z. Chen, Y.X. Zhang, G.X. Lu, G. Lin, F. Gong, and Y.Q. Tan. 2019. Novel inactivating mutations in the FSH receptor cause premature ovarian insufficiency with resistant ovary syndrome. *Reprod Biomed Online*. 38:397-406.

Hellstrand, E., A. Nowacka, D. Topgaard, S. Linse, and E. Sparr. 2013. Membrane Lipid Co-Aggregation with α-Synuclein Fibrils. *Plos One*. 8:e77235.

Hemmingsen, S.M., C. Woolford, S.M. Vandervies, K. Tilly, D.T. Dennis, C.P. Georgopoulos, R.W. Hendrix, and R.J. Ellis. 1988. Homologous Plant and Bacterial Proteins Chaperone Oligomeric Protein Assembly. *Nature*. 333:330-334.

Hershko, A., A. Ciechanover, H. Heller, A.L. Haas, and I.A. Rose. 1980. Proposed Role of Atp in Protein Breakdown - Conjugation of Proteins with Multiple Chains of the Polypeptide of Atp-Dependent Proteolysis. *P Natl Acad Sci-Biol*. 77:1783-1786.

Hershko, A., D. Ganoth, J. Pehrson, R.E. Palazzo, and L.H. Cohen. 1991. Methylated Ubiquitin Inhibits Cyclin Degradation in Clam Embryo Extracts. *J Biol Chem*. 266:16376-16379.

Hershko, A., H. Heller, S. Elias, and A. Ciechanover. 1983. Components of Ubiquitin-Protein Ligase System. Resolution, Affinity Purification, and Role in Protein Breakdown. *J Biol Chem*. 258:8206-8214.

Hetz, C., J. Castilla, and C. Soto. 2007. Perturbation of endoplasmic reticulum homeostasis facilitates prion replication. *J Biol Chem*. 282:12725-12733.

Hetz, C., M. Russelakis-Carneiro, K. Maundrell, J. Castilla, and C. Soto. 2003. Caspase-12 and endoplasmic reticulum stress mediate neurotoxicity of pathological prion protein. *Embo J*. 22:5435-5445.

Hetz, C., K.Z. Zhang, and R.J. Kaufman. 2020. Mechanisms, regulation and functions of the unfolded protein response. *Nat Rev Mol Cell Bio*. 21:421-438.

Higuchi, M., K. Tagai, K. Takahata, and H. Endo. 2025. Advances in PET imaging of protein aggregates associated with neurodegenerative disease. *Nat Rev Neurol*. 21:506–522.

Hipp, M.S., P. Kasturi, and F.U. Hartl. 2019. The proteostasis network and its decline in ageing. *Nat Rev Mol Cell Bio*. 20:421-435.

Hipp, M.S., S.H. Park, and F.U. Hartl. 2014. Proteostasis impairment in protein-misfolding and aggregation diseases. *Trends Cell Biol*. 24:506-514.

Hoffstrom, B.G., A. Kaplan, R. Letso, R.S. Schmid, G.J. Turmel, D.C. Lo, and B.R. Stockwell. 2010. Inhibitors of protein disulfide isomerase suppress apoptosis induced by misfolded proteins. *Nat Chem Biol*. 6:900-906.

Holdgaard, S.G., V. Cianfanelli, E. Pupo, M. Lambrughi, M. Lubas, J.C. Nielsen, S. Eibes, E. Maiani, L.M. Harder, N. Wesch, M.M. Foged, K. Maeda, F. Nazio, L.R. de la Ballina, V. Dötsch, A. Brech, L.B. Frankel, M. Jäättelä, F. Locatelli, M. Barisic, J.S. Andersen, S. Bekker-Jensen, A.H. Lund, V.V. Rogov, E. Papaleo, L. Lanzetti, D. De Zio, and F. Cecconi. 2019. Selective autophagy maintains centrosome integrity and accurate mitosis by turnover of centriolar satellites. *Nat Commun*. 10:4176.

Hoozemans, J.J.M., E.S. van Haastert, P. Eikelenboom, R.A.I. de Vos, J.M. Rozemuller, and W. Scheper. 2007. Activation of the unfolded protein response in Parkinson's disease. *Biochem Bioph Res Co*. 354:707-711.

Hoozemans, J.J.M., R. Veerhuis, E.S. Van Haastert, J.M. Rozemuller, F. Baas, P. Eikelenboom, and W. Scheper. 2005. The unfolded protein response is activated in Alzheimer's disease. *Acta Neuropathol*. 110:165-172.

Horovitz, A., T.H. Reingewertz, J. Cuéllar, and J.M. Valpuesta. 2022. Chaperonin Mechanisms: Multiple and (Mis)Understood? *Annu Rev Biophys*. 51:115-133.

Hruban, Z., R.G. Kleinfeld, B. Spargo, R.W. Wissler, and H. Swift. 1963. Focal Cytoplasmic Degradation. *Am J Pathol*. 42:657-683.

Htet, P.H., E. Avezov, and E. Lauga. 2024. Fluid mechanics of luminal transport in actively contracting endoplasmic reticulum. *Elife*. 13:RP93518.

Hu, J.J., Y. Shibata, P.P. Zhu, C. Voss, N. Rismanchi, W.A. Prinz, T.A. Rapoport, and C. Blackstone. 2009. A Class of Dynamin-like GTPases Involved in the Generation of the Tubular ER Network. *Cell*. 138:549-561.

Hurst, S., B.E. Vos, M. Brandt, and T. Betz. 2021. Intracellular softening and increased viscoelastic fluidity during division. *Nat Phys*. 17:1270-1276.

Ingolia, N.T., L.F. Lareau, and J.S. Weissman. 2011. Ribosome Profiling of Mouse Embryonic Stem Cells Reveals the Complexity and Dynamics of Mammalian Proteomes. *Cell*. 147:789-802.

Ito, Y., M. Yamada, H. Tanaka, K. Aida, K. Tsuruma, M. Shimazawa, I. Hozumi, T. Inuzuka, H. Takahashi, and H. Hara. 2009. Involvement of CHOP, an ER-stress apoptotic mediator, in both human sporadic ALS and ALS model mice. *Neurobiol Dis*. 36:470-476.

Jacob, F., and J. Monod. 1961. Genetic Regulatory Mechanisms in Synthesis of Proteins. *J Mol Biol*. 3:318-356.

Jayaraj, G.G., M.S. Hipp, and F.U. Hartl. 2020. Functional Modules of the Proteostasis Network. *Csh Perspect Biol*. 12:a033951.

Jeffery, W.R. 2015. Closing the Wounds: One Hundred and Twenty Five Years of Regenerative Biology in the Ascidian. *Genesis*. 53:48-65.

Jiang, H., S.S. Wang, Y.J. Huang, X.N. He, H.G. Cui, X.L. Zhu, and Y.X. Zheng. 2015. Phase Transition of Spindle-Associated Protein Regulate Spindle Apparatus Assembly. *Cell*. 163:108-122.

Jiang, H.Y., and R.C. Wek. 2005. Phosphorylation of the α-subunit of the eukaryotic initiation factor-2 (eIF2α) reduces protein synthesis and enhances apoptosis in response to proteasome inhibition. *J Biol Chem*. 280:14189-14202.

Jin, Y., W. Awad, K. Petrova, and L.M. Hendershot. 2008. Regulated release of ERdj3 from unfolded proteins by BiP. *Embo J*. 27:2873-2882.

Johnston, H.E., and R.S. Samant. 2021. Alternative systems for misfolded protein clearance: life beyond the proteasome. *Febs J*. 288:4464-4487.

Johnston, J.A., C.L. Ward, and R.R. Kopito. 1998. Aggresomes: A cellular response to misfolded proteins. *J Cell Biol*. 143:1883-1898.

Kadauke, S., M.I. Udugama, J.M. Pawlicki, J.C. Achtman, D.P. Jain, Y. Cheng, R.C. Hardison, and G.A. Blobel. 2012. Tissue-Specific Mitotic Bookmarking by Hematopoietic Transcription Factor GATA1. *Cell*. 150:725-737.

Kaganovich, D., R. Kopito, and J. Frydman. 2008. Misfolded proteins partition between two distinct quality control compartments. *Nature*. 454:1088-1095.

Kaisari, S., D. Sitry-Shevah, S. Miniowitz-Shemtov, A. Teichner, and A. Hershko. 2017. Role of CCT chaperonin in the disassembly of mitotic checkpoint complexes. *P Natl Acad Sci USA*. 114:956-961.

Kampinga, H.H., and E.A. Craig. 2010. The HSP70 chaperone machinery: J proteins as drivers of functional specificity. *Nat Rev Mol Cell Bio*. 11:579-592.

Karagöz, G.E., D. Acosta-Alvear, and P. Walter. 2019. The Unfolded Protein Response: Detecting and Responding to Fluctuations in the Protein-Folding Capacity of the Endoplasmic Reticulum. *Csh Perspect Biol*. 11:a033886.

Kaushik, S., and A.M. Cuervo. 2018. The coming of age of chaperone-mediated autophagy. *Nat Rev Mol Cell Bio*. 19:365-381.

Kawaguchi, T., K. Miyazawa, S. Moriya, T. Ohtomo, X.F. Che, M. Naito, M. Itoh, and A. Tomoda. 2011. Combined treatment with bortezomib plus bafilomycin A enhances the cytocidal effect and induces endoplasmic reticulum stress in U266 myeloma cells: Crosstalk among proteasome, autophagy-lysosome and ER stress. *Int J Oncol*. 38:643-654.

Keene, C.D., C.M.P. Rodrigues, T. Eich, M.S. Chhabra, C.J. Steer, and W.C. Low. 2002. Tauroursodeoxycholic acid, a bile acid, is neuroprotective in a transgenic model of Huntington's disease. *P Natl Acad Sci USA*. 99:10671-10676.

Kelly, J.J., D. Tranter, E. Pardon, G. Chi, H. Kramer, L. Happonen, K.M. Knee, J.M. Janz, J. Steyaert, C. Bulawa, V.O. Paavilainen, J.T. Huiskonen, and W.W. Yue. 2022. Snapshots of actin and tubulin folding inside the TRiC chaperonin. *Nat Struct Mol Biol*. 29:420-429.

Kendrew, J.C., G. Bodo, H.M. Dintzis, R.G. Parrish, H. Wyckoff, and D.C. Phillips. 1958. 3-Dimensional Model of the Myoglobin Molecule Obtained by X-Ray Analysis. *Nature*. 181:662-666.

Kirstein-Miles, J., A. Scior, E. Deuerling, and R.I. Morimoto. 2013. The nascent polypeptide-associated complex is a key regulator of proteostasis. *Embo J*. 32:1451-1468.

Klaips, C.L., G.G. Jayaraj, and F.U. Hartl. 2018. Pathways of cellular proteostasis in aging and disease. *J Cell Biol*. 217:51-63.

Klopfenstein, D.R.C., F. Kappeler, and H.P. Hauri. 1998. A novel direct interaction of endoplasmic reticulum with microtubules. *Embo J*. 17:6168-6177.

Knoll, M., and E. Ruska. 1932. The Electron Microscope. *Z Phys*. 78:318-339.

Kohli, E., S. Causse, V. Baverel, L. Dubrez, N. Borges-Bonan, O. Demidov, and C. Garrido. 2021. Endoplasmic Reticulum Chaperones in Viral Infection: Therapeutic Perspectives. *Microbiol Mol Biol R*. 85:e0003521.

Konno, T., P. Parutto, C.C. Crapart, V. Davi, D.M.D. Bailey, M.A. Awadelkareem, C. Hockings, A.I. Brown, A. Agrawal, J.E. Chambers, M.J. Vander Werp, K.M. Koning, L.M. Elfari, S. Steen, E. Metzakopian, L.M. Westrate, E.F. Koslover, and E. Avezov. 2024. Endoplasmic reticulum morphology regulation by RTN4 modulates neuronal regeneration by curbing luminal transport. *Cell Rep*. 43:114357.

Konrad, C.G. 1963. Protein Synthesis and Rna Synthesis during Mitosis in Animal Cells. *J Cell Biol*. 19:267-277.

Kopito, R.R. 2000. Aggresomes, inclusion bodies and protein aggregation. *Trends Cell Biol*. 10:524-530.

Kors, S., and A.L. Schlaitz. 2024. Dynamic remodelling of the endoplasmic reticulum for mitosis. *J Cell Sci*. 137:jcs261444.

Koslover, E.F., C.K. Chan, and J.A. Theriot. 2017. Cytoplasmic Flow and Mixing Due to Deformation of Motile Cells. *Biophys J*. 113:2077-2087.

Kraft, F., P. Rodriguez-Aliaga, W. Yuan, L. Franken, K. Zajt, D. Hasan, T.-T. Lee, E. Flex, A. Hentschel, A.M. Innes, B. Zheng, D.S. Julia Suh, C. Knopp, E. Lausberg, J. Krause, X. Zhang, P. Trapane, R. Carroll, M. McClatchey, A.E. Fry, L. Wang, S. Giesselmann, H. Hoang, D. Baldridge, G.A. Silverman, F.C. Radio, E. Bertini, A. Ciolfi, K.A. Blood, J.-M. de Sainte Agathe, P. Charles, G. Bergant, G. Cuturilo, B. Peterlin, K. Diderich, H. Streff, L. Robak, R. Oegema, E. van Binsbergen, J. Herriges, C.J. Saunders, A. Maier, S. Wolking, Y. Weber, H. Lochmuller, S. Meyer, A. Aleman, K. Polavarapu, G. Nicolas, A. Goldenberg, L. Guyant, K. Pope, K.N. Hehmeyer, K.G. Monaghan, A. Quade, T. Smol, R. Caumes, S. Duerinckx, C. Depondt, W. Van Paesschen, C. Rieubland, C. Poloni, M. Guipponi, S. Arcioni, M. Meuwissen, A.C. Jansen, J. Rosenblum, T.B. Haack, M. Bertrand, L. Gerstner, J. Magg, O. Riess, J.B. Schulz, N. Wagner, M. Wiesmann, J. Weis, T. Eggermann, M. Begemann, A. Roos, M. Hausler, T. Schedl, M. Tartaglia, J. Bremer, S.C. Pak, J. Frydman, M. Elbracht, and I. Kurth. 2024. Brain malformations and seizures by impaired chaperonin function of TRiC. *Science (New York, N.Y.)*. 386:516-525.

Kraskiewicz, H., and U. FitzGerald. 2012. InterfERing with endoplasmic reticulum stress. *Trends Pharmacol Sci*. 33:53-63.

Kucharski, T.J., P.E. Minshall, M. Moustafa-Kamal, A.S. Turnell, and J.G. Teodoro. 2017. Reciprocal Regulation between 53BP1 and the Anaphase-Promoting Complex/Cyclosome Is Required for Genomic Stability during Mitotic Stress. *Cell Rep*. 18:1982-1995.

Kumar, D., B. Golchoubian, I. Belevich, E. Jokitalo, and A.L. Schlaitz. 2019. REEP3 and REEP4 determine the tubular morphology of the endoplasmic reticulum during mitosis. *Mol Biol Cell*. 30:1377-1389.

Labbadia, J., and R.I. Morimoto. 2015. The Biology of Proteostasis in Aging and Disease. *Annual Review of Biochemistry*. 84:435-464.

Lai, C.S.W., J. Preisler, L. Baum, D.H.S. Lee, H.K. Ng, J. Hugon, K.F. So, and R.C.C. Chang. 2009. Low molecular weight Aβ induces collapse of endoplasmic reticulum. *Mol Cell Neurosci*. 41:32-43.

Lawless, M.W., A.K. Mankan, S.G. Gray, and S. Norfis. 2008. Endoplasmic reticulum stress - A double edged sword for Z alpha-1 antitrypsin deficiency hepatoxicity. *Int J Biochem Cell B*. 40:1403-1414.

Leder, A., G. Mas, V. Szentgyörgyi, R.P. Jakob, T. Maier, A. Spang, and S. Hiller. 2025. A multichaperone condensate enhances protein folding in the endoplasmic reticulum. *Nat Cell Biol*.

Lee, H., J.Y. Noh, Y. Oh, Y. Kim, J.W. Chang, C.W. Chung, S.T. Lee, M. Kim, H. Ryu, and Y.K. Jung. 2012. IRE1 plays an essential role in ER stress-mediated aggregation of mutant huntingtin via the inhibition of autophagy flux. *Hum Mol Genet*. 21:101-114.

Lee, M.G., and P. Nurse. 1987. Complementation Used to Clone a Human Homolog of the Fission Yeast-Cell Cycle Control Gene Cdc2. *Nature*. 327:31-35.

Levinthal, C. 1968. Are There Pathways for Protein Folding. *J Chim Phys Pcb*. 65:44-45.

Lewis, M.J., and H.R.B. Pelham. 1985. Involvement of Atp in the Nuclear and Nucleolar Functions of the 70 Kd Heat-Shock Protein. *Embo J*. 4:3137-3143.

Lewy, F., and M. Lewandowsky. 1912. Handbuch der Neurologie. *Berlin: Julius*

Springer. 3:920–933.

Li, C.M., J. Kang, J. Baek, Y. Kim, H. Park, and Y.K. Jung. 2024. Cytosolic FKBPL and ER-resident CKAP4 co-regulates ER-phagy and protein secretion. *Nat Commun*. 15:7886.

Li, J.M., Z.Y. Cai, L.P. Vaites, N. Shen, D.C. Mitchell, E.L. Huttlin, J.A. Paulo, B.L. Harry, and S.P. Gygi. 2021. Proteome-wide mapping of short-lived proteins in human cells. *Mol Cell*. 81:4722-4735.

Li, Y.A., S.J. Li, and H.J. Wu. 2022. Ubiquitination-Proteasome System (UPS) and Autophagy Two Main Protein Degradation Machineries in Response to Cell Stress. *Cells-Basel*. 11:851.

Li, Z.Y., X.F. Tian, X.M. Ji, J.J. Wang, H.X. Chen, D.M. Wang, and X. Zhang. 2020. ULK1-ATG13 and their mitotic phospho-regulation by CDK1 connect autophagy to cell cycle. *Plos Biol*. 18:e3000288.

Liang, J.R., E. Lingeman, S. Ahmed, and J.E. Corn. 2018. Atlastins remodel the endoplasmic reticulum for selective autophagy. *J Cell Biol*. 217:3354-3367.

Liao, T., R. Li, P. Lu, Y. Liu, R. Yang, H. Guo, Z. Wu, R. Wang, L. Yuan, Z. Hu, H. Gao, and F. Li. 2024. Molecular Basis of VCPIP1 and P97/VCP Interaction Reveals Its Functions in Post-Mitotic Golgi Reassembly. *Adv Sci (Weinh)*. 11:e2403417.

Lindner, A.B., R. Madden, A. Dernarez, E.J. Stewart, and F. Taddei. 2008. Asymmetric segregation of protein aggregates is associated with cellular aging and rejuvenation. *P Natl Acad Sci USA*. 105:3076-3081.

Liu, B.D., L. Larsson, A. Caballero, X.X. Hao, D. Öling, J. Grantham, and T. Nyström. 2010. The Polarisome Is Required for Segregation and Retrograde Transport of Protein Aggregates. *Cell*. 140:257-267.

Liu, B.D., L. Larsson, V. Franssens, X.X. Hao, S.M. Hill, V. Andersson, D. Höglund, J. Song, X.X. Yang, D. Öling, J. Grantham, J. Winderickx, and T. Nyström. 2011. Segregation of Protein Aggregates Involves Actin and the Polarity Machinery. *Cell*. 147:959-961.

Liu, B.T., Y. Han, and S.B. Qian. 2013. Cotranslational Response to Proteotoxic Stress by Elongation Pausing of Ribosomes. *Mol Cell*. 49:453-463.

Liu, X., H.W. Wang, Z. Dou, K. Ruan, D.L. Hill, L. Li, Y.Y. Shi, and X.B. Yao. 2020. Phase separation drives decision making in cell division. *J Biol Chem*. 295:13419-13431.

Liu, X.L., S. Oh, and M.W. Kirschner. 2022. The uniformity and stability of cellular mass density in mammalian cell culture. *Front Cell Dev Biol*. 10:1017499.

Liu, Y., X. Zhang, W.T. Chen, Y.L. Tan, and J.W. Kelly. 2015. Fluorescence Turn-On Folding Sensor To Monitor Proteome Stress in Live Cells. *J Am Chem Soc*. 137:11303-11311.

Liu, Z., G.L. Liu, J. Wang, M. Xiong, and A.S. Lee. 2023. ER chaperone GRP78/BiP translocates to the nucleus under stress and acts as a transcriptional regulator. *P Natl Acad Sci USA*. 120:e2303448120.

Liu, Z.Y., S.J. Xiang, B. Chen, J. Li, D.C. Zhu, H.J. Xu, and S. Hu. 2024. Parkinson Disease -Targeted Nanocapsules for Synergistic Treatment: Combining Dopamine Replacement and Neuroinflammation Mitigation. *Adv Sci*. 11:2404717.

Lu, G., J. Yi, A. Gubas, Y.T. Wang, Y.H. Wu, Y. Ren, M. Wu, Y. Shi, C.X. Ouyang, H.W.S. Tan, T.R. Wang, L.M. Wang, N.D. Yang, S. Deng, D.J. Xia, R.H. Chen,

S.A. Tooze, and H.M. Shen. 2019. Suppression of autophagy during mitosis via CUL4-RING ubiquitin ligases-mediated WIPI2 polyubiquitination and proteasomal degradation. *Autophagy*. 15:1917-1934.

Lu, J.N., T. Wu, B. Zhang, S.K. Liu, W.J. Song, J.J. Qiao, and H.H. Ruan. 2021. Types of nuclear localization signals and mechanisms of protein import into the nucleus. *Cell Commun Signal*. 19:60.

Lu, L., M.S. Ladinsky, and T. Kirchhausen. 2009. Cisternal Organization of the Endoplasmic Reticulum during Mitosis. *Mol Biol Cell*. 20:3471-3480.

Lu, M., C.N. Christensen, J.M. Weber, T. Konno, N.F. Läubli, K.M. Scherer, E. Avezov, P. Lio, A.A. Lapkin, G.S.K. Schierle, and C.F. Kaminski. 2023. ERnet: a tool for the semantic segmentation and quantitative analysis of endoplasmic reticulum topology. *Nat Methods*. 20:569-579.

Lu, M., F.W. van Tartwijk, J.L.Q.J. Lin, W. Nijenhuis, P. Parutto, M. Fantham, C.N. Christensen, E. Avezov, C.E. Holt, A. Tunnacliffe, D. Holcman, L. Kapitein, G.S.K. Schierle, and C.F. Kaminski. 2020. The structure and global distribution of the endoplasmic reticulum network are actively regulated by lysosomes. *Sci Adv*. 6:eabc7209.

Lukacs, G.L., and A.S. Verkman. 2012. CFTR: folding, misfolding and correcting the ΔF508 conformational defect. *Trends Mol Med*. 18:81-91.

Ly, J., K.H. Xiang, K.C. Su, G.B. Sissoko, D.P. Bartel, and I.M. Cheeseman. 2024. Nuclear release of eIF1 restricts start-codon selection during mitosis. *Nature*. 635:490–498.

Mackeh, R., D. Perdiz, S. Lorin, P. Codogno, and C. Poüs. 2013. Autophagy and microtubules - new story, old players. *J Cell Sci*. 126:1071-1080.

Maity, H., A.N. Muttathukattil, and G. Reddy. 2018. Salt Effects on Protein Folding Thermodynamics. *J Phys Chem Lett*. 9:5063-5070.

Majid, N., and R.H. Khan. 2023. Protein aggregation: Consequences, mechanism, characterization and inhibitory strategies. *Int J Biol Macromol*. 242:125123.

Malhas, A., C. Goulbourne, and D.J. Vaux. 2011. The nucleoplasmic reticulum: form and function. *Trends Cell Biol*. 21:362-373.

Marzec, M., D. Eletto, and Y. Argon. 2012. GRP94: An HSP90-like protein specialized for protein folding and quality control in the endoplasmic reticulum. *Bba-Mol Cell Res*. 1823:774-787.

Massacci, G., L. Perfetto, and F. Sacco. 2023. The Cyclin-dependent kinase 1: more than a cell cycle regulator. *Brit J Cancer*. 129:1707-1716.

Massey, A.J., D.S. Williamson, H. Browne, J.B. Murray, P. Dokurno, T. Shaw, A.T. Macias, Z. Daniels, S. Geoffroy, M. Dopson, P. Lavan, N. Matassova, G.L. Francis, C.J. Graham, R. Parsons, Y.K. Wang, A. Padfield, M. Comer, M.J. Drysdale, and M. Wood. 2010. A novel, small molecule inhibitor of Hsc70/Hsp70 potentiates Hsp90 inhibitor induced apoptosis in HCT116 colon carcinoma cells. *Cancer Chemoth Pharm*. 66:535-545.

Masui, Y., and C.L. Markert. 1971. Cytoplasmic Control of Nuclear Behavior during Meiotic Maturation of Frog Oocytes. *J Exp Zool*. 177:129-145.

Mateju, D., T.M. Franzmann, A. Patel, A. Kopach, E.E. Boczek, S. Maharana, H.O. Lee, S. Carra, A.A. Hyman, and S. Alberti. 2017. An aberrant phase transition of stress granules triggered by misfolded protein and prevented by chaperone function. *Embo J*. 36:1669-1687.

Mazroui, R., S. Di Marco, R.J. Kaufman, and I.E. Gallouzi. 2007. Inhibition of the ubiquitin-proteasome system induces stress granule formation. *Mol Biol Cell*. 18:2603-2618.

Mazzarello, P. 2002. Emilio veratti and the first applications of the «black reaction» to muscle research: A historical account. *Rendiconti Lincei*. 13:273-288.

Mazzarello, P., A. Calligaro, V. Vannini, and U. Muscatello. 2003. The sarcoplasmic reticulum: its discovery and rediscovery. *Nat Rev Mol Cell Bio*. 4:69-74.

McAinsh, A.D., and G.J.P.L. Kops. 2023. Principles and dynamics of spindle assembly checkpoint signalling. *Nat Rev Mol Cell Bio*. 24:543-559.

McIntosh, J.R., and T. Hays. 2016. A Brief History of Research on Mitotic Mechanisms. *Biology-Basel*. 5:55.

McPhee, M., G. Dellaire, and N.D. Ridgway. 2024. Mechanisms for assembly of the nucleoplasmic reticulum. *Cell Mol Life Sci*. 81:415.

Meacham, G.C., C. Patterson, W.Y. Zhang, J.M. Younger, and D.M. Cyr. 2001. The Hsc70 co-chaperone CHIP targets immature CFTR for proteasomal degradation. *Nat Cell Biol*. 3:100-105.

Melo, E.P., T. Konno, I. Farace, M.A. Awadelkareem, L.R. Skov, F. Teodoro, T.P. Sancho, A.W. Paton, J.C. Paton, M. Fares, P.M.R. Paulo, X. Zhang, and E. Avezov. 2022. Stress-induced protein disaggregation in the endoplasmic reticulum catalysed by BiP. *Nat Commun*. 13:2501.

Miettinen, T.P., J.H. Kang, L.F. Yang, and S.R. Manalis. 2019. Mammalian cell growth dynamics in mitosis. *Elife*. 8:e44700.

Miller, S.B.M., A. Mogk, and B. Bukau. 2015. Spatially Organized Aggregation of Misfolded Proteins as Cellular Stress Defense Strategy. *J Mol Biol*. 427:1564-1574.

Milo, R. 2013. What is the total number of protein molecules per cell volume? A call to rethink some published values. *Bioessays*. 35:1050-1055.

Mochida, K., and H. Nakatogawa. 2022. ER-phagy: selective autophagy of the endoplasmic reticulum. *Embo Rep*. 23:e55192.

Mogk, A., B. Bukau, and H.H. Kampinga. 2018. Cellular Handling of Protein Aggregates by Disaggregation Machines. *Mol Cell*. 69:214-226.

Moore, A.S., S.M. Coscia, C.L. Simpson, F.E. Ortega, E.C. Wait, J.M. Heddleston, J.J. Nirschl, C.J. Obara, P. Guedes-Dias, C.A. Boecker, T.L. Chew, J.A. Theriot, J. Lippincott-Schwartz, and E.L.F. Holzbaur. 2021. Actin cables and comet tails organize mitochondrial networks in mitosis. *Nature*. 591:659-664.

Moreno, J.A., M. Halliday, C. Molloy, H. Radford, N. Verity, J.M. Axten, C.A. Ortori, A.E. Willis, P.M. Fischer, D.A. Barrett, and G.R. Mallucci. 2013. Oral Treatment Targeting the Unfolded Protein Response Prevents Neurodegeneration and Clinical Disease in Prion-Infected Mice. *Sci Transl Med*. 5:206ra138.

Morris, J.A., A.J. Dorner, C.A. Edwards, L.M. Hendershot, and R.J. Kaufman. 1997. Immunoglobulin binding protein (BiP) function is required to protect cells from endoplasmic reticulum stress but is not required for the secretion of selective proteins. *J Biol Chem*. 272:4327-4334.

Morrow, C.S., T.J. Porter, N. Xu, Z.P. Arndt, K. Ako-Asare, H.J. Heo, E.A.N. Thompson, and D.L. Moore. 2020. Vimentin Coordinates Protein Turnover at the Aggresome during Neural Stem Cell Quiescence Exit. *Cell Stem Cell*.

26:558-568.

Mosquera, J.V., M.C. Bacher, and J.R. Priess. 2021. Nuclear lipid droplets and nuclear damage in Caenorhabditis elegans. *Plos Genet*. 17:e1009602.

Mukherjee, S., M. Poudyal, K. Dave, P. Kadu, and S.K. Maji. 2024. Protein misfolding and amyloid nucleation through liquid-liquid phase separation. *Chem Soc Rev*. 53:4976-5013.

Mymrikov, E.V., M. Daake, B. Richter, M. Haslbeck, and J. Buchner. 2017. The Chaperone Activity and Substrate Spectrum of Human Small Heat Shock Proteins. *J Biol Chem*. 292:672-684.

Nakajima, S., H. Kato, S. Takahashi, H. Johno, and M. Kitamura. 2011. Inhibition of NF-κB by MG132 through ER stress-mediated induction of LAP and LIP. *Febs Lett*. 585:2249-2254.

Nigg, E.A. 2001. Mitotic kinases as regulators of cell division and its checkpoints. *Nat Rev Mol Cell Bio*. 2:21-32.

Nissley, D.A., Y. Jiang, F. Trovato, I. Sitarik, K.B. Narayan, P. To, Y.Z. Xia, S.D. Fried, and E.P. O'Brien. 2022. Universal protein misfolding intermediates can bypass the proteostasis network and remain soluble and less functional. *Nat Commun*. 13:3081.

Niu, Y., J.G. Pemberton, Y.J. Kim, and T. Balla. 2024. Phosphatidylserine enrichment in the nuclear membrane regulates key enzymes of phosphatidylcholine synthesis. *Embo J*. 43:3414-3449.

Nmezi, B., J.Q. Xu, R. Fu, T.J. Armiger, G. Rodriguez-Bey, J.S. Powell, H.Q. Ma, M. Sullivan, Y.P. Tu, N.Y. Chen, S.G. Young, D.B. Stolz, K.N. Dahl, Y. Liu, and Q.S. Padiath. 2019. Concentric organization of A- and B-type lamins predicts their distinct roles in the spatial organization and stability of the nuclear lamina. *P Natl Acad Sci USA*. 116:4307-4315.

Nourbakhsh, K., A.A. Ferreccio, M.J. Bernard, and S. Yadav. 2021. TAOK2 is an ER-localized kinase that catalyzes the dynamic tethering of ER to microtubules. *Dev Cell*. 56:3321-3333.

Novikoff, A.B., H. Beaufay, and C. De Duve. 1956. Electron microscopy of lysosomerich fractions from rat liver. *The Journal of biophysical and biochemical cytology*. 2:179-184.

Nunziante, M., K. Ackermann, K. Dietrich, H. Wolf, L. Gädtke, S. Gilch, I. Vorberg, M. Groschup, and H.M. Schätzl. 2011. Proteasomal Dysfunction and Endoplasmic Reticulum Stress Enhance Trafficking of Prion Protein Aggregates through the Secretory Pathway and Increase Accumulation of Pathologic Prion Protein. *J Biol Chem*. 286:33942-33953.

Nurse, P., P. Thuriaux, and K. Nasmyth. 1976. Genetic-Control of Cell-Division Cycle in Fission Yeast Schizosaccharomyces-Pombe. *Mol Gen Genet*. 146:167-178.

Odle, R.I., S.A. Walker, D. Oxley, A.M. Kidger, K. Balmanno, R. Gilley, H. Okkenhaug, O. Florey, N.T. Ktistakis, and S.J. Cook. 2020. An mTORC1-to-CDK1 Switch Maintains Autophagy Suppression during Mitosis. *Mol Cell*. 77:228-240.

Ogrodnik, M., H. Salmonowicz, R. Brown, J. Turkowska, W. Sredniawa, S. Pattabiraman, T. Amen, A.C. Abraham, N. Eichler, R. Lyakhovetsky, and D. Kaganovich. 2014. Dynamic JUNQ inclusion bodies are asymmetrically inherited in mammalian cell lines through the asymmetric partitioning of vimentin. *P Natl Acad Sci USA*. 111:8049-8054.

Oh, S., C. Lee, W.L. Yang, A. Li, A. Mukherjee, M. Basan, C.Z. Ran, W. Yin, C.J. Tabin, D. Fu, X.S. Xie, and M.W. Kirschner. 2022. Protein and lipid mass concentration measurement in tissues by stimulated Raman scattering microscopy. *P Natl Acad Sci USA*. 119.

Okabe, K., N. Inada, C. Gota, Y. Harada, T. Funatsu, and S. Uchiyama. 2012. Intracellular temperature mapping with a fluorescent polymeric thermometer and fluorescence lifetime imaging microscopy. *Nat Commun*. 3:705.

Olzscha, H., S.M. Schermann, A.C. Woerner, S. Pinkert, M.H. Hecht, G.G. Tartaglia, M. Vendruscolo, M. Hayer-Hartl, F.U. Hartl, and R.M. Vabulas. 2011. Amyloid-like Aggregates Sequester Numerous Metastable Proteins with Essential Cellular Functions. *Cell*. 144:67-78.

Ong, D.S.T., T.W. Mu, A.E. Palmer, and J.W. Kelly. 2010. Endoplasmic reticulum Ca2+ increases enhance mutant glucocerebrosidase proteostasis. *Nat Chem Biol*. 6:424–432.

Ong, J.Y., and J.Z. Torres. 2020. Phase Separation in Cell Division. *Mol Cell*. 80:9-20.

Ostermann, J., A.L. Horwich, W. Neupert, and F.U. Hartl. 1989. Protein Folding in Mitochondria Requires Complex-Formation with Hsp60 and Atp Hydrolysis. *Nature*. 341:125-130.

Owyong, T.C., and Y.N. Hong. 2022. Emerging fluorescence tools for the study of proteostasis in cells. *Curr Opin Chem Biol*. 67.

Palade, G.E. 1955. A Small Particulate Component of the Cytoplasm. *J Biophys Biochem Cy*. 1:59-68.

Palade, G.E., and K.R. Porter. 1954. Studies on the Endoplasmic Reticulum .1. Its Identification in Cells Insitu. *J Exp Med*. 100:641-+.

Palozola, K.C., G. Donahue, H. Liu, G.R. Grant, J.S. Becker, A. Cote, H.T. Yu, A. Raj, and K.S. Zaret. 2017. Mitotic transcription and waves of gene reactivation during mitotic exit. *Science*. 358:119-122.

Parashar, S., R. Chidambaram, S.L. Chen, C.R. Liem, E. Griffis, G.G. Lambert, N.C. Shaner, M. Wortham, J.C. Hay, and S. Ferro-Novick. 2021. Endoplasmic reticulum tubules limit the size of misfolded protein condensates. *Elife*. 10:e71642.

Patterson, C. 1956. Age of Meteorites and the Earth. *Geochim Cosmochim Ac*. 10:230-237.

Paweletz, N. 2001. Walther Flemming: pioneer of mitosis research. *Nat Rev Mol Cell Bio*. 2:72-75.

Pelham, H.R.B. 1984. Hsp70 Accelerates the Recovery of Nucleolar Morphology after Heat-Shock. *Embo J*. 3:3095-3100.

Pelham, H.R.B. 1986. Speculations on the Functions of the Major Heat-Shock and Glucose-Regulated Proteins. *Cell*. 46:959-961.

Peng, J., G. Liang, S. Inan, Z. Wu, D.J. Joseph, Q.C. Meng, Y. Peng, M.F. Eckenhoff, and H.F. Wei. 2012. Dantrolene ameliorates cognitive decline and neuropathology in Alzheimer triple transgenic mice. *Neurosci Lett*. 516:274-279.

Pérez, J.M.H. 2024. Alpha 1-Antitrypsin Deficiency. *New Engl J Med*. 391:336-342.

Perutz, M.F., M.G. Rossmann, A.F. Cullis, H. Muirhead, G. Will, and A.C.T. North. 1960. Structure of Haemoglobin: A Three-Dimensional Fourier Synthesis at 5.5-A. Resolution, Obtained by X-Ray Analysis. *Nature*. 185:416-422.

Pessa, J.C., J. Joutsen, and L. Sistonen. 2024. Transcriptional reprogramming at the intersection of the heat shock response and proteostasis. *Mol Cell*. 84:80-93.

Pfeifer, C.R., M.P. Tobin, S. Cho, M. Vashisth, L.J. Dooling, L.L. Vazquez, E.G. Ricci-De Lucca, K.T. Simon, and D.E. Discher. 2022. Gaussian curvature dilutes the nuclear lamina, favoring nuclear rupture, especially at high strain rate. *Nucleus-Phila*. 13:129-143.

Piña, F., F. Yagisawa, K. Obara, J.D. Gregerson, A. Kihara, and M. Niwa. 2018. Sphingolipids activate the endoplasmic reticulum stress surveillance pathway. *J Cell Biol*. 217:495-505.

Pina, F., B. Yan, J.J. Hu, and M. Niwa. 2023. Reticulons bind sphingolipids to activate the endoplasmic reticulum cell cycle checkpoint, the ER surveillance pathway. *Cell Rep*. 42:113403.

Piña, F.J., and M. Niwa. 2015. The ER Stress Surveillance (ERSU) pathway regulates daughter cell ER protein aggregate inheritance. *Elife*. 4:e06970.

Pobre, K.F.R., G.J. Poet, and L.M. Hendershot. 2019. The endoplasmic reticulum (ER) chaperone BiP is a master regulator of ER functions: Getting by with a little help from ERdj friends. *J Biol Chem*. 294:2098-2108.

Pohl, C., and S. Jentsch. 2009. Midbody ring disposal by autophagy is a post-abscission event of cytokinesis. *Nat Cell Biol*. 11:65-70.

Porter, K.R. 1953. Observations on a Submicroscopic Basophilic Component of Cytoplasm. *J Exp Med*. 97:727-750.

Porter, K.R., A. Claude, and E.F. Fullam. 1945. A Study of Tissue Culture Cells by Electron Microscopy - Methods and Preliminary Observations. *J Exp Med*. 81:233-246.

Powers, E.T., and W.E. Balch. 2013. Diversity in the origins of proteostasis networks - a driver for protein function in evolution. *Nat Rev Mol Cell Bio*. 14:237-248.

Preissler, S., J.E. Chambers, A. Crespillo-Casado, E. Avezov, E. Miranda, J. Perez, L.M. Hendershot, H.P. Harding, and D. Ron. 2015. Physiological modulation of BiP activity by trans-protomer engagement of the interdomain linker. *Elife*. 4:e08961.

Preissler, S., C. Rato, L.A. Perera, V. Saudek, and D. Ron. 2017. FICD acts bifunctionally to AMPylate and de-AMPylate the endoplasmic reticulum chaperone BiP. *Nat Struct Mol Biol*. 24:23-29.

Preissler, S., C. Rato, Y.H. Yan, L.A. Perera, A. Czako, and D. Ron. 2020. Calcium depletion challenges endoplasmic reticulum proteostasis by destabilising BiP-substrate complexes. *Elife*. 9:e62601.

Preissler, S., and D. Ron. 2019. Early Events in the Endoplasmic Reticulum Unfolded Protein Response. *Csh Perspect Biol*. 11:a033894.

Prieto-Garcia, C., V. Matkovic, T. Mosler, C.X. Li, J. Liang, J.A. Oo, F. Haidle, I. Macinkovic, A. Cabrera-Orefice, R. Berkane, G. Giuliani, F.F. Xu, A.C. Jacomin, I. Tomaskovic, M. Basoglu, M.E. Hoffmann, R. Rathore, R. Cetin, D. Boutguetait, S. Bozkurt, M.C.H. Cañás, M. Keller, J. Busam, V.J. Shah, I. Wittig, M. Kaulich, P. Beli, W.P. Galej, I. Ebersberger, L.K. Wang, C. Münch, A. Stolz, R.P. Brandes, W.K.F. Tse, S. Eimer, D.Y.R. Stainier, S. Legewie, K. Zarnack, M. Müller-McNicoll, and I. Dikic. 2024. Pathogenic proteotoxicity of cryptic splicing is alleviated by ubiquitination and ER-phagy. *Science*. 386:768-776.

Prostko, C.R., M.A. Brostrom, and C.O. Brostrom. 1993. Reversible Phosphorylation

of Eukaryotic Initiation-Factor 2-Alpha in Response to Endoplasmic Reticular Signaling. *Mol Cell Biochem*. 128:255-265.

Prouty, W.F., M.J. Karnovsky, and A.L. Goldberg. 1975. Degradation of Abnormal Proteins in Escherichia-Coli Formation of Protein Inclusions in Cells Exposed to Amino-Acid Analogs. *J Biol Chem*. 250:1112-1122.

Pyronnet, S., J. Dostie, and N. Sonenberg. 2001. Suppression of cap-dependent translation in mitosis. *Gene Dev*. 15:2083-2093.

Radons, J. 2016. The human HSP70 family of chaperones: where do we stand? *Cell Stress Chaperon*. 21:379-404.

Rai, A.K., J.X. Chen, M. Selbach, and L. Pelkmans. 2018. Kinase-controlled phase transition of membraneless organelles in mitosis. *Nature*. 559:211-216.

Ratner, S. 1979. The dynamic state of body proteins. *Ann N Y Acad Sci*. 325:188-209.

Ratner, S., D. Rittenberg, A.S. Keston, and R. Schoenheimer. 1940. Studies in protein metabolism XIV. The chemical interaction of dietary glycine and body proteins in rats. *J Biol Chem*. 134:665-676.

Reggio, A., V. Buonomo, R. Berkane, R.M. Bhaskara, M. Tellechea, I. Peluso, E. Polishchuk, G. Di Lorenzo, C. Cirillo, M. Esposito, A. Hussain, A.K. Huebner, C.A. Hübner, C. Settembre, G. Hummer, P. Grumati, and A. Stolz. 2021. Role of FAM134 paralogues in endoplasmic reticulum remodeling, ER-phagy, and Collagen quality control. *Embo Rep*. 22:e52289.

Reinle, K., A. Mogk, and B. Bukau. 2022. The Diverse Functions of Small Heat Shock Proteins in the Proteostasis Network. *J Mol Biol*. 434:167157.

Resende, R., E. Ferreiro, C. Pereira, and C.R. De Oliveira. 2008. Neurotoxic effect of oligomeric and fibrillar species of amyloid-beta peptide 1-42: Involvement of endoplasmic reticulum calcium release in oligomer-induced cell death. *Neuroscience*. 155:725-737.

Richter, K., M. Haslbeck, and J. Buchner. 2010. The Heat Shock Response: Life on the Verge of Death. *Mol Cell*. 40:253-266.

Ritossa, F. 1962. A New Puffing Pattern Induced by Temperature Shock and Dnp in Drosophila. *Experientia*. 18:571-573.

Rossi, A.M., and C.W. Taylor. 2020. Reliable measurement of free Ca2+ concentrations in the ER lumen using Mag-Fluo-4. *Cell Calcium*. 87:102188.

Rousseau, E., B. Dehay, A. Ben-Haïem, Y. Trottier, M. Morange, and A. Bertolotti. 2004. Targeting expression of expanded polyglutamine proteins to the endoplasmic reticulum or mitochondria prevents their aggregation. *P Natl Acad Sci USA*. 101:9648-9653.

Ruan, L.H., C.K. Zhou, E.L. Jin, A. Kucharavy, Y. Zhang, Z.H. Wen, L. Florens, and R. Li. 2017. Cytosolic proteostasis through importing of misfolded proteins into mitochondria. *Nature*. 543:443-446.

Ruddock, L.W. 2012. Low-Molecular-Weight Oxidants Involved in Disulfide Bond Formation. *Antioxid Redox Sign*. 16:1129-1138.

Rujano, M.A., F. Bosveld, F.A. Salomons, F. Dijk, M.A.W.H. van Waarde, J.J.L. van der Want, R.A.I. de Vos, E.R. Brunt, O.C.M. Sibon, and H.H. Kampinga. 2006. Polarised asymmetric inheritance of accumulated protein damage in higher eukaryotes. *Plos Biol*. 4:2325-2335.

Rutkevich, L.A., and D.B. Williams. 2011. Participation of lectin chaperones and thiol oxidoreductases in protein folding within the endoplasmic reticulum. *Curr Opin*

Cell Biol. 23:157-166.

Sabatini, D.D., and M. Adesnik. 2013. Christian de Duve: Explorer of the cell who discovered new organelles by using a centrifuge. *P Natl Acad Sci USA*. 110:13234-13235.

Sackton, K.L., N. Dimova, X. Zeng, W. Tian, M.M. Zhang, T.B. Sackton, J. Meaders, K.L. Pfaff, F. Sigoillot, H.T. Yu, X.L. Luo, and R.W. King. 2014. Synergistic blockade of mitotic exit by two chemical inhibitors of the APC/C. *Nature*. 514:646-649.

Sadovsky, R.G., S. Brielle, D. Kaganovich, and J.L. England. 2017. Measurement of Rapid Protein Diffusion in the Cytoplasm by Photo-Converted Intensity Profile Expansion. *Cell Rep*. 18:2795-2806.

Sakagami, Y., T. Kudo, H. Tanimukai, D. Kanayama, T. Omi, K. Horiguchi, M. Okochi, K. Imaizumi, and M. Takeda. 2013. Involvement of endoplasmic reticulum stress in tauopathy. *Biochem Bioph Res Co*. 430:500-504.

Samanta, S., S.H. Yang, B. Debnath, D. Xue, Y.T. Kuang, K. Ramkumar, A.S. Lee, M. Ljungman, and N. Neamati. 2021. The Hydroxyquinoline Analogue YUM70 Inhibits GRP78 to Induce ER Stress-Mediated Apoptosis in Pancreatic Cancer. *Cancer Res*. 81:1883-1895.

Sanchón, A.C., H.S. Kumar, M. Mantovani, I. Osinnii, J.M. Mateos, A. Kaech, D. Shcherbakov, R. Akbergenov, and E.C. Böttger. 2021. ER-misfolded proteins become sequestered with mitochondria and impair mitochondrial function. *Commun Biol*. 4:1350.

Sanger, F., and H. Tuppy. 1951. The Amino-Acid Sequence in the Phenylalanyl Chain of Insulin .1. The Identification of Lower Peptides from Partial Hydrolysates. *Biochem J*. 49:463-481.

Sawyer, E.M., L.E. Jensen, J.B. Meehl, K.P. Larsen, D.A. Petito, J.H. Hurley, and G.K. Voeltz. 2024. SigmaR1 shapes rough endoplasmic reticulum membrane sheets. *Dev Cell*. 59:2566-2577.

Schachtele, C.F., D.L. Anderson, and P. Rogers. 1968. Mechanism of Canavanine Death in Escherichia Coli .2. Membrane-Bound Canavanyl-Protein and Nuclear Disruption. *J Mol Biol*. 33:861-868.

Schlaitz, A.L. 2014. Microtubules as key coordinators of nuclear envelope and endoplasmic reticulum dynamics during mitosis. *Bioessays*. 36:665-671.

Schlaitz, A.L., J. Thompson, C.C.L. Wong, J.R. Yates, and R. Heald. 2013. REEP3/4 Ensure Endoplasmic Reticulum Clearance from Metaphase Chromatin and Proper Nuclear Envelope Architecture. *Dev Cell*. 26:315-323.

Schleyer, M., and W. Neupert. 1985. Transport of Proteins into Mitochondria: Translocational Intermediates Spanning Contact Sites between Outer and Inner Membranes. *Cell*. 43:339-350.

Schmidt, M., A. Rohe, C. Platzer, A. Najjar, F. Erdmann, and W. Sippl. 2017. Regulation of G2/M Transition by Inhibition of WEE1 and PKMYT1 Kinases. *Molecules*. 22.

Schopf, F.H., M.M. Biebl, and J. Buchner. 2017. The HSP90 chaperone machinery. *Nat Rev Mol Cell Bio*. 18:345-360.

Schröder, M., and R.J. Kaufman. 2005. ER stress and the unfolded protein response. *Mutat Res-Fund Mol M*. 569:29-63.

Schuldiner, M., and B. Schwappach. 2013. From rags to riches - The history of the

endoplasmic reticulum Preface. *Bba-Mol Cell Res*. 1833:2389-2391.

Seibel, N.M., J. Eljouni, M.M. Nalaskowski, and W. Hampe. 2007. Nuclear localization of enhanced green fluorescent protein homomultimers. *Anal Biochem*. 368:95-99.

Sengupta, P., P. Satpute-Krishnan, A.Y. Seo, D.T. Burnette, G.H. Patterson, and J. Lippincott-Schwartz. 2015. ER trapping reveals Golgi enzymes continually revisit the ER through a recycling pathway that controls Golgi organization. *P Natl Acad Sci USA*. 112:E6752-E6761.

Sengupta, S., A.B. Sami, J.C. Gatlin, and D.L. Levy. 2025. Proteasome inhibition induces microtubule-dependent changes in nuclear morphology. *iScience*. 28:111550.

Senovilla, L., I. Vitale, I. Martins, M. Tailler, C. Pailleret, M. Michaud, L. Galluzzi, S. Adjemian, O. Kepp, M. Niso-Santano, S.S. Shen, G. Mariño, A. Criollo, A. Boilève, B. Job, S. Ladoire, F. Ghiringhelli, A. Sistigu, T. Yamazaki, S. Rello-Varona, C. Locher, V. Poirier-Colame, M. Talbot, A. Valent, F. Berardinelli, A. Antoccia, F. Ciccosanti, G.M. Fimia, M. Piacentini, A. Fueyo, N.L. Messina, M. Li, C.J. Chan, V. Sigl, G. Pourcher, C. Ruckenstuhl, D. Carmona-Gutierrez, V. Lazar, J.M. Penninger, F. Madeo, C. López-Otín, M.J. Smyth, L. Zitvogel, M. Castedo, and G. Kroemer. 2012. An Immunosurveillance Mechanism Controls Cancer Cell Ploidy. *Science*. 337:1678-1684.

Serpico, A.F., F. Febbraro, C. Pisauro, and D. Grieco. 2022. Compartmentalized control of Cdk1 drives mitotic spindle assembly. *Cell Rep*. 38:110305.

Sharma, R., M.M.D. Pramanik, B. Chandramouli, N. Rastogi, and N. Kumar. 2018. Understanding organellar protein folding capacities and assessing their pharmacological modulation by small molecules. *Eur J Cell Biol*. 97:114-125.

Shen, B.R., P.L. Zheng, N.N. Qian, Q.Z. Chen, X. Zhou, J.J. Hu, J.G. Chen, and J.L. Teng. 2019. Calumenin-1 Interacts with Climp63 to Cooperatively Determine the Luminal Width and Distribution of Endoplasmic Reticulum Sheets. *iScience*. 22:70-80.

Shi, L.J., C.G. Yang, M.Y. Zhang, K.N. Li, K.Y. Wang, L. Jiao, R.M. Liu, Y.Y. Wang, M. Li, Y. Wang, L. Ma, S.X. Hu, and X. Bian. 2024. Dissecting the mechanism of atlastin-mediated homotypic membrane fusion at the single-molecule level. *Nat Commun*. 15:2488.

Shibata, N., A. Hirano, M. Kobayashi, T. Siddique, H.X. Deng, W.Y. Hung, T. Kato, and K. Asayama. 1996. Intense superoxide dismutase-1 immunoreactivity in intracytoplasmic hyaline inclusions of familial amyotrophic lateral sclerosis with posterior column involvement. *J Neuropath Exp Neur*. 55:481-490.

Shibata, Y., T. Shemesh, W.A. Prinz, A.F. Palazzo, M.M. Kozlov, and T.A. Rapoport. 2010. Mechanisms Determining the Morphology of the Peripheral ER. *Cell*. 143:774-788.

Shively, J.M. 1974. Inclusion-Bodies of Prokaryotes. *Annu Rev Microbiol*. 28:167-187.

Shuda, M., C. Velásquez, E.D. Cheng, D.G. Cordek, H.J. Kwun, Y. Chang, and P.S. Moore. 2015. CDK1 substitutes for mTOR kinase to activate mitotic cap-dependent protein translation. *P Natl Acad Sci USA*. 112:5875-5882.

Sivan, G., R. Aviner, and O. Elroy-Stein. 2011. Mitotic Modulation of Translation Elongation Factor 1 Leads to Hindered tRNA Delivery to Ribosomes. *J Biol Chem*. 286:27927-27935.

Sivan, G., and O.E. Stein. 2008. Regulation of mRNA translation during cellular division. *Cell Cycle*. 7:741-744.

Smith, E.M., and C.G. Proud. 2008. cdc2-cyclin B regulates eEF2 kinase activity in a cell cycle- and amino acid-dependent manner. *Embo J*. 27:1005-1016.

Soltysik, K., Y. Ohsaki, T. Tatematsu, J.L. Cheng, and T. Fujimoto. 2019. Nuclear lipid droplets derive from a lipoprotein precursor and regulate phosphatidylcholine synthesis. *Nat Commun*. 10:473.

Son, S., J.H. Kang, S. Oh, M.W. Kirschner, T.J. Mitchison, and S. Manalis. 2015. Resonant microchannel volume and mass measurements show that suspended cells swell during mitosis. *J Cell Biol*. 211:757-763.

Sontag, E.M., F. Morales-Polanco, J.H. Chen, G. McDermott, P.T. Dolan, D. Gestaut, M.A. Le Gros, C. Larabell, and J. Frydman. 2023. Nuclear and cytoplasmic spatial protein quality control is coordinated by nuclear-vacuolar junctions and perinuclear ESCRT. *Nat Cell Biol*. 25:699-713.

Spear, J.S., and K.A. White. 2023. Single-cell intracellular pH dynamics regulate the cell cycle by timing the G1 exit and G2 transition. *J Cell Sci*. 136:jcs260458.

Spokoini, R., O. Moldavski, Y. Nahmias, J.L. England, M. Schuldiner, and D. Kaganovich. 2012. Confinement to Organelle-Associated Inclusion Structures Mediates Asymmetric Inheritance of Aggregated Protein in Budding Yeast. *Cell Rep*. 2:738-747.

Spriggs, K.A., M. Bushell, and A.E. Willis. 2010. Translational Regulation of Gene Expression during Conditions of Cell Stress. *Mol Cell*. 40:228-237.

Srivastava, S.P., M.V. Davies, and R.J. Kaufman. 1995. Calcium Depletion from the Endoplasmic-Reticulum Activates the Double-Stranded Rna-Dependent Protein-Kinase (Pkr) to Inhibit Protein-Synthesis. *J Biol Chem*. 270:16619-16624.

Stevens, F.J., and Y. Argon. 1999. Protein folding in the ER. *Semin Cell Dev Biol*. 10:443-454.

Stewart, M.P., J. Helenius, Y. Toyoda, S.P. Ramanathan, D.J. Muller, and A.A. Hyman. 2011. Hydrostatic pressure and the actomyosin cortex drive mitotic cell rounding. *Nature*. 469:226-230.

Stojkovska, I., W.Y. Wani, F. Zunke, N.R. Belur, E.A. Pavlenko, N. Mwenda, K. Sharma, L. Francelle, and J.R. Mazzulli. 2022. Rescue of α-synuclein aggregation in Parkinson's patient neurons by synergistic enhancement of ER proteostasis and protein trafficking. *Neuron*. 110:436-451.

Stonyte, V., E. Boye, and B. Grallert. 2018. Regulation of global translation during the cell cycle. *J Cell Sci*. 131:jcs220327.

Straus, W. 1958. Colorimetric Analysis with N, N-Dimethyl-Para-Phenylenediamine of the Uptake of Intravenously Injected Horseradish Peroxidase by Various Tissues of the Rat. *J Biophys Biochem Cy*. 4:541-550.

Straus, W. 1964. Cytochemical Observations on Relationship between Lysosomes and Phagosomes in Kidney and Liver by Combined Staining for Acid Phosphatase and Intravenously Injected Horseradish Peroxidase. *J Cell Biol*. 20:497-507.

Strnad, P., N.G. McElvaney, and D.A. Lomas. 2020. Alpha1-Antitrypsin Deficiency. *New Engl J Med*. 382:1443-1455.

Taguchi, N., N. Ishihara, A. Jofuku, T. Oka, and K. Mihara. 2007. Mitotic phosphorylation of dynamin-related GTPase Drp1 participates in mitochondrial

fission. *J Biol Chem*. 282:11521-11529.
Tahmasebi, S., N. Sonenberg, J.W.B. Hershey, and M.B. Mathews. 2019. Protein Synthesis and Translational Control: A Historical Perspective. *Csh Perspect Biol*. 11:a035584.
Tanenbaum, M.E., N. Stern-Ginossar, J.S. Weissman, and R.D. Vale. 2015. Regulation of mRNA translation during mitosis. *Elife*. 4:e07957.
Tang, D.M., H.B. Yuan, O. Vielemeyer, F. Perez, and Y.Z. Wang. 2012. Sequential phosphorylation of GRASP65 during mitotic Golgi disassembly. *Biol Open*. 1:1204-1214.
Tao, T.Q., J.L. Wang, X.R. Wang, Y. Wang, H.M. Mao, and X.H. Liu. 2019. The PERK/Nrf2 pathway mediates endoplasmic reticulum stress-induced injury by upregulating endoplasmic reticulophagy in H9c2 cardiomyoblasts. *Life Sci*. 237:116944.
Tavender, T.J., J.J. Springate, and N.J. Bulleid. 2010. Recycling of peroxiredoxin IV provides a novel pathway for disulphide formation in the endoplasmic reticulum. *Embo J*. 29:4185-4197.
Tedesco, B., L. Vendredy, V. Timmerman, and A. Poletti. 2023. The chaperone-assisted selective autophagy complex dynamics and dysfunctions. *Autophagy*. 19:1619-1641.
Tessarz, P., M. Schwarz, A. Mogk, and B. Bukau. 2009. The Yeast AAA Chaperone Hsp104 Is Part of a Network That Links the Actin Cytoskeleton with the Inheritance of Damaged Proteins. *Mol Cell Biol*. 29:3738-3745.
Thomas, J.M. 2012. The birth of X-ray crystallography. *Nature*. 491:186-187.
Thornton, B.R., and D.P. Toczyski. 2003. Securin and B-cyclin/CDK are the only essential targets of the APC. *Nat Cell Biol*. 5:1090-1094.
Tipton, A.R., and G.J. Gorbsky. 2022. More than two populations of microtubules comprise the dynamic mitotic spindle. *J Cell Sci*. 135:jcs258745.
Tissieres, A., H.K. Mitchell, and U.M. Tracy. 1974. Protein Synthesis in Salivary Glands of Drosophila Melanogaster: Relation to Chromosome Puffs. *J Mol Biol*. 84:389-398.
Tomasetti, C., J. Poling, N.J. Roberts, N.R. London, M.E. Pittman, M.C. Haffner, A. Rizzo, A. Baras, B. Karim, A. Kim, C.M. Heaphy, A.K. Meeker, R.H. Hruban, C.A. Iacobuzio-Donahue, and B. Vogelstein. 2019. Cell division rates decrease with age, providing a potential explanation for the age-dependent deceleration in cancer incidence. *P Natl Acad Sci USA*. 116:20482-20488.
Torres, A.K., V. Fleischhart, and N.C. Inestrosa. 2024. Mitochondrial unfolded protein response (UPR): what we know thus far. *Front Cell Dev Biol*. 12:1405393.
Torres, M., K. Castillo, R. Armisén, A. Stutzin, C. Soto, and C. Hetz. 2010. Prion Protein Misfolding Affects Calcium Homeostasis and Sensitizes Cells to Endoplasmic Reticulum Stress. *Plos One*. 5:e15658.
Tyedmers, J., A. Mogk, and B. Bukau. 2010. Cellular strategies for controlling protein aggregation. *Nat Rev Mol Cell Bio*. 11:777-788.
Vallin, J., and J. Grantham. 2019. The role of the molecular chaperone CCT in protein folding and mediation of cytoskeleton-associated processes: implications for cancer cell biology. *Cell Stress Chaperon*. 24:17-27.
Vedrenne, C., D.R. Klopfenstein, and H.P. Hauri. 2005. Phosphorylation controls CLIMP-63-mediated anchoring of the endoplasmic reticulum to microtubules.

Mol Biol Cell. 16:1928-1937.

Veratti, E. 1961. Investigations on Fine Structure of Striated Muscle Fiber. *J Biophys Biochem Cy*. 10:1-59.

Verwilst, P., K. Kim, K. Sunwoo, H.R. Kim, C. Kang, and J.S. Kim. 2019. Revealing Protein Aggregates under Thapsigargin-Induced ER Stress Using an ER-Targeted Thioflavin. *Acs Sensors*. 4:2858-2863.

Veyron, S., G. Oliva, M. Rolando, C. Buchrieser, G. Peyroche, and J. Cherfils. 2019. A Ca2+-regulated deAMPylation switch in human and bacterial FIC proteins. *Nat Commun*. 10:1142.

Vidal, R., B. Caballero, A. Couve, and C. Hetz. 2011. Converging Pathways in the Occurrence of Endoplasmic Reticulum (ER) Stress in Huntington's Disease. *Curr Mol Med*. 11:1-12.

Vincenz-Donnelly, L., and M.S. Hipp. 2017. The endoplasmic reticulum: A hub of protein quality control in health and disease. *Free Radical Bio Med*. 108:383-393.

Vincenz-Donnelly, L., H. Holthusen, R. Körner, E.C. Hansen, J. Presto, J. Johansson, R. Sawarkar, F.U. Hartl, and M.S. Hipp. 2018. High capacity of the endoplasmic reticulum to prevent secretion and aggregation of amyloidogenic proteins. *Embo J*. 37:337-350.

Walter, P., and G. Blobel. 1981. Translocation of Proteins across the Endoplasmic-Reticulum .3. Signal Recognition Protein (Srp) Causes Signal Sequence-Dependent and Site-Specific Arrest of Chain Elongation That Is Released by Microsomal-Membranes. *J Cell Biol*. 91:557-561.

Walther, D.M., P. Kasturi, M. Zheng, S. Pinkert, G. Vecchi, P. Ciryam, R.I. Morimoto, C.M. Dobson, M. Vendruscolo, M. Mann, and F.U. Hartl. 2015. Widespread Proteome Remodeling and Aggregation in Aging. *Cell*. 161:919-932.

Wang, B.W., Z.H. Zhao, M.C. Xiong, R. Yan, and K. Xu. 2022. The endoplasmic reticulum adopts two distinct tubule forms. *P Natl Acad Sci USA*. 119:e2117559119.

Wang, J., J. Lee, D. Liem, and P. Ping. 2017. Gene encoding Hsp70 chaperone BiP in the endoplasmic reticulum. *Gene*. 618:14-23.

Wang, L., and C.C. Wang. 2023. Oxidative protein folding fidelity and redoxtasis in the endoplasmic reticulum. *Trends Biochem Sci*. 48:40-52.

Wang, L., X. Wang, and C.C. Wang. 2015. Protein disulfide-isomerase, a folding catalyst and a redox-regulated chaperone. *Free Radical Bio Med*. 83:305-313.

Wang, L., L.H. Zhang, Y.B. Niu, R. Sitia, and C.C. Wang. 2014. Glutathione Peroxidase 7 Utilizes Hydrogen Peroxide Generated by Ero1α to Promote Oxidative Protein Folding. *Antioxid Redox Sign*. 20:545-556.

Wang, S.Y., H. Tukachinsky, F.B. Romano, and T.A. Rapoport. 2016. Cooperation of the ER-shaping proteins atlastin, lunapark, and reticulons to generate a tubular membrane network. *Elife*. 5:e18605.

Wang, Y.N., S.L. Li, M. Mokbel, A.I. May, Z.Z. Liang, Y.L. Zeng, W.Q. Wang, H.H. Zhang, F.F. Yu, K. Sporbeck, L.W. Jiang, S. Aland, J. Agudo-Canalejo, R.L. Knorr, and X.F. Fang. 2024. Biomolecular condensates mediate bending and scission of endosome membranes. *Nature*. 635:1204-1210.

Ward, C.L., S. Omura, and R.R. Kopito. 1995. Degradation of CFTR by the Ubiquitin-Proteasome Pathway. *Cell*. 83:121-127.

Watson, J.D., and F.H.C. Crick. 1953a. Genetical Implications of the Structure of Deoxyribonucleic Acid. *Nature*. 171:964-967.

Watson, J.D., and F.H.C. Crick. 1953b. Molecular Structure of Nucleic Acids - a Structure for Deoxyribose Nucleic Acid. *Nature*. 171:737-738.

Welch, W.J., and J.P. Suhan. 1985. Morphological-Study of the Mammalian Stress Response - Characterization of Changes in Cytoplasmic Organelles, Cytoskeleton, and Nucleoli, and Appearance of Intranuclear Actin-Filaments in Rat Fibroblasts after Heat-Shock Treatment. *J Cell Biol*. 101:1198-1211.

Wheeler, J.R., T. Matheny, S. Jain, R. Abrisch, and R. Parker. 2016. Distinct stages in stress granule assembly and disassembly. *Elife*. 5:e18413.

Wilker, E.W., M.A.T.M. van Vugt, S.A. Artim, P.H. Huang, C.P. Petersen, H.C. Reinhardt, Y. Feng, P.A. Sharp, N. Sonenberg, F.M. White, and M.B. Yaffe. 2007. 14-3-3σ controls mitotic translation to facilitate cytokinesis. *Nature*. 446:329-332.

Williams, D.C., R.M. Vanfrank, W.L. Muth, and J.P. Burnett. 1982. Cytoplasmic Inclusion-Bodies in Escherichia-Coli Producing Biosynthetic Human Insulin Proteins. *Science*. 215:687-689.

Wilson, D.I.I.I., M.R. Cookson, L. van den Bosch, H. Zetterberg, D.M. Holtzman, and I. Dewachter. 2023. Hallmarks of neurodegenerative diseases. *Cell*. 186:693-714.

Wirth, A.J., M. Platkov, and M. Gruebele. 2013. Temporal Variation of a Protein Folding Energy Landscape in the Cell. *J Am Chem Soc*. 135:19215-19221.

Wiseman, R.L., J.S. Mesgarzadeh, and L.M. Hendershot. 2022. Reshaping endoplasmic reticulum quality control through the unfolded protein response. *Mol Cell*. 82:1477-1491.

Woerner, A.C., F. Frottin, D. Hornburg, L.R. Feng, F. Meissner, M. Patra, J. Tatzelt, M. Mann, K.F. Winklhofer, F.U. Hartl, and M.S. Hipp. 2016. Cytoplasmic protein aggregates interfere with nucleocytoplasmic transport of protein and RNA. *Science*. 351:173-176.

Wright, M.T., and L. Plate. 2021. Revealing functional insights into ER proteostasis through proteomics and interactomics. *Exp Cell Res*. 399:112417.

Wu, H. 1995. Studies on Denaturation of Proteins XIII. A Theory of Denaturation. *Advances in Protein Chemistry*. 46:6-26.

Wu, H.Y., L.C. Wang, B.M. Sow, D. Leow, J. Zhu, K.M. Gallo, K. Wilsbach, R. Gupta, L.W. Ostrow, C.J.J. Yeo, R.M. Sobota, and R. Li. 2024. TDP43 aggregation at ER-exit sites impairs ER-to-Golgi transport. *Nat Commun*. 15:9026.

Wu, X.D., and T.A. Rapoport. 2018. Mechanistic insights into ER-associated protein degradation. *Curr Opin Cell Biol*. 53:22-28.

Xu, F., W.Q. Du, Q. Zou, Y.T. Wang, X. Zhang, X.D. Xing, Y. Li, D.C. Zhang, H.M. Wang, W.H. Zhang, X.Y. Hu, X. Liu, X.L. Liu, S.J. Zhang, J.Q. Yu, J.H. Fang, F.J. Li, Y. Zhou, T.Q. Yue, N. Mi, H.T. Deng, P. Zou, X.W. Chen, X.R. Yang, and L. Yu. 2021. COPII mitigates ER stress by promoting formation of ER whorls. *Cell Res*. 31:141-156.

Xu, F.F., and L.K. Wang. 2024. Deciphering ER stress-unfolded protein response relationship by visualizing unfolded proteins in the ER. *Cell Rep*. 43:114358.

Xu, L., Y. Xiang, and J.J. Hu. 2023. Molecular basis of Climp63-mediated ER lumen spacing. *J Cell Sci*. 136:jcs260976.

Yan, Y.H., C. Rato, L. Rohland, S. Preissler, and D. Ron. 2019. MANF antagonizes nucleotide exchange by the endoplasmic reticulum chaperone BiP. *Nat Commun*. 10:541.

Yu, Q.N., X. Liu, J.W. Fang, H.H. Wu, C. Guo, W. Zhang, N.P. Liu, C. Jiang, Q. Sha, X. Yuan, Z.K. Wang, and K. Qu. 2023. Dynamics and regulation of mitotic chromatin accessibility bookmarking at single-cell resolution. *Sci Adv*. 9:eadd2175.

Zaal, K.J.M., C.L. Smith, R.S. Polishchuk, N. Altan, N.B. Cole, J. Ellenberg, K. Hirschberg, J.F. Presley, T.H. Roberts, E. Siggia, R.D. Phair, and J. Lippincott-Schwartz. 1999. Golgi membranes are absorbed into and reemerge from the ER during mitosis. *Cell*. 99:589-601.

Zaher, H.S., and R. Green. 2009. Fidelity at the Molecular Level: Lessons from Protein Synthesis. *Cell*. 136:746-762.

Zamecnik, P.C. 1969. An Historical Account of Protein Synthesis, with Current Overtones - a Personalized View. *Cold Spring Harb Sym*. 34:1-16.

Zamecnik, P.C., M.L. Stephenson, J.F. Scott, and M.B. Hoagland. 1957. Incorporation of C-14-Atp into Soluble Rna Isolated from 105,000 X G Supernatant of Rat Liver. *Fed Proc*. 16:275-275.

Zhang, I.R.X., J.H. Ren, S. Vadrevu, M. Raghavan, and L.S. Satin. 2020. ER stress increases store-operated Ca2+ entry (SOCE) and augments basal insulin secretion in pancreatic beta cells. *J Biol Chem*. 295:5685-5700.

Zhang, W., Z.J. Zhang, Y. Xiang, D.D. Gu, J.N. Chen, Y.F. Chen, S.X. Zhai, Y. Liu, T. Jiang, C. Liu, B. He, M. Yan, Z.F. Wang, J. Xu, Y.L. Cao, B. Deng, D.S. Zeng, J. Lei, J.X. Zhuo, X.X. Lei, Z.J. Long, B.L. Jin, T.S. Chen, D. Li, Y.D. Shen, J.J. Hu, S. Gao, and Q.T. Liu. 2024. Aurora kinase A-mediated phosphorylation triggers structural alteration of Rab1A to enhance ER complexity during mitosis. *Nat Struct Mol Biol*. 31:219-231.

Zhang, Y., I. Sinning, and S. Rospert. 2017. Two chaperones locked in an embrace: structure and function of the ribosome-associated complex RAC. *Nat Struct Mol Biol*. 24:611-619.

Zhao, G., M.K. Jia, S.C. Zhu, H. Ren, G.P. Wang, G.W. Xin, M.J. Sun, X.Y. Wang, Q.Y. Lin, Q. Jiang, and C.M. Zhang. 2024. Mitotic ER-mitochondria contact enhances mitochondrial Ca influx to promote cell division. *Cell Rep*. 43:114794.

Zhou, C.K., B.D. Slaughter, J.R. Unruh, A. Eldakak, B. Rubinstein, and R. Li. 2011. Motility and Segregation of Hsp104-Associated Protein Aggregates in Budding Yeast. *Cell*. 147:1186-1196.

Zhou, C.K., B.D. Slaughter, J.R. Unruh, F.L. Guo, Z.L. Yu, K. Mickey, A. Narkar, R.T. Ross, M. McClain, and R. Li. 2014. Organelle-Based Aggregation and Retention of Damaged Proteins in Asymmetrically Dividing Cells. *Cell*. 159:530-542.

List of the Publication

Du Shoukang, Wang Yuhan, Chen Bowen, Xie Shuangshuang, Chan Kuan Yoow, Hay David C, Chew Ting Gang (2025) Clearance of protein aggregates during cell division *eLife* 13:RP96675.